Durham E-Theses

Steady-State and Ultrafast Fluorescence Depolarisation in Rigid-Rod Conjugated Polymers

VAUGHAN, HELEN,LOUISE

How to cite:

VAUGHAN, HELEN,LOUISE (2010) *Steady-State and Ultrafast Fluorescence Depolarisation in Rigid-Rod Conjugated Polymers*, Durham theses, Durham University. Available at Durham E-Theses Online: http://etheses.dur.ac.uk/223/

Use policy

The full-text may be used and/or reproduced, and given to third parties in any format or medium, without prior permission or charge, for personal research or study, educational, or not-for-profit purposes provided that:

- a full bibliographic reference is made to the original source
- a link is made to the metadata record in Durham E-Theses
- the full-text is not changed in any way

The full-text must not be sold in any format or medium without the formal permission of the copyright holders.

Please consult the full Durham E-Theses policy for further details.

Academic Support Office, Durham University, University Office, Old Elvet, Durham DH1 3HP
e-mail: e-theses.admin@dur.ac.uk Tel: +44 0191 334 6107
http://etheses.dur.ac.uk

Abstract

Steady-State and Ultrafast Fluorescence Depolarisation in Rigid-Rod Conjugated Polymers

Helen Louise Vaughan

Polarised spectroscopic techniques were used to investigate the underlying physics of steady-state and ultrafast fluorescence depolarisation in conjugated polymers. Depolarisation is due to fluorescence anisotropy: the angular difference between the absorption and emission transition dipole moments of a molecule. Polarised spectroscopy results from a polymer with a flexible backbone, poly (9,9-di(ethylhexyl)fluorene) were compared with those from two rigid backbone polymers: methyl-substituted ladder-type poly (*para*-phenylene) and the newly synthesised naphthylene ladder-type polymer (2,6-NLP). This revealed that there is an intrinsic anisotropy directly associated with the molecular backbone. This work is the first reported on 2,6-NLP.

Fluorescence anisotropy was shown to be dependent upon the conjugation length; the transition dipole moments show larger angles for short lengths, tending to a minimum as the length increases. For rigid-rod polymers, this behaviour is replicated at each vibronic position. In the flexible polymer, planarisation of the backbone elongates the excited state over more conjugated bonds, changing the angle between the transition dipole moments, whereas in rigid-rod polymers, such elongation can only be electronic.

Linear dichroism results obtained for all the polymers has shown the angle between the absorption transition dipole moment and the molecular backbone is large and that the emission transition dipole moment is aligned with the backbone. Off-chain to on-chain transition dipole moments arise from transitions from localised to delocalised states suggesting that the excited state in conjugated polymers is delocalised.

Time-dependent measurements show that the main fluorescence depolarisation mechanism occurs in under 5 ps for both flexible and rigid polymers. The ultrafast timescale and the similarity of the two systems requires the process to be electronic in origin and not linked to a physical deformation.

This work proposes that ultrafast fluorescence depolarisation is a result of the delocalisation of the electronic state as the conjugation length extends over more of the polymer.

Steady-State and Ultrafast Fluorescence Depolarisation in Rigid-Rod Conjugated Polymers

by

Helen Louise Vaughan

A thesis submitted to the Faculty of Science,

University of Durham for the degree of Doctor of Philosophy

Department of Physics

University of Durham

December 2009

Overview - A comprehensive abstract

Steady-State and Ultrafast Fluorescence Depolarisation in Rigid-Rod Conjugated Polymers

Helen Louise Vaughan

This thesis contains experimental results of the photophysical behaviour of blue emitting conjugated polymers and discusses how these can be used to further the understanding of the fundamental processes involved. In particular, an answer for the problem of ultrafast fluorescence depolarisation has been sought.

Fluorescence depolarisation is the result of an angular difference between the absorption and emission transition dipole moments on a molecule. This is also referred to as the fluorescence anisotropy and the angles can be measured by polarised spectroscopies. By monitoring the change in angle and how it relates to the conjugated backbone, the intra-chain processes governing excitation energy transfer can be categorised. These processes are linked to the photoluminescence efficiency of the molecule and evaluating the processes assists in the manufacture of efficient light emitting devices.

Two families of blue emitting conjugated polymers, both used in light emitting devices, were studied. In particular, a polymer with a flexible backbone, poly (9,9-di(ethylhexyl) fluorene) (PF2/6), and two with rigid backbones, ladder-type polymers poly (*para*-phenylene)s (MeLPPP and 2,6-NLP), were investigated via fluorescence anisotropy. This thesis contains the first photophysical results published about 2,6-NLP.

The flexible polymer, PF2/6 presented a large anisotropy loss that was dependent upon the excitation wavelength except at low energy excitation wavelengths. Therefore depolarisation is thought to occur as a result of excitation migration from higher energy states to lower energy states. A smaller fluorescence anisotropy loss was observed in shorter versions of this polymer. The short oligomers are unable to support excitation energy migration and the anisotropy loss was explained as a change in dipole orientation associated with the elongation of the excited state as a result of planarisation of the backbone. It is postulated that, in longer chains, both processes take place.

The rigid polymers, MeLPPP and 2,6-NLP, were investigated to further understand the effect of structural motion on fluorescence depolarisation. The fluorescence anisotropy was once again dependent upon the excitation wavelength, therefore fluorescence depolarisation is a result of an electronic process. It was observed that the angle of the absorption transition dipole moment is dependent upon the conjugation length. As the conjugation length increases the angle of absorption transition dipole tends to the same angle as the emission transition dipole moment. It was hypothesised that as the excited state elongates, it encompasses more covalent bonds and the state, and its associated transition dipole moment, becomes more aligned with the backbone.

The natural anisotropy of the three polymers was also found: 0.32 ± 0.04 for PF2/6 and 0.36 ± 0.05 for the ladder polymers. These values, which are less than the maximum for parallel dipole moments, show that there was an intrinsic anisotropy loss associated with the structure of the polymer. An angle between the two transition dipole moments also means that at least one of them lies at an angle to the molecular backbone.

The molecular backbones of the three polymers were oriented in stretched polyethylene films and the degree of orientation was measured by three different methods. The methods used, x-ray diffraction; polarised Raman spectroscopy and a polarised fluorescence anisotropy technique, were in good agreement and the angle of the backbones relative to the stretch orientation was found.

Using the aligned films and the polarised absorption technique, linear dichroism, the angle between the absorption transition dipole moments and the backbone was found. The absorption transition dipole was found to be off-axis for short conjugation lengths and that the angle between the backbone and the transition dipole moment decreased as the conjugation length increased. The data were used to show that the emission transition dipole, associated with longer conjugation lengths, was parallel the backbone. The off-axis transition dipole moments are thought to arise from transitions from localised states to delocalised states, suggesting that the absorption transition dipole moment is localised and the emission transition moment is delocalised.

The polymers were also investigated by time-resolved fluorescence anisotropy which allows a study of the intrinsic anisotropy loss. It was found that the anisotropy loss evolves on the same time scale for both the flexible polymer and the rigid polymer, further confirming the presence of a similar process in both systems. The results of these experiments were limited by the detection system's resolution, but it was confirmed that the intrinsic loss must occur in under 5 ps. The ultrafast timescale for this depolarisation strongly suggests that it must be electronic in origin and not linked to a physical deformation of the polymer.

From the results in this thesis, it is proposed that the ultrafast depolarisation observed in these, and other conjugated polymers, is a result of the delocalisation of the electronic state as the conjugation length extends over more of the polymer.

Preface

The work contained in this thesis was carried out in the Organic Electroactive Materials Group and with its collaborators between 2003-2008. The following publications result from the work contained within this thesis.

Chapter 4 *An investigation into the excitation migration in polyfluorene solutions via temperature dependent fluorescence anisotropy.* H. L. Vaughan, F. B. Dias and A. P. Monkman Journal of Chemical Physics **122**(1) 014902 (2005)

Chapter 5 *On the angular dependence of the optical polarisation anisotropy in ladder-type polymers.* H. L. Vaughan, L.-O. Pålsson, B. S. Nehls, A. Farrell, U. Scherf and A. P. Monkman Journal of Chemical Physics **128**(4) 044709 (2008)

Chapter 6 *A concentration effect on the oriented microstructure in tensile drawn polyfluorene-polyethylene blend.* M. Knaapila, H. L. Vaughan, T. P. A. Hase, R. C. Evans, R. Stepanyan, M. Torkkeli, H. D. Burrows, U. Scherf and A. P. Monkman Macromolecules **43** (1) 299305 (2010)

Other original work was carried out during the tenure of this PhD. Several publications resulted from this but are not included within this thesis.

- *Polarized optical spectroscopy applied to investigate two poly(phenylene vinylene) (PPV) polymers with different side structures*
  L.-O. Pålsson, H. L. Vaughan and A. P. Monkman Journal of Chemical Physics **125**(16) 164701 (2006)
  (contribution: developed fabrication technique for stretched polyethylene-conjugated polymer films, sample fabrication and performed some spectroscopic measurements.)

- *Orientation of triplet and singlet transition dipole moments in polyfluorene, studied by polarised spectroscopies.*
  S. M. King, H. L. Vaughan and A. P. Monkman Chemical Physics Letters **440** 268 - 272 (2007).
  (contribution: sample fabrication and performed the steady-state polarised spectroscopic experiments.)

- *On the determination of anisotropy in polymer thin films. A comparative study of optical techniques*
  M. Campoy-Quiles, J. Nelson, P. G. Etchegoin, D. D. C. Bradley, V. Zhokhavets, G. Gobsch, H. L. Vaughan, A. P. Monkman, O. Ingans, N. K. Persson, H. Arwin, M. Garriga, M. I. Alonso, G. Herrmann, M. Becker, W. Scholdei, M. Jahja, and C. Bubeck, Physica Status Solidi A. Special Edition **5** 1270 - 1273(2008)
  (contribution: performed spectroscopic ellipsometric measurements using the "Durham" technique as outlined in the published article.)

Contents

List of Figures

List of Tables

Declaration

The material contained in this thesis has not been submitted for the examination of any other degree, or part thereof at the University of Durham or any other institution. The material contained in this thesis is the work of the author except where formally acknowledged by reference.

Copyright

The copyright of this thesis rests with the author. No quotation from it should be published without her prior consent and information derived from it should be acknowledged.

Acknowledgments

"I can no other answer make, but, thanks, and thanks."

William Shakespeare
Twelfth Night, Act III, Scene III

I would like to thank many people and acknowledge that without their help this thesis would never have been completed. Much of the thanks has to go to: my supervisor Professor Andy Monkman who always listened to my ridiculous ideas and never laughed; to Dr Lars-Olof Pålsson for getting me into research and making it such fun; to Professor Peter Hatton for saying what I needed to hear, whether I wanted to hear it or not; to Dr Tom Hase, Dr Matti Knaapila and the guys at the XMaS Beamline at ESRF for looking after me, writing beamline proposals and being convinced that the work was worth doing; to Dr Fernando Dias for teaching me how to use the laser and not to take science experiments too personally; to Professor Hugh Burrows and the Department of Chemistry, University of Coimbra for hosting me for a fabulous month and to the office, especially Dr Simon King and Dr-in-waiting Edward Snedden for just for being there when I needed you.

A heartfelt thank you goes to Professor Greg Scholes, Dr Arvindas Ruseckas and Dr Johannes Geirschner, all of whom are experts in the field of ultra-fast depolarisation in conjugated polymers and all of whom took time to speak with me about the results contained in this thesis at OP 2009 in Beijing, June 2009. They were all complimentary and supportive of my work, resulting in a much needed boost of my confidence.

Thanks also go to the Engineering and Physical Research Council who funded my period of study. I was fortunate enough to be given a Durham University Teaching Fellowship supported by the County Durham Economic Partnership (CDEP), the Ogden Trust and the MacRobert Trust. This gave me the opportunity to spend a year in Easington Community School teaching, making resources and making very good friends with the students and the teachers.

Particularly special expressions of my utmost gratitude go to Dr Nathan and Mrs Lucy Courtney for their understanding, Jenny Radcliffe for her never ending LaTeX knowledge and Dr-in-waiting Helen Armstrong for being the better Helen and never turning me away.

My final thank you goes to my family: my Mum and Dad who have always had faith in me even when I have not.

Thank you

Helen L Vaughan
December 2009

For my parents:
Judith and Geoff Vaughan.

Chapter 1

Introduction

1.1 Lighting, displays and organic polymers

The provision of artificial lighting in homes and offices allows us to work in the dark, increasing our daily productivity. Electrical lighting, an improvement on the naked flames of fires and candles, has allowed factories and shops to stay open twenty-four hours a day with less risk of fires and other accidents. It is an invention that allows us to drive safely at night and decorate our Christmas trees without fear of setting them alight.

However, since Joseph Swann's invention of the incandescent light bulb one hundred and thirty years ago, there has been a desire for brighter, smaller, less expensive, more versatile lighting solutions. Most common lighting is still based on this early design of a heated wire filament encased in a thin glass ball or bulb. Light created in this way has to be passed through a coloured filter to access the full colour range of the rainbow. For example, coloured light bulbs used for decoration are made with tinted glass. This method, however, reduces the accessible amount of light from the bulb and decreases the overall efficiency of a coloured lighting system. Also, traditional incandescent light bulbs emit a high percentage of energy as heat instead of light and today, with an apparent energy crisis looming, the efficiency of these devices has become increasingly important.

Other current lighting solutions are based on fluorescent strip lights which emit light as a result of electrical discharge through a mercury vapour which then excites a fluorescent compound. They are significantly more efficient than light bulbs but they produce a stark blue-coloured white light that can be uncomfortable to look at. The energy saving "ECO" bulbs, which are based on this concept are slow to reach their maximum brightness, are not compatible with dimmer switches and may flicker making them uncomfortable for some people. The mercury necessary for their operation is a known health hazard and is subject to regulation.

All these lighting devices are rigid and brittle and the range of applications they can be used for is limited. Semiconductor light emitting diode (LED) devices are a more attractive option for lighting not only because they have the sought-after high luminescence efficiency but also because they can be mass produced cheaply in a range of shapes, colours and sizes. They are much thinner than other light sources and are used for lighting large panel displays. A further problem is that semiconductors produce narrow colour bands and to get an apparent white light at least three bands must be combined. The different colours of the bands means that illuminated objects do not always reflect their true colours. Hence LED's are not usable in many lighting applications where colour is important, for example, hospital lighting.

In our technological age we receive information from directly illuminated displays: signs, televisions, traffic lights, computer screens, even electric razors have a display. One of the more successful display technologies is the liquid crystal display (LCD) which is used in devices such as, televisions, digital watch faces, mobile phones and computer screens.

Even some of the latest generation of technologies have properties that are not conducive to all commercial applications: they are all rigid and those that include a glass container (light bulbs, fluorescence tubes and LCDs) are prone to breaking. The true aim for the lighting and display community is a totally flexible, unbreakable device that covers the whole white light spectrum.

The solution to the mechanical issues is a device which is made entirely of plastic. Plastic has the advantage of low mass, ease of processing and flexibility allowing large scale projects to be undertaken. But most plastics are electrical insulators which is a considerable drawback for an electronic device. However, there is one family of organic polymers that can conduct a current as well as emit light. Understanding the physical and electronic properties of these conjugated polymers is the purpose of the work described in this thesis. Of key interest is the microscopic relationship between the physical and electronic processes as this aids in the development of new, more efficient polymers.

1.2 Conjugated polymers

Polymers are long chain organic molecules comprised of repeated units connected in the form of a covalently bonded carbon backbone. In insulating polymers all the carbon atoms are joined with single bonds and the bonding electrons are localised and requires a great deal of energy to be excited. Conjugated polymers however have a carbon backbone that alternates between single and double covalent bonds. In the double bond, a π-bond, the electrons are not as tightly bound to the carbon atom (delocalised) and need less energy to become excited. The highest occupied molecular orbital (HOMO) is the *pi* orbital and the lowest unoccupied molecular orbital (LUMO) is the pi^{star} orbital. Transitions between the HOMO and LUMO are the primary electronic transition. Furthermore, the wavefunction of the HOMO and LUMO can extend over several adjacent monomer units which lowers the energy further such that it corresponds to the energy of visible light. These delocalised electrons allow the molecule absorb and emit light, whilst still retaining the usual physical properties of plastics.

The first of these conjugated polymers was produced in 1977, by doping a single chain polymer, polyacetylene, with halogen ions producing an electrically conducting polymer.[1] Twenty years later, the first observation of luminescence from a conjugated polymer under an applied electric current was reported and their potential as a new light source was revealed.[2]

The chemical structure and the number of repeating units of a conjugated polymer controls the energetic separation of the HOMO and LUMO and therefore the colour of the emitted

light. Consequently, by changing the chemical structure of the backbone it is possible to modify the colour of emitted light. Emission bands of conjugated polymers are typically broad, thus making it easier to make white light devices than with semiconductor LEDs. Instead of a single polymer that emits a single colour, two or more polymers can be mixed in a solution enabling any colour to be produced. It is also possible to synthesise polymers that have two differently emitting units within them, enabling the development of a white-light emitting polymer.

1.3 Organic light emitting diodes (OLEDs)

The ultimate aim for the use of conjugated polymers is to create an efficient light emitting device such as an organic light emitting diode (OLED), which can be used for display or lighting. Whilst a single polymer layer will emit light when a current is passed through it as demonstrated by Burroughes *et al.*,[2] more recent devices have more than one layer. Typical

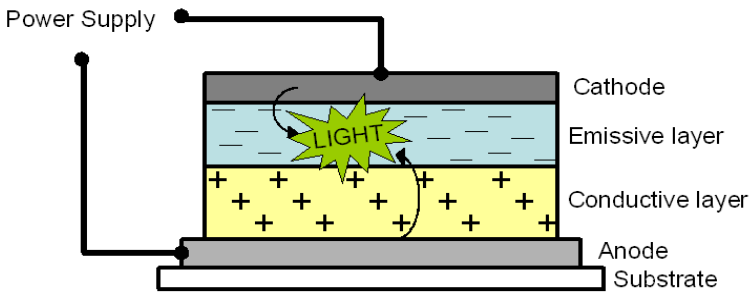

Figure 1.1: Schematic diagram of an organic light emitting diode (OLED) mounted on a substrate, showing the electrical connections (anode and cathode) and the active polymer layer (conductive and emissive sub-layers). In the emissive layer there are free electrons (denoted by -) and in the conductive layer there is a deficit of electrons (holes, denoted by +). Electrons and holes recombine emitting light when current is passed from the anode to the cathode.[3] Figure based on a schematic in Blythe, T (2008) *Electrical Properties of Polymers* Cambridge University Press pp 401.[3]

OLEDs are comprised of five layers (as shown in Figure 1.1): a transparent substrate; a transparent anode; a conductive layer (typically a conjugated polymer); an emissive polymer layer; and, a cathode (typically a metal). When a current is applied, positive charges (holes) are injected into emissive layers where they recombine with negative charges (electrons), emitting light. White-light emitting devices can be made by building several emissive layers made from different polymers or by using a blend of polymers in a single layer or on a single molecule with multiple chromophores.[3]

Manufacture of OLEDs is simpler than traditional LEDs because the polymers are organic and they can be dissolved in a wide range of organic solvents and used as an ink. Thin films can be deposited on a wide range of materials, such as glass, plastic and metals using existing printing techniques[4–6] such as ink jet printing.[7,8] These techniques allow thin patterned films of polymer to be created easily and OLEDs and other polymer electronics can be manufactured much more cheaply than current devices, for example, semiconductor LEDs and LCDs.

Each layer in an OLED is no thicker than 100 nm (100 times thinner than a human hair) meaning that the total device thickness is dominated by the substrate. Therefore, a massive advertising billboard can be made up of smaller segments without worrying about their structural integrity. Similarly, these devices can be made as small as television pixels.

Increasingly, OLEDs are being used in devices that are competing with visual display technologies, because OLEDs can create a full colour display and they respond to an electronic switching signal faster than most LCDs. They have a further advantage over LCDs: they do not need a backlight. This removes the need for backlighting and makes a display brighter with sharper images. OLEDs also have a wider viewing angle and more lifelike colours.[7,9]

Although OLEDs have a clear advantage, and indeed there are several products containing OLEDs based on small molecules are already on the consumer market.[10–12]

Making polarised polymer devices is sometimes straightforward because some polymers can be printed on to substrates with an alignment layer. However, the polymer's properties in respect to polarised light, whether it be absorption or emission, is still not fully understood.

1.4 Polarised light and polarisers

Electromagnetic radiation is a transverse wave as shown in Figure 1.2. If the radiation has a wavelength between 380 nm and 700 nm it can be observed with the naked eye and is referred to as visible light. The electric and magnetic fields of the radiation are perpendicular to each other. By convention, the direction of the electric field determines the polarisation of the radiation.

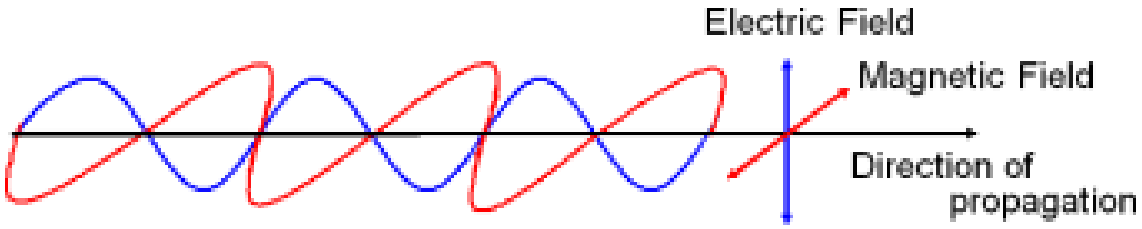

Figure 1.2: Schematic diagram of electromagnetic radiation showing the electric field (blue) and the magnetic field (red) which are both transverse to the direction of propagation (black). The polarisation is defined as the direction of the electric field. Figure based on schematics in Hecht, E (1998) *Optics 3rd Edition* Addison Wesley pp 46.[13]

Typically light sources such as the sun and incandescent light bulbs produce unpolarised light i.e. many individual waves each with different polarisations. Specific orientations of the electric field or polarisations of light can be selected in several ways e.g. by using a polarising medium. Polarisers are materials that are optically anisotropic, usually due to an orientation within the material. The simplest form of polariser is a stretched plastic sheet that has been coated in an iodine based ink and is commercially known as Polaroid.[13] Since the polymer chains are all aligned with the stretching direction, the ink on them is also similarly oriented.

The basic principle of this kind of polariser is that the light waves with their electric fields parallel to the aligned chains are absorbed by the ink whereas the waves polarised perpendicular to the chains pass through unaffected. Unpolarised light contains many waves with a component of their electric field parallel to the dye. These components will be absorbed whereas components perpendicular will be allowed through. Hence a simple thin film can be used to polarise light and the resulting light is said to be linearly polarised. The distribution of polarised light produced by polarisers is described in detail in Chapter 2.

Some crystals can also be used to polarise light. The atomic structure and, hence, the distribution of the electrons, in these crystals is anisotropic. The interaction between the light and the electrons causes refraction. Anisotropic crystals will have two or more refractive indices. This means that linearly polarised light is refracted differently depending on the orientation of the crystal. When unpolarised light enters this sort of crystal, the two orthogonal components of the electric field are refracted by different amounts. It is, therefore, possible to select a single polarisation of light. Scattering from particles and reflection from a planar medium are other means of producing linearly polarised light from unpolarised light.

The procedure of selecting a single linear polarisation of light will mean there is a significant drop in intensity. The inclusion of a polariser in any optical system reduces the intensity of the light. In a display or lighting application this has the additional disadvantage of wasting light and, therefore, reducing the efficiency of the device.

1.5 Transition dipole moments

Movement of an electron from a lower energy state in an atom to a higher energy state requires the absorption of electro-magnetic radiation (light) and the transition from a higher energy state to a lower energy state, emits light.

The electronic structure of conjugated polymers is such that when a *pi*-electron in the double bond makes a transition between HOMO and LUMO, the light absorbed or emitted is typically in the visible.

The interaction of the electric field of the light and the electronic structure of the molecule leads to the formation of a transition dipole. A transition between orbitals is governed by a property called the transition dipole moment. It is the orientation of the dipole which gives the probability of absorbing linearly polarised light and determines the polarisation of emitted light. By determining the orientation of the dipoles with respect to the polymer's backbone it is possible to make predictions about the mechanism governing the change in polarisation between absorbed and emitted light.

Understanding the electronic processes between absorption and emission in conjugated polymers will advance the knowledge of the fundamentals of polymer photophysics. These properties are linked to the efficiency of emission of light from the polymers and thus the efficiency of the OLED. A thorough understanding of polarisation will also help in creating more efficient polymers and thus more efficient devices.

1.6 Aims and objectives

The aim of this thesis is to investigate the absorption and emission properties of two types (flexible and rigid) of blue-emitting conjugated polymers. In particular, this thesis reports on a newly synthesised polymer (naphthylene-ladder-type poly (*para*-phenylene) (2,6-NLP)) for which no photophysics has previously been reported. Two properties of interest are excitation migration and the orientation of the transition dipole moments which will be measured by investigating the polarisation behaviour.

When a photon is absorbed and an electron makes a transition to a higher energy level an excitation is formed. In conjugated polymers the excitation, called an exciton, is an excited state whereby an interaction between an electron and a hole keeps the two carriers correlated in the excited state. Excitation migration occurs as this exciton moves between units on a polymer chain or between chains. This movement can change the difference in orientation between absorption and emission transition dipole moments. The migration of excitations in the polymer is of great fundamental interest in the field of conjugated polymers. The processes by which the excitons (electron and hole bound pair) move along the chain (intra-chain motion) before they recombine are linked to the luminescence efficiency of a particular polymer. The luminescence efficiency, the ratio of emitted energy to absorbed energy, of an isolated polymer in a solution is very high (90 %). In a deposited film, however, this efficiency drops to under half that in the solution. The polymer chains are much closer to each other in a film and the excitons can move among many more chains to the lowest energy state before they emit. Migration between chains (inter-chain motion) requires energy, thus reducing the energy of an emitted photon. Moreover the exciton can find quenching sites (such as defects) more easily which decrease the luminescence efficiency. This has a significant consequence for making efficient devices and it is vital to control or remove processes that inhibit high efficiencies.

To be able to fully differentiate between the inter-chain processes that can occur in a film and intra-chain processes that occur intrinsically, it is essential to start by isolating the electronic and vibronic processes that occur on an individual chain. Work carried out to investigate excitation migration in isolated chains is reported in this thesis. Steady-state polarised fluorescence spectroscopic experiments were undertaken to investigate intra-chain electronic processes.

The theoretical basis of the work described in the thesis is covered in Chapter 2 which covers both the fundamentals of polarisation of light and the photophysics of molecules. Particular attention is given to the two types of conjugated polymers (flexible and non-flexible or ladder) used in the work including the first ever report on the photophysics of the new ladder-type polymer 2,6-NLP. These polymers were chosen as they appear from previous work to be of special interest for the particular optical applications described earlier. A wide range of experimental techniques were employed and Chapter 3 describes the fundamental aspects of them, with more details being given, as appropriate, in the later chapters. The bulk of the

thesis describes the experimental results: Chapters 4 and 5 cover the steady state fluorescence experiments to obtain data on the basic behaviour of the molecules and measure the angle between absorption and emission transition dipole moments; Chapter 6 reports on the X-ray diffraction studies and the polarised Raman spectroscopic investigations into finding the angle the absorption transition dipole moments make with the conjugated backbone; and in Chapter 7, the results of time resolved polarised fluorescence measurements are presented to gain an understanding of the rate of the depolarisation between absorption and emission and it's connection with the inter-chain electronic processes. Finally, in Chapter 8, the results of these experiments are discussed in the context of furthering the understanding of the photophysics of conjugated polymers and their contribution to improving optical applications.

Chapter 2

Photophysics and Conjugated Polymers

2.1 Introduction

This chapter contains an introduction to the physics that underlies the experiments performed and the results obtained in this thesis. As the experiments concentrate on the interaction between polarised light and conjugated polymers, this chapter begins with a brief discussion of light, specifically, linearly polarised light. It is followed by explanation of how bonding occurs in molecules and why the electronic properties of conjugated polymers arise. The next section concentrates on photophysics: the study of the interaction of light with materials. Finally, there is a review of previously published information about the conjugated polymers used in this work.

2.2 Light

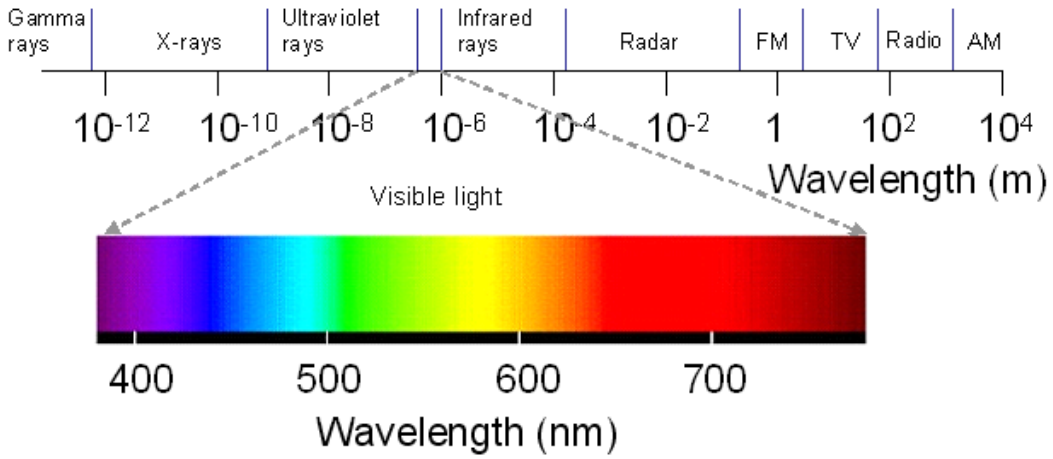

Figure 2.1: Schematic diagram to show the electromagnetic spectrum. The figure shows that the names given to different length waves and highlights the relationship between wavelength and colour of visible light. Adapted from a table in M. Chapple (1997) *The complete A-Z Physics handbook* p. 75.[14]

Electromagnetic (EM) radiation is a transverse wave in which electric and magnetic fields oscillate at 90 ° to each other, as shown in Figure 1.2. The type and name of radiation is characterised by the wavelength (λ), as shown in Figure 2.1. Waves with length between 380 nm and 700 nm can be observed by the human eye and are referred to as the visible spectrum and commonly called light.

The intensity of the electric and magnetic fields of EM radiation can be derived from Maxwell's equations.[15] The electric field vector ($\boldsymbol{E}$) of a light wave can be described mathematically as:

$$\boldsymbol{E} = E_0 \sin(2\pi\nu t + \theta) \tag{2.1}$$

where E_0 is the amplitude of the wave, ν is the frequency of the light, (where the speed of light, $c = \nu\lambda$) t is the time from $t = 0$ and θ represents the initial phase of the wave. The phase indicates the position of the wave, be it peak, trough or somewhere in between, at $t = 0$. The phase can also give information on the relative positions of the peaks of two different EM waves.

2.2.1 Polarised light

As the wave propagates, the electric field vector traces a pattern in the plane perpendicular to the direction of travel (z-axis), which can be described using orthogonal co-ordinates (x and y) in this plane. An important property of light, its polarisation, is defined by the pattern the electric vector traces, as shown in Figure 2.2. If the individual waves that make up a beam of light are such that the direction of the electric vector does not change with time, the wave is said to be linearly, or plane, polarised, as shown in Figures 2.2(a) and (b). If the direction of the electric field vector changes uniformly with time, then elliptically (c) or circularly (d) polarised light are produced.

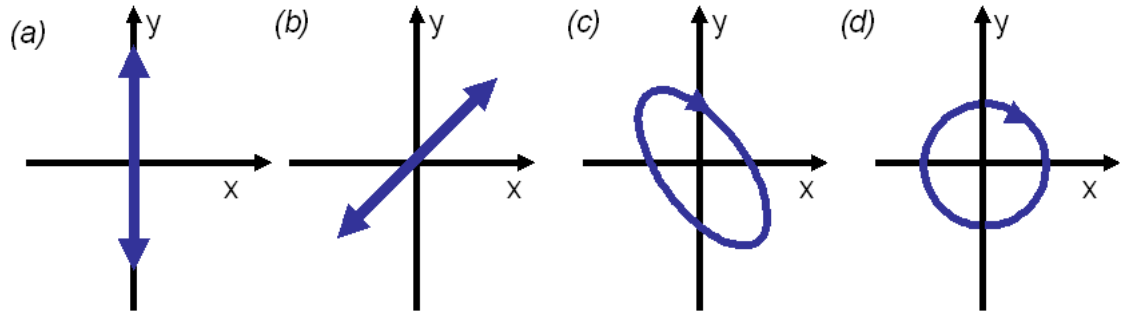

Figure 2.2: Schematic diagrams of the pattern traced out by the electric field vector of an electromagnetic wave. The wave is travelling out of the page. In (a) and (b) the vector does not change with time and the light is classed as linearly (or plane) polarised. The angle that the vector makes with the y-axis determines the angle of polarisation of the wave. Also shown, in (c) and (d), is the pattern when the vector changes uniformly with time which results in elliptically (c) and circularly (d) polarised light. Diagrams adapted from Feynman *et al.* (1965) pp 33-2[16]

Light from an isotropic source (e.g. the sun or a filament light bulb) contains light waves with different polarisation directions which are emitted randomly in time. At any moment the resultant electric field vector of the light will be different from one moment to the next and this produces an ever changing polarisation state, rather than just one. This type of light is called unpolarised light.

It is possible to select a specific orientation of linearly polarised light from unpolarised light for use in optical systems, for example, the backlighting for liquid crystal displays. In the experiments described in this thesis, the absorption and emission of linearly polarised light is used to reveal some of the electronic properties of the conjugated polymers. Selecting and detecting a specific orientation of the polarisation of light requires the use of polarisers, which only allow the transmission of a particular, chosen electric field direction.

2.2.2 Polarisers

A polariser is a material that affects the two orthogonal components of the electric field differently, enabling them to be separated and thus producing light of a defined polarisation. In this section, only polarisers that produce linearly polarised light are described[a].

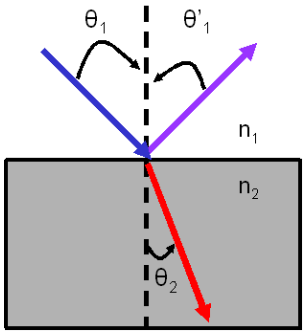

Figure 2.3: Schematic diagram to show the path of a light beam as it reaches the interface of two materials with different refractive indices. The diagram shows that the the incident beam of light (blue) is both reflected (purple) and refracted (red) when it reaches the interface. The angle of incidence (θ_1) is equal to the angle of reflection (θ_1') and the angle of refraction is calculated from Snell's Law given in equation 2.2. The dotted line indicates the normal, from which all angles are measured. Diagram adapted from Tipler, P (1999) *Physics for Scientists and Engineers* p. 1041[17]

When light strikes the boundary between two materials, it may be reflected or transmitted through the second material. When light passes from one material (e.g. air) to another (e.g. glass) its velocity and direction are changed by the process of refraction, which is a result of the interaction between the electric field of the light with the electronic distribution (electron density) in the material. The extent of this refraction is measured by the index of refraction, n. Snell's Law describes the angle of refraction, θ_2, i.e. the angle to the normal that the light makes as it passes from one material (with index of refraction, n_1) to another (with index of refraction n_2). Snell's Law also depends upon the angle of incidence (θ_1) at the boundary of the two materials. See Figure 2.3 for further clarity of the angles involved. Snell's Law is written mathematically as:[17]

$$\frac{\sin\theta_2}{\sin\theta_1} = \frac{n_1}{n_2} \tag{2.2}$$

Birefringent crystals, such as quartz and calcite, have two refractive indices which affect the two orthogonal polarisation components of the incident light differently, so that the transmitted light is split into the two components. There is a direction in the crystal, the optic axis, where both polarisations propagate with the same velocity. The lower refractive index causes one polarisation to be refracted less than the other ray. Therefore, by controlling the angles of entry and exit of unpolarised light, it is possible to construct a polariser which produces linearly polarised light. Specifically, Glan-Thompson polarisers, which use this principle, were used in the experiments reported in this thesis.

[a] There are other types of polarisers that can create circularly polarised light from plane polarised light. These are known as quarter wave plates. More details of these polarisers can be found in Hecht, E (1998) *Optics 3rd Edition* Addison Wesley

Glan-Thompson polarisers are formed from two calcite prisms held together by glycerine or mineral oil.[13] The prisms are shaped such that the component of light perpendicular to the optic axis is totally internally reflected at the interface resulting in the transmission of one polarisation only. These types of polarisers are frequently used in optical experiments that require a high degree of resultant polarisation. They are very useful in experimental situations because they have a large acceptance angle[b] and can cover a wavelength range from 350 nm to 2.3 μm. With a suitable cement they can also be used in the ultra-violet region of the spectrum (down to 240 nm).[18]

Absorption of one polarised component is another method of selecting polarisation from unpolarised light. These dichroic materials include Polaroid and other thin films. As will be explained in section 2.3 on electronic transitions, molecules (and indeed crystals) will absorb the component of the electric field parallel to its dipole and allow transmission of the perpendicular electric field components, resulting in linearly polarised light.

Light can also be linearly polarised by scattering (for example from atoms and dust particles) or by reflection from a plane surface (for example a pool of water or a window). The latter can only occur at a specific angle dependent on the reflecting medium. Whilst these two processes commonly occur around us, neither of the two methods were used to create polarised light for the experiments.

2.2.3 Malus's Law

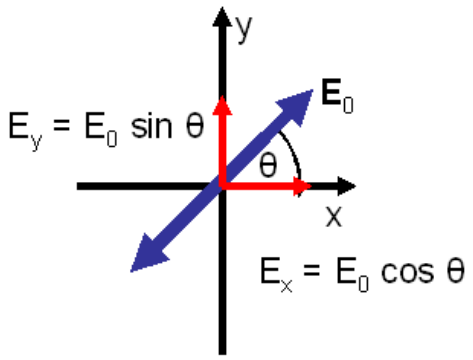

Figure 2.4: A schematic to show the two orthogonal electric field components of linearly polarised light. The resultant electric field, E_0, is split into components along the x and y axes.

In all cases, selecting a single plane polarisation from an isotropic source reduces the intensity of the light. As has already been noted, linear polarisers select a specific orientation of unpolarised light. The electric field vector of an incoming light wave can be considered to be composed of two components: one parallel to the transmission axis (E_x) and the other orthogonal to it (E_y) as shown in Figure 2.4. The electric field vector that passes through a polariser is dependent upon the angle that it makes with the transmission axis.

[b] The acceptance angle is the range of angles of incidence of the incoming beam that still produces polarised light.

If the electric field E_0, makes an angle θ with the transmission axis then the two components can be written as:

$$\begin{aligned} E_x &= E_0 \cos\theta \\ E_y &= E_0 \sin\theta \end{aligned} \tag{2.3}$$

The E_x component passes through the polariser unaffected, whereas the E_y is affected by the polariser (for example, in a thin film polariser it is absorbed).

Since the intensity of light is proportional to the square of the electric field, the initial intensity of light I_0 is equal to E_0^2. As such, the intensity transmitted through the polariser, I, is given by:

$$\begin{aligned} I = E_x^2 &= E_0^2 \cos^2\theta \\ \therefore \quad I &= I_0 \cos^2\theta \end{aligned} \tag{2.4}$$

This is known as Malus's Law. When light is passed through a pair of polarisers the intensity of the transmitted light will depend on the angle between the transmission axes, being at a maximum when they are parallel (and equal to I_0) and decreasing as the angle increases, eventually becoming zero when the axes are orthogonal. In a series of perfect polarisers, where successive pairs of polarisers are rotated to non-orthogonal angles, some light will be transmitted. At each polariser in the series, the intensity of light and the plane of polarisation will be changed, so only the incident parallel component is transmitted. The final intensity can be determined by successive applications of Malus's Law. This phenomenon can be used effectively in the laboratory by monitoring the intensity of light through two polarisers to ensure that they are aligned with each other.

2.3 Light, energy and electronic orbitals

The energy of the electromagnetic radiation, E, is directly related to its wavelength by the following relation

$$E = \frac{hc}{\lambda} \tag{2.5}$$

where h is Planck's constant and c and λ have been previously defined. Since the wave carries a quantised amount of energy, light is often considered to consist of particles called photons and quantum mechanics is used to describe the processes. The two descriptions of light, as a wave or a particle, are complementary and this duality is fundamental to the nature of light: depending on the phenomenon observed one description or the other is used. In the work described here, for example, polarisation is essentially a wave property whereas the absorption and emission processes are photon based.[15,16,19]

2.3.1 How is light connected to atomic structure?

Atoms show distinct spectra with the hydrogen atom being the simplest. From this spectrum, Rydberg and Ritz developed a mathematical equation to describe the wavelength of light emitted in hydrogen.[15]

The Rydberg-Ritz equation is:[15]

$$\frac{1}{\lambda} = R_H\left(\frac{1}{n_a^2} - \frac{1}{n_b^2}\right) \qquad n_a = 1, 2, ... \qquad n_b = 2, 3, ... \tag{2.6}$$

where λ is the wavelength, R_H is the Rydberg constant for hydrogen and n_a and n_b are integers. Rydberg's work was purely heuristic and did not lead to any deeper understanding of the under lying physics.

The hydrogen atom, with only one electron, was the first atom to be understood at a quantum mechanical level. This was achieved by Bohr, by assuming that the electron could only exist in quantised energy levels.[15] Electronic transitions between energy levels requires a change of energy in the form of electromagnetic radiation. For a transition from a lower level to higher level, electromagnetic radiation is absorbed. For a transition the other way around, electromagnetic radiation is emitted. This is shown in Figure 2.5.

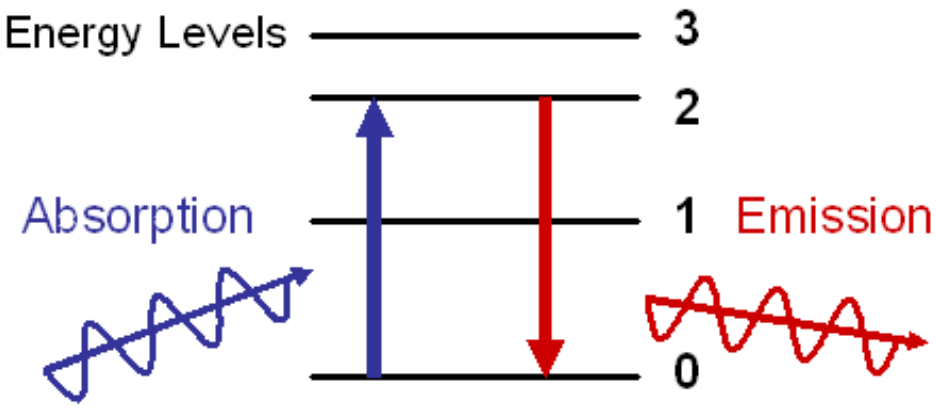

Figure 2.5: Schematic diagram showing four energy levels that could arise in an atom. Also shown are vertical transitions between levels. The upward (blue) arrow corresponds to the absorption of electromagnetic radiation and the downward (red) arrow corresponds to the emission of electromagnetic radiation.

Due to its single electron hydrogen has a relatively simple set of energy levels. Bohr related the n_a and n_b in Rydberg's equation (equation 2.6) and the transition between the levels, and produced a series of emission lines that matched the previously recorded spectrum of hydrogen. Atoms other than hydrogen contain a nucleus surrounded by a cloud of multiple electrons. The electrons are still constrained to be in quantised energy levels.

The energy E_n of a particular level n can be calculated by the following equation:[17]

$$E_n = -\left(\frac{1}{(4\pi\epsilon_0)}\right)^2 \frac{me^4}{2\hbar^2}\frac{Z^2}{n^2} \tag{2.7}$$

where m is the mass of the electron, ϵ_0 is the electric constant, $\hbar$ is Planck constant divided by 2 π and Z is the atomic number of the atom. Bohr's model was also able to derive the Rydberg constant, R_H in equation 2.6 from fundamental constants.

Each transition between different levels in the atom has a different energy and consequently a different wavelength. It is possible to use the above equation to calculate the wavelength of electromagnetic radiation emitted for each transition.

Conversely, by observing the wavelength of the electromagnetic radiation emitted, it is possible to evaluate the energy levels of an atom. Each atom has a characteristic set of energy levels. This translates to a characteristic set of absorption and emission lines which makes up the spectrum of the atom. Locating the absorption and/or emission lines can help identify the atoms in a system.

Molecules have more complex energy levels, due to the interaction between the electrons which form inter-atomic bonds. The basic concept remains: the transition between energy levels results in the emission or absorption of electromagnetic radiation. This will be discussed in a later section.

2.3.2 Probability of a transition and transition dipole moments

An electronic transition does not occur simply because electronic states exist in a system. Absorption can only occur when the incident photon has energy greater or equivalent to the energy separation of the two states. Even then, the transition is not guaranteed.

The incident photon carries with it an electric field which must perturb the ground state in such a way that it resonates with the higher state. Only then can the photon be absorbed. The electric field of the light perturbs the charge distribution from one stable configuration to one that resembles that of the excited state. This change in charge distribution induces a dipole.[20–23] For this reason the perturbation is considered to be a transition dipole moment, $\vec{\mu}_{i\to f}$, and is a function of the initial and final state wavefunctions (ψ_i and ψ_f):

$$\vec{\mu}_{i\to f} = \langle \psi_f \mid e\vec{r} \mid \psi_i \rangle \tag{2.8}$$

where e is the charge on an electron and $\vec{r}$ is the unit vector of the dipole.

As a vector has magnitude and orientation, there is strong absorption when the electric field vector of the incident light is linearly polarised parallel to the absorption transition dipole moment. The absorption becomes weaker as the angle between the two vectors increases. The strength of the absorption transition depends on the magnitude of the absorption transition dipole moment by a dimensionless property called the transition oscillator strength $f_{i\to f}$ which is linked to the wavelength of the transition:[15]

$$f_{i\to f} = \left[\frac{8\pi^2 m_e c}{3e^2 h}\right] \frac{1}{\lambda} \mid \vec{\mu}_{i\to f} \mid^2 \tag{2.9}$$

where m_e is the rest mass of the electron. $f_{i\to f}$ is governed by quantum mechanical selection rules which allow or forbid a transition; they include a change in electron spin; a change in wavefunction parity; a change in angular momentum and the overlap of the two orbitals during a transition. A value of $f = 1$ means the transition is allowed whereas for a value of 0, the transition is forbidden. The transition oscillator strength can be determined through absorbance experiments, further details are presented in section 2.5.1.

There is also an emission transition dipole moment that governs the radiative relaxation (emission) from an excited state to the ground state. Here, the excited state is perturbed such that the emitted photon's electric field is linearly polarised parallel to the emission transition dipole moment.

The probability of a transition is determined by Fermi's Golden Rule[15,17]

$$\Gamma_{i\to f} = \frac{2\pi}{\hbar} \mid \langle \psi_f \mid \hat{H}(\vec{r}) \mid \psi_i \rangle \mid^2 g(E_f)t \tag{2.10}$$

where Γ is the probability of the transition between the initial and final states, $g(E_f)$ is the density of states, t is the time and $\hat{H}$ is the Hamiltonian operator that is dependent upon the orientation of the dipole. The probability is proportional to the square of the cosine of the angle that the transition dipole moment makes with the vertical.

The transition dipole moments are a fundamental property of any atom or molecule as they determine the strength and orientation of the transition. This is important in the understanding of electronic processes that occur in molecules. The transition dipole moments become increasingly important for oriented molecules as they will determine the polarisation of absorbed and emitted light.

2.3.3 Atomic orbitals

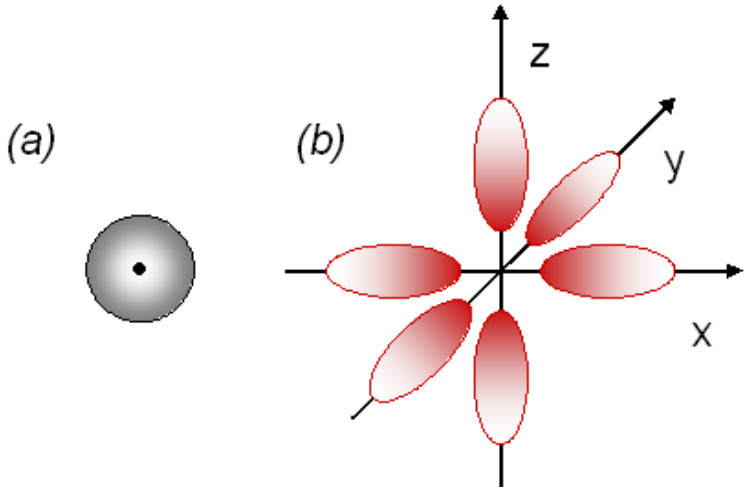

Figure 2.6: Schematic to show two types of atomic orbitals. Sharp (s-) orbitals are spherical in shape (a) and principal (p-) orbitals have 6 lobes, one in each axial direction (c). Figure adapted from Kotz *et* al. (1996).[24]

Electrons in atoms and molecules are forced into different energy levels due to the Pauli Exclusion Principle.[15] This principle states that fermions cannot exist in the same quantum state. Electrons are fermions that have a spin state of 1/2 or -1/2, thus two electrons can have the same energy but different quantum spin states. Extra electrons are forced into additional quantum states which may be in higher energy levels. The increased number of energy levels increases the number of possible transitions that an electron can undergo. Each of these transitions has an associated absorption (and emission) wavelength, unless it is forbidden by quantum mechanical rules.

Also associated with the increased number of electrons is the change in shape of electron orbital. The number of electrons in each energy level follows $2n^2$, where n is the number of the energy level. The first four electrons are placed in two sharp (s-) orbitals that are spherical in shape. The next six electrons are placed in placed in three principal (p-) orbitals. The three p-orbitals are perpendicular to each other and shaped like dumbbells as shown in Figure 2.6 (b). These are referred to as p_x, p_y and p_z orbitals to distinguish their orientation. Further electrons are added into five diffuse (d-) orbitals and seven fundamental (f-) orbitals (though not necessarily in this sequential order). Their shapes are more difficult to describe though they can be found in *Chemical Bonding* by A. Companion[25] and *Basic Inorganic Chemistry* by Cotton and Wilkinson[26] respectively.

The shape of the s- and p- orbitals becomes particularly important when discussing bonding in organic molecules.

2.3.4 Molecular orbitals

As atoms are brought together, their electron orbitals begin to overlap. This overlap is the beginning of a chemical bond between the atoms. When atoms are held together in this way they are said to be a molecule. There are three types of bond that form in organic molecules, the σ-bond, the π-bond and the δ-bond. Only the first two are important for further discussion within conjugated polymers and the latter will be discussed only briefly.

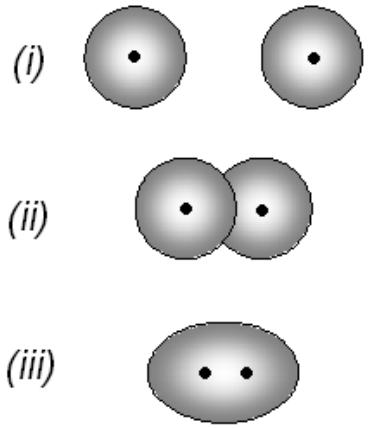

Figure 2.7: Schematic diagram to show the formation of a sigma bond between two atoms with s-orbitals. (i) the atoms and their orbitals are spherical and separated but as they are brought together (ii) their orbitals overlap. The nuclei are equally repelled and attracted and their orbitals coalesce to form a molecular orbital (iii). The bond between the two atoms is called a σ bond. Diagram adapted from Companion, A (1979) p. 46.[25]

A σ-bond is formed when two atoms and their spherical s-orbitals come into close proximity and the electrons become attracted to the opposite nucleus. This draws the nuclei together, until they reach a stable position where the attraction is equal to the repulsion. At this point the orbitals hybridise and the electrons are shared between the two nuclei and form an orbital that encompasses both atoms. This is called a molecular orbital (MO). The σ-bond is created from a "bonding" σ-orbital and an "anti-bonding" $\sigma^\star$-orbital (higher energy). The process described above is shown in Figure 2.7.

σ-bonds can also be formed between two collinear p-orbitals or between a p-orbital and an s-orbital. This latter bond requires hybridisation between the orbitals to form a sp-hybrid orbital that has the shape of a squashed sphere. Since both electrons are involved in holding the atoms together and are localised between the atoms, the σ- bond is particularly strong.

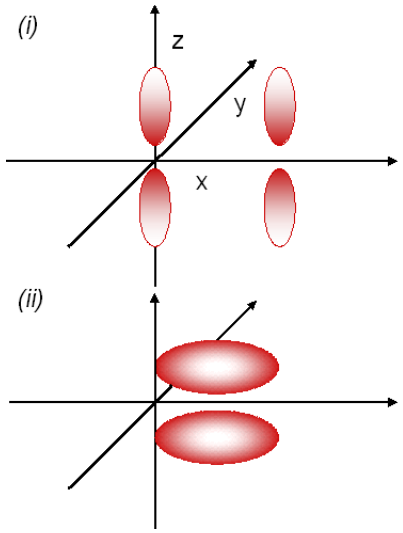

Figure 2.8: Schematic diagram to show the formation of a π-bond in two molecules with electrons in the p_z-orbitals. The atoms only have four electrons each and the p_z-orbitals are shown for clarity. As they are brought together (i) the p_z-orbitals overlap. The nuclei are equally repelled and attracted and their orbitals coalesce to form a molecular orbital (ii). The bond between the two atoms is called a π-bond. Diagram adapted from Companion, A (1979) p. 50.[25]

π-bonds, by contrast, are quite weak. These bonds form as a result of the orbital overlap between two parallel p-orbitals. As the atoms are brought together, the p_z-orbitals overlap and coalesce and the electrons are delocalised above and below the x-axis. The π-bond is created from a π-orbital and an anti-bonding $\pi^\star$-orbital (which has higher energy). This is shown in Figure 2.8.

The third type of bonding, δ bonding, occurs between d-orbitals which are found in large atoms. These atoms are not usually present in conjugated polymers [c].

Molecules are not solely comprised of one type of bonding. Indeed, it is common that the p-orbitals will form both σ- and π-bonds with an adjacent atom. This is called a double bond. Molecules containing double bonds are called unsaturated molecules whereas those with only single bonds are called saturated molecules. For example, in methane (CH_4) each of the carbon atom's four electrons overlap with one from a hydrogen atom creating four σ- bonds. The same applies to ethane (C_2H_6) where there is only one bond between each atom (one bond between the two carbon atoms and one from each hydrogen to the adjacent carbon atom.). However, in ethene (also called ethylene C_2H_4), as shown in Figure 2.9, due to the lower number of hydrogen atoms it is necessary for the carbon atoms to bond together

[c] Further details of this type of bonding can be found in several texts including *Chemical Bonding* by A. Companion.[25] and *Basic Inorganic Chemistry* by Cotton and Wilkinson.[26]

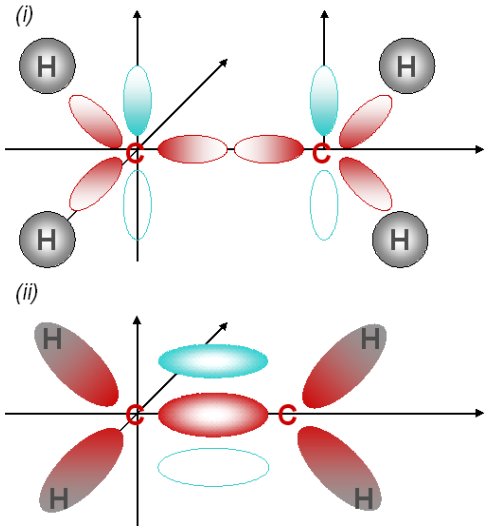

Figure 2.9: Schematic diagram to show the bonding in ethylene. Ethylene C_2H_4, contains two carbon atoms and four hydrogen atoms (i). As the atoms are brought together, molecular orbitals, (bonds) start to form. There is a σ-bond between each hydrogen and carbon atom and one between the two carbon atoms. The electrons in the p_z-orbital (coloured blue for clarity) form a π-bond which has a lower state and higher energy state above and below the molecule.

twice and create a double bond (a σ-bond and a π-bond). A σ-bond forms between each of the carbon and hydrogen atoms. A σ-bond between the carbon atoms is also formed from the p_x-orbitals and this forms the backbone of the molecule. The electrons remaining in the p_z-orbital form a ground state π-orbital or higher energy, $\pi^\star$-orbital, above and below the molecule.[4,20]

The MO that exist as a result of bonds between atoms are also involved in electronic transitions. Absorption transitions occur between the highest (energy) occupied molecular orbital (HOMO) and the lowest (energy) unoccupied molecular orbital (LUMO), whereas emission transitions occur from the LUMO to the HOMO. The electrons in an unsaturated bond are delocalised and the π-bond is weak and transitions can easily occur between the π-orbital (the HOMO) and the $\pi^\star$-orbital (the LUMO).

The part of the molecule where transitions in the visible part of the spectrum can occur are called chromophores. These can be a single monomer unit, or more usually encompass a series of monomer units. The chromophores result in absorption and emission spectra that are characteristic of specific molecules. For example, some dyes, such as Coumarin, have an chromophore that can absorb and emit visible light.[27] Typically, the spectra of molecules are broad, compared with the line-like spectra of atoms. The reasons for this will be discussed later.

A special set of molecules that interact with light is the family of conjugated polymers.

2.3.5 Bonding in polymers

A polymer is a long chain molecule with a structure comprised of a repeating series of smaller molecular units as shown in Figure 2.10. These small units are called monomers and make up the polymer's backbone. Polymers are often organic materials, in the sense that their main chemical components are carbon and hydrogen. Polymers can occur naturally, for example, the polysaccharide, cellulose, is grown in the cell walls of plants, or they can be synthesised. Limiting the polymer synthesis allows the length of the polymer to be controlled and polymer lengths can vary from two to ten monomers (an oligomer) to many thousands of monomers.

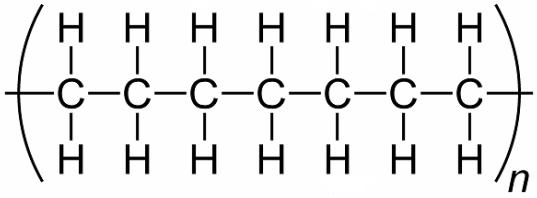

Figure 2.10: Chemical structure of typical polymer polyethylene. The structure shows a section of the polymer containing seven repetitions of the monomer unit H-C-H (CH_2).

Polymers are more commonly referred to as plastics and are used for many practical purposes which utilise one or more of their properties. They are used, for example, as lightweight and flexible packaging such as drinks bottles or magazine wrappers. Polymers can be solution processed, meaning they can be dissolved in a solvent and then painted on surfaces, such as most paints and nail varnishes. Most importantly of all, most polymers are cheap to buy and manufacture.

2.3.6 Bonding and orbitals in conjugated polymers

Conjugated polymers are a family of organic polymers that are of special interest to many scientists. Their backbone is comprised of alternating single and double carbon-carbon bonds i.e. they follow the pattern C—C=C—C=C—C=C where C—C represents a single σ-bond and the C=C represents a double bond (comprised of a σ- and π-bond). This is shown in the conjugated polymer, polyacetylene (Figure 2.11). The repeating alternating pattern is called conjugation and is the distinguishing feature of all conjugated polymers. Conjugation can pass through aromatic groups, such as phenyl rings, which can form part the polymer backbone. The length of the polymer chain which contains this unbroken alternating pattern is referred to as the conjugation length and acts as a chromophore.

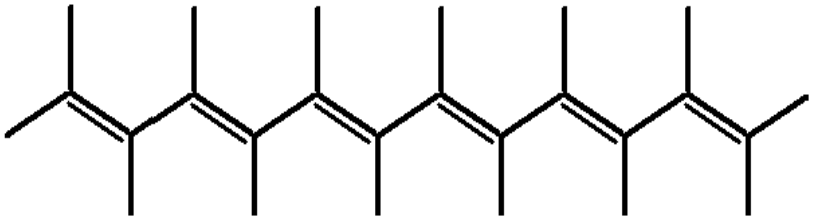

Figure 2.11: Chemical structure of the first synthesised conjugated polymer, polyacetylene. The structure shows a section of the polymers containing six repetitions of the monomer unit CH—CH=CH. The carbon-carbon single bonds are longer than the carbon-carbon double bonds.

Normally in σ- and π-bonds the electrons are localised between two atoms. However, in conjugated polymers, the molecular orbitals created by π-bonds can coalesce because of their close proximity to each other. This forms an extended π-bond that encompasses the whole of the conjugated segment.

The extended delocalisation, due to an increased conjugation length, lowers the energy gap of a possible transition. The extended π-bond creates a more complex and larger MO and makes the photophysics of conjugated polymers different from that of small molecules. The energy difference of the HOMO and LUMO (also the energy difference between the π- and $\pi^{\star}$-orbital) corresponds to the UV-visible region of the electromagnetic spectrum. Hence as the conjugation length decreases, the corresponding wavelength of light absorbed or emitted is blue-shifted. It is the fact that the emission from these polymers can be in the UV-visible region that makes optical manufacturers interested in conjugated polymers. Conjugated polymers also have many of the same properties that their unconjugated counterparts possess; they are cheap, lightweight, flexible and can be processed by (usually organic) solution. They are an ideal candidate for cheap, lightweight, flexible optical displays.

2.3.7 Conjugation length distribution

In a conjugated polymer, the π-bonds extend over the length of unbroken conjugation. This is often referred to as the *conjugation length*.[28] The conjugation length is not a fixed length for a specific polymer and can vary from chain to chain. It is controlled by several factors including the length of the polymer, defects created during synthesis, and unwanted kinks in the chain. Collectively, these factors give rise to the conjugation length distribution and it is this distribution that makes the photophysics of these polymers different from short molecules (e.g. dyes) and inorganic semiconductors.

Breaks in the conjugation arising as a result of imperfect synthesis, may be due the formation of a monomer unit or during polymerisation. For example, defects in the polymer backbone may not maintain the alternating pattern of single and double bonds, thus causing a break in conjugation. Defects can arise from left-over catalyst, mis-bonding or left-over starting materials.

Breaks in conjugation can also be caused by non-linear polymer growth. During polymerisation, monomers can bond to each other at various angles which will deviate from the initial direction of growth. This in turn breaks the extended conjugation. It is expected that the monomer units bond end-to-end to each other to form a linear chain. However, if sites available for bonding on the chain are not collinear, the resulting backbone will have a saw-tooth pattern, instead of being straight.

The polymer methyl-substituted ladder-type poly (para-phenylene) (MeLPPP), one of the polymers studied in this thesis, is believed to suffer from this non-linear growth problem. It is believed that the polymer grows linearly initially. However, after it has reached a length of several tens of units, it can bond with another chain of a similar length. Instead of bonding parallel to one of the chains, it is hypothesised that it bonds at approximately 60 ° to create a herringbone pattern as shown in Figure 2.12.[29,30]

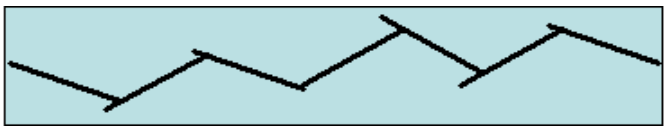

Figure 2.12: A schematic to show how MeLPPP may form a herringbone pattern during synthesis. It is thought that the polymer grows linearly in one direction before it joins with another linear segment.[29–31] The diagram shows how the linear segments of the polymer, fuse together at approximately 60 °. The linear segments may be joined at each end or part way along the adjacent segment.

Other physical disruptions to the continuous conjugation are thought to include a twist between adjacent monomers in the polymer. In this case, the substituent groups on neighbouring monomers interact and force the monomers to rotate around the molecular axis.

Another synthesis problem is controlling the length of the polymer chain and in turn the conjugation length distribution. For relatively short polymers, of about 20 units in length and shorter oligomers, such as those that have been studied here, the total length of the polymer often determines the conjugation length. This is certainly the case if the polymer is defect free and the monomer units are in a straight line.

2.3.8 Polydispersity

During polymerisation, it is difficult to produce chains of a specific length; the end product usually contains a range of lengths. However some control is possible, for example controlling the temperature of the reaction also controls the rate of polymerisation. The distribution of polymer lengths synthesised is called the polydispersity.

The polydispersity, P, is the ratio of the weight average molecular weight (M_W) to the number average molecule weight (M_n).[32]

$$P = \frac{M_W}{M_n} \tag{2.11}$$

These two averages are weighted means, M_W is weighted with the molecular weight:

$$M_W = \frac{\sum_{i=1}^{m} N_i M_i^2}{\sum_{i=1}^{m} N_i M_i} \tag{2.12}$$

whereas the M_n is a number average:

$$M_n = \frac{\sum_{i=1}^{m} N_i M_i}{\sum_{i=1}^{m} N_i} \tag{2.13}$$

The value of the polydispersity is always greater than one, but the closer this value is to unity, the smaller the distribution of chain lengths. When the value is low, it is possible to estimate the length of each chain.

Since the conjugation length of a polymer is dependent upon the length of a polymer, the conjugation length distribution is dependent upon the polydispersity of a batch of polymer. The polydispersity, therefore, needs to be considered when many molecules are studied simultaneously e.g. in a solution or film.

The spectra that are produced by conjugated molecules are very complex. This is partially because of the distribution of conjugation lengths which is analogous to the density of states, but also because of the nature of the excited state.

2.4 The nature of the excited state

The crystal structure of inorganic semiconductors gives rise to energy bands in the place of discrete atomic levels. The bands are two electronic states, a valence band and a conduction band, that are separated by an energy gap that must be overcome before electrons can transport a current. This gap can be overcome by thermal energy and an electron is promoted from the valence band to the conduction band and leaves an oppositely charged "hole" behind. The quasiparticle that describes the interaction between the electron and hole is called an exciton.[33]

The π-bond in conjugated polymers is created two electronic orbitals, a π- orbital and a $\pi^\star$-orbital. The two electronic orbitals responsible for the π-bond were interpreted with the semiconductor band theory and was originally applied to them shortly after their discovery.[34–36]

More recent research has challenged the applicability of the semiconductor band model for conjugated polymers. The electrons in this semiconductor band theory model are "nearly free" leading to excitons with a small binding energy. However, experiments have shown that conjugated polymers have a high exciton binding energy.[37–39] The form of the excited state has been extensively investigated[28] and the electrons have been observed to have strong localisation to a small conjugated unit. Most importantly, spectra have shown detailed structure that comes from coupling of the excitons to the molecule's vibrational modes. This has led to the creation of a theory which is now used in models, theories and experimental analysis of conjugated polymers.

2.4.1 Excitons in conjugated polymers

This new theory is descriptively named the molecular exciton model. It assumes that the excitations are tightly bound a result of a Coulomb interaction between the electron and hole.[40,41] The basis of this thesis relies on this theory that the excitons formed are tightly bound, indeed localised, to an individual chain. The size of the exciton is determined by the spectroscopic unit (conjugation length) to which it is localised.[42] As stated earlier, the size of the conjugation length can vary as a result of aggregation, defects or kinks in the polymer chain. Recent work has suggested that gentle twists and bends of the polymer chain do not completely change the localisation of an excited state.[43]

The behaviour of the electron-hole pair can be correlated over different distances. Excitons localised to the same chromophore (also termed conjugation length) are tightly bound to it, have a close separation between electron and hole, and are called "Frenkel" excitons.[28] If the electron-hole pair is extended over two adjacent molecules (that is, the electron and hole are on two different molecules) or two different segments of the same molecule, the exciton is called a "charge-transfer" exciton and the electron and hole are able to recombine but over a longer timescale than ordinary fluorescence. The charge separation (caused by the separation of the electron and hole) causes a permanent dipole in the system which can be altered with a polar solvent. A larger electron-hole separation results in a "Wannier-Mott" exciton. These excitons have a low binding energy and are able to move more easily.[28]

Conjugated polymers support both Frenkel excitons (localised on one unit) and charge transfer excitons because they can support a permanent dipole. The two types of polymers used it this study are believed to support Frenkel excitons in non-polar solvents.

It is currently believed that the ground state is delocalised and that after excitation the first excited state of a single conjugated polymer is localised.[44–46] However, work contained in this thesis questions this assumption. *Dynamic localisation* on the femtosecond timescale has been theorised to occur in a number of long chain polymers[47,48] and dendrimers.[49,50] It is a result of conformational motion or nuclear motion that forces the exciton to relocate from its ground state configuration.[43]

2.4.2 Polarons

Under an applied electric field, an exciton can disassociate into its constituent free charges. The electron, hole and their interaction field are known as a polaron pair. If the pair are still correlated but not bound they are known as a geminate pair. As the electron and hole separate further, they lose their correlation and are effectively free charges. The vibronic energy from a chain distortion, a phonon, and the free charge constitute a polaron. The free charges can recombine and emit at a defect or reform an exciton. Polaron pairs alter the orbital picture of conjugated polymers and create a set of energy levels between the existing HOMO and LUMO.

The consideration of geminate pairs, polaron pairs and the charges is important for light emitting devices as they aid the electrical conduction. These pairs can also be formed by charge injection which is a key step in OLED operation. The manufacturers of photovoltaic devices made from conjugated polymers also have to consider free charges, as it is the dissociation of excitons that is vital for their function.

2.4.3 Singlet and triplet states

As electrons and holes are fermions, both with spin = 1/2 and they follow Pauli's Exclusion Principle and therefore two fermions can exist in the same energy level if they have opposite spin. The exciton, a correlated electron-hole pair, can exist in a ground state with spin = 0. This is called a singlet state and the ground state is given the abbreviation S_0.

A photon has a spin = 1 and the absorption of a photon cannot change the spin of one of the electrons. Excitation via absorption creates another singlet state which is the first excited state S_1. No change of spin is required for a transition between singlet states meaning that the transition is allowed.

A state with the total spin = ± 1 can also exist; and is called the triplet state (T_1). Here a change of electron spin is required to form a triplet state meaning that these energy levels cannot be accessed by photon absorption. Similarly the transition from an excited triplet state to the singlet ground state is quantum mechanically spin forbidden. Triplet states can be formed through intersystem crossing from the S_1 state and during polaron recombination in OLED devices. Since the radiative (emissive) transition is not allowed from the triplet state, the device's efficiency can be compromised by the presence of triplet states.

Singlet-singlet transitions are only considered in this thesis, particularly the $S_0 \rightarrow S_1$ and $S_1 \rightarrow S_0$ transitions. These correspond to an absorption transition and an emission transition respectively.

2.4.4 Energy Transfer Processes

After absorption of energy, the excited state can undergo one of many processes that can change the energy of the exciton. Energy can be transferred along a conjugated polymer (excitation or exciton migration) or it can be transferred between adjacent molecules via reabsorption, incoherent hopping to lower energy states or Förster resonance transfer.[28,51] Other effects can also result in a change in energy of the excited state and, most importantly, a change in the observed photophysics.

Excitation energy can be transferred from one spectroscopic unit to another. This may be on the same polymer chain (intra-chain transfer) or between different molecules (inter-chain transfer). These processes are both shown in Figure 2.13. The transfer can occur by exciton migration (or hopping) between spectroscopic units or by Förster transfer.[28,51,53–59]

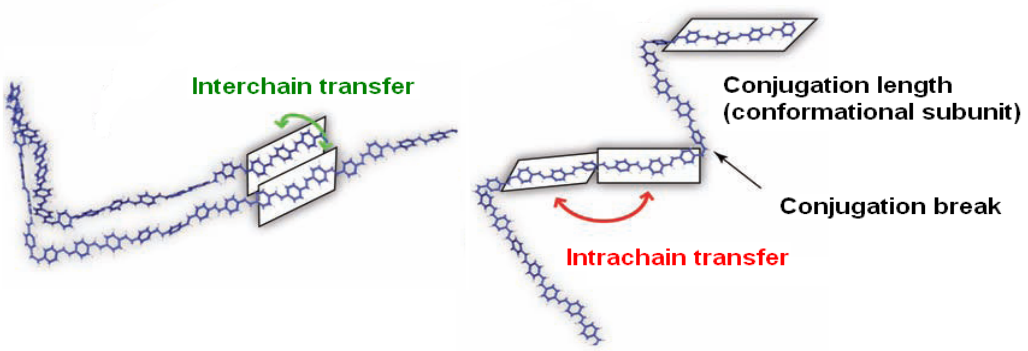

Figure 2.13: A schematic to show how energy can transfer between conjugation lengths either on separate chains or to different parts of the same chain. The diagram shows a segment of the chain with continuous conjugation, this is referred to as a conjugation length or conformational subunit. These conjugation lengths are limited by conjugation breaks. The diagram shows interchain transfer (green) which occurs between two conjugation lengths on separate chains and intra-chain transfer (red) which occurs between units on the same chain. The diagram is taken from and adapted from Collini, E *et al.* Science (2009)[52]

Förster transfer can occur between two spectroscopic units where there is a spectral overlap between the absorption of one molecule and the emission of the other. This transfer system also relies on the close proximity of the molecules (< 6 nm) and the relative orientations of the transition dipole moments.[51] The left of Figure 2.13 shows the relative positions of two conjugation lengths, on separate chains, required for interchain transfer, such as Förster transfer. Full details of Förster transfer can be found in section 2.4.5.

An exciton can hop to energetically lower states (longer conjugation lengths) and will eventually become locally trapped (for example, by a break in conjugation or a defect) or reach the longest conjugation length supported by the system. The right of Figure 2.13 shows multiple conjugation lengths on a polymer chain: some of which are separated by conjugation breaks. In a system with enough thermal energy to overcome defects, the exciton can make hops to energetically higher states and the hopping process can continue until the lowest energy (longest) site is reached. The hopping process is dispersive and dependent upon the number of sites that an exciton can move to. If the exciton is of high energy, there are many sites to choose from, but as its energy decreases so does the number of available sites. By creating a low energy exciton, it is forced to remain in the same position and it is possible to monitor any changes that the exciton undergoes. This technique is called *site-selective spectroscopy* and is achieved by exciting a polymer at the very red-edge of the absorption spectrum.[51,60]

Both excitation migration[61–66] and dynamic localisation produce a difference between the ground (S_0) and excited (S_1) states which can be observed through simple absorption and emission comparison studies. The process of absorption typically creates an exciton with excess energy and it will rapidly migrate through the system to the lowest state.

Observing these energy transfer processes in isolation can allow a more detailed picture of the photophysics of conjugated polymers to be created.

2.4.5 Inter-molecular processes

Whilst single molecular spectroscopy is a new and upcoming field[67,68] it has been more usual to experimentally observe a solution or thin film containing many thousands of polymer chains. This will have the marked effect of increasing the absorption and emission in comparison to a single molecule, as well as broadening of the absorption and emission spectra. The latter will be discussed in full in the following section on spectroscopy of conjugated polymers.

In this section we briefly discuss two electronic processes that are affected by the close proximity of another molecule (specifically a second conjugated polymer). Then the physical effect of having many oriented polymers is outlined.

Förster transfer

Förster transfer is the name given to the energy transfer process between two optically active units. This typically takes place between two adjacent molecules which act as a donor and an acceptor respectively. This transfer rate, k_T, is proportional to the spectral overlap[d] of the two units, $J(\lambda)$, the alignment of their transition dipole moments, κ, and the close proximity of the units, r:

$$k_T \propto \left(\frac{1}{r}\right)^6 \kappa^2 J(\lambda) \tag{2.14}$$

The Förster radius is the distance between the donor and acceptor such that the Förster transfer competes equally with the donor's radiative decay rate. This distance is typically less than 6 nm.[51]

Förster Transfer is also known as resonance energy transfer as it occurs between two transition dipoles that are resonating at the same natural frequency. Förster Transfer occurs between the donor's emission transition dipole moment and the acceptor's absorption transition dipole moment and does not involve the emission and reabsorption of a photon. Efficient transfer can only occur where there is a spectral overlap between the emission spectrum of the donor molecule and the absorption spectrum of the acceptor and the relative orientations (small angle between) of the transition dipole moments are similar.[51]

This type of energy transfer can also take place between spectroscopic units on adjacent conjugated polymer chains. It can happen because there is a spectral overlap of the donor and acceptor and the rigidity of the chains keeps the transition dipole moments almost parallel to each other. It has also been theorised that this kind of transfer could take place along one chain if it were coiled back on itself. To decrease the possibility of Förster Transfer it is important to keep the conjugated polymers at a separation of above a few nanometres. This can be done by using highly dilute solutions and allows the photophysics of isolated molecules to be investigated.

[d] between the emission of the donor and absorption the acceptor

Aggregates

Molecules can cluster together and interact, creating aggregates in concentrated solutions or in a film. The clusters can have a fixed spatial arrangement (a "Super molecular" structure) or a disoriented shape.

In some cases, the close proximity of the molecular orbitals causes them to overlap and create a new MO which is different to that of a single molecule. The new molecular orbitals can even encompass the whole aggregate.[69] This has the effect of changing the positions of the HOMO and LUMO from that of a single molecule. For example, the gap between the HOMO and LUMO may be reduced causing a red shift in the spectrum associated with the absorption transition.

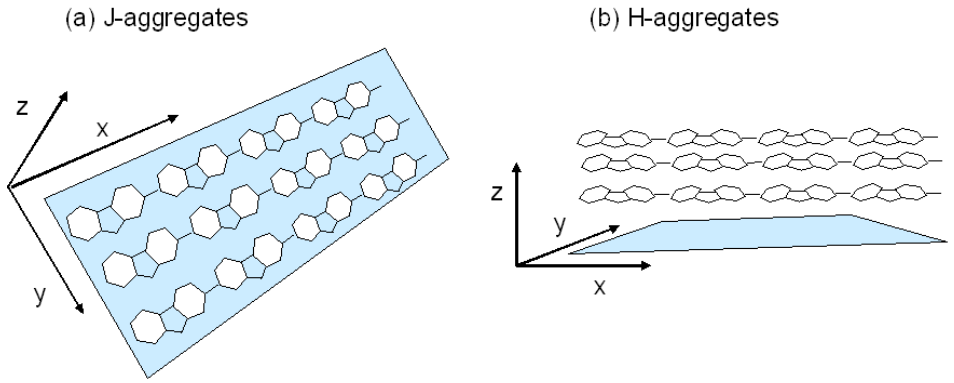

Figure 2.14: Schematic diagram to show the possible arrangement of molecules in a J-aggregate and in an H-aggregate. The diagram shows a long chain molecule which lies in the x-y plane. In J-aggregates the molecules form an array in the plane of the molecule (the x-y plane). In H-aggregates the molecules stack perpendicular to the plane of the molecule. The plane of the molecule has been coloured blue.

There are two main types of super molecular structures that can form as a result of aggregation. These are J- and H-aggregates and are shown in Figure 2.14.

J-aggregates have molecules arranged in the plane of the molecule in a parallel array. The MO of the aggregate is spread out over the entire array, which reduces the energy gap between the HOMO and LUMO. As a result the absorption spectrum from a J-aggregate is shifted to longer wavelengths compared with an individual molecule. The spectrum from J-aggregates is characterised by a sharp absorption peak that is red-shifted from the broad peak of isolated molecules. This spectrum is characteristic of the size of aggregate.[70]

H-aggregates have molecules arranged perpendicular to the plane of the molecule. The molecules are assembled parallel, but above one another. Again the MOs from the individual molecules coalesce and encompass the aggregate. In H-aggregates, this increases the energy gap between the HOMO and LUMO . This results in spectral shift to shorter wavelengths as compared to the individual wavelengths. H-aggregates can often be identified through their broad spectra that is blue shifted with respect to the isolated molecule.

It is unlikely that a molecular system will form purely J- or H-aggregates[71] unless the forces between the molecules are particularly strong. It is more probable that there is a mixture of one super molecular structure, a set of disordered clusters and some isolated molecules with all three phases contributing different percentages depending on the molecule. However, a significant proportion of either of these super structures can be identified through basic spectroscopic techniques such as absorption and emission spectroscopy.[69,71]

2.4.6 Crystallites

The term crystallite is used throughout this thesis to refer to individual molecules that have clustered together to form an ordered structure in solid state. One of the polymers used in the photophysical investigations in the later chapters of this work, PF2/6, can form aligned crystallites that have a hexagonal cross-section.[72] The crystallites formed in PF2/6 are described in Chapter 6.

2.4.7 Phase segregation

In a blend of two or more polymers, identical molecules can form domains instead of homogenising. This is known as phase segregation and can happen on a microscopic or macroscopic scale. The domains in a phase segregated blend can form aligned crystallites or disordered aggregates. This is a phenomenon that is explained in more detail and investigated in Chapter 6.

2.4.8 Orientational order.

Another important aspect of many molecule systems is the way that the molecules are ordered, whether it be a system with a small number of isolated molecules; a system with many molecules; or even highly structured crystallite. The relative orientation of the molecules is very important when calculating angularly dependent quantities. For example, when locating a specific molecular bond relative to a fixed laboratory framework or transition dipole moments determined through polarised spectroscopies.[23,73]

A system is said to be isotropic if all of the molecules are randomly oriented within a sample. An example of an isotropic system, used in this work, is a dilute solution of a conjugated polymer. If the molecules in a system have a preferential alignment direction, then this system is referred to as anisotropic. Examples of anisotropic systems include liquid crystals, stretched films in which the molecules align with the stretch direction and super molecular structures like J-aggregates.

A anisotropic system with a unique preferential direction of orientation is called a uniaxial distribution. An example of a uniaxial distribution is shown in Figure 2.15. The long axis of all the molecules are oriented within a cone around the unique axis. This is defined to be the Z axis of the system. A system may be neither isotropic nor perfectly uniaxial. The molecules in the system may have some preferential orientation, but there may be a wider angular distribution around that orientation axis.

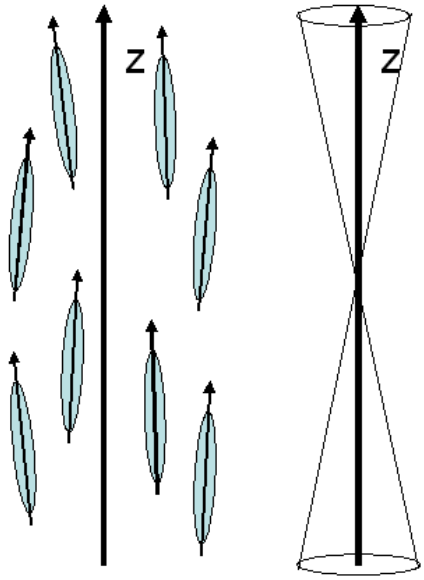

Figure 2.15: A schematic diagram to show an example of a uniaxial distribution. The diagram shows eight molecules that have their long axis aligned at a small angle ($> 10\,^{\circ}$) to the orientation direction Z. The diagram on the right is another way to represent a uniaxial distribution of similar molecules. It shows the the range ($> 10\,^{\circ}$) of all the possible angles that a molecule can make with the orientation axis. Figure adapted from diagrams in E.W. Thulstrup (1989),[23] J. Michl (1995)[73] and A. Rodger and B. Norden (1997).[21]

The distribution of molecules is mathematically represented by an orientational distribution function, $f(\Omega)$:

$$\int f(\Omega)\,\mathrm{d}\Omega = 1. \tag{2.15}$$

where Ω is a solid angle pertaining to the system, integrating over which encompasses all the molecules in the system.

The distribution of orientations has to be taken into account when calculating average angular quantities. i.e:

$$\langle a \rangle = \int a(\Omega)\, f(\Omega)\,\mathrm{d}(\Omega) \tag{2.16}$$

where $a(\Omega)$ is an angularly dependent quantity.[73]

The orientation distribution function is important in deriving the distribution of excited molecules by polarised light (see section 2.5.5) and from that, the average angle between the absorption and emission transition dipole moments, as will be seen in section 2.5.7.

2.4.9 Orientation factors (Order parameters)

The orientation distribution can be described by an orientation factor, also called an order parameter. The orientation factors are used to represent the alignment of one of the molecular axes to the orientation direction. This property of aligned samples can be experimentally found via x-ray diffraction and polarised spectroscopies (as reported in Chapter 6). These factors are an indicator of how well the molecules are uniaxially aligned and can give the average angle a molecular backbone makes with alignment direction.[21] What follows here is a derivation of the order parameter.

2.4.10 Derivation of the order parameter for a uniaxial "rod-like" molecule

The order parameter depends on two sets of co-ordinates; those in the laboratory frame (X,Y,Z) and those in the molecular frame (x,y,z). These two frames are shown in Figure 2.16.[23,73] The relationship between these frames, allows the definition of the orientation factors which are used to represent the alignment of one of the molecular axes (x,y,z) to the orientation direction (Z axis).

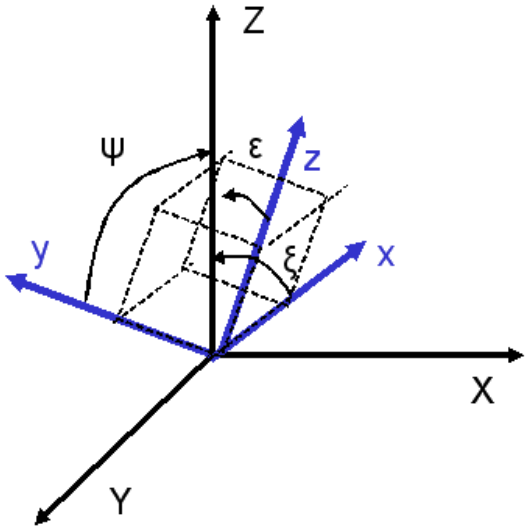

Figure 2.16: A schematic to show the relationship between the laboratory frame (Black, X,Y,Z) and molecular frame (Blue, x,y,z). The figure also shows the angles (ψ, ξ and ε) between each of the molecular axes with the Z-axis in the laboratory frame. The longest axis of the molecule is defined as the z-axis. Figure adapted from diagrams in E.W. Thulstrup (1989),[23] J. Michl (1995)[73] and A. Rodger and B. Norden (1997)[21]

The orientation factors, K_{uv} are defined by the following integrals where u and v are any one of the angles ϕ, ξ, ε (as shown in Figure 2.16):

$$K_{uv} = \int f(\Omega)\, \cos u\, \cos v\, \mathrm{d}\Omega = \langle \cos u\, \cos v \rangle \tag{2.17}$$

The orientation factors can be expressed as the elements of Saupe orientation matrices.[21,23]

$$\mathbf{S} = \begin{pmatrix} S_{xx} & S_{xy} & S_{xz} \\ S_{yx} & S_{yy} & S_{yz} \\ S_{zx} & S_{zy} & S_{zz} \end{pmatrix}$$

where the S_{ij} represent the matrix elements and the order parameters in each microscopic direction.

For uniaxial orientation, for example, conjugated polymers are long chain rod-like molecules that can align in uniaxial micro crystallites, the matrix elements take the form[21]

$$S_{ij} = \frac{1}{2}(3K_{uv}\delta_{uv}) = \frac{1}{2}(3\langle \cos u \cos v \rangle - \delta_{uv}) \tag{2.18}$$

where δ_{uv} is a Kronecker delta.

It is most common to define the longest axis of the molecule as the z-axis, meaning for a rod-like molecule, such as a conjugated polymer, with one long axis twice (or more) the length of the other two dimensions, the matrix elements simplify further: $S_{xx} = S_{yy} = 1/2S_{zz}$. Since, S_{zz} is the primary molecular axis the order parameter for a rod-like molecule, Φ, can be written as:

$$\Phi = \frac{1}{2}(3\langle\cos^2\varepsilon\rangle - 1) \tag{2.19}$$

where ε is the angle between the orientation direction and the molecular axis as shown in Figure 2.16. In the case of rod-like molecules polymers is also the polymer's backbone

The order parameter can vary between 0 (indicating an isotropic sample) to 1 (indicating perfectly aligned). In an oriented sample, the value will reflect a distribution of possible backbone orientations. In a homogeneous uniaxial distribution, equation 2.19 can be used to determine the statistical average angle for ε. The molecules, whilst oriented, actually have individual ε that lie within a cone of the average angle (as schematically shown in Figure 2.15).

If the system contains two or more unevenly sized domains of different backbone orientations the average angle is skewed in favour of the larger domain. In this situation, the order parameter and angle ε cannot be relied upon. This is an important consideration for blends that form phase segregated aggregates.

The order parameter can be determined through X-ray diffraction, polarised Raman spectroscopy or fluorescence anisotropy experiments carried out on an aligned film. All three of these techniques are explained in detail in Chapter 6.

2.4.11 Aligning molecules

It is possible to align molecules in a variety of ways: Polyfluorenes and other liquid crystalline polymers can be cast onto a rubbed polyimide surface and, upon heating, will align almost perfectly with the ridged surface, whereas other molecules such as para-phenylenes need to be incorporated into an anisotropic host such as liquid crystals ($0.5 \leq \Phi \leq 0.7$)[74,75] or stretched polyethylene.

Incorporating conjugated polymers into polyethylene will create a blend with regions of micro crystallinity. If the crystallites within these regions do not align with the imposed stretch direction, then the blend is not a homogeneous uniaxial distribution.

2.5 Spectroscopy of conjugated polymers.

So far, this chapter has described the fundamentals of the absorption and emission of light and the electronic behaviour of simple molecules. This section covers the interaction of conjugated polymers with light, which is the subject of the work in this thesis. It deals with the processes of absorbance and emission (specifically, fluorescence), polarised absorbance and fluorescence and factors that cause the depolarisation of fluorescence

2.5.1 Absorbance and absorption spectra

An important property of conjugated systems is the amount of light absorbed by the sample. The absorbance, A, of a sample is described with a simple equation, the Beer-Lambert Law,[22] which states:

$$A = \ln(I_0/I_x) \tag{2.20}$$

where I_x is the intensity of the light at position x within the sample and I_0 is the intensity before the light enters the sample. The absorbance is dependent on how well the sample absorbs at each frequency, ν, (called the molar extinction coefficient, $\epsilon(\nu)$), the concentration of the sample, $[c]$, and its thickness, l such that:

$$A = \epsilon(\nu)[c]l \tag{2.21}$$

The log of the absorbance is referred to as the optical density ($\mathrm{OD} = \ln A$) and the absorbance of the sample as a function of frequency (or wavelength as in equation 2.5) is called the absorption spectrum. The energy required to promote an electron from the lowest state (ground state or HOMO in a conjugated polymer) to the higher state (an excited state: LUMO) is equal to the energy gap between the two states. In a system with more than one energy level (for example, a molecule), the molar extinction coefficient is dependent on the frequency of the illuminating light because of the physical limitations on the possible transitions that are available within a molecule. Small molecules with few transitions present sharp absorption curves at frequencies corresponding to the transitions.

To determine the relative strength of an electronic transition, it is necessary to integrate the molar extinction coefficient whole absorption spectrum, which can be written mathematically as:[20]

$$f_{i\to f} = 6.25 \times 10^{25} \int \epsilon(\nu)\ d\nu \tag{2.22}$$

where $f_{i\to f}$ is the transition oscillator strength for an absorption transition.

The oscillator strength is a quantum mechanical property that is linked to the magnitude of the transition dipole moment (see equation 2.8 in section 2.3.2). By studying the absorption spectrum of a molecule is it is possible to retrieve information about the magnitude of the absorption transition dipole moment. In this thesis, the transitions considered are between singlet-states which are have strong oscillator strengths ($f \sim 1$) enabling them to be observed.

Larger, more complex molecules, such as conjugated polymers produce absorption spectra with broad peaks centered on the frequencies of the transitions. The broadening is due to the conjugation length distribution. The range of possible lengths, often thought of to be a Gaussian distribution, inhomogeneously broadens the sharp peaks.

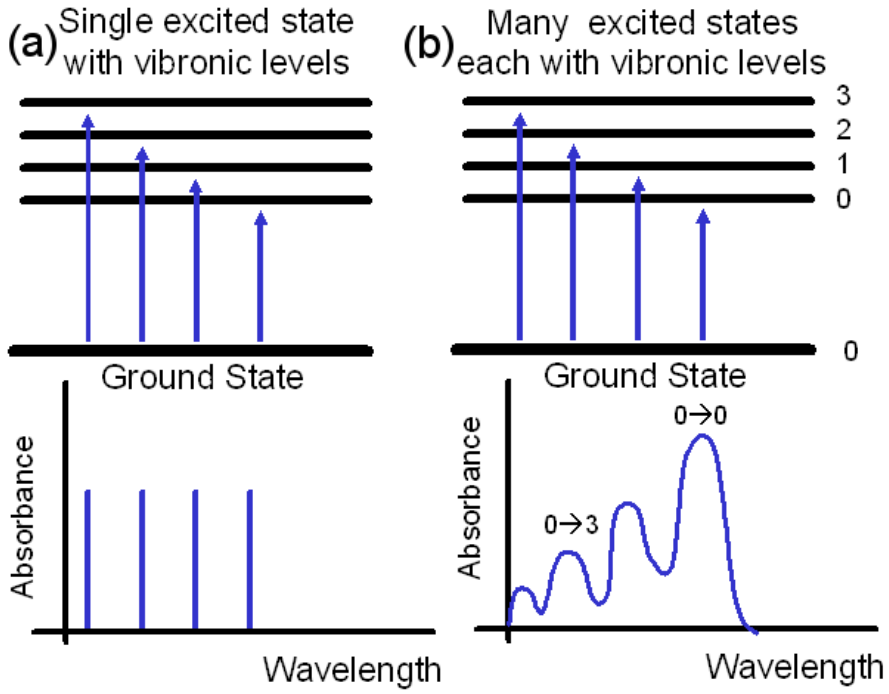

Figure 2.17: A schematic showing the energy levels within a molecule and the corresponding representation of the corresponding absorption spectrum. In (a) the spectrum is created by transitions from the ground state to different vibronic levels. The spectrum is sharp and well defined the absorbance intensities are the same because, in this example, the oscillator strength is the same for each transition. In (b) the spectrum is created by transitions from the ground state to different electronic levels that have vibronic levels coupled within them. The spectrum contains peaks from vibronic transitions which are inhomogeneously broadened as a result of the conjugation length distribution.

In a more complex system, like a conjugated polymer, there is strong coupling between electronic and vibrational levels (due to molecular degrees of freedom e.g. rotation of a side group) which results in multiple vibrational levels within an electronic level as shown in Figure 2.17 (a). Where there are many electronic levels, an electron can be promoted from the ground state to any of the vibronic levels within the electronic states (Figure 2.17 (b)) which means that the molecule can absorb over a wide range of energies. This produces a characteristic absorption spectrum which has pronounced vibronic features. The absorption spectrum will be broadened by the presence of the conjugation length distribution and usually the vibronic features are masked in a broad curve.

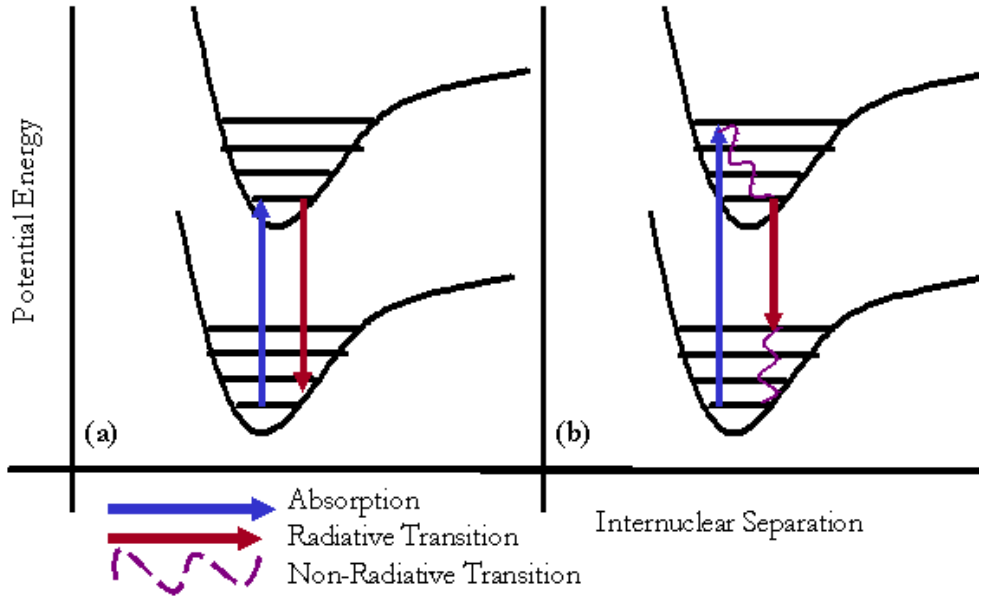

Figure 2.18: Jabłoński Diagrams to show absorption and emission between energy levels in a molecule. The diagram shows two electronic levels made of multiple vibrational levels. In (a) the transition is purely electronic whereas in (b) there are non-radiative transitions through the vibronic levels known as internal conversion.

The Franck-Condon Principle[51,76] states that the time taken for a transition, typically on the order of 10^{-15} seconds, is much faster than the time needed for a rearrangement of the atoms in the molecule. Therefore the ground and the excited state have the same configuration during the transition. This results in a vertical transition on a Jabłoński diagram which used to show the states in a molecule (see Fig 2.18(a)). In terms of quantum mechanics, where electronic and vibronic states are represented by wavefunctions, transitions occur between states with the greatest wavefunction overlap.

2.5.2 Emission and fluorescence spectra

An electron in an excited state can relax back down to the ground state and dissipate the absorbed energy in a number of ways. These are grouped into radiative and non-radiative relaxation and are both shown on the Jabłoński diagram in Figure refabsem1

Radiative relaxation refers to the emission of energy as a photon, which has an energy equal to the energy gap between the two states. If the transition from upper to ground state is allowed by the quantum mechanical selection rules then the emission is virtually instantaneous (on the picosecond to nanosecond timescale) and known as fluorescence. If intersystem crossing takes place and the spin of an electron changes such that a pair have parallel spin, then the emission can come from a triplet state and is called phosphorescence. This latter transition is quantum mechanically "not allowed" and occurs on the microsecond to second timescale.

Non-radiative relaxation refers to the energy of the excited state being released in a non-emissive way. Some of these processes have already been discussed in an earlier section on the nature of the excited state (Section 2.4). The energy can be released as molecular vibrations (or rotations) and can change the conformation of the molecule, the orientation of the molecule or simply the temperature of the system. One way to gauge the luminescence efficiency of the system, and indeed determine if non-radiative processes are taking place, is to measure its photoluminescence quantum yield which is the ratio of absorbed energy to emitted energy.

Structure in fluorescence spectra

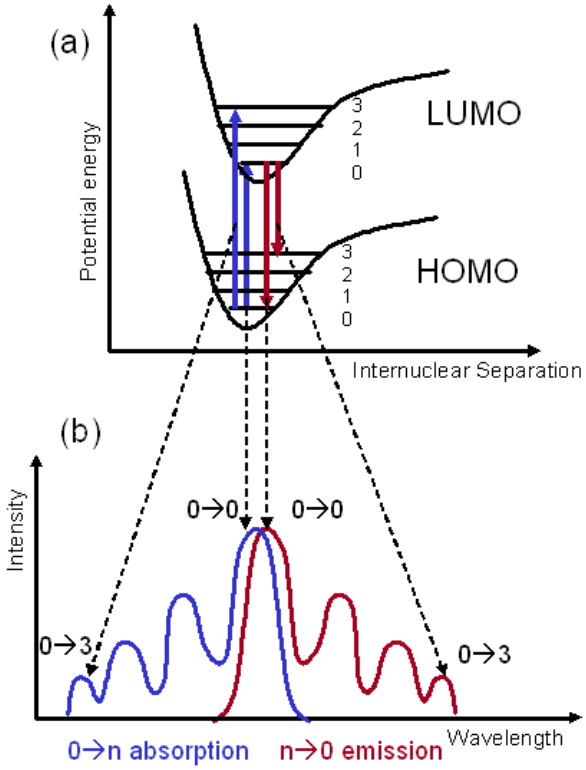

Figure 2.19: A schematic to show the origin of vibronic structure in absorption and fluorescence spectra. The vibronic levels in both the HOMO (ground) and LUMO (excited) electronic state, (a) give rise to peaks (vibronic shoulders) in the absorption and emission spectra, (b). If the energetic spacings of the vibronic levels are the same in each MO then the absorption (blue) and emission (red) spectra are mirror images of each other.

Fluorescence spectra give the energetic position of the electronic and vibronic states as shown in Figure 2.19. Kasha's Rule[51,76] states that the downward electronic transition will occur preferentially from the lowest vibronic state in the upper electronic level because the wave-function overlap between this state and the ground state is the largest. Internal conversion in the excited state ensures that the excitation is in the lowest vibronic state (see Figure 2.18 (b)). The distribution of electronic and vibrational energy levels also has an effect on the range of energies that can be emitted and thus of the structure and width of the *fluorescence*

spectrum. If the transition is purely electronic as in Figure 2.18 (a), the emission is the same as the absorption. But in a complex system, an excited state can undergo more than one different transition back to the ground state. For example, in Figure 2.18 (b) there is a non-radiative transition to lower vibronic levels and an electronic transition will result in an energetically shifted spectrum. Spectra of different shapes result from transitions from completely different energy levels that are accessed via energy transfer.

By Kasha's Rule and the Franck-Condon Principle the strongest absorption transitions should be between the HOMO and the purely electronic LUMO which is directly above it. Similarly the strongest emission transition will occur between the purely electronic LUMO and the HOMO. These are known as the 0-0 transitions. If the vibrational spacings in both the ground and excited state are the same, then it can be expected that vibronic replicas in the emission spectrum are a mirror image of those in the absorption spectrum as shown in Figure 2.19. The peaks from vibronic transitions are often visible as "vibronic shoulders" on the edge of the peak from the electronic transition. The 0-0 absorption and emission transitions are of the same energy if the emission transition is is immediate and the excited state does not undergo a energetic change.

The excited state can undergo a relaxation to a lower energetic state as result of molecular conformational motion or the solvent cage can relax around the excited molecule. Both processes will lower the energy of the excited state before emission. This results in a difference between the absorption 0-0 line and the emission 0-0 line and is called the Stokes' Shift. Measuring the Stokes' shift can be used to monitor the changes that occur after absorption, but before emission.

2.5.3 Spectral shifts due to solvents: solvatochromism

The absorption and emission spectrum of a molecule is also dependent upon the solvent cage that surrounds it. In highly polar solvents, the charge distribution of the molecule is distorted by the close proximity of the solvent molecules. This can lead to a shift to longer (bathochromic) or shorter (hypsochromic) wavelengths. It is usual that this is seen as a small blue shift for polymers in a polar solvent such as chloroform.

2.5.4 Polarised spectroscopy

Since the absorption and emission of a photon is dependent upon the orientation of the transition dipole moment, polarised spectroscopy can give extra information about the orientation of transitions within a molecule.

In some molecules the absorption transition dipole moment and the emission transition dipole moment are parallel but in conjugated polymers they are often differently oriented. Figure 2.20 shows a schematic of the positions of the transition dipole moments relative to each other and the polymer backbone. The angles are fully defined in the following sections.

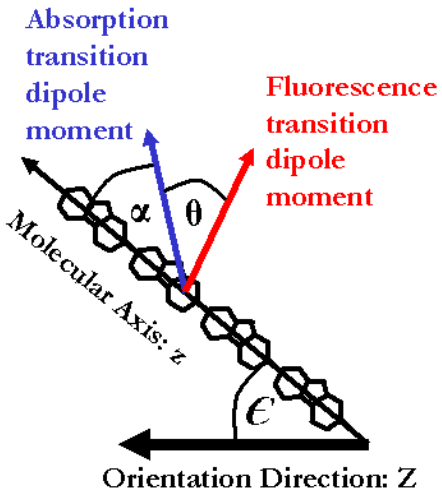

Figure 2.20: Schematic to show the molecular directions and angles between the transition dipole moments. The molecular z-axis (backbone) is at angle ε to the orientation (stretch) direction Z-axis. The blue arrow shows the absorption transition dipole moment which is at an angle α to the molecular axis: the fluorescence transition dipole moment (shown by the red arrow) is at an angle θ to the absorption transition dipole moment. These angles are used in the text to derive various theoretical relationships.

The orientation of the transition dipole moments arises from the spatial extent of the electronic state.[43] Locating and monitoring the orientations of the transition dipole moments is therefore a legitimate technique for determining the change in exciton localisation in conjugated polymers. This can be achieved through various methods of polarised spectroscopy.

2.5.5 Polarised Absorption: Linear Dichroism

As has been discussed earlier in this chapter (Section 2.3.2 on transition dipole moments), absorption is governed by the transition dipole moments. That is, only light polarised parallel to the molecule's absorption transition dipole moments will be absorbed.

When an isotropic sample is illuminated with unpolarised light, light of sufficient energy for the transition will be absorbed without a polarisation preference. However, when either the sample is oriented or the incoming light is polarised the absorption process becomes anisotropic. In the case where an oriented material is illuminated with isotropic light, light polarised parallel to the orientation of the absorption transition dipole moments is absorbed and light polarised perpendicular is transmitted. These materials act as polarisers (see Section 2.2.2). On the other hand, where an isotropic sample is illuminated with plane polarised light, only the molecules with a component of their absorption transition dipole moments parallel to the incoming polarisation will be absorbed.

In an experiment, polarised light corresponds to a light polarised within a narrow angular distribution and only a small distribution of molecules will absorb and become excited. This is called photoselection, as only those molecules are be excited and can participate in further electronic processes.[51,77]

Photoselection causes the excitation of a distribution of molecules with an angle ε to the Z-axis with a probability of $f(\varepsilon)\mathrm{d}\varepsilon$. The probability of absorption is a function of the orientation distribution and is proportional to $\cos^2\varepsilon$. The distribution of excited molecules created is symmetric about Z-axis. The number of molecules in the angle between $\varepsilon+\mathrm{d}\varepsilon$ is proportional to sin ε dε. Therefore the distribution of photoselected molecules created by plane polarised light is:[51]

$$f(\varepsilon)\mathrm{d}\varepsilon = \cos^2\varepsilon \sin\varepsilon \mathrm{d}\varepsilon \tag{2.23}$$

This is applicable only for a single photon exciting a molecule.

When both sample and light are oriented the sample again acts like a polariser, i.e. it is dichroic. When the sample and the light are parallel the absorption will be intense, but when they are orthogonal, considerably fewer will be absorbed. It is possible to investigate the orientation of the absorption transition dipole moments and therefore molecular alignment in the sample using polarised light.[21,73]

Linear Dichroism (LD) is the difference between the absorption of light polarised parallel ($A_\parallel$) and perpendicular ($A_\perp$) to the sample's orientation direction:

$$LD = A_\parallel - A_\perp \tag{2.24}$$

Individual electronic transitions have a single absorbance transition dipole moment. In a linear dichroism experiment this is observed as a constant linear dichroism value for the absorbance region.[21] Each absorption transition dipole moment will present a value of LD corresponding to its orientation in the sample. Measuring the LD can be used to locate multiple transitions in a spectrum (provided they are oriented differently to each other). The angle between the absorption transition dipole moment and the polymer backbone (α, shown in Figure 2.20) can be determined via:[21]

$$\frac{LD}{3A_{ISO}} = \frac{1}{2}(3\langle\cos^2\alpha\rangle - 1)\Phi \tag{2.25}$$

where $A_{ISO} = \frac{1}{3}(A_\parallel + 2A_\perp)$ and is the isotropic absorption. The angle, α, found through experiments, should be treated as an effective angle that represents multiple molecules. The order parameter of the system, Φ, indicates how well aligned the molecular axis is within a sample as discussed in sections 2.4.9 and 2.4.10.

If the order parameter is known from other experiments, then linear dichroism experiments and equation 2.25 can be used to estimate the absorption transition dipole moment.

2.5.6 Polarised Fluorescence: Fluorescence Anisotropy

To achieve polarised fluorescence from conjugated polymers the fluorescence transition dipole moments need to be parallel. It is often simple enough to align the molecules in a matrix (or with an electric field). Therefore, when the molecules emit, they will emit with the same polarisation.

The angular distribution of the polarisation direction will be dependent upon how well aligned the fluorescence transition dipole moments and the molecule are. If the molecules are very well oriented then the fluorescence ratio ($F_{\parallel}/F_{\perp}$) will be high and the fluorescence will be highly polarised.

In the case of an aligned film, the sample can be illuminated with unpolarised light as this will not affect the emission polarisation. This method is not particularly efficient as some of the light will not be absorbed and, therefore, wasted. It would be more efficient to illuminate this aligned system with light polarised parallel to the absorbance transition dipole moment.

When polarised light illuminates an isotropic distribution and the process of photoselection occurs (see section 2.5.5), a subset of the molecules with part of their absorbance transition dipole moment parallel to incoming light, are excited. It is from these molecules that the fluorescence can occur.

For the ideal system of rigid, immobile molecules with their absorbance transition dipole moments parallel to their emission transition dipole moments, photoselection will result in highly polarised emission. (At least as high as the incoming polarisation.)

In a more typical experiment, where the molecules are flexible and able to rotate, such as in a solution and their absorption and emission transition dipole moments are not collinear, the emission is not polarised. This is called fluorescence depolarisation.

The extent of the depolarisation can be measured with fluorescence anisotropy. Recording the difference between light emitted with the same polarisation as the incident light and that emitted in a perpendicular direction gives the fluorescence anisotropy, $\langle r \rangle$, of the system:[51,78]

$$\langle r \rangle \;=\; \frac{I_{\parallel} - I_{\perp}}{I_{\parallel} + 2I_{\perp}} \tag{2.26}$$

where $I_{alignment}$ is the intensity of the emission, and $\parallel$ and $\perp$ are the relative alignment of the excitation and emission polarisers.

The denominator of equation 2.26 arises from the total fluorescence, I_T which is the sum of the intensity in the three laboratory directions X, Y and Z.[51] The directions are shown in Figure 2.16.

$$I_T = \sum_i I_i = I_X + I_Y + I_Z \tag{2.27}$$

each $I_{direction}$ is a sum of the angular intensity components in the direction of the laboratory axis. If the Z-axis is classed as the vertical, then $I_Z = I_{\parallel}$ for vertically polarised light and $I_Y = I_X = I_{\perp}$ and so $I_T = I_{\parallel} + 2I_{\perp}$.

2.5.7 Derivation of fluorescence anisotropy

To derive the relationship between the value of fluorescence anisotropy and the angle between the absorption and emission transition dipole moments it is necessary to first consider a single, isolated molecule that neither bends nor rotates, with absorption and emission transition dipole moments that are collinear and aligned along the backbone.

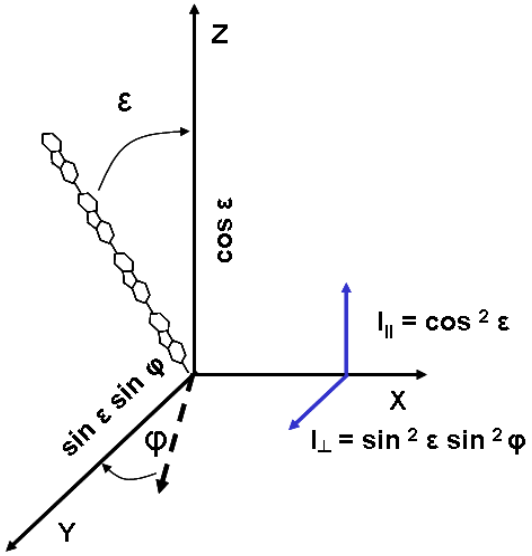

Figure 2.21: Emission intensities for a single molecule in a coordinate system. The angle ε is the angle between the polymer backbone and the Z-axis and φ between the backbone and the Y-axis. If the absorption and emission transition moments are collinear and the excitation is parallel to the Z-axis then the emission can be split into two orthogonal components (see equation 2.29). Taken and adapted from Lakowicz J. (1999) *Principles of Fluorescence Spectroscopy* p. 293

The molecules is held at an angle ε to the Z-axis and the relevant angles are shown in Figure 2.21. The excitation beam is polarised parallel to the Z-axis and the emitted light will be parallel to that absorbed. It will be comprised of two components parallel and perpendicular to the excitation polarisation.

$$I_{\parallel} = I_0 \cos^2 \varepsilon \, \mathrm{d}\varepsilon \tag{2.28}$$

$$I_{\perp} = I_0 \sin^2 \varepsilon \, \mathrm{d}\varepsilon \sin^2 \phi \tag{2.29}$$

These relations are derived for a single molecule. In a solution containing several thousand molecules, the orientation distribution function around Z-axis must be taken into account. Photoselection will preferentially excite molecules with a component of their absorption transition dipole moment parallel to the Z-axis. This means that all molecules oriented with angle ϕ to the Y-axis will be excited with equal probability. This probability depends upon the average angle ϕ takes in the XY-plane.

The average value for $\sin^2 \phi$ term across all molecules and all angles is:

$$\langle \sin^2 \phi \rangle = \frac{\int_0^{2\pi} \sin^2 \phi \; d\phi}{\int_0^{2\pi} d\phi} = \frac{1}{2} \tag{2.30}$$

Substituting equation 2.30 into equations 2.28 and 2.29 results in equations being solely in terms of ε. Many molecules are distributed about the Z-axis with a probability $f(\varepsilon)$, therefore the equations 2.28 and 2.29 have to be integrated over the angle ε to take this distribution into account. (Note: it is only necessary to integrate between 0 and 90 °.):

$$I_{\parallel} = \int_0^{\frac{\pi}{2}} f(\varepsilon)\cos^2\varepsilon \, \mathrm{d}\varepsilon = k\langle cos^2\varepsilon\rangle \tag{2.31}$$

$$I_{\perp} = \int_0^{\frac{\pi}{2}} f(\varepsilon)\sin^2\varepsilon \, \mathrm{d}\varepsilon = \frac{k}{2}\langle\sin^2\varepsilon\rangle \tag{2.32}$$

where k is a constant of the system. Substituting these relations into equation 2.26 gives the fluorescence anisotropy, $\langle r\rangle$, as a function only of the angle between the backbone and the Z-axis, ε, that is:

$$\langle r\rangle \;=\; \frac{(3\langle\cos^2\varepsilon\rangle - 1)}{2} \tag{2.33}$$

To determine the maximum fluorescence anisotropy of a real system, it is necessary to find the maximum value of $\langle\cos^2\varepsilon\rangle$. Using the distribution of photoselected molecules as in equation 2.23, the value of $\langle\cos^2\varepsilon\rangle$ for collinear absorption and emission transition dipole moments is given by:[51]

$$\langle\cos^2\varepsilon\rangle = \frac{\int_0^{\frac{\pi}{2}}\cos^2\varepsilon f(\varepsilon)\mathrm{d}\varepsilon}{\int_0^{\frac{\pi}{2}} f(\varepsilon)\mathrm{d}\varepsilon} = \frac{3}{5} \tag{2.34}$$

substituting this value into equation 2.33 gives a maximum anisotropy of 2/5 (0.40). This value is smaller than would be found for an isolated molecule.

The difference in orientation between the absorption and emission transition dipole moments, θ, (as shown in Figure 2.20) results in a further loss of anisotropy. This has a similar relationship between the angle and the fluoresecence anisotropy as in equation 2.33. The relationship needs to take the photoselection distribution into account (2/5) and thus the equation for fluorescence anisotropy for non-collinear transition dipole moments becomes:[51]

$$\langle r\rangle \;=\; \left(\frac{(3\langle\cos^2\varepsilon\rangle - 1)}{2}\right)\left(\frac{(3\langle\cos^2\theta\rangle - 1)}{2}\right) \tag{2.35}$$

$$\;=\; \frac{2}{5}\left(\frac{(3\langle\cos^2\theta\rangle - 1)}{2}\right) \tag{2.36}$$

This equation gives the average angular displacement undergone by all the transition dipoles for an isotropic ensemble. Thus the anisotropy at a finite time after excitation can have a value between $-0.20 \leq \langle r\rangle \leq 0.40$.[79] Values over 0.40 are only possible for multi-photon excitation processes.[51]

Zero anisotropy: The magic angle

A value of zero for the anisotropy correlates to an average angle of 54.7°. This is the magic angle and represents an isotropic or randomly oriented distribution. The magic angle, β, occurs when:

$$I_{\parallel} = I_{\perp} \tag{2.37}$$

from equation 2.26. Substituting in equations 2.28 and 2.29 gives:

$$I_0 \ \cos^2 \beta = I_0 \ \frac{\sin^2 \beta}{2} \tag{2.38}$$

This is only true when $\beta = 54.7°$. Since the two orthogonal components are equal, the emission distribution is isotropic. The magic angle is used as a setting for polarisers. By illuminating a system with light polarised at 54.7° it is possible to simulate illumination with unpolarised light.

Non-zero anisotropy

Anisotropy values between 0.40 and zero represent angles between 0° and 54.7° Lower anisotropy values correspond to angles greater than 54.7°, the magic angle, and 90°. A value of −0.2 represents a system where the absorption and emission dipoles are orthogonal.

A small negative angle i.e. close to, but not equal to, zero cannot necessarily be trusted to give a true estimate of the angle between absorption and emission transition dipole moments. Instead a small negative value often represents a randomly oriented distribution with a large standard error on the measurement.

Fluorescence anisotropy can be used to investigate isotropic dilute solutions and films. In films, a distribution that is aligned in plane of the film gives a value of 0.10 because all the transition dipole moments are parallel to the film surface.[73]

The anisotropy can only have the maximum value of 0.40 when the emission transition dipole moment is aligned with the excitation polarisation. This means that the emission must originate from exactly the same state that was originally excited. The maximum value is rarely seen because physical motions and inter- and intra-chain processes can change the orientation of the transition dipole moments before emission. In solutions rotation can be stopped using high viscosity solvents. Processes such as excitation migration and conformational motion of a molecule can result in a new spectroscopic unit which has a differently oriented transition dipole moment. Both processes can result in a large fluorescence anisotropy loss.

Fluorescence anisotropy loss has been used to evaluate the angular separation of absorption and emission transition dipole moments in this work.

2.5.8 Fluorescence anisotropy loss processes

Fluorescence anisotropy loss can arise from many processes; these are introduced below.

Rotation

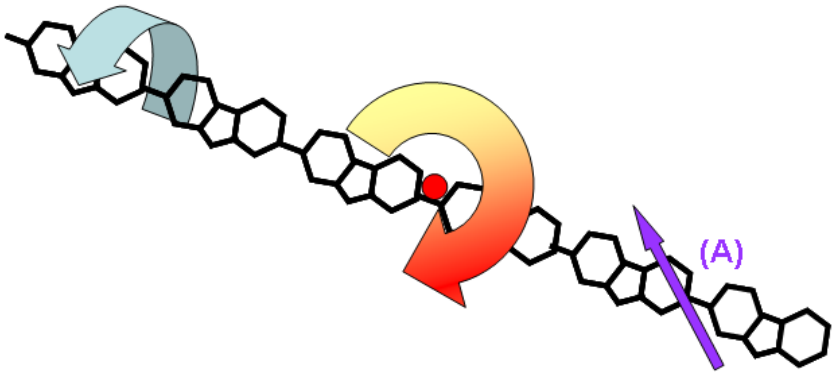

Figure 2.22: Schematic to show how rotation of molecule changes the orientation of the transition dipole moments. The diagram shows two ways that the molecule can rotate: around an axis through the backbone (blue arrow) and around an axis that passes through the centre of the molecule (red arrow, axis indicated by a red circle). If a chromophore is constrained to remain at point (A) and the molecule rotates about its centre, the orientation of the transition dipole moment will also rotate. If the molecule rotates (spins) round its backbone, the orientation of the transition dipole will also change.

In a mobile (free to rotate) molecule where the absorbance transition dipole moment and the emission transition dipole moment are collinear, the anisotropy loss is most likely due to rotation. The whole molecule can rotate about its centre, as shown in Figure 2.22. As the molecule rotates, so too does the location of the emission transition dipole moment. This will be recorded as an anisotropy loss. It is possible to calculate the rate of rotation from the angular change (measured via fluorescence anisotropy) and the fluorescence lifetime. This is possible because the fluorescence anisotropy can only be recorded during the fluorescence lifetime.

It follows therefore that if the rotation time is very much greater than the fluorescence lifetime, the molecule will not rotate appreciably and the anisotropy value will be high. (Close to, if not identical to, the natural anisotropy of the molecule.)

Correspondingly, if the rotation time is much less than the fluorescence lifetime, then the molecule is able to rotate considerably, then all of the polarisation will be lost and fluorescence anisotropy will be zero. Rotation rate, or rotational correlation time, Θ, can be observed through time resolved decays and the anisotropy as a function of time for a system that rotates is:[80]

$$\langle r(t) \rangle = r_0 e^{-t/\Theta}. \tag{2.39}$$

Energy Transfer

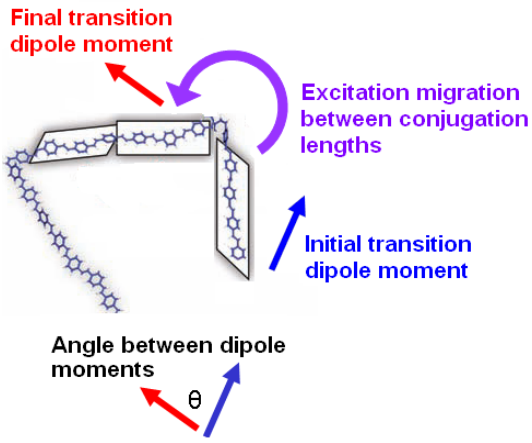

Figure 2.23: A schematic to show how the process of intra-chain excitation migration depolarises the fluorescence. The exciton transfers from an original excited state that has an emission transition dipole moment parallel to absorbance transition dipole moment to a final excited state which has an emission transition dipole moment that is at an angle θ from the absorbance transition dipole moment. This causes a depolarisation of the fluorescence. The excitation migration process can only occur when there is sufficient additional excitation energy. The schematic of the molecule was taken from Collini, E *et al.* Science (2009) and then adapted.

In an immobile molecule, a cause of fluorescence anisotropy loss is energy transfer from the initially excited state to another site of lower energy, which can be on another chain or on the same molecule (excitation migration). Figure 2.23 shows how these processes occur. If the absorbance transition dipole moment is not collinear with the emission transition dipole moment of the final state, then the polarisation is lost by energy transfer. Figure 2.23 shows fluorescence depolarisation due to intra-chain excitation migration. If excitation migration does not occur then the excitation will remain on the original site and the absorbance transition dipole moment and emission transition dipole moment will be parallel and no anisotropy will be lost.

The excitation migration process requires additional energy from the absorption process; without it, the excitation is constrained to the initially excited state. Therefore, this anisotropy loss process can be studied by varying the excitation energy incident on the molecules (via site-selective spectroscopy).

2.5.9 Conformational twisting

Some molecules can undergo conformational relaxation. That is, the parts of the molecule can rotate, twist or bend to achieve a lower energy conformation. In the case where adjacent segments can twist relative to each other, for example the adjacent phenylene rings in a conjugated polymer, this conformational twisting can reduce the fluorescence anisotropy values.[81,82] The twisting between rings can planarise a molecule which can extend the conjugation length by a small number of bonds. This results in an excited state that is in a different conformation to the excited state.

The change in the conformation between the ground and excited state may be accompanied by a change in transition dipole orientation. For example, distortions in the ground state may produce an off-axis absorption transition dipole moment. When the state is extended over more bonds in the excited state, the effect of the distortions is lessened and the emission transition dipole moment is more aligned with the aforementioned axis and not parallel to the absorption transition dipole. The fluorescence anisotropy will therefore be reduced.

Aggregation and donor-acceptor transfer

When molecules bond together to form dimers (small aggregates), or large macromolecules, the emission transition dipole moments of the individual molecules are randomly oriented within the aggregate. When the molecules are in such close proximity, the excitation migration transfer process can occur very much more easily and it is more probable that the lowest energy state can be accessed. This state will have a differently oriented transition dipole moment and the polarisation will be lost. Hence aggregation reduces fluorescence anisotropy.

Reabsorption and scattering

If the concentration of a material, for example, in a solution, is high, the probability that an emitted photon is reabsorbed is similarly high. A molecule can be excited if it has a component of its absorbance transition dipole moment parallel to the incoming light. If the emitted light is at an angle to the absorbance transition dipole moment then the emission can excite a second molecule which will emit at a further angle from the original polarisation.

As an extreme example, consider a situation where the concentration is high and the exciting light is polarised vertically. The first molecule to be excited emits with polarisation at an angle θ from the vertical. This emission excites another molecule, which emits up to 2θ from the vertical. Over the whole solution, multiple reabsorption processes will occur and there will be no preferential emission polarisation angle that reaches the detector and hence all the anisotropy will be lost.

Scattering and reabsorption processes are inherently linked to the fluorescence and will therefore take place on the same timescale as the fluorescence lifetime of the molecule. These processes can occur in any solution. However, it can be reduced to a very small proportion by keeping the concentration low. In the experiments carried out here, the absorption was kept below 0.1 OD. Scattered polarised light from the molecules or any of the components in the optical system will also affect the recorded anisotropy. However this is usually very low for dilute solutions.[51] Working with low concentration solutions allows fluorescence anisotropy measurements to be taken that are not masked by the presence of reabsorpton and scattering.

Alignment of polarisers

The fluorescence anisotropy values can be only valid if the polarisers in the optical set-up are aligned. This can be checked by testing known emission rotators, e.g. perylene or coumarin, into a steady-state system.

2.5.10 Fluorescence kinetics

The excited state does not always relax immediately; indeed it may exist for up to several nanoseconds. This is enough time for many intra- and inter-chain processes to occur. The excited state does not relax periodically, it relaxes randomly. A way to gauge the number of molecules in an excited state is to observe the fluorescence intensity decay with time:[51,77]

$$I(t) = I_0 \exp(-t/\tau) \tag{2.40}$$

where I_0 is the initial emission intensity, *I(t)* is the emission intensity after time t and τ is the natural lifetime of the state. τ incorporates a great deal of information about the excited state and how it relaxes because it is the inverse of the sum of all the possible decay rates both radiative, k_r and non-radiative, k_{nr}:

$$\tau = \left(\sum k_r + \sum k_{nr} \right)^{-1} \tag{2.41}$$

It is easier to measure the radiative decay than the non-radiative decay but it is possible to gauge the non-radiative decay rate through the efficiency of the radiative decay. The photoluminescence quantum yield, Φ_f, is the ratio of emission to absorption. This is the same as the ratio of the rate of emitted photons to the rate of the absorbed photons, k_{abs}:

$$\Phi_f = \frac{k_r}{k_{abs}} \tag{2.42}$$

In a closed system, with a finite number of electrons, when equilibrium is reached the rate of absorption is equal to the rate of relaxation by any route,

$$k_{abs} = \sum k_r + \sum k_{nr} \tag{2.43}$$

So the quantum yield can be written as:

$$\Phi_f = \frac{k_r}{\sum k_r + \sum k_{nr}} \tag{2.44}$$

The fluorescence lifetime, τ_f, is inversely proportional to the fluorescence decay rate $k_f = 1/\tau_f$. If the only emission observed is the fluorescence, then $k_r = k_f = 1/\tau_f$. The photoluminescence quantum yield can be simply written as a ratio:

$$\Phi_f = \frac{\tau}{\tau_f} \tag{2.45}$$

Importantly, the intensity can now be written as a series of exponential terms involving many fluorescence lifetimes, each representing a different radiative decay route:

$$I(t) = \sum_{i=1}^{n} I_i \exp(-t/\tau_{fi}) \tag{2.46}$$

This is the key equation is used in analyzing fluorescence decays.

The kinetics of fluorescence anisotropy

Since the fluorescence is dependent on time, so too is the fluorescence anisotropy, and this can reveal further information about a system.[51,80] Equation 2.26 can be modified to involve a time dependence, giving:

$$\langle r(t)\rangle \;=\; \frac{I_{\parallel}(t) - I_{\perp}(t)}{I_{\parallel}(t) + 2I_{\perp}(t)} \tag{2.47}$$

For a single fluorescence lifetime and a single anisotropy loss process e.g. rotation, the time resolved fluorescence anisotropy can be written as:

$$\langle r(t)\rangle = r_0 \exp(-t/\tau_r) \tag{2.48}$$

where r_0 is the anisotropy immediately after excitation determined by the natural anisotropy of the molecule and τ_r is the rotation lifetime. In this special case it is easy to see that if $I_{\parallel}(t)$ and $I_{\perp}(t)$ can be recorded then the rotational lifetime can be determined by fitting an exponential curve to the data. The analysis becomes more complicated, but not impossible, for systems with multiple fluorescence lifetimes and many anisotropy decay channels, such as conjugated polymers. Chapter 7 describes the method, measurements and analysis procedure for these complex systems.

2.6 Introduction to the conjugated polymers studied

This section provides an insight into the previously published properties of the polymers used in this investigation. Two types of polymers that emit blue light were used. The first set of polymers, polyfluorenes, are flexible whereas the second set, ladder-type poly(para-phenylene)s are completely rigid.

2.6.1 Polyfluorenes (PF2/6 and PFO)

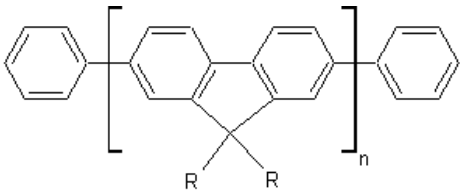

Figure 2.24: Basic repeat unit of a substituted polyfluorene. Substituents, side groups, can be added at the "9" position, marked R.

Poly(9,9- dialkylfluorene) contains the necessary conjugated backbone and energy structure to give vibrant and more importantly highly efficient blue fluorescence. The molecule can be easily synthesised by two different routes, giving a variety of molecular weights, and with innovative substituents, or co-polymerisations, a wide range of emissive colour can be achieved.[83,84] There has been a great deal of work done on developing, characterising and understanding the polyfluorenes family.[85]

The basic structure of the PF family is shown in Figure 2.24. It has two phenyl rings connected with a methine bridge with a substituent (side group) at the "9" position marked R in the figure. Since the synthesis of the first soluble PF in 1993,[86] different synthesis routes

(either Suzuki[87] or Yamamoto couplings[88]) have been used to tailor both the substituents or the molecular weight.[89] PFs are considered to be semi rigid-rod polymers and this is an adequate description for understanding some of the physical processes, e.g. revolution in a solvent.[90] However, rigid tends to mean inflexible and rod implies straight: neither of which are explicitly true for PFs. Due to the single bond between the monomer units, the each unit can undergo some degree of torsional motion. The polymer has been investigated via X-ray diffraction and found to be twisted, meaning torsional motion would planarise the molecule.[91] The bond angles between the monomer units is approximately 20 °, resulting in a backbone that is slightly buckled. For this reason they are often referred to as wormlike polymers.[85]

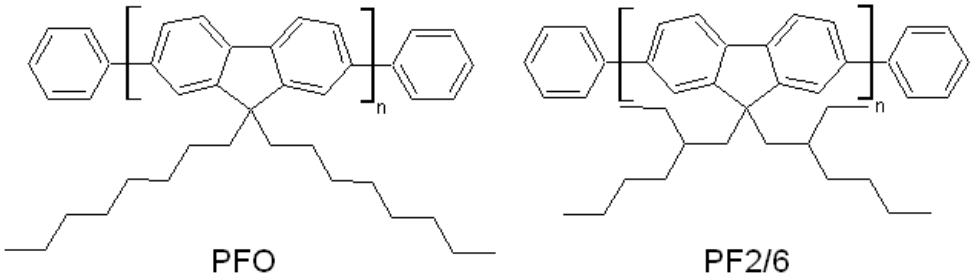

Figure 2.25: Basic repeat unit and end groups of the two polyfluorenes used in this work: poly[9,9-di(octyl)fluorene] and Poly[9,9-di(ethylhexyl)fluorene].

Different substituents added to the "9" position change the solubility, phase and morphology of the polymer in solution or film.[85] For example, the two PFs used in this work: poly[9,9-di(octyl)fluorene] (PFO, sometimes called PF8) and poly[9,9-di(ethylhexyl)fluorene] (PF2/6), both shown in Figure 2.25, have different side chains and different photophysical responses. PFO has long side groups, 8 carbon atoms in a single chain, which are normally at a large angle to the backbone. This is known as the α-phase and produces blue emission. However, by lowering the temperature[92,93] or using poor solvents[94–96] the side chains are forced into a new alignment.[e] The side chains are able to interact and planarise the backbone. This is known as the β-phase and has a characteristic low energy absorption and emission spectra that is dominated by vibronic shoulders. The β-phase quenches the emission from the normal phase and lowers the quantum yield.[97]

PF2/6 also has a side group of 8 carbon atoms, but the configuration of the side group is such that it does not interact with the backbone.[98] The structure does not allow the chain to planarise and PF2/6 only exists in the α-phase. The absorption and emission spectra for both PFs in their α-phase are very similar.[99]

Long chain PFs support several different conjugation lengths leading to a large conjugation length distribution.[100] This partially broadens the absorption spectrum such that its vibronic replicas cannot be resolved. This broad spectra makes site-selective spectroscopy particularly useful for investigating these polymers. Fytas *et al.* have hypothesised that the average conjugation length supported on a chain is 12 units long.[90]

[e] Poor solvents refer to ones in which the polymer is almost insoluble.

The emission spectrum of PFs is dominated by vibronic replicas of the main transition (0-0 line shown in Figure 2.19). These polymers show a relatively large Stokes' shift which is typically explained as a result of torsional motion in the backbone. However, the quantum yields are very high (∼80%) for both PFO and PF2/6 suggesting that there are few non-radiative relaxations.[101]

Like many polymers, PFs are subject to photodegredation, specifically, photo-oxidation which produces a carbonyl group forms at the "9" position in place of the side group. During the polymer synthesis, incomplete alkylation creates mono-alkylated sites that are prone to oxidation.[102] They can also be created by overheating, especially in air or in unsealed devices[103,104] and it is important to store samples in a cool, dark, dry place. These sites are called keto defects and act as a low energy trap for excitations and result in a yellow emission.[105–107] There is also an accompanying reduction in the quantum yield.[108] In films and concentrated solutions, PFs sometimes form small aggregates that lower the energy of the emission which produces green emission.[109]

PFs are thermotropic liquid crystals, which means that above their melt temperature (between $100-170\,^{\circ}\mathrm{C}$) the polymer chains can be forced into an alignment. This typically comes from a suitably aligned substrate, like a rubbed polyimide layer.[110–113] This technique has been used successfully to get dichroic ratios of up to 25, though due to its more compact side chains PF2/6 shows a higher dichroic ratio than PFO when aligned.[109,111] Films aligned in this way have been utilised in Durham University to discover the anisotropic refractive indices[114] and the helical packing structure of PF2/6.[72,96,115,116] PFO has also been aligned in stretched polyethylene, a technique used to good effect within this work.[117]

2.6.2 Ladder-type poly(*para*-phenylene)s (MeLPPP and 2,6-NLP)

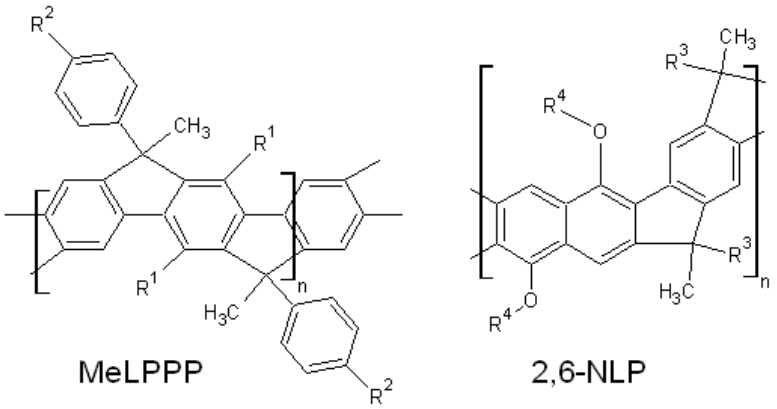

Figure 2.26: The molecular structure of the two ladder-type polymers used (MeLPPP and 2,6-NLP). $\mathbf{R^1}$ and $\mathbf{R^2}$ are alkyl groups. $\mathbf{R^3}$=1,4-$\mathbf{C_6H_4}$-$\mathbf{C_{10}H_{21}}$ and $\mathbf{R^4}$=$\mathbf{C_8H_{17}}$

Ladder-type poly (*para*-phenylenes) (LPPPs) are another set of highly efficient blue light emitters that can be used in LEDs.[67,118–120] Their emission spectra are similar to that of PFs but their structure is different. This allows a direct comparison between the two sets of polymers and the further understanding of photophysics based on structural properties.

LPPPs have a methine bridge between adjoining (neighbouring) phenyl rings[121] as shown in Figure 2.26 giving them a "ladder"-like appearance. The bridge means that adjacent phenylene rings cannot under go the conformational relaxation that PFO and PF2/6 suffer from.[122,123] They are a planar rigid-rod polymer.

The absorption and fluorescence spectra are mirror images of each other and dominated by a series of very well defined vibronic shoulders energetically separated by the inter-ring C-C stretching vibrational mode. The Stokes' shift is very small (∼4 nm) and the photoluminescence quantum yield is very high (∼90 %).[57,120,124] These are a direct consequence of the rigid backbone which limits the number of molecular geometries available to the ground and excited states.[125] The spectra are inhomogeneously broadened by the conjugation length distribution which can be accessed through site-selective spectroscopy. Since the backbone is already planarised, it does not form a phase equivalent to the α-phase of the PFs. Instead LPPPs are more like the PF β-phase and the absorption and emission spectra of LPPPs and PF β-phase are very similar.

Two variants of the ladder-type polymers were used in this work. The monomer structure of methyl-substituted-LPPP (MeLPPP),[121,126] and the newly synthesised poly(naphthylene - phenylene) (2,6-NLP),[127] are shown in Figure 2.26. MeLPPP has a LPPP structure with an additional methyl side group. 2,6-NLP is slightly different as it has a naphthylene unit in the conjugated backbone which further constricts any torsional motion. MeLPPP has been investigated for nearly fifteen years whereas it is believed 2,6-NLP has not been investigated prior to this work.

During the synthesis of MeLPPP to high molecular weights, it is believed that the chain does not polymerise in a straight line. Instead, after a given length, the polymer grows at an angle to the chain, estimated to be at 60 ° to the original chain.[29–31] This results in a lightning bolt shaped polymer and it is believed that separate spectroscopic units (chromophores) can exist on each part of the chain.[67] This is shown in Figure 2.12. 2,6-NLP is free from these branches but there is a small bond angle between the phenyl ring and the naphthylene rings which produces a wavelike polymer. This wave-pattern is not thought to be big enough to break the conjugation. MeLPPP is hypothesised to support conjugation units with an average length between 7 and 12 monomer units.[128–130]

It has been reported that there is a very low concentration of keto defects at the methine bridge in MeLPPP[131] and the polymer has always been considered to be unaffected by changes in temperature.[132] But in films of MeLPPP, there is a broad yellow-green (low energy) emission band that is conspicuously absent in solutions.[45,119,131,133–136] This has led to the assumption that MeLPPP forms aggregates in films.[131] Very recent work has shown that thermal cycling of the polymer can induce this band, suggesting the polymer is susceptible to oxidation defects.[105,137] However, single molecule spectroscopy has not shown inter-chain defects[122] and the low energy emission can be eliminated by doping MeLPPP into a suitable host matrix, thus verifying the aggregation theory.

Studies of the electronic energy transfer in MeLPPP has suggested that singlet exciton transfer is enhanced by the planarised backbone,[64,138–141] and using it in devices would provide a fast response in LEDs, lasers and solar cells.[142–145] MeLPPP has one of the highest photoluminescence quantum yields in film of 30 - 40%. In laboratory-made devices it has been found to have an electroluminescence quantum yield of ∼60%[146] which promises highly efficient LEDs in the future.

2.6.3 Summary

The polymers investigated in this work have been chosen because of their potential to be used as the active medium in light emitting devices. Indeed polyfluorenes have recently been used in to make LEDs,[83,84,147] including highly polarised LEDs.[148,149] Investigating the photophysics of the polymers and understanding the electronic and physical behaviour of the polymers in isolation and in polymer blends is of interest to researchers and device manufacturers. By comparing the results from a flexible polymer with those from a perfectly rigid polymer, an interpretation of the photophysics in the context of polymer structure and conformation can be made.

Chapter 3

Experimental Details

3.1 Introduction

This chapter presents details of the experimental techniques and methods used to investigate the photophysics of the conjugated polymers. A list of the polymers used, from where they were obtained and a detailed description of the methods used to make solutions, spun films and aligned films is presented. An account is then given of the main spectroscopic techniques used. Finally, a detailed set of instructions for future users of the equipment available in the OEM group at Durham University is provided.

3.2 The properties of the conjugated polymers used

As noted in Chapter 2, the main polymers studied in this work were two representatives of two different classes. The results from flexible Polyfluorene derivatives poly[9,9-di(ethylhexyl)fluorene] (PF2/6) and an oligomer of (9,9-dioctylfluorene) (PFO) were compared with the rigid ladder–type poly (*para*-phenylene) (-LPPP) derivatives methyl-substituted-LPPP (MeLPPP) and naphthylene-LPPP (2,6-NLP). The monomer unit structures of all four polymers can be found in Figure 2.25 and 2.26. In addition to the four main polymers, a short spectroscopic study on the effect of the PF2/6 chain length was undertaken. Two short chain polymers (or oligomers) of PF2/6, PF2/6$_{N=20}$ and PF2/6$_{N=10}$ were used for this study. N refers to the number of repeat units in the oligomer.

Oligomer Name	Abbreviation	Chain Length	Polydispersity
Poly[9,9-di(ethylhexyl)fluorene]	PF2/6	Long chain ($\sim$ 60)	1.80
Poly[9,9-di(ethylhexyl)fluorene]	PF2/6$_{N=20}$	$\sim$ 20	1.70
Poly[9,9-di(ethylhexyl)fluorene]	PF2/6$_{N=10}$	$\sim$ 10	1.65
Poly[9,9-dioctylfluorene]	PFO$_{N=3}$	$\sim$ 3	1.00
Methyl-substituted-LPPP	MeLPPP	Long chain ($\sim$ 60)	1.3
Poly(naphthylene-phenylene)	2,6-NLP	$\sim$ 21	1.7

Table 3.1: Table of polymer properties used in this study including name, chain lengths (number of monomer units) and polydispersities, P, (distribution of chain lengths) of the polymers used.

Table 3.1 contains information on the chain structures of all the compounds used in this study. It includes the abbreviations used throughout the rest of this thesis, the approximate chain length (number of monomer units) of the polymer chains used and the polydispersity (see section 2.3.8). The polydispersity is a measure of the distribution of the chain lengths around a mean value. A value of one indicates that all the chains are the same length. This is typically the case for short chain oligomers. A higher value indicates that there is a range of chain lengths. The polydispersity information was provided by the synthetic chemists who made the polymers and were obtained from gel permeation chromatography.[31]

Five of the materials used in this work were provided by Professor U. Scherf from the University of Wüppertal, Germany, whose group synthesised and purified them. The oligomer, $PFO_{N=3}$), was donated by Dr M. Tavasli from Durham University, UK, who performed the synthesis and purification.

The synthesis and purification technique of PF2/6 and two of its oligomers $PF2/6_{N=20}$, $PF2/6_{N=10}$ can be found in work by Fukuda *et al.*[86]and Grell *et al.*[98] The three-unit oligomer of PFO ($PFO_{N=3}$) was synthesised directly via Suzuki Coupling[86,87] and is monodisperse (i.e. polydispersity = 1). MeLPPP was synthesised and purified by a method first described by Scherf *et al.*[121,126] Whilst 2,6-NLP was created by a novel microwave assisted synthesis by Nehls *et al.*[127]

Sample preparation was carried out by the author as part of this thesis work, but no further synthesis or purification of the polymers was carried out after they had been received.

3.3 Sample preparation

3.3.1 Solutions

Dilute solutions of the polymers were prepared in the high purity ($< 99\%$) solvents methylcyclohexane (MCH) and Toluene (both purchased from Romil). The concentration of the solution is stated in the relevant chapters and never fell below 3 mg/L ($\sim 2 \times 10^{-4}\%$ weight for weight). It was necessary to use solutions with a maximum absorption optical density below 0.1 to avoid reabsorption of the emission by the sample and thus complicating the spectra. This had the benefit of increasing the chain separation thus limiting possible aggregation and inter-chain energy transfer effects as well. In all cases the solutions were mixed with magnetic followers, stirring for several hours to ensure the mixture was homogeneous.

Solutions were held in 10 mm quartz cuvettes which had been thoroughly cleaned before use. Cuvettes were cleaned by filling them with a dilute nitric acid solution (4 parts water to 1 part acid) and leaving them for approximately 12 hours before rinsing with water, acetone and isopropanol. Finally, the cuvettes were dried with nitrogen. This cleaning process was employed to remove any residual material (e.g. grease, another polymer, organic solvent) before use.

3.3.2 Spun cast films

One method to make a polymer film with a uniform thickness is to spin cast a solution onto a clean disc of fused silica or optical grade glass with 10 mm diameter. The substrates were cleaned thoroughly before use using a similar technique to that described above for the cuvettes. Initially, they were left in diluted nitric acid for at least 8 hours, then they were rinsed in de-ionised water before being put into a sonication bath first of acetone and then of isopropanol. The substrates were then dried in a stream of nitrogen and handled with clean tweezers. The film thicknesses were approximately 100 μm.

Solutions with concentration of 10 mg/mL of the polymers in toluene were made and allowed to stir with magnetic followers for at least 12 hours. In most cases, the polymer dissolved with simple stirring. Occasionally, due to the low laboratory temperature, it was necessary to heat the solutions to $\sim 30\,^{\circ}$C to dissolve any residual solid.

100 μL of the solution were drop cast onto the disc which was spun at 2500 rpm for 60 seconds. Previous experience had shown there was no need to dry them further.[150] The films were used almost immediately or stored in a cool, dark, dry cupboard until they were required.

3.3.3 Aligned films

To be able to understand the photophysics in relation to the orientation of the polymer backbone it is necessary to locate the direction of the polymer chain. Hence, the need for aligning all the polymer chains in one direction within the sample. Clearly, it is significantly easier to align chains in a solid film rather than in a solution because the random motions will destroy the uniaxial directionality.

It is possible to align PFO and PF2/6 by casting a film (as described above) on to an aligned substrate (typically rubbed polyimide on glass).[141,151,152] By heating the polymer above its melting point it is possible to force the backbone to epitaxially align with the grooves in the rubbed polyimide layer. It was not possible to use the same technique to align the ladder-type polymers (LPPP) due to their high melting point. An attempt to measure the melting point was investigated by differential scanning calorimetry (DSC) with the assistance of Professor Marder's group at the Department of Chemistry at Durham University. The polymer was not observed to melt despite being elevated to temperatures of $\sim 200\,^{\circ}$C. It was therefore necessary to develop a method to align this polymer.

The technique that was used was a successful adaption of that outlined by Hagler *et al.*[55] for aligning guest polymers in stretched polyethylene (PE) host . A solution with a concentration 8 mg/mL of spectrophotometric grade PE and fresh o-xylene (<97%) (both purchased from Aldrich) was heated to approximately 120 °C whilst being stirred vigorously with a magnetic follower. Heating to this temperature also served to boil off residual water within the solution. Any water present in the solution causes the resulting films to become very brittle with air pockets (bubbles). When the PE had dissolved in the o-xylene the temperature was reduced to 80 - 90 °C and a warmed solution of the conjugated polymer and o-xylene was then added. The concentration of conjugated polymer to PE was varied between 0.25 % and 15.00 % depending on the experimental requirements. The solution was stirred for approximately 10 minutes before it was poured out into clean, ice-chilled Petri dishes. An example of the resulting films is shown in Figure 3.1.

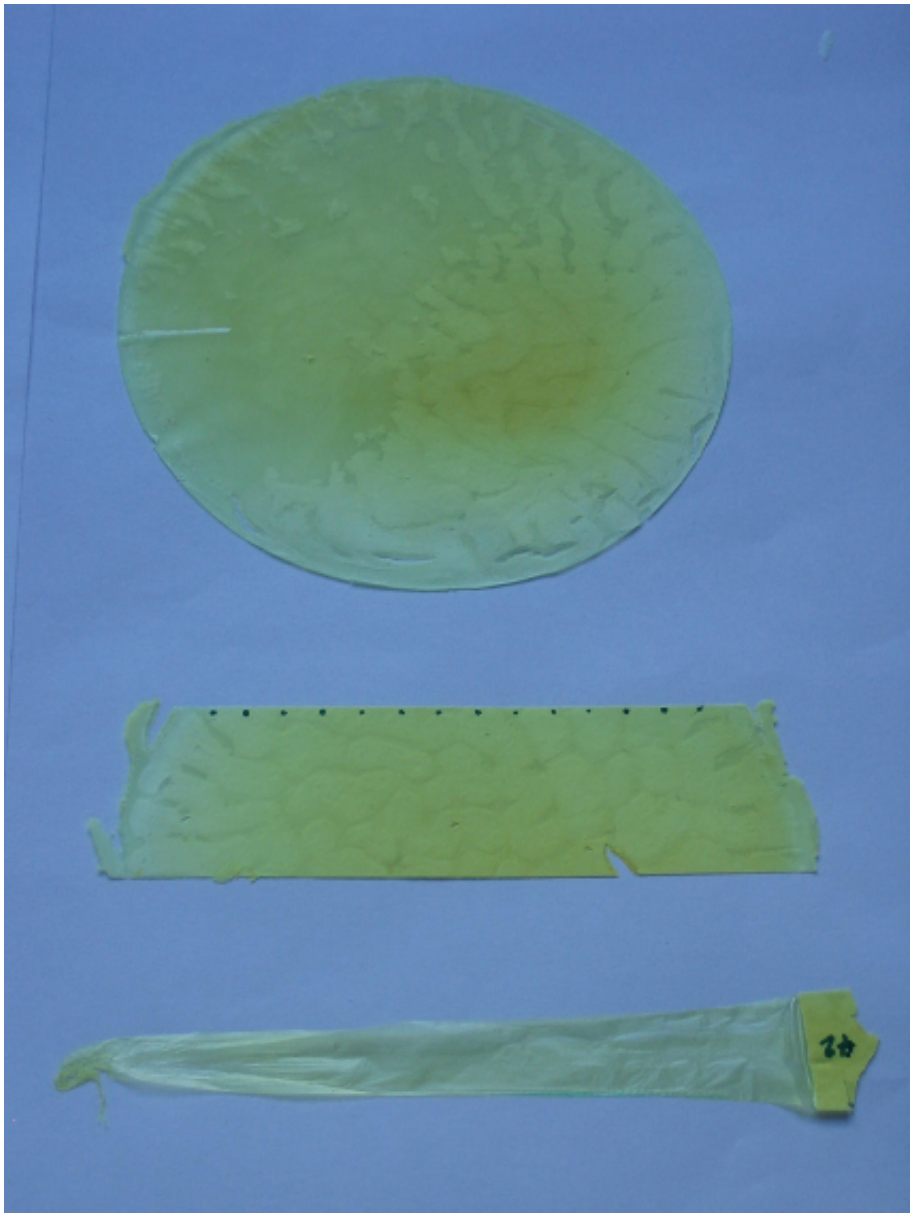

Figure 3.1: A photograph of three polyethylene films containing 2,6-NLP. The figure shows three stages of the sample preparation. The top image shows a film removed from a Petri dish after cooling. The middle image shows a strip of the film cut to a width of 1 – 2 cm and marked with permanent pen at 5 mm intervals, in preparation for the stretching procedure. The bottom image shows a film that has been stretched 28 times its original length.

After cooling and drying, the resulting films were then sliced into strips 1 - 2 cm wide and up to the diameter of the dish in length. They were then marked at 5 mm intervals with a permanent pen. An example of these films is shown in the photograph in Figure 3.1.

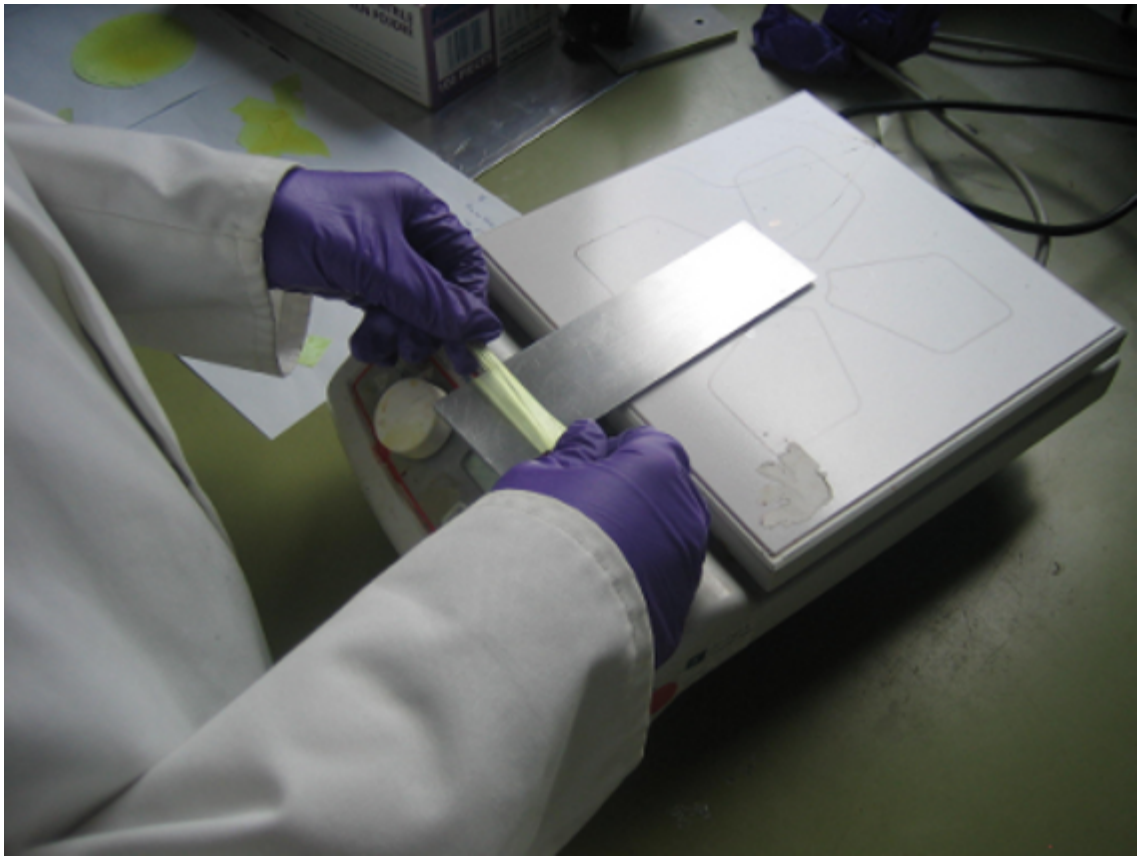

Figure 3.2: Photograph to show the experimental arrangement required to stretch a polyethylene host. A strip of polyethylene film is held over a heated plate. Once it becomes warm the two ends of the film are drawn apart. This method allows the film to be stretched up to 40 times its original length.

The films were held over a clean metal plate resting on a hot-plate heated to a temperature of approximately 110 °C (as shown in Figure 3.2). The warmed films were slowly stretched by hand. Once stretched, the films were remeasured and stretch ratios of 30 - 40 times the original length were frequently obtained. The films were then mounted on clean glass microscope slides. This particular method was first published by the author in 2006.[75]

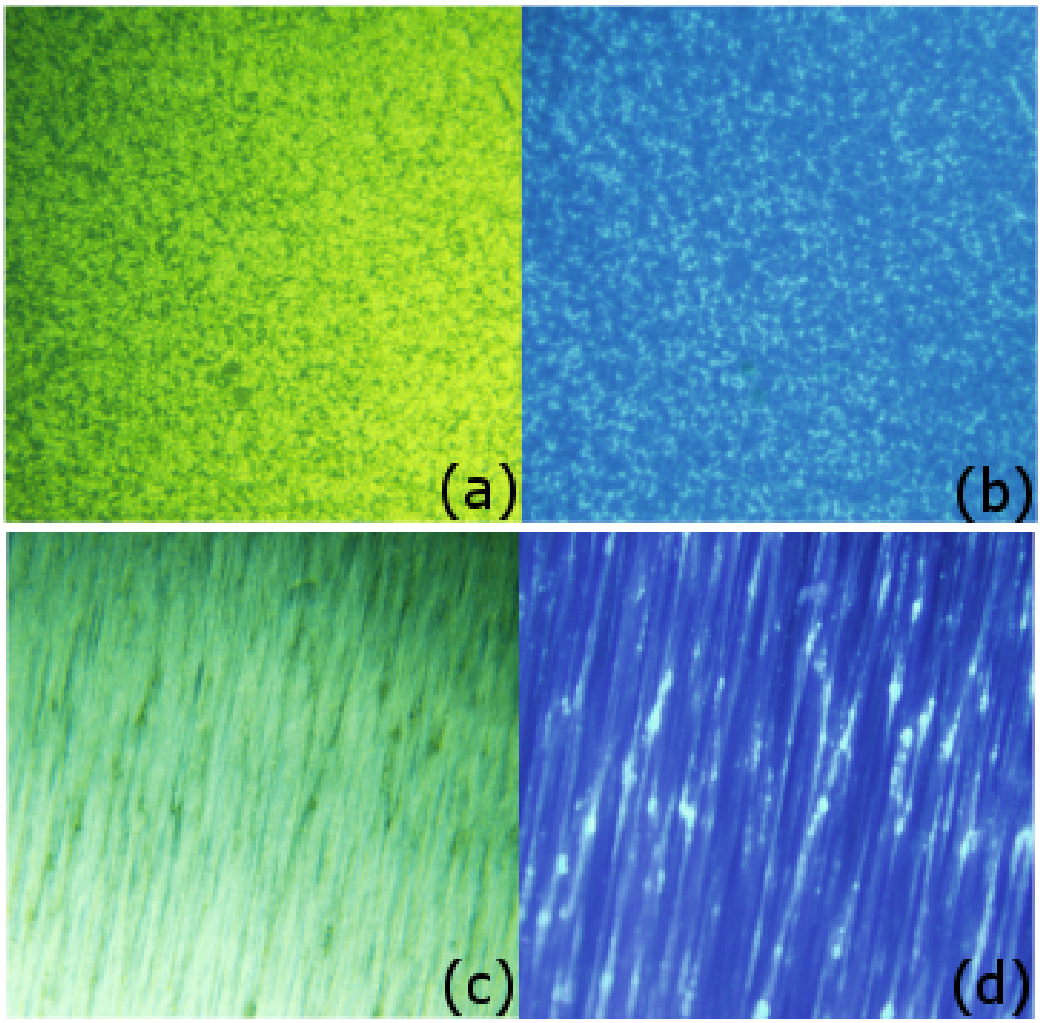

Figure 3.3: Ordinary (a) and fluorescence (b) microscope images of 2,6-NLP in an unaligned polyethylene film. Ordinary (c) and fluorescence (d) microscope images of 2,6-NLP in a stretch-aligned polyethylene film. (Stretched 34 times). The images demonstrate that stretching the film results in alignment of the 2,6-NLP. All the fluorescence microscopy images were taken with an Olympus BX51M transmitted and reflected light microscope for epi-fluorescence illumination with the assistance of Dr Carmen Morán at the University of Coimbra, Portugal.

Fluorescence microscope images were taken of the stretched films at University of Coimbra, Portugal, during a visit by the author. An Olympus BX51M transmitted and reflected light microscope in epifluorescence mode (excitation and detection from above the film) and filter set types U-MNU2 (360 nm - 370 nm excitation band width and 400 nm dichroic mirror) was used. This filter set allowed emission of wavelength greater than 405 nm to be observed. The images from early films are shown in Figure 3.3. Figure 3.3 (c) shows the film alignment and Figure 3.3 (d) shows that the emission comes from areas of the films that have been oriented.

3.4 Experimental equipment

3.4.1 Spectrometers

Simple absorption and emission spectra were taken on commercially available equipment. By placing polarisers into the optical path of these machines, linear dichroism and fluorescence anisotropy measurements could be taken. A linear dichroism spectrometer was also designed and built. These are described below.

3.4.2 Perkin Elmer Lambda 19 spectrophotometer

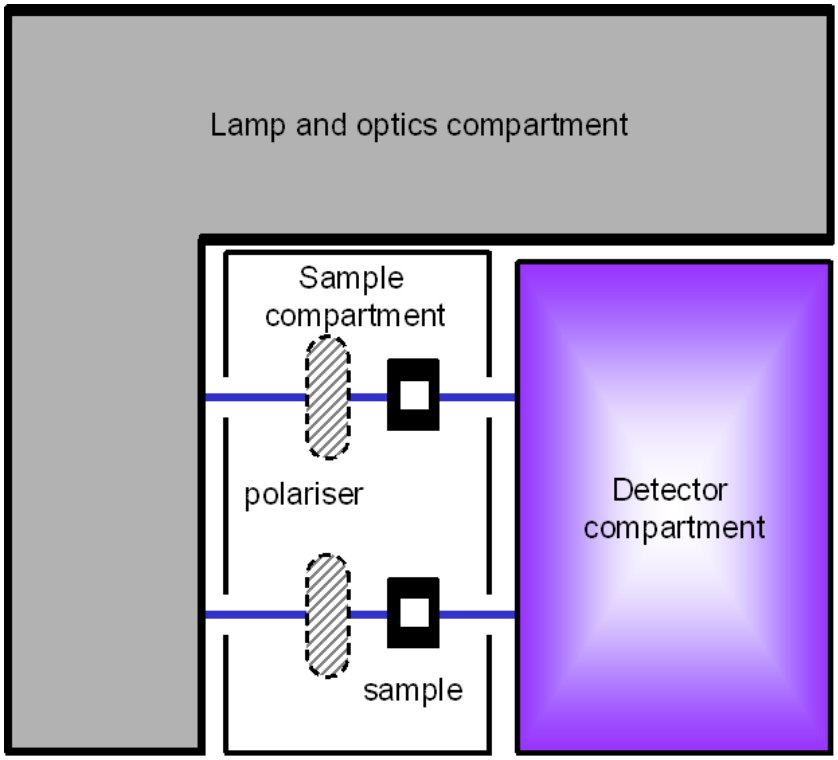

Figure 3.4: Schematic diagram of the spectrometer used for the isotropic and polarised absorption measurements. The polarisers were placed in the sample compartment, in front of the sample. The sample under test was placed in the holder at the bottom as shown on the figure. A blank, but otherwise identical sample was placed in the holder shown at the top of the figure.

Isotropic absorption spectra were taken with a *Perkin Elmer Lambda 19* spectrophotometer which can be used to study the absorption from the ultra-violet (∼190 nm) to the near infra-red (∼3200 nm). A schematic of this equipment is shown in Figure 3.4. The machine is equipped with a deuterium lamp for the UV and a tungsten lamp for the visible and near infrared regions, of the spectrum. It employs a double beam ratio recording operation: the beam from the selected lamp is split in two, the first passes straight through a reference sample and the second through the sample under investigation. The difference between the two intensities is recorded and used to create a full absorption spectrum. A variety of sample holders can be placed into the equipment allowing the study of both films or solutions (which are held in 10 mm cuvettes).

3.4.3 Linear dichroism measurements in absorption spectrophotometer

Polarised absorption spectra (linear dichroism measurements) could be recorded by inserting a matching pair of Glan-Thompson polarisers in the optical path of the beam (shown in Figure 3.4). An aligned film is rotated around the beam to collect spectra parallel and perpendicular to the polarisers.

3.4.4 Linear dichroism measurements with a transmission spectrometer

A transmission spectrometer was designed to allow linear dichroism (LD) measurements to be taken directly, and was built along an optical bench. A line diagram of this experimental set-up is shown in Figure 3.5. The optical components along the light path consisted of a tungsten lamp, a Bentham Monochromator, a Glan-Thompson polariser, a Hinds photoelastic modulator (PEM), the sample which was held at 45° to the plane of the bench and an amplified photodiode which detected the incoming light.

The intensity of light transmitted through the sample was recorded with the photodiode.

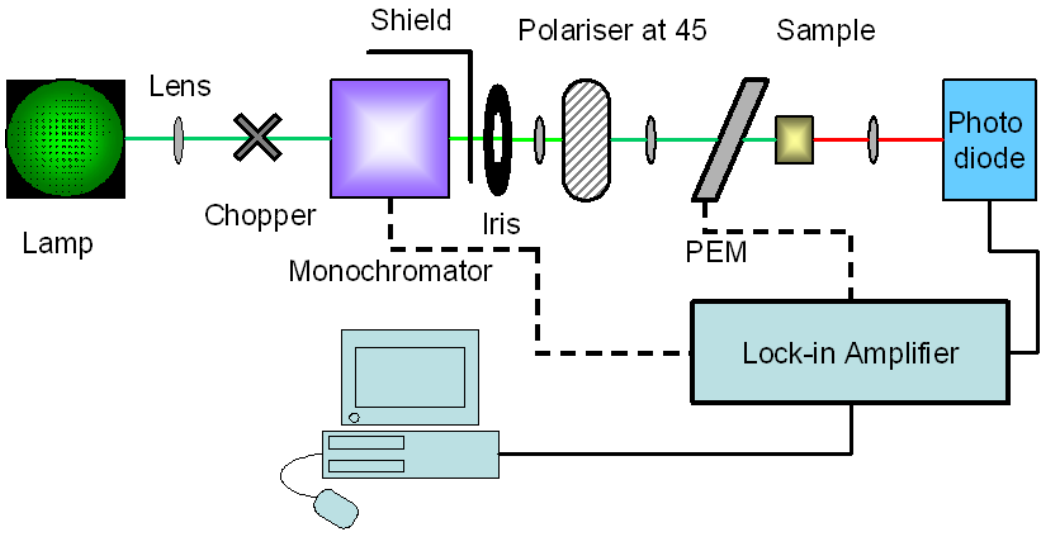

Figure 3.5: Schematic diagram of the home-built apparatus used for linear dichroism measurements. The illumination came from a tungsten lamp and was passed through a series of optics including a monochromator. The shield and iris were used to stop stray non-monchromated light passing into the rest of the experiments. The light was passed through a polariser at 45° to the horizontal bench. Aligned samples were also held at this angle. The light passed through the sample and then was focused onto a photodiode. Either the PEM or the chopper was used with the lock-in amplifier. The PEM was only used for polarised absorption measurements and the chopper for isotropic absorption measurements.

The signal was modulated by the chopper or the PEM and detected in conjunction with the lock-in amplifier. The use of the PEM and the 45° polariser meant polarised transmission could be recorded. The PEM was used as a half-wave plate and the polarisation of light was modulated between parallel and perpendicular to the alignment of the sample. The difference in transmission of these two polarisations was recorded. The intensity of the lamp used had a strong wavelength dependence. The differential transmission spectrum was divided by the

lamp spectrum to correct for this. Inverting the differential transmission gives the LD. The system was controlled by a LABVIEW 7.0 program specifically written for the task. The version used was modified by the author from an original program written by Mr A Smith at the Department of Physics, Durham University.

3.4.5 Jobin-Yvon Fluorolog-3 spectrofluorimeter

Steady-state emission spectra were taken with a Jobin-Yvon Fluorolog-3 spectrofluorimeter equipped with a xenon lamp which allowed excitation in the visible (between 300 nm and 550 nm) and a photomultiplier tube for detection from the UV to IR (between 240 nm to 1000 nm). A monochromated beam of light illuminates the sample and the emission is recorded with the photomultiplier tube. The Fluorolog has a right angle geometry (also known as L-format geometry[51]) which means the emission is collected at 90 ° to the excitation beam. The emission is recorded as a function of wavelength and saved to the computer. A photodiode collects a reflected excitation beam that allows the behaviour of the lamp to be monitored. This output allows the spectra to be corrected for any fluctuations in the intensity of the lamp. Equipped with double excitation and emission monochromators, the system is sufficiently precise to reliably take data in 1 nm increments. The fluorolog has a range of different sample holders to allow either solutions or films to be investigated. A photograph of the film holder is shown in Figure 3.6.

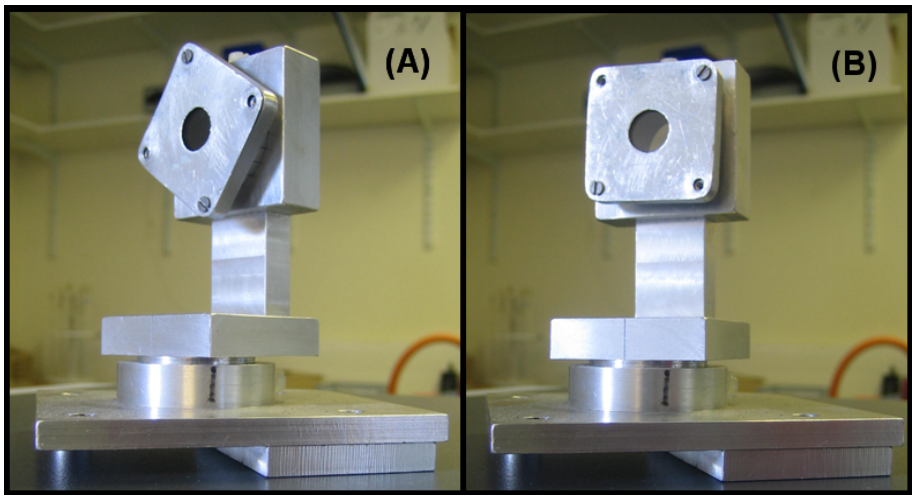

Figure 3.6: Photographs of the film holder used in the spectrofluorimeter in two different orientations (A and B). The film is held in the top part of the holder and can be rotated 360 ° around the horizontal axis. The holder can be orientated in the vertical axis.

3.4.6 Fluorescence anisotropy measurements in Fluorolog-3

The fluorolog used has motorised, computer controllable Glan-Thompson polarisers which could be rotated allowing a full range of angles to be investigated. For fluorescence anisotropy measurements the excitation polariser was set vertical and the emission polariser rotated to vertical or horizontal to record the polarised emission spectra of the polymer. Equation 2.26 thus becomes:

$$\langle r \rangle = \frac{I_{vv} - G_1 I_{vh}}{I_{vv} + 2G_1 I_{vh}} \tag{3.1}$$

where $I_{ex,em}$ is the emission intensity and v and h denote the vertical and horizontal alignment of the polarisers held in the excitation (ex) and emission (em) port. $G_1 = I_{hv}/I_{hh}$, is the instrumental polarisation correction factor and is discussed in detail below.

The spectra were taken with an interval of 2 nm, an integration time of 5 seconds and a 1 nm slit width. It took approximately 30 minutes to complete the measurements for an anisotropy value at any one excitation wavelength. The fluorolog was programmed to take the relevant spectra for excitation wavelengths across the absorption spectrum of the polymer, thus creating an excitation anisotropy spectrum.

Excitation anisotropy spectra were also taken as a function of temperature. Solutions were held within a custom designed cuvette: an 80 cm glass tube with a quartz cuvette fused to the end. The open end was sealed with a rubber bung. A Janis Research Company VNF-100 liquid nitrogen cryostat was used to reach temperatures between 330 K and 180 K.

The same measurements were also taken for films, both isotropic and aligned. The films were held in a specially designed holder, shown in Figure 3.6. The filmholder has two degrees of freedom, meaning that a film can be positioned in almost any orientation. The holder can be rotated around the vertical axis to fix the angle of incidence of the excitation beam on the film. This was fixed at 30°. An aligned film can be rotated and the stretch direction fixed at any angle to the vertical.

A program was written by the author in Microcal Origin to analyse the anisotropy data. The program removed a standard background estimated from the last 20 data points in a file, where there was no emission, and used the equation 3.1 to calculate the fluorescence anisotropy. The automation of both parts of the experiment allowed it to be repeated several times.

3.4.7 Polarisation correction factor, G_1

Optical instruments such as photodetectors often have a dependency on polarisation. This needs to be corrected for by use of the apparatus polarisation response factor.

The apparatus polarisation response factor, G_1 in equation 3.1, can be measured from two emission spectra:[51]

$$G_1 = \frac{I_{hv}}{I_{hh}} \tag{3.2}$$

where $I_{ex,em}$ is the emission intensity and v and h denote the vertical and horizontal alignment of the polarisers. The G_1 factor was measured for a dilute solution of the laser dye Coumarin 6 (Photonic Solutions) in Ethanol (Romil). This dye was chosen because it is highly emissive in the fluorescence wavelength range of the polymers used in this work. The G_1 factor was found to be independent of excitation wavelength and the value used in later analysis was created from the average of several repeated measurements.

3.4.8 Time-correlated single photon counting (TCSPC) - Principle

Time correlated single photon counting is a method of measuring the time between absorption and emission from a molecule. The measurement can be used to identify excited state lifetimes and investigate transfer rates between two or more excited states. The name of the experiment aptly describes the technique, the detector counts individual photons as a function of the time they are emitted from the sample. A variable monochromated laser source is used to trigger the counting system and excite the sample. The counter is stopped when emission from the sample is detected. The time from excitation to emission is recorded and a histogram of results is built-up over multiple repetitions of the experiment.

The single photon counting technique is similar to using a stopwatch to measure a a sprinter's time over 100 m. There is a "*start*" signal that starts the counting and an equivalent "*stop*" signal. The equipment in TCSPC is significantly more sophisticated, but the principle is the same.

The sample and a trigger diode connected to the MCP are excited by the laser with a pulse every 13.1 ns (i.e. at 76.3 MHz). A single photon is emitted from the sample and this starts the charging of capacitor in the MCP at a known charging rate. The next photon from the laser triggers the diode connected to the MCP and acts as a "*stop*" signal, stopping the capacitor from charging further. The voltage on the capacitor is related to the time between the "*start*" and "*stop*", $T_{start \rightarrow stop}$. Since the time between the the excitation pulses is always

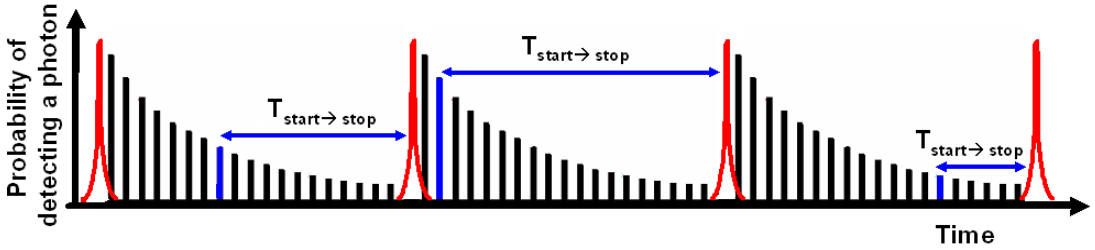

Figure 3.7: Schematic diagram of the reverse single photon counting method. The black lines represent the probability of detecting a single emitted photon, the blue bar represents the detection of a photon and the "*start*" signal and the red peak represents the trigger signal from the laser and the "*stop*" signal. It is referred to as the reverse single photon counting method because typical TCSPC systems have the trigger as the start and detection as the stop signal. Figure adapted from Professor Monkman's post-graduate lecture notes.

fixed at $T_{pulse} = 13.1$ ns, $T_{start \rightarrow stop}$ is also related to the time between the sample excitation and the emission of a single photon, T_{photon}:

$$T_{photon} = T_{pulse} - T_{start \rightarrow stop} \tag{3.3}$$

This is shown diagrammatically in Figure 3.7. A histogram of the T_{photon} times can be built up over long exposure times. After the successful detection of a photon the MCP has to recharge and cannot detect further photons emitted in a single T_{pulse} time period.

Conventional TCSPC systems start to count with the trigger signal and stop upon the detection of a photon. However, this conventional method will not respond with a high repetition rate from the laser and the T_{photon} times it can be used to resolve are quite long in comparison to the system used here. The system used in this work is a reverse single photon counting method and is suitable for resolving lifetimes between 4 ps (the channel width) and 13.1 ns (the time between pulses). Therefore it is not suitable for long emission lifetimes such as phosphorescent materials which have long lifetimes.[51] But it is more than ample for fluorescent lifetime studies which are typically on the nanosecond scale.[51]

3.4.9 Time-correlated single photon counting - Equipment

The single photon counting set-up used to investigate the fluorescence lifetime and anisotropy decays of the polymers in this work were taken with a system built and calibrated at the Physics Department, Durham University by Dr F. B. Dias. A line diagram of the experimental set-up is shown in Figure 3.8.

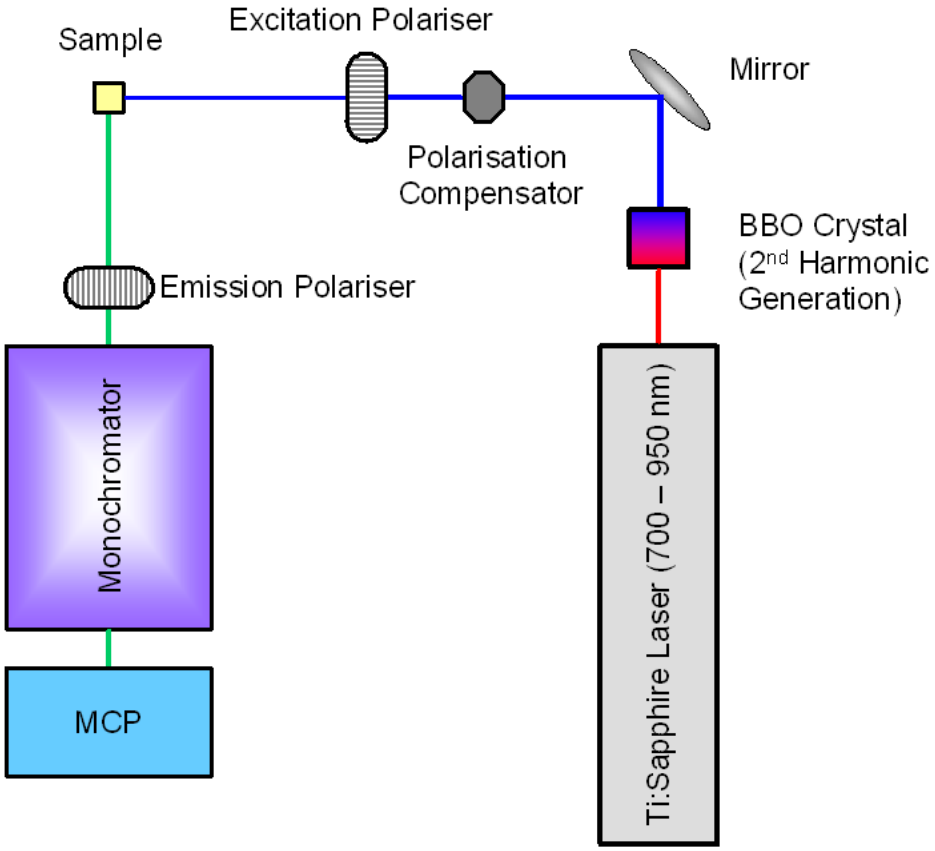

Figure 3.8: Schematic diagram of the apparatus used for time correlated single photon counting measurements. A Ti:Sapphire laser (with output wavelengths between 700 nm and 950 nm) is frequency doubled in a beta barium borate (BBO) crystal. A Berek polarisation compensator is used to rotate the laser beam to vertical (or horizontal for the anisotropy decay measurements). The beam passes through a polariser before illuminating the sample. The light emitted from the sample is collected at 90° from the excitation beam to stop specular reflection entering the detector. Solution samples were held in 10 mm cuvettes. Films were placed at an angle of 60° to the excitation beam. The emitted light passed through a double monochromator onto a microchannel plate (MCP) connected to the control computer.

A Ti:Sapphire laser (Mira 900, Coherent) with a narrow pulse width (> 2 ps) was frequency doubled (using a beta barium borate (BBO) crystal). The wavelength could be tuned between 350 nm and 475 nm depending upon experimental requirements. The beam was vertically polarised, initially by rotating the horizontal beam and then passing it through two separate Glan-Thompson polarisers, to ensure it was highly polarised. The sample, either a solution in a quartz cuvette or a film, mounted at 45° was illuminated by this beam. Emission collection optics, perpendicular to the excitation beam, allowed the emission to pass through a polariser and a double monochromator (Acton Spectra Pro 2300i) before being collected by a micro-channel plate (MCP) which covers a total time of with a detection channel width of 3.26 ps. The system has an instrument response function of 22 ps and, after deconvolution, features as short as 4 ps can be resolved.[138] The addition of a rotatable polariser in the emission optics allows the set-up to be used to collect time-resolved fluorescence anisotropy measurements using the TCSPC method.[153–159]

The response time of the system was recorded by scattering the laser beam from a sample. For dilute solutions (typically used in these investigations) the scattering rate is low and the solution is replaced with a suspension of Ludox (colloidal silica beads) in water. The response time varied from ~ 25 ps for solutions to ~ 30 ps for solid state samples. The small variation arises from the slight difference in experimental geometries required for the different types of samples.

The apparatus polarisation response factor, G_1, was determined through long time tail matching of Coumarin 6 (from Exiton Dyes Ltd) in Ethanol (from Romil) at each excitation wavelength.[80] The polarised TCSPC system and the analysis procedure, outlined by O'Connor and Phillips,[80] was tested at 430 nm with Coumarin 6 in ethylene glycol (from Aldrich) and both the fluorescence lifetime and the rotational lifetime were found to be the same as that found previously.[160] This check was repeated at each excitation wavelength and gave the same result. A further check of the response function was made by using polarised decays to form the sum $I_{ISO} = I_{vv} + 2I_{vh}$ which was the same as the isotropic emission.

3.4.10 Time-correlated single photo counting - Data acquisition

An isotropic decay (emission polariser oriented to the magic angle $I_M(t)$ of $\sim 55\,^\circ$) and two polarised decays (emission polariser oriented parallel and perpendicular to the excitation polariser) were recorded for each excitation wavelength at two different emission wavelengths. The set of decays were recorded twice.

The emission polariser was aligned at the magic angle, parallel or perpendicular relative to the vertically polarised excitation, in order to collect polarised decays $I_M(t)$, $I_{\|}(t)$ and $I_{\perp}(t)$ respectively. The integration times were the same for both polarised decays and were kept as short as possible to give at least 6,000 counts (no more than 600 s). The laser was deemed to be stable for these durations.

The magic angle decays for different wavelengths (listed in Chapter 7) were deconvoluted with the instrument response function and analysed globally to determine the fluorescence lifetimes that were then used in the simultaneous fitting of the two polarised decays. The fits were used to create a model of the anisotropy decay. The model was then used to determine the anisotropy decay times.

The time response of the system (as described above) was taken before every measurement as it is used in the deconvolution procedure.

3.4.11 Time-correlated single photon counting - Data analysis

The "Globals" deconvolution fitting software package developed at the Laboratory for Fluorescence Dynamics at the University of Illinois at Urbana-Champaign was used. The analysis technique employed here fits each decay as a series of exponentials (as in equation 2.46). Both the fluorescence lifetime and pre-exponential amplitudes can be varied in the fitting procedure. The quality of the fit is indicated by the result of a least-squares fitting and a value of χ^2 close to unity is deemed an appropriate fit for the data. This procedure creates a reconstructed intensity decay for the time which is masked by the response time of the system. Each decay can be deconvoluted separately or as a group of related decays. The former is typically used to investigate decays from molecules about which there is limited knowledge. The latter, the global analysis technique, is used to study two or more linked decays. Two separate cases of global analysis were used in this work.

Global analysis can be used to investigate multiple radiative species. The fluorescence lifetimes of these species will be the same, however their pre-exponential intensities will depend upon the emission wavelength recorded. By recording decays at two or more emission wavelengths, the surety of the lifetimes can be assured by fitting for these common values and their relative amplitudes. This technique is particularly useful for determining the fluorescence lifetimes of isotropic decays. Global analysis can also be used for polarised decays recorded at the same emission wavelength. The anisotropic component, for example excitation migration, will have the same lifetime for both components, however, it will occur as a decay time (negative amplitude) in the emission decay parallel to the excitation and a rise time (positive amplitude) in the decay perpendicular to the excitation. These decays can also be fitted together to determine the anisotropy decay time.

3.5 Other experiments

Raman spectroscopy, x-ray diffraction and a technique for order parameter determination were also used and are fully described in Chapter 6.

Chapter 4

Fluorescence Anisotropy in Polyfluorene

4.1 Introduction

This chapter describes temperature dependent fluorescence anisotropy measurements carried out in dilute solutions of poly[9,9-di(ethylhexyl)fluorene] (PF2/6) and three of its oligomers. It was published in the *Journal of Chemical Physics* in 2005 under the title of *An investigation into the excitation migration in polyfluorene solutions via temperature dependent fluorescence anisotropy.*[161]

Fluorescence anisotropy processes are associated with energy loss processes. Therefore, by studying the fluorescence anisotropy, a more thorough understanding of certain energy losses (and associated efficiency losses) can be studied. The information pertaining to loss processes can help chemists design more efficient molecules and device engineers make more efficient devices. For example, if a molecule rotates, additional long alkyl chains could be attached to stop this rotation.

Fluorescence anisotropy measurements were used to estimate the natural anisotropy of the PF2/6 polymer and shorter chain oligomers of the same monomer unit. The natural anisotropy is a measure of the angular separation between the absorption and emission transition dipole moments. Any deviation from the maximum 0.40 value can be considered as an anisotropy loss. This information was then used as a baseline for subsequent work on locating the angular position of these transition dipole moments relative to the polymer backbone. There is particular interest in the conjugated polymer Polyfluorene (PFO) because it emits in the blue region of the electromagnetic spectrum.

Natural anisotropy measurements can be used to estimate what happens to an excited state in the time between its creation (via absorption) and before it relaxes (via emission, in this case fluorescence). For example, an anisotropy loss can be linked to an excitation migration or an energy transfer process. In small molecules it is usually explained by physical rotation of the whole molecule or conformational changes of the chemical structure of the molecule. Other loss processes have been described in detail in Chapter 2 section 2.5.8.

The temperature dependent results reported in this chapter strongly suggest that there are two different anisotropy loss mechanisms. Both migration of the excited state and the rotation of part of the chain alter the position of the fluorescence transition dipole moment with respect to the absorption transition dipole moment. As a result, the anisotropy is less than its maximum, $\langle r \rangle = 0.40$, and the natural anisotropy was estimated to be 0.32. It was found that both these processes occurred in polymers of over 20 units in length, but the excitation

migration process dominated at high temperatures. By studying oligomers of short length where excitation migration is impossible, it was possible to reveal that excitation migration was temperature independent whereas the twisting of the polymer chain is dependent upon temperature. The results of the experiments presented here were also used to verify the theory that PF2/6 polymer undergoes both conformational twisting of the backbone and excitation migration, which was first postulated by Dias *e*t al. in 2003.[54]

4.2 Previous research

Time-resolved fluorescence studies of PF2/6 had previously been carried out by Dias *et al.* at the Instituto de Technologia Química e Biológica, Oeiras, Portugal, in collaboration with the OEM group at Durham University. The work revealed that the fluorescence intensity (I) from the singlet excited state was best described by using biexponential behaviour,[54] i.e. $I = A_1\ e^{-t/\tau_1} + A_2\ e^{-t/\tau_2}$. The two lifetimes ($\sim$ 370 ps and $\sim$ 40 ps) were found to be independent of solvent polarity, indicating that the two processes are intra-molecular. The longer lifetime was presumed to be the main decay mechanism for the polymer because it was present for all excitation wavelengths. The shorter lifetime was found to be energy dependent and appeared as a decay time when it is collected on the blue peak (high energy) of the emission spectrum and as a rise time when it is collected at the red-edge (lower energies). The longer lifetime component was also shown to be temperature independent, while the shorter lifetime component was found to be a function of temperature thus confriming the idea that the longer lifetime is the main decay route. In the temperature range 233 K to 313 K, the shorter lifetime varied between 100 ps and 30 ps respectively. The short lifetime was also found to be dependent on solvent viscosity.

Dias *et al.* compared the results from PF2/6 to those from an inflexible polymer, methyl-substituted ladder-type poly(*para*-phenylene)(MeLPPP).[54] MeLPPP is also a blue emitting conjugated polymer, that closely resembles polyfluorene derivatives, with the notable exception that each phenyl ring is doubly bridged to each adjacent ring, shown in Figure 2.26. This double bridge structure removes possible conformational twisting about the backbone axis. Dias *et al.*[54] found that MeLPPP has only one long lifetime, suggesting that the shorter lifetime in PF2/6 arises from a physical motion of the PF2/6 backbone. It was argued that a possible explanation was that the polymer undergoes a small torsional motion between two adjacent phenylene rings along the polymer backbone. The authors also argued that the initially excited state is in an energetically unfavourable 'twisted' arrangement and that the states can undergo conformational relaxation, or un-twisting, that makes the structure more planar. It was noted in their work, that the final state of the polymer would not be entirely planar and that the proposed rotation between the bonds would be very small.

Other theories about the nature of the short component were discussed by Dias *et al.* The theories included vibrational relaxation of the excited state and excitation migration to a longer conjugation length. Vibrational relaxation typically occurs on the femtosecond scale[162] which is beyond the temporal resolution of the system Dias *et al.*[54] used. Vibrational

relaxation would be a factor of ∼10,000 faster than the shorter lifetime that was measured and was ruled out by Dias *et al.*[54] Excitation migration is likely to occur as PF2/6 can support many chromophores but this process is unlikely to be affected by solvent viscosity. Although there was strong evidence for the conformational motion argument, excitation migration (in the form of exciton hopping to energetically lower states) could not be totally ruled out by Dias *et al.*[54]

The work presented in this chapter was designed to clarify the processes that occur in PF2/6 after excitation. Site-selective temperature dependent fluorescence anisotropy was used to separate the processes and the results here show that both migration and conformational relaxation of the lowest excited state contribute to the energy relaxation process.

4.3 Experimental

Sample preparation

The polyfluorene derivative poly[9,9-di(ethylhexyl)fluorene] (PF2/6) in long chain polymer form (PF2/6) and two oligomers with chain lengths of twenty and ten units ($PF2/6_{N=20}$ and $PF2/6_{N=10}$ respectively) were investigated in dilute methylcyclohexane (MCH) solution. A shorter polyfluorene derivative (9,9-dioctylfluorene) (PFO) oligomer with three units was also investigated in the same way. Higher viscosity solvents, decalin and hexadecane, were also used to make solutions of $PF2/6_{N=10}$. The absorption of the solutions was kept below an optical density of 0.1 to avoid any possible aggregate effects and re-absorption of emission because both processes are known to lower the fluorescence anisotropy value.

Steady-state fluorescence anisotropy measurements

Fluorescence anisotropy measurements were taken with the procedure outlined in Chapter 3. Anisotropy temperature profiles were made in solution above the melting point of MCH; the range between 220 K and 330 K was specifically studied. Excitation anisotropy activation spectra were created using excitation wavelengths across the polymer's absorption spectrum. This was done at room temperature (∼ 290 K) and at 220 K.

4.4 Results

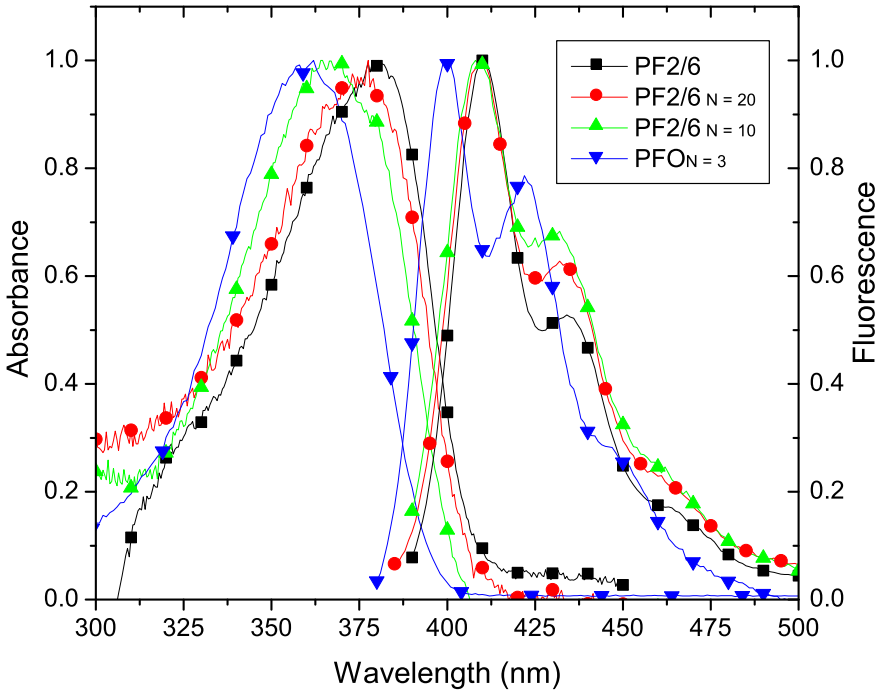

Figure 4.1: Absorption and emission spectra of the polyfluorene derivatives in dilute MCH solution: the long chain polymer of poly [9,9-di(ethylhexyl)fluorene] PF2/6; (Black line, squares); the oligomers PF2/6$_{N=20}$ (Red line, circles) and PF2/6$_{N=10}$ (Green line, triangles) and (9,9-dioctylfluorene) PFO$_{N=3}$ (Blue line, inverted triangles). These spectra were taken at 20 °C and the excitation wavelength for emission spectra was 380 nm.

Poly (9,9-di(ethylhexyl)fluorene) (PF2/6), its shorter oligomers: PF2/6$_{N=20}$, PF2/6$_{N=10}$, and PFO$_{N=3}$, have broad absorption spectra that encompass a significant portion of the UV and blue visible spectrum particularly between 325 nm and 400 nm, (as shown in Figure 4.1). The absorption maximum wavelength shifts to longer wavelengths as the number of repeat units increases.

The emission of all four molecules, when excited at 380 nm, (also Figure 4.1), produce very similar emission spectra with three clear vibrational bands at 420 nm, 435 nm and 465 nm. PFO$_{N=3}$, is the exception; it is blue shifted by 20 nm. The emission from the longest three macromolecules is almost indistinguishable apart from the change in relative intensity of the first and second vibrational peak.

The shift towards longer absorption maxima is not seen in emission maxima. This means there is a decrease in the "effective" Stokes's shift with increasing monomer units. The "classical" Stokes's shift is a measure of the conformational relaxation energy lost due to a relaxation of the initial excited state chain geometry into its lowest energy excited state geometry. However, in conjugated polymer systems energy migration can also contribute to

this difference in energy, yielding a larger "apparent" Stokes's shift. Therefore, in conjugated polymers, the measured Stokes's shift cannot be used simply as a direct measure of either energy migration or conformational relaxation.

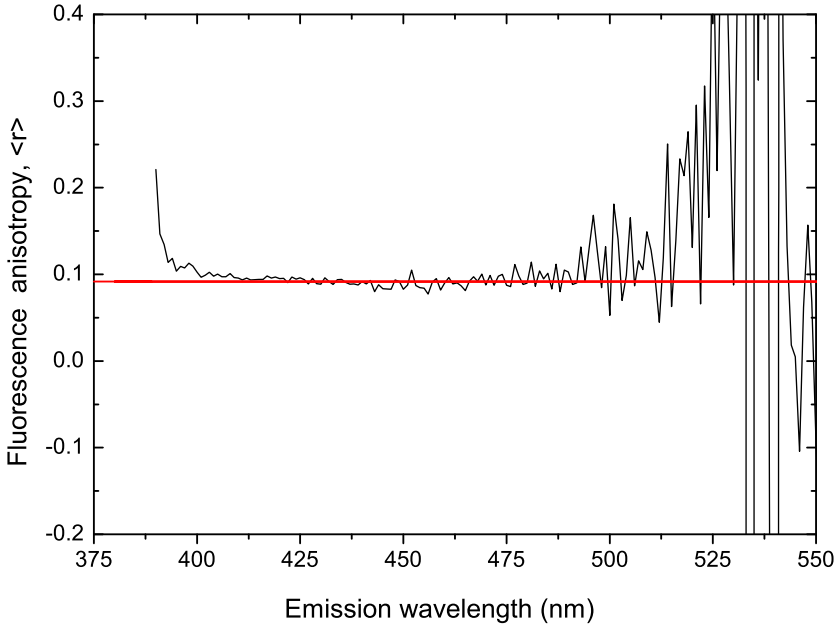

Figure 4.2: Fluorescence anisotropy of PF2/6 as a function of emission wavelength in a solution of MCH excited at 384 nm. The straight line highlights the average value of anisotropy ($\langle r \rangle$) across the excitation spectrum ($\langle r \rangle = 0.09 \pm 0.01$). The noise at the ends of the spectrum, is caused by very low intensity at the edges of the emission spectrum.

An example of the fluorescence anisotropy spectrum for PF2/6 in methylcyclohexane (MCH, viscosity ~ 0.67 mPa s at 25 °C[163]) is shown in Figure 4.2. It was found, for all the macromolecules, that the fluorescence anisotropy does not vary greatly with the emission wavelength. The fluorescence anisotropy value for a single excitation wavelength was taken as the average value across the whole fluorescence spectrum and was used to create the excitation anisotropy spectrum. In the example in Figure 4.2 the excitation wavelength is 384 nm (absorption maximum) and the average fluorescence anisotropy value across the emission spectrum is $\langle r \rangle = 0.09 \pm 0.01$.

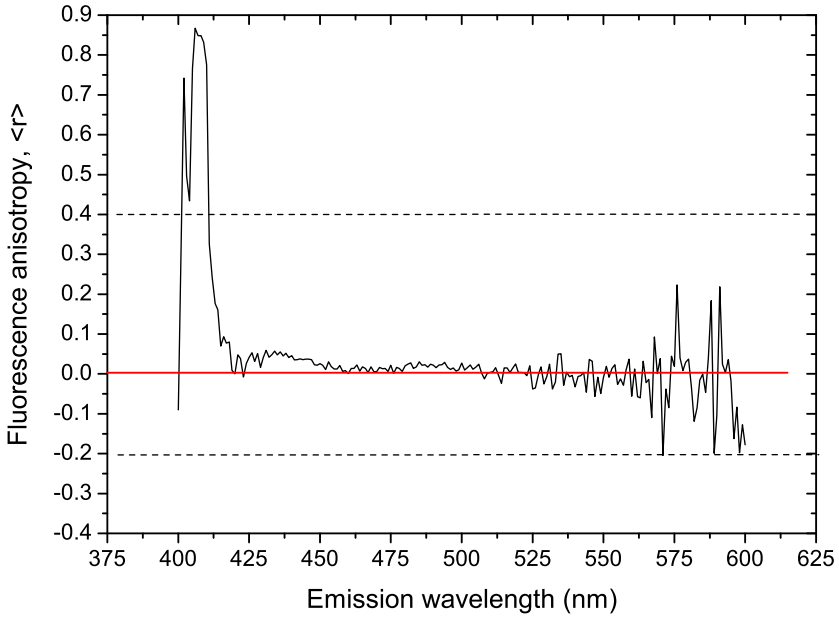

Figure 4.3: Fluorescence anisotropy of perylene in a solution of hexadecane. The straight line highlights the value of fluorescence anisotropy across the excitation spectrum (zero). The noise at the ends of the spectrum is caused by very low intensity at the edges of the emission spectrum. The dotted lines show the limits of the fluorescence anisotropy.

Fluorescence anisotropy is commonly lost through rotation of the molecule: to demonstrate this the fluorescence anisotropy of perylene in MCH is shown in Figure 4.3. The fluorescence anisotropy value is zero within the bounds of experimental error across the fluorescence spectrum. Perylene is a small molecule, comprised of five phenyl rings and is known to rotate very quickly, consequently losing all fluorescence anisotropy rapidly.[164] PF2/6 has a non-zero fluorescence anisotropy in solutions of low viscosity for almost all excitation wavelengths across its absorption band. It is therefore assumed that the system does give reliable ansiotropy values and that rotation of PF2/6 is very slow compared with its short fluorescence lifetime.

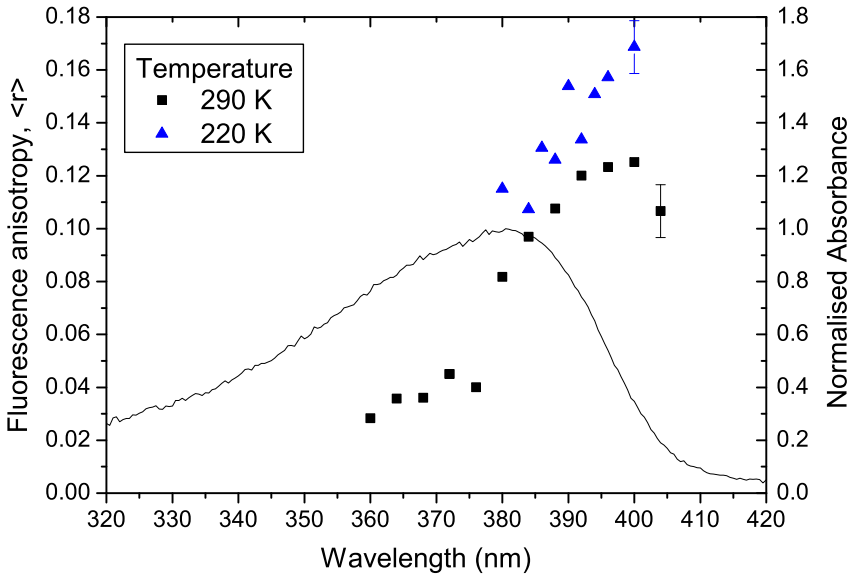

Figure 4.4: Excitation anisotropy spectra of PF2/6 in MCH showing an excitation wavelength dependence. The average fluorescence anisotropy value increases to a plateau level at longer excitation wavelengths. The measurements taken at 220 K (triangles) and 290 K (squares). Also shown is the normalised PF2/6 absorption spectrum. Representative error bars are shown on the graph.

It was found that the fluorescence anisotropy depended upon the excitation wavelength. The fluorescence anisotropy for excitation wavelengths across the absorption band or excitation anisotropy spectrum, of PF2/6 in MCH, shown in Figure 4.4, is excitation wavelength dependent. At room temperature, the fluorescence anisotropy value for excitation at the peak of the absorption spectrum ($\lambda_{ex} = 384$ nm) is significantly less than the value for excitation at the red-edge of the spectrum ($\lambda_{ex} = 400$ nm). At even shorter excitation wavelengths ($\lambda_{ex} \sim 360$ nm) the increased excess energy leads to very low fluorescence anisotropy $\langle r \rangle \sim 0.02 \pm 0.01$. The increase in the fluorescence anisotropy value reaches a plateau at $\langle r \rangle \sim 0.12 \pm 0.01$ at long wavelengths ($\lambda_{ex} > 390$ nm) and remains approximately constant. The small drop in value at $\lambda_{ex} = 404$ nm is thought to have been caused by the low intensity emitted at this excitation wavelength.

Figure 4.4 also shows the anisotropy values at 220 K. Lowering the temperature of the solution did not change the emission wavelength dependence. But lowering the temperature did increase the steady-state anisotropy value at the edge of the absorption spectra. Decreasing temperature shows an increase in the value of the anisotropy at the red-edge. At the peak absorption wavelength, it appears the value of anisotropy is independent of temperature.

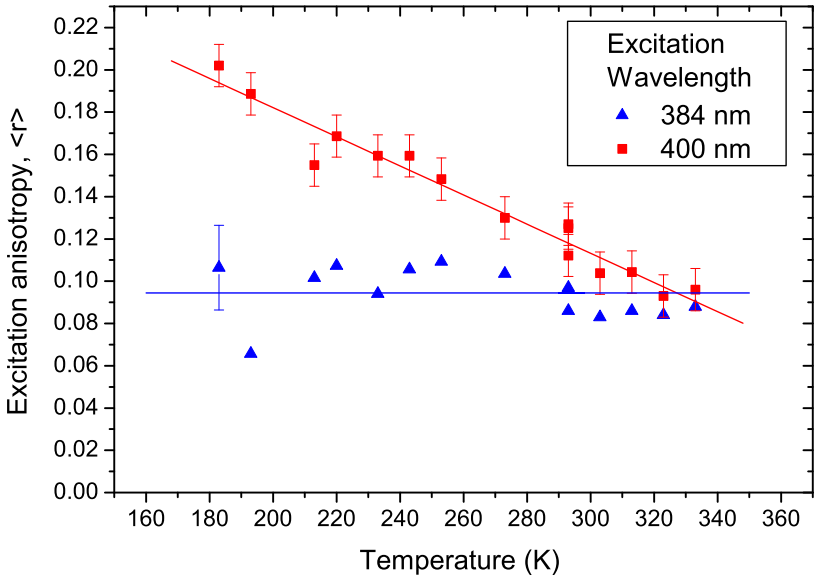

Figure 4.5: Fluorescence anisotropy temperature profile of PF2/6 in MCH for two different excitation wavelengths. Fluorescence anisotropy measurements were taken with excitation wavelengths at the blue peak (λ_{ex} = 384 nm triangles) and at the red edge (λ_{ex} = 400 nm squares) of the absorption band. The average anisotropy values when excited at the red-edge are temperature dependent whereas the anisotropy values when excited at the blue peak are constant within the error for all the temperatures studied. Linear trendlines and representative error bars are shown on the graph.

The temperature dependence of the anisotropy value at the edge and the peak of the absorption spectrum is shown in Figure 4.5. The anisotropy value is approximately constant ($\langle r \rangle \sim 0.09 \pm 0.01$) at the peak of the absorption spectrum (λ_{ex} = 384 nm) and is temperature dependent at the red-edge (λ_{ex} = 400 nm). At the red-edge the anisotropy increases with a drop in temperature; by extrapolating these results to the boiling point of liquid nitrogen (77 K) a value of $\langle r \rangle = 0.28 \pm 0.04$ was obtained. Extrapolating to absolute zero (0 K) provides an estimate for the natural anisotropy of 0.32 ± 0.04: this differs from the theoretical maximum value 0.40. This estimate is also very close to the results found for the poly(*p*-phenylenevinylene) (PPV) oligomers[78,165] and poly(2-methoxy,5-(2'-ethyl-hexoxy)-p-phenylenevinylene)(MEH-PPV)[166] in inert matrices. In those studies it was found that anisotropy values between 0.35 - 0.36 for long chain polymers.[78,165,166]

The value of natural anisotropy (r_0) estimated here corresponds to the average angle between the absorption and emission transition dipole moments (θ). In Chapter 2, the relationship between the anisotropy and the angle θ for an isotropic system is described by equation 2.36. Using this equation, the average angle between the absorption and emission dipoles can be calculated to be $\theta = 21° \pm 6°$. It should be noted that just above room temperature all excitation wavelengths produce the same values ($\langle r \rangle \sim 0.09 \pm 0.01$).

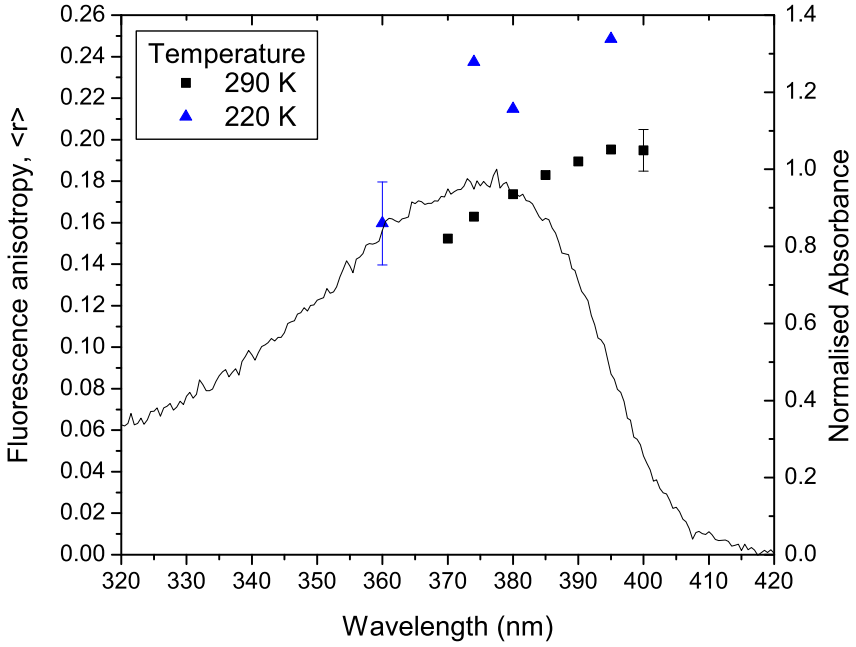

Figure 4.6: Excitation anisotropy spectra of PF2/6$_{N=20}$ in MCH showing an excitation wavelength dependence. The average anisotropy value increases to a plateau level at longer wavelengths. The measurements taken at 220 K (triangles) and 290 K (squares). Also shown is the normalised PF2/6$_{N=20}$ absorption spectrum. Representative error bars are shown on the graph.

PF2/6 is a long chain polymer with, on average, $\sim$ 60 fluorene units per chain; as the number of units is decreased the behaviour of the solutions changes. The room temperature anisotropy of a molecule with twenty fluorene units (PF2/6$_{N=20}$), as seen in Figure 4.6, is $\langle r \rangle$ = 0.19 $\pm$ 0.01 at λ_{ex} = 395 nm, almost double that of PF2/6 (Figure 4.4). This corresponds to a significant change in the natural anisotropy of the molecules. Equation 2.36, which is applicable since rotation has been eliminated, shows the movement of the transition dipole is approximately 10 $^\circ$ less for the short chain oligomer than for the long chain polymer.

The excitation anisotropy spectrum of PF2/6$_{N=20}$ is similar in shape to that of the long chain polymer (Figure 4.4), with an increase to $\langle r \rangle$ = 0.19 $\pm$ 0.01 at which point the anisotropy remains approximately constant for increased excitation wavelengths. At low temperatures, temperature dependent behaviour is observed again, but here, both the blue peak and red-edge excitation wavelengths produce increased anisotropy values.

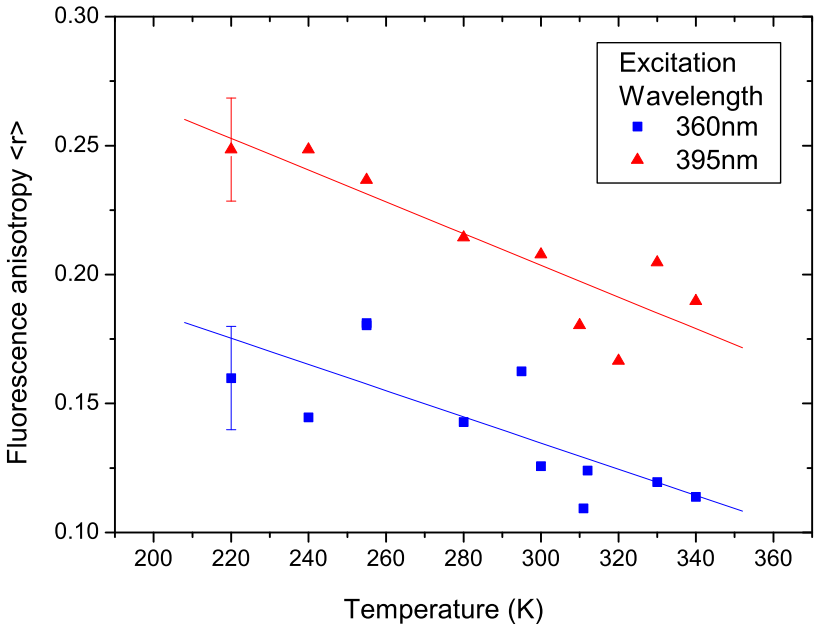

Figure 4.7: Anisotropy temperature profile of PF2/6$_{N=20}$ in MCH for two different excitation wavelengths. Anisotropy measurements taken close to the absorption maximum, at the blue peak (λ_{ex} = 360 nm triangles) and at the red-edge (λ_{ex} = 395 nm squares) of the absorption band. Both excitation wavelengths produce average anisotropy values that are temperature dependent. Linear trendlines and representative error bars are shown on the graph.

Figure 4.7 shows that for excitation at the red-edge of the absorption spectrum, the anisotropy of PF2/6$_{N=20}$ has a similar temperature dependence to that of the polymer, PF2/6. Figure 4.4 also shows that for excitation close to the absorption maximum which occurs at the blue peak of its absorption band, the fluorescence anisotropy has a small temperature dependence, which is different from the polymer. This suggests that the mechanism governing the loss of anisotropy in PF2/6$_{N=20}$ is not fully activated even with high-energy photons. The trend for both chosen excitation wavelengths in PF2/6$_{N=20}$ is almost parallel, which suggests that the same process is responsible for anisotropy loss at both edges of the absorption spectrum. This oligomer contains an average of twenty monomer units and Fytas *et al.* have hypothesised that the conjugation length in polyfluorenes spans an average of ∼12 units.[90] It is, therefore, unlikely that the shorter oligomers can support multiple sites that an exciton can migrate to and in turn, this suggests that energy migration is unlikely to be the main anisotropy loss process.

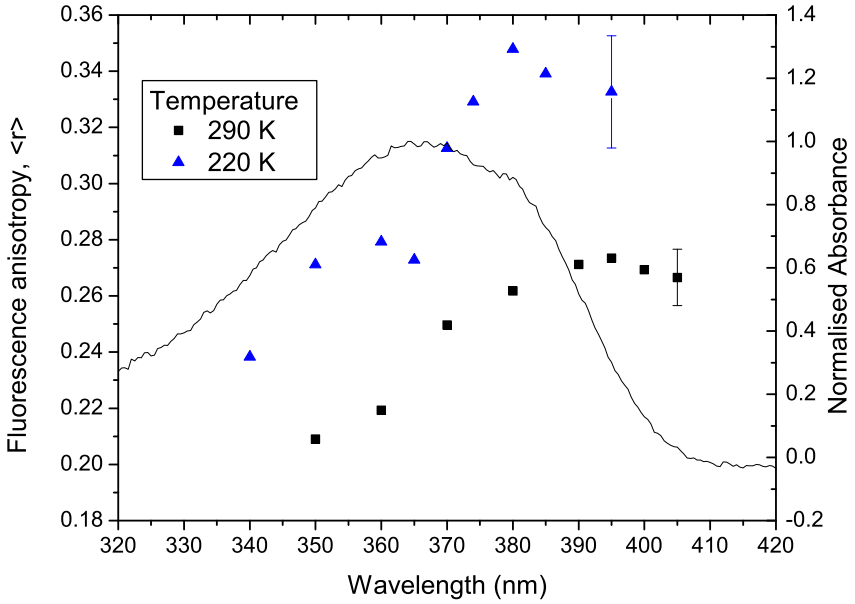

Figure 4.8: Excitation anisotropy spectra of PF2/6$_{N=10}$ in MCH showing an excitation wavelength dependence. The average anisotropy value increases to a plateau level at longer excitation wavelengths. The measurements taken at 220 K (triangles) and 290 K (squares). Also shown is the normalised PF2/6$_{N=10}$ absorption spectrum. Representative error bars are shown on the graph.

Truncating the oligomer to only ten units long, PF2/6$_{N=10}$, produces a blue shift in its absorption spectrum. The peak of this spectrum is at 360 nm and the edge at 385 nm as shown in Figure 4.1. The emission spectrum, however, is very similar to the longer chains and the only difference occurs in the intensity of the vibronic shoulder at around 440 nm. The excitation anisotropy spectrum follows the same trend as the longer PF2/6$_{N=20}$, but has a significantly greater value of anisotropy as shown in Figure 4.8. It shows a distinct increase and has a plateau area beginning at $\lambda_{ex} = 390$ nm, at the edge of its absorption band. At reduced temperatures, the anisotropy further increases almost to the maximum value, $\langle r \rangle = 0.40$, and the plateau region begins at a slightly lower excitation wavelength at $\lambda_{ex} = 384$ nm.

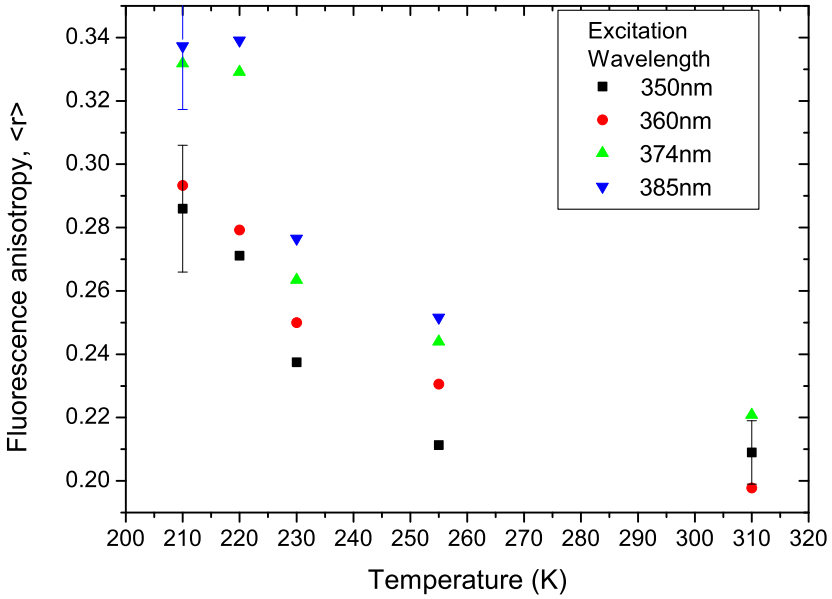

Figure 4.9: Anisotropy temperature profile of PF2/6$_{N=10}$ in MCH for four different excitation wavelengths. Anisotropy measurements taken at the blue peak of the absorption band: λ_{ex} = 350 nm squares, at λ_{ex}= 360 nm circles, at λ_{ex} = 374 nm triangles and at the edge of the absorption band: λ_{ex} = 385 nm inverted triangles. All the excitation wavelengths produce an exponential-like temperature dependent curve.

The results of an investigation into the temperature dependence of the anisotropy of PF2/6$_{N=10}$ are shown in Figure 4.9. Unlike the longer molecules, the anisotropy temperature dependence of this short oligomer is no longer a linear relation.

The change in anisotropy with temperature shown in Figure 4.9 is much greater than that shown in Figure 4.7 for PF2/6$_{N=20}$. This stronger dependence on temperature is assumed to be due to the faster rotation of the smaller molecule, as smaller molecules are less hindered by viscous drag in rotating about their centres. Similar behaviour has been noticed previously by Egelhaaf *et al.* who found that the rotational lifetimes of polyenes increased with chain length.[167] The rotation of a molecule is a significant anisotropy loss process as explained in section 2.5.8. As the molecule rotates about its centre point so does its fluorescence transition dipole moment.

The rotation can only be observed via fluorescence within the molecule's fluorescence lifetime and can only affect the observed fluorescence anisotropy during this time.[51] If the rotation time is appreciatively shorter than the fluorescence lifetime then the molecule will rotate significantly, depolarising the fluorescence and a fluorescence anisotropy value of zero is observed. If the rotation time is much longer compared with the fluorescence lifetime then the molecule remains stationary and the fluorescence anisotropy is unaffected.

The rotational correlation time (or the anisotropy decay time), Θ, for a spherical molecule is related to the fluorescence anisotropy by the Perrin equation.[51]

$$\frac{r_0}{r} = 1 + \frac{\tau}{\Theta} \tag{4.1}$$

where $\Theta = (\eta V)/(TR)$, T is the temperature, R is the gas constant, ν is the solvent viscosity and V is the volume that a molecule takes up.

Figure 4.9 shows that the fluorescence anisotropy is not zero at any point: hence it can be concluded that the rotational correlation time is shorter than the fluorescence lifetime. At low temperatures, the fluorescence anisotropy approaches the high natural anisotropy value: therefore, the rotational correlation time must increase as the temperature decreases.

The fluorescence lifetime of PF2/6 is quoted by Dias *et al.* to be of the order of a few hundred picoseconds. The rotational correlation time of polymeric PF2/6 must be longer than the fluorescence lifetime for an anisotropy greater than zero to be observed. The anisotropy decay process must be created by either a physical process in the molecule or a much faster electronic process.

As mentioned earlier, it is unlikely that such a small oligomer can support more than one conjugation length and as with PF2/6$_{N=20}$, the absorption and emission should occur at the same site. Most likely, the majority of the emission comes from the site initially excited and the whole molecule undergoes some form of electronic intra-chain relaxation, conformational twisting of the oligomer backbone, or as a rotation of the whole molecule.

To further investigate the nature of the possible physical motion, the behaviour of PF2/6$_{N=10}$ in solvents with very different viscosities decalin (3.35 mPa s at 25 °C) and hexadecane (3.03 mPa s at 25 °C) was investigated. The results are shown in Figure 4.10. The measurements in the more viscous solutions show the same profile as the oligomer in MCH, but the plateau region in the hexadecane solution begins at a lower wavelength than in both decalin and in MCH. This is because the high viscosity solvent prevents rotational motion so that the absorption and emission transition dipole moments remain in their original orientation. The maximum anisotropy values at the red-edge, (λ_{ex}= 380 nm) for both these new solvents are higher than those in MCH: for hexadecane $\langle r \rangle = 0.34 \pm 0.01$ and for decalin $\langle r \rangle = 0.30 \pm 0.01$ which compare with $\langle r \rangle = 0.27 \pm 0.01$ for MCH solutions. This corresponds to a difference in anisotropy of 0.07, between the MCH and hexadecane solutions, which is equivalent to an average movement of the transition dipole orientation by approximately 3 °.

The most probable cause for the major anisotropy loss in this oligomer is rotation. Figure 4.9 can be fitted to the Perrin equation which shows that the temperature dependence is independent of excitation wavelength, whereas the results for the longer molecules PF2/6 and PF2/6$_{N=20}$ have indicated a strong dependence on the wavelength. Lowering the temperature

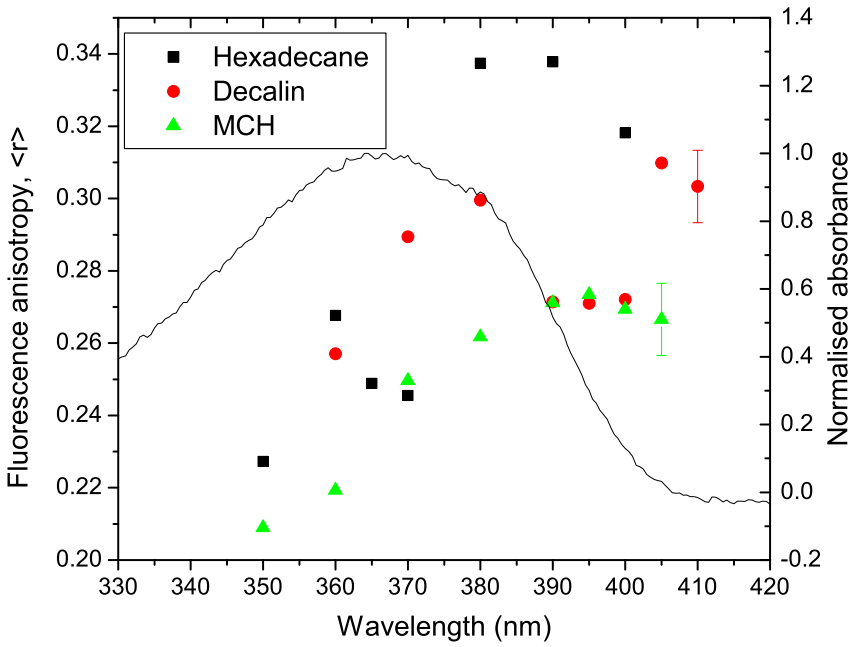

Figure 4.10: Excitation anisotropy spectrum of PF2/6$_{N=10}$ in MCH (triangles), decalin (circles) and hexadecane (squares). Measurements taken at 290 K. The average anisotropy value increases to a plateau level at longer excitation wavelengths. The plateau level is dependent on solvent viscosity; the most viscous solvent, hexadecane, presents the highest plateau and the least viscous solvent, MCH, presents the lowest average anisotropy. Also shown is the normalised PF2/6$_{N=10}$ in MCH absorption spectrum. Representative error bars are shown on the graph.

will decrease the vibrational energy in the solvent effectively increasing the solvent's viscosity. The results in Figure 4.10 show that highly viscous solvents can hinder the motion greatly. The proposed backbone conformational change is a twist of adjacent phenylene rings and not a bend towards each other. Hence it is more likely that PF2/6$_{N=10}$ undergoes a rotation of the whole molecule.

The reason that this oligomer can exhibit more rotation than PF2/6 is purely because of its short length compared with the other oligomers. As such it can be used to confirm that the other oligomers are not rotating significantly within their fluorescence lifetimes.

It is still worth noting that the theoretical maximum anisotropy value was not reached either at low temperatures or in viscous solvents. This implies that there could be an other much faster, anisotropy decay mechanism that is responsible for an anisotropy loss from 0.40 to $\sim$ 0.36.

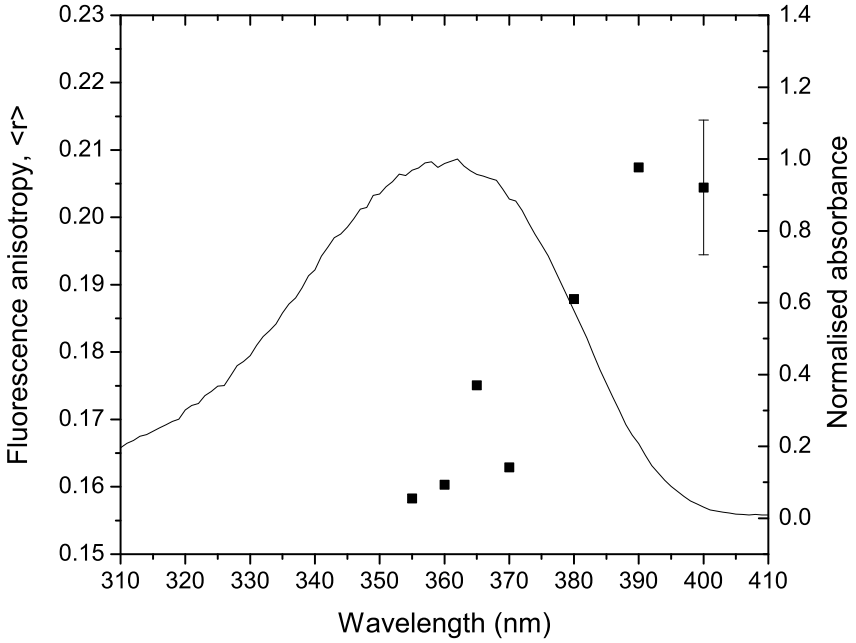

Figure 4.11: Excitation anisotropy spectra of PF2/O$_{N=3}$ in MCH at room temperature showing an excitation wavelength dependence. The average anisotropy value increases to a plateau level at longer wavelengths. Also shown is the normalised PFO$_{N=3}$ absorbance spectrum. Representative error bars are shown on the graph.

Reducing the size of the molecule to three units (PFO$_{N=3}$) produces anisotropy values that as seen in Figure 4.11 are lower than PF2/6$_{N=10}$ and approximately equivalent to that of PF2/6$_{N=20}$. But the small molecule still shows the same excitation anisotropy profile as the longer macromolecules. In the case of the shortest molecule, rotational motion would be expected to dominate, but, even here, very high levels of anisotropy can be observed meaning rotation is inefficient. This serves to confirm that rotation in longer chains is also a rather inefficient anisotropy loss mechanism and can be considered negligible when discussing the major reasons for fluorescence anisotropy loss in polyfluorene polymers.

4.5 Discussion

The purpose of the experiments described in this chapter was to investigate the nature of the anisotropy loss and understand the photophysical processes that occur in poly[9,9-di(ethylhexyl)fluorene] (PF2/6).The anisotropy loss (deviation from the theoretical anisotropy maxima of 0.40) observed in all of the polymers could be due to a number of photophysical behaviours, including rotation of the chain, twisting or bending of the chain and excitation migration.

When a chain is unable to rotate, the observed change in dipole orientation could arise from conformational relaxation of the chain. Upon photoexcitation an excited state with the same geometry as the ground state is created. The excited state relaxes into a lower energy state by distorting the local geometry of the molecule. The relaxation would appear as a chromic shift and the new configuration will have a differently oriented transition dipole moment to the initial geometry (i.e. different from the absorption transition dipole moment) resulting in a loss of fluorescence anisotropy.

The resultant chromic shift, Stokes's shift, (shown in Figure 4.1), between absorption and fluorescence is made up of several possible components including the process described above, a possible shift due to chain flexibility and solvatochromic effects. It is not possible in these experiments to distinguish between the contributions of these processes to the overall chromic shift and therefore whether conformational relaxation is a fluorescence anisotropy loss process in PF2/6.

The excited states of conjugated polymers are excitonic. Excitons can migrate along the chain from one spectroscopic unit (or chromophore) to another of lower energy through incoherent hops (see Section 2.4 in Chapter 2). This process corresponds to a chromic shift in the emission spectrum from the absorption spectrum which would not be discernible from neither the Stokes's shift created by the flexibility of the PF2/6 monomer unit or from the solvatochromic effect of studying these materials in solution. Since the orientation of a transition dipole is determined by the chromophore's position along the flexible chain, exciton migration will also reorientate a dipole from its initial orientation (i.e. parallel to the absorption transition dipole) and reduce the fluorescence anisotropy (as explained in Chapter 2).

PF2/6 is has a significant Stokes's shift as seen in in Figure 4.1 which gives an indication of the electronic processes that can occur in the polymer. The polymeric version of PF2/6 has many possible chromophores along its length and excitation migration can occur to energetically lower states. Although this and intra-chain vibrations contribute to the inhomogeneously broadened absorbance spectrum and Stokes's shift, the major cause of the shift is attributed to the flexibility of the polymer. The PF2/6 monomer unit has only one methine bridge bond between adjacent phenyl rings and as such conformational relaxation (twisting) of the excited site can occur. Either conformational twisting or excitation migration exist in PF2/6 and could be responsible for the anisotropy recorded.

The anisotropy of PF2/6 was found to be dependent upon the excitation wavelength (Figure 4.4) indicating that the anisotropy loss is dependent upon excess energy. The anisotropy value increases almost linearly until it reaches a maximum plateau. This plateau region begins at the lowest excitation energy at which the anisotropy loss process can occur, i.e. there must be sufficient energy in the system for the loss process to be activated. Such processes, that do not occur at low excitation energies, are commonly referred to as a "red-edge" effect. Red-edge effects are common in organic compounds and the results in Figures 4.4, 4.6, 4.8 and 4.10 are all analogous to the results of site selective spectroscopy.[168] Thermal energy will affect both exciton motion, (limiting how far it is able to move) and conformational motion (simply by freezing out the vibrations that cause the relaxation of the excited state). When an initially excited state is created at a low energy site, the exciton cannot easily locate a nearby site of lower energy to migrate to within its excitation lifetime and, therefore, emission occurs from the initial site. By using low energy excitation wavelengths, which reduces the excess energy, a single electronic site can be probed with limited exciton hopping. Excess thermal energy will also assist the anisotropy loss process and exciton hopping. Thus at lower temperatures, the red-edge plateau region occurs at a shorter wavelength (i.e. the system saturates at a higher energy) as shown in Figures 4.4 and 4.8.

Typically, in low viscosity solutions, this dependency upon excitation energy is attributed to rotational motion of the molecule which causes the depolarisation. This is especially the case for small molecules such as perylene. When a small molecule can undergo rapid rotation in solution, all fluorescence anisotropy is lost as shown in Figure 4.3.

Figure 4.2 shows that there is incomplete fluorescence anisotropy loss in PF2/6. This only implies that this molecule does not rotate fully within its fluorescence lifetime. However, PF2/6 is a long chain compared with the small molecule perylene and is known to form an open coil structure in solution with a persistence length of twelve repeat units.[90] Its rate of rotation is approximately $10^6 - 10^5$ s^{-1} (from Figure 9 in ref.[90]) and, therefore, in a fluorescence lifetime of 400 ps, the molecule rotates through approximately 0.1 °. The long chain molecule can, therefore, be considered static in all solvents.

Since the anisotropy of PF2/6 is not at the inferred maximum value of the natural anisotropy of $\langle r \rangle = 0.32 \pm 0.04$ (value determined via extrapolation from Figure 4.5) at the red-edge the loss in anisotropy at these low energy sites must arise from a process other than exciton motion and rotation. It follows that at higher excitation energies, on the blue peak of the absorbance spectrum, the anisotropy loss is a combination of this "unknown" process and exciton migration.

The flexibility of PF2/6 suggests that this "unknown" anisotropy loss process is due to conformational relaxation and this was investigated in molecules with limited excitation migration. Oligomers comprised of only a few units cannot support as many spectroscopic units as a long polymer chain. It has been estimated that the spectroscopic unit of PF2/6 encompasses between eight and twelve monomer units.[90] Therefore the oligomers used here, of 10 and 20

units, can be considered to support one or at most two chromophores. Excitation migration to a lower energy site cannot occur simply because lower energy sites do not exist on these chains. When an oligomer is excited, the excitation is energetically constrained to remain in the initial site. The increased anisotropy value of smaller macromolecules, compared with PF2/6 support this explanation. The high value of anisotropy presented by $PF2/6_{N=10}$ shows that the sites available for migration are extremely limited, yet the fluorescence anisotropy is not at the theoretical maximum. Since the oligomers are considerably shorter than PF2/6, it is concluded that the presumption that they undergo negligible rotation is now erroneous. Indeed, the data in Figure 4.9 indicates that $PF2/6_{N=10}$ is rotating, although it does not undergo a complete rotation within its fluorescence lifetime like perylene. The shortest oligomer ($PFO_{N=3}$), must also rotate faster than the polymer in low viscosity solvents, yielding lower anisotropy values than $PF2/6_{N=10}$.

$PF2/6_{N=10}$ solutions of high viscosity solvents, hexadecane and decalin, reveals much higher anisotropy values (see Figure 4.10). The increased viscosity hinders rotation and the oligomer is almost stationary in these solvents during its fluorescence lifetime. Since excitation migration is not possible within $PF2/6_{N=10}$, the data suggests that there is only one site in this oligomer because of the similar trend in temperature dependency for all the excitation wavelengths as shown in Figure 4.8 and 4.11. It is worth noting that the natural anisotropy or the PF2/6 molecule and not the maximum 0.40, f is observed in the data from the oligomer in hexadecane. This suggests that there is an anisotropy loss process inherent to the PF2/6 monomer.

$PF2/6_{N=20}$ does not show the same temperature dependency as $PF2/6_{N=10}$ (comparing Figures 4.7 and 4.9) and can be considered stationary. Therefore, the anisotropy loss of the longer oligomer, $PF2/6_{N=20}$, can be attributed to an internal mechanism, e.g. twisting, that changes the orientation of the dipole, rather than molecular rotation.

It is concluded that only conformational relaxation can be responsible for the anisotropy loss in the oligomers when they are held in place with a high viscosity solvent.

The same conformational motion must also exist in PF2/6 since it contains the same monomer unit. $PF2/6_{N=20}$ and $PF2/6_{N=10}$ are almost linear chains; therefore, exciton migration along the chain should not change the anisotropy greatly. However, there is a significant variation in anisotropy with excitation wavelength; approximately 0.05 over the region $\lambda_{ex} = 370$ nm to 395 nm for both oligomers (note the error is $\pm$ 0.01). From equation 2.36 it is possible to calculate the angle between the absorption and emission transition dipoles for $\lambda_{ex} = 370$ nm and $\lambda_{ex} = 395$ nm (Example: $PF2/6_{N=20}$; $\theta_{370} = 38.9\,^\circ$ and $\theta_{395} = 35.7\,^\circ$). The difference in angle is approximately $3\,^\circ$ in both oligomers. This is the extra movement undergone by the transition dipole when it is excited with a high energy compared with when it is excited with low energy. The small difference highlights the importance of the conformation relaxation process.

The emission spectra from the polymer, PF2/6$_{N=20}$ and PF2/6$_{N=10}$, (Figure 4.1) are very similar, in energetic position and in structure, suggesting that excitation tends to a site of the same conjugation length regardless of overall molecular length. Given that conformational relaxation gives rise to the Stokes's shift in the oligomers, the emission must occur from a low energy conformational state, proving that both anisotropy processes (presumed to be excitation migration and conformational relaxation) occur in the polymer. In the PFO$_{N=3}$, a different low energy emission state exists reflecting its shorter conjugation length.

To confirm this hypothesis about the processes in the polymer, the temperature dependent results are considered. Excitation of the polymer at high energy wavelengths (in the blue region of the absorbance spectrum) yields temperature independent anisotropy profiles, indicating the process that causes the loss of anisotropy has a very low activation energy. Exciting the polymer with low energy wavelengths and thus effectively selecting specific sites on the chain results in a temperature dependent fluorescence anisotropy. The two different gradients confirm the idea of two separate anisotropy loss processes.

When repeated with the shorter oligomers, the temperature dependence is different (Figure 4.7) i.e. excitation at all energies yields fluorescence anisotropy which is temperature dependent. Since this can only be conformational relaxation in PF2/6$_{N=20}$, it can be deduced that this process is dependent on both the excitation and thermal energy. The temperature dependent behaviour of the oligomer is also apparent in the polymer when it is excited on the red-edge of the absorbance spectrum. This provides strong confirmation that the polymer does undergo conformational motion.

From the difference in the temperature dependent behaviour of the polymer and the oligomer, it can be seen that chain relaxation plays a very important role in the fluorescence anisotropy loss. In the case of the oligomers where exciton migration has little or no effect, a large thermally activated fluorescence anisotropy loss is observed and must be due to purely intramolecular relaxation. It is also noted that excitation on the blue peak of the absorption band also yields a lower value of $\langle r \rangle$, which indicates that these sites can structurally relax by a greater extent in the excited state or they are more distorted in the ground state. At the blue peak there is greater excess excitation energy available to assist the conformational relaxation process. Therefore, the excited state is able to undergo further twisting when excited at the blue peak than at the red-edge. The previous time-resolved work by Dias *et al.*,[54] indicated that the PF2/6 molecules planarises over its fluorescence lifetime as a result of torsional motion between adjacent phenylene rings.

Planarisation, on its own, should not reduce the anisotropy value because the proposed twisting motion is perpendicular to the chain axis and because the orientation of the emission transition dipole which is presumed to be along the chain backbone, it should therefore be unaffected. However, planarisation can act to extend a chromophore and therefore change its properties. Westenhoff *et al.*[81,82] postulated that the planarisation of a similar polymer, poly(dioctyl-bithiophene) (PDOPT), increased the conjugation length of the chromophore.

Extending the conjugation length to over additional bonds will change the shape of the excited state from the ground state. Any distortions that exist in the ground state conformation will directly affect the orientation of the absorption transition dipole. As the excited state encompasses more bonds, the effect of the distortion on the emission transition dipole will be less and therefore the transition dipole moments will no longer be parallel. The planarisation and its associated extension of the chromophore will therefore be observed as a loss of anisotropy.

For the long chain polymer, PF2/6, either Förster energy transfer or excitation tunneling between conjugation lengths gives rise to loss of anisotropy by excitation migration. The anisotropy loss due to this will be greater than that by any structural relaxation processes. Given that the experiments were carried out in dilute solution, these processes must be intra-chain but it is not possible to differentiate between them. Since PF2/6 is a loose coil it may be possible for excitations to undergo energy transfer between non-neighbouring chain segments if two parts of the chain come into close contact within the coil. However, clearly not all anisotropy is lost which indicates that this process is rather inefficient and clearly, singlet excitons have rather limited intra-chain mobility in the isolated chain regime.

4.6 Conclusions

The experiments described in this chapter have shown that fluorescence anisotropy can be used to probe single sites along conjugated polymer chains held in low viscosity solvents. This is achieved by using reduced temperatures and long chains which possess a long rotational time. Both techniques reduce the rotational motion of the molecule to a negligible level.

It is concluded from the results that the proposal of Dias *et al.*, that PF2/6 undergoes excitation migration and conformational twisting in the excited state, is correct. Conformational twisting occurs solely within oligomers of ten units or less because excitation migration cannot occur. Furthermore, low temperature single-site spectroscopy has been used to show that the natural anisotropy of PF2/6 is 0.32 ± 0.04 corresponding to an angle between the absorption and emission transition dipole moments (θ) of $21\,^\circ \pm 6\,^\circ$.

If the conformational motion can be removed completely, for example by using a rigid-rod like polymer, then the excitation migration along the chain and its anisotropy loss can be studied directly. In particular, the anisotropy loss related to extending the conjugation length in the excited state can be investigated. Therefore in the next chapter, the same experiments were carried out on two rigid ladder-type polymers to study their behaviour.

Chapter 5

Fluorescence Anisotropy of Ladder-type Poly(*para*-phenylene)

5.1 Introduction

This chapter describes the temperature dependent fluorescence anisotropy measurements carried out on two ladder type poly(*para*-phenylene) conjugated polymers which were published in the *Journal of Chemical Physics* under the title *On the angular dependence of the optical polarisation anisotropy in ladder-type polymers* .[169]

The previous chapter showed that anisotropy loss in poly[9,9-di(ethylhexyl)fluorene] (PF2/6) was due to a combination of electronic and physical processes, specifically: exciton migration and a conformational twist of the backbone. It was not possible to study either of these processes in isolation.

To solely investigate the excitation migration the study in Chapter 4 was repeated with a polymer that is rigid and, therefore, cannot twist. Ladder-type poly(*para*-phenylenes) (LPPP) are blue emitting conjugated polymers that have a similarly shaped emission spectrum to PF2/6 in the solution phase. LPPPs are planar ribbon-like molecules that have two bonds between each phenyl ring in their backbone whereas PF2/6 only has one (see Figures 2.25 and 2.26).[85,89] This double methine bridge limits (if not entirely eliminates) the torsional motion of the backbone. It is hypothesised here that any anisotropy loss would, therefore, be due to exciton migration or another unidentified electronic process.

To investigate the fluorescence polarisation loss, the steady-state fluorescence anisotropy results of two different ladder-type polymers (methyl-substituted ladder-type poly(*para*-phenylene)(MeLPPP) and poly(naphthylene-phenylene) (2,6-NLP)) are reported. By using dilute solutions of high viscosity solvents, inter-chain transfer and rotation of the polymer were eliminated, allowing only exciton transfer along the chain to be monitored in the experiments.

Low temperature fluorescence anisotropy measurements were used to estimate the natural anisotropy of the two polymers. This information is subsequently used in Chapter 6 as a baseline for locating the position of the absorption and emission transition dipole moments relative to the polymer backbone.

Another major result was finding that the excitation anisotropy profiles do not follow the same pattern as for PF2/6: instead of reaching a maxima on the red-edge, these polymers yield curves that are consistent with the vibronic structure of their absorption spectra. These results were used to investigate angular separation of the absorption and emission transition dipole moments as a function of the conjugation length distribution.

This chapter also contains the first report of the photophysics of 2,6-NLP. The initial absorption and emission results were used to confirm that this polymer is indeed rigid as has been claimed in the literature.[127]

5.2 Previous research

The photophysics of methyl-substituted ladder-type poly(*para*-phenylene) MeLPPP, has been extensively studied. MeLPPP, first synthesised in 1991, is a blue emitting polymer that reportedly has very few structural defects.[131,132] More importantly, it has a double methine bridge between neighbouring phenyl rings which limits torsional conformational motion and results in a planar configuration. This allows comparison with more flexible polymers such as PF2/6.

The rigidity of the polymer backbone also reduces the number of vibrational modes available in the chain. This reduces the inhomogeneous broadening of the absorption and emission spectra and gives a sharp well defined vibronic structure in both spectra. The rigidity of the polymer is also evidenced by a small Stokes's shift which shows there is little structural change in the excited state.

Due to its long side groups, , this polymer is not believed to form aggregates in solution (as explained in Chapter 2), so spectra are a result from excitons located on single chains.[45,119,128] The fluorescence spectrum from the polymer in the solid state is dominated by the same vibronic structure that is present in the solution spectrum. It has also been reported that there is a broad yellow emissive band (around $\sim$ 560nm)[45,119,131] from films which is absent in dilute solution. This is considered to be either an aggregate state[105,134] or an on-chain defect created through heating in air.[137] Aggregate states lower the fluorescence yield and will also facilitate rapid depolarisation of a system (see section 2.5.8 in Chapter 2).

Both MeLPPP and 2,6-NLP, are comprised of a linear array of chromophores. However, MeLPPP is thought to branch during synthesis which gives rise to chain segments at 60 ° to each other[67] (see Figure 2.12) which could cause the conjugation to break and new spectroscopic units (or chromophores) to form.

2,6-NLP is a newly synthesised polymer for which, it is believed, no photophysics has been reported prior to publication of this thesis. As can be seen in Figure 2.26 it has a different chemical structure from MeLPPP, however the rigid backbone is similar. The main difference between the polymers is that 2,6-NLP has a double phenylene group (or naphthalene group) in its monomer unit. This group should make the polymer backbone more rigid and less prone to branching defects but it will mean that the backbone is not totally linear.

5.3 Experimental

Sample preparation

The two different ladder-type poly(*para*-phenylene) polymers, methyl-substituted poly (*para*-phenylene) (MeLPPP) and naphthalene - substituted ladder-type poly (naphthalene -phenylene) (2,6-NLP) were investigated in dilute solution. Details of their synthesis can be found in Scherf *e*t al. (1992)[126] and Nehls *e*t al. (2005)[127] for MeLPPP and 2,6-NLP respectively. The organic solvent methylcyclohexane (MCH) was used and the absorption of the solutions was kept deliberately below 0.1 O.D. for MeLPPP (corresponding to a concentration of 5 mg/mL) and 0.05 for 2,6-NLP (corresponding to a concentration of 3 mg/mL). Such low concentrations were used to avoid reabsorption of the initially emitted photons. Reabsorption is a process known to lower the fluorescence anisotropy of the system (see section 2.5.8 in Chapter 2). Solutions were held in 10 mm quartz cuvettes.

Unaligned films of both polymers were spun from 10 mg/mL toluene solution as described in section 3.3.2. The typical maximum absorbance of these films was 0.3 O.D. at the absorption maximum.

Steady-state fluorescence anisotropy

Fluorescence anisotropy measurements were taken with the procedure outlined in Chapter 3 (specifically section 3.4.6). Anisotropy temperature profiles were made above the freezing point of MCH and just below its boiling point (in particular the temperature range between 220 K and 330 K was studied). Excitation anisotropy spectra were created by using excitation wavelengths across the polymer's absorption spectrum. This was done at room temperature ($\sim$ 290 K) and at 220 K.

5.4 Steady-state spectroscopy results and discussion

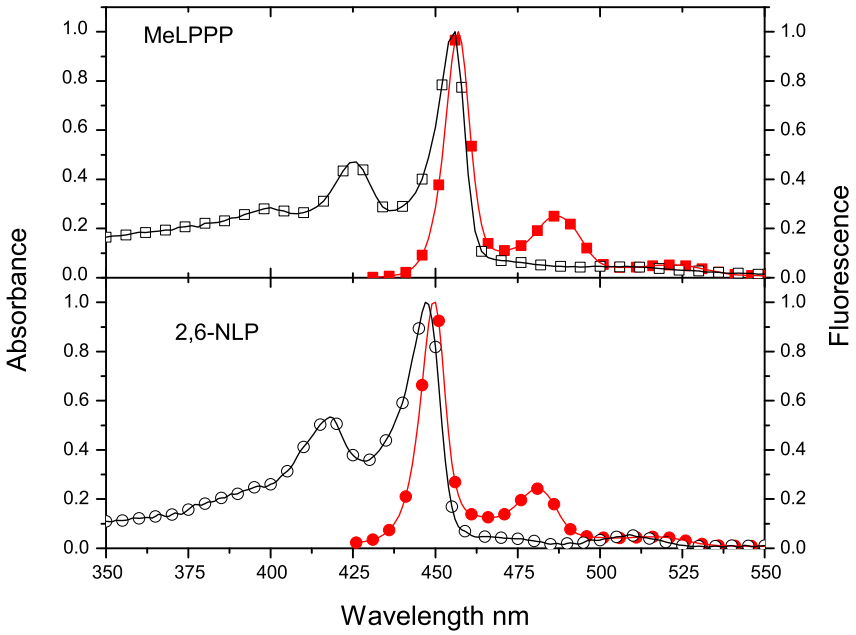

Figure 5.1: Absorption (open symbols) and emission (filled symbols) spectra of MeLPPP (Top: squares) and 2,6-NLP (Bottom: circles) in MCH at 20 °C. The excitation wavelength for both emission spectra was 420 nm. The figure shows the detailed vibronic structure of all the spectra and the $>$ 3 nm separation (Stokes's shift) between the absorbance and emission maxima of both polymers.

The absorption and emission (excitation wavelength of 420 nm) of both methyl- substituted ladder-type poly (*para*-phenylene) (MeLPPP) and naphthylene-substituted ladder-type poly (*para*-phenylene) (2,6-NLP) in methylcyclohexane (MCH) solution are shown in Figure 5.1.

There are several similarities between the spectra of the two polymers. Both absorption spectra and both emission spectra are well structured, the spacings of the vibronic shoulders are the same and the separation in wavelength between the main absorbance and emission is small for both polymers.

The absorption spectra of MeLPPP is narrow and well structured showing a small amount of inhomogeneous broadening. The absorption peaks in MeLPPP are located at 425 nm and 455 nm, the latter being the very strong 0-0 transition. The absorption spectrum of 2,6-NLP is similarly structured but is red-shifted by 5 nm from that of MeLPPP, with two maxima at 420 nm and 450 nm. The similarities in the absorption spectra, indicate that the ground state of these polymers is similar, not only in energy, because their absorbance maxima are close in wavelength, but also in structural conformation. Given that it is accepted that MeLPPP has a planar conformation[126,170,171] it can be assumed that 2,6-NLP has a similarly planar structure in the ground state.

The structure of the absorption spectrum of MeLPPP is mirrored in the emission spectrum of the polymer solution. Under excitation at 420 nm (shown in Figure 5.1), and indeed all excitation wavelengths across the absorbance spectrum (not shown), the emission spectra is narrow, well-structured and has a main emission peak (0-0 transition) and a vibronic replica. In MeLPPP, the main peak and replica are at approximately 457 nm and 487 nm respectively.

The emission spectra of 2,6-NLP is similarly an almost mirror image of its absorbance spectrum. Like MeLPPP, it has a main emission peak and a first vibronic replica at 453 nm and 483 nm respectively. The 0-0 transition dominates in both the absorption and emission spectra and the vibronic spacings in the ground and excited states are similar suggesting adherence to the Mirror Rule (see section 2.5.2 for full details). This further confirms that the conformation of these two states in MeLPPP and 2,6-NLP are structurally similar and that there is very little, if any, motion of the polymer's backbone.

The difference in energy between the absorption peak and the emission peak is called the Stokes's shift and is classically taken as a measure of the conformational relaxation energy within a system, (see section 2.5.2). However, in conjugated polymers, excitation energy migration or other ultra-fast electronic processes supplement the relaxation process and increase the difference between the absorption and emission energies. Since this difference in the ladder-type polymers is very small relative to a spectral shift of ~ 1 nm in MeLPPP and ~ 3 nm in 2,6-NLP, the contribution of these processes to the apparent Stokes's shift must also be very small. It is thus a confirmation of the polymer's limited conformational motion.

This small Stokes's shift could also be created by limited energetic relaxation of the excited state. If the excited state relaxes to a more energetically stable state of lower energy, it is appears as a large energetic shift of the emission maximum from the absorbance maximum. Instead, the results here (Figure 5.1), showing a very small spectral shift between the 0-0 transitions, suggest that the excited state is in an energetically stable form and the energy of the excited state does not change from creation to emission. The results also confirm that there is little structural relaxation of the chain in the excited state, thus confirming that the polymer is rigid. It does not prove that the exciton is unable to move to an energetically lower state, but it does prove that if there is exciton migration, the change in energy is small.

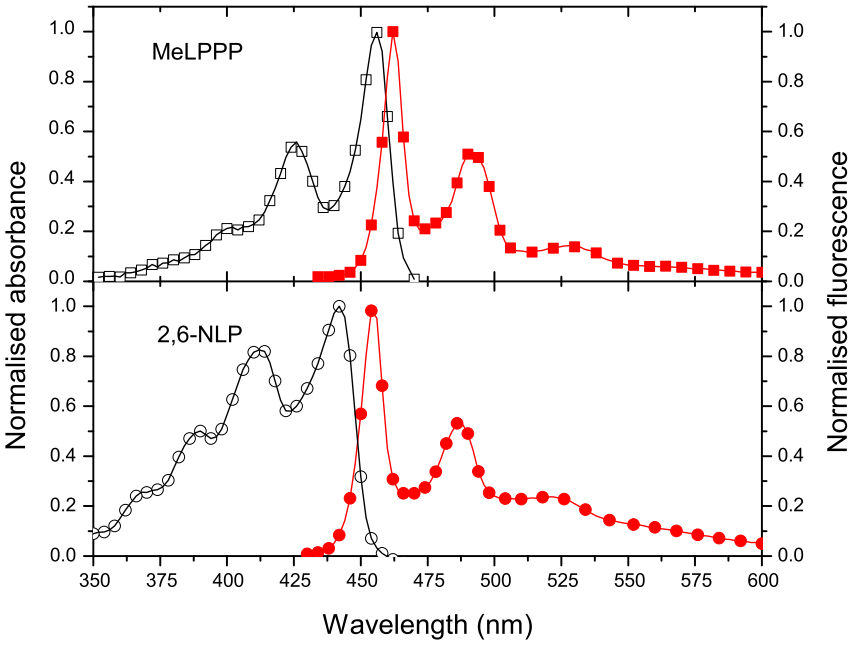

Figure 5.2: Absorbance (empty symbols) and emission (filled symbols) spectra of MeLPPP (Top: squares) and 2,6-NLP (Bottom: circles) in thin spun cast films at 20 °C. The excitation wavelength for both emission spectra was 430 nm. The figure shows the detailed vibronic structure of all the spectra and the $>$ 3 nm separation (Stokes's shift) between the absorbance and emission maxima of both polymers.

Figure 5.2 shows the absorbance and emission spectra of thin spun cast films of MeLPPP and 2,6-NLP. Again the spectra of the two polymers are similar in structure. The absorption and emission spectra of the films show a slight blue-shift relative to that in solution. The films do not show a broad peak in the yellow, characteristic of aggregate or defect effects, but the main emission peak is subject to reabsorption and is reduced in intensity compared with that of a solution. The simple spectra here have established the rigidity of the ladder polymers and that the solution and the solid-state samples investigated are free from aggregated defects.

5.5 Fluorescence anisotropy results

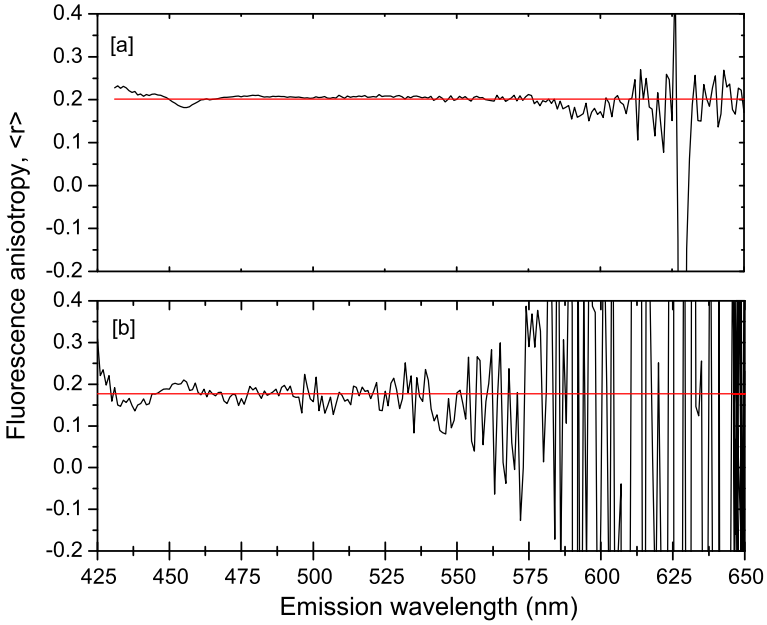

Figure 5.3: (a) Fluorescence anisotropy of MeLPPP in a solution of MCH excited at 420 nm. The average value of anisotropy $\langle r \rangle = 0.20 \pm 0.01$ is indicated with a straight line. (b) Fluorescence anisotropy of 2,6-NLP in a solution of MCH excited at 420 nm. The average value of anisotropy at $\lambda_{ex} = 475$ nm, $\langle r \rangle = 0.18 \pm 0.01$, is indicated with a straight line. The noise at the very edge of the spectra is caused by low emission in this region.

Figures 5.3 (a) and (b) show selected fluorescence anisotropy spectra of the polymer-MCH solutions when excited at 420 nm. There are some significant differences between the fluorescence anisotropy results of the two polymers. The anisotropy of MeLPPP (Figure 5.3 (a)) is constant, within experimental error, across the whole of its emission spectrum and, as such, by averaging the values over a wide emission wavelength range (460 nm - 500 nm) the anisotropy was determined to be $\langle r \rangle = 0.20 \pm 0.01$. This procedure was not possible for 2,6-NLP, as the emission anisotropy spectrum is more noisy (Figure 5.3 (b)). Therefore the anisotropy was determined by averaging over a smaller emission wavelength range. The noise at the long wavelength end of the spectrum is due to the low emission intensity from this polymer. In subsequent work reported in this thesis, where the excitation wavelength is varied, the anisotropy value used was always taken at $\lambda_{em} = 485$ nm (unless otherwise stated), which is on the edge of the secondary maximum of its fluorescence spectrum. Also, the anisotropy value in this region showed the least variation. In Figure 5.3 (b), $\langle r(\lambda_{ex=420nm}) \rangle = 0.18 \pm 0.01$.

It is noted that in Figure 5.3 the anisotropy deviates slightly from the 'average', that is indicated with a red line, in the emission wavelength range between 425 and 450 nm. This wavelength range corresponds to the absorbance region of the two polymers, where there is very little emission. The fluorescence intensity here is very low and as such the associated errors will be larger than for other parts of the spectra.

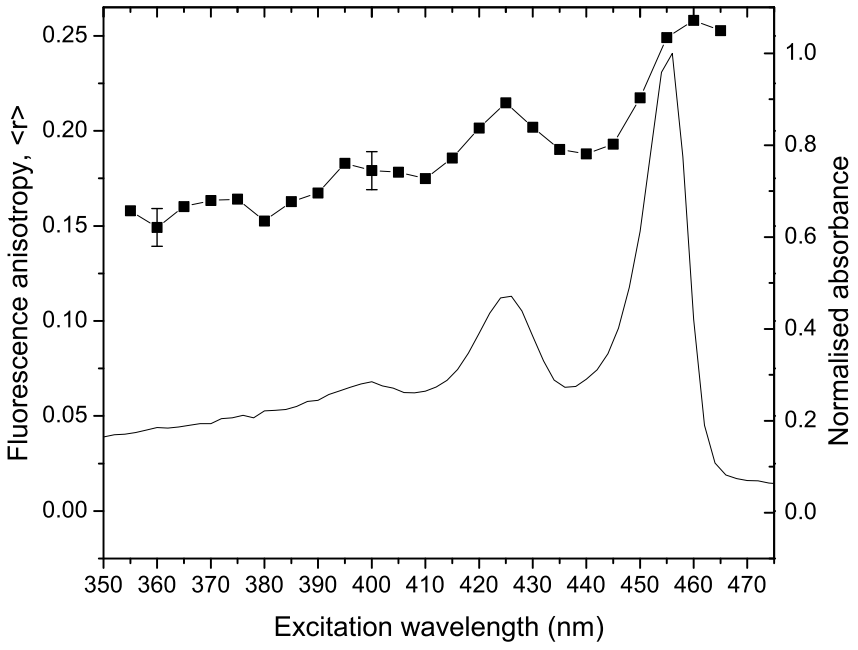

Figure 5.4: Excitation anisotropy spectrum of MeLPPP in a solution of MCH at 290 K (squares) with the normalised absorption spectrum. Representative error bars are shown on the graph.

By varying the excitation wavelengths, excitation anisotropy spectra for the polymers were created and the results are shown in Figures 5.4 and 5.5. The spectral position of the emission is independent of the excitation wavelength but Figure 5.4 shows that the fluorescence anisotropy of MeLPPP in MCH at room temperature is clearly wavelength dependent. There are two distinct peaks in the excitation anisotropy spectrum, at $\lambda_{ex} = 425$ nm and $\lambda_{ex} = 455$ nm, separated by a region of even greater loss in fluorescence anisotropy (between 435 nm to 445 nm). All of these features correspond directly to the polymer's absorption spectrum. The fluorescence anisotropy values for these peaks are not equal (detailed in Table 5.1) and these values of anisotropy correspond to different angles between the absorption and emission transition dipoles (these can be calculated via eq.2.36) and are also presented in Table 5.1.

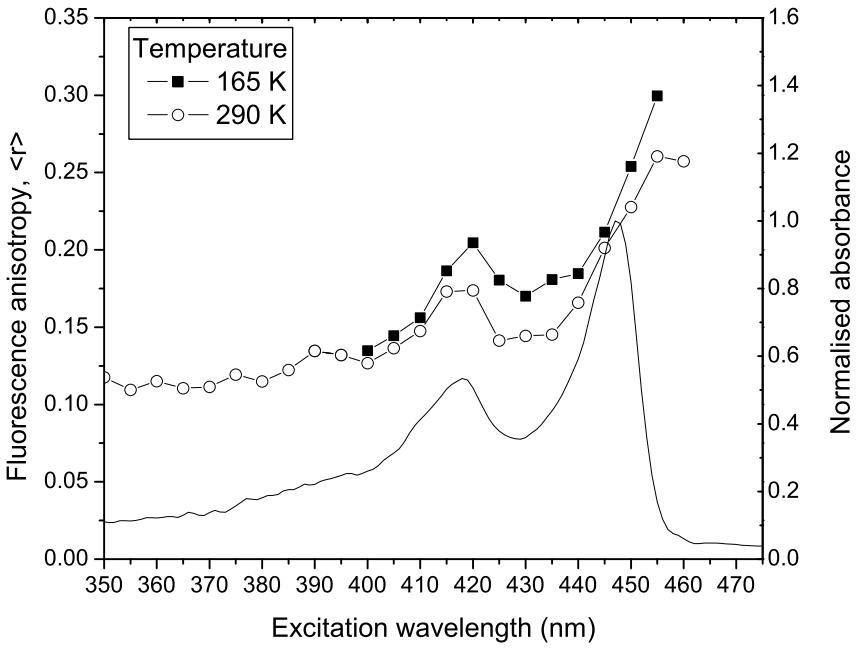

Figure 5.5: Excitation anisotropy spectrum of 2,6-NLP in a solution of MCH at 290 K (circle) and 165 K (squares) with the normalised absorption spectrum. Representative error bars are shown on the graph.

The same excitation wavelength dependent behaviour is seen in 2,6-NLP (Figure 5.5). The excitation anisotropy spectrum, at both room temperature (290 K) and at a significantly lower temperature (165 K), follows the shape of the absorption. The peaks in the room temperature activation spectrum for 2,6-NLP occur at $\lambda_{ex} = 420$ nm and $\lambda_{ex} = 450$ nm. At both temperatures, the two anisotropy peaks have different values meaning that the angles between the absorption and emission transition dipoles as detailed in Table 5.1.

The plateau region between the two peaks lies between 425 nm and 435 nm and the fluorescence anisotropy value in this region there is also dependent upon the temperature. The fluorescence anisotropy values and the angle between absorption and emission transition dipole moments as calculated using equation 2.36 are presented in Table 5.1.

It is worth noting that Figures 5.4 and 5.5, corresponding to MeLPPP and 2,6-NLP, are direct analogues of the excitation anisotropy spectrum data shown in Chapter 4 which relate to the non-ladder, flexible polymer PF2/6. Both ladder-type polymers present higher red-edge anisotropy values than PF2/6 ($\sim 0.26 \pm 0.01$ for MeLPPP compared with 0.13 ± 0.01 for PF2/6.) The other main difference is the shape of the excitation wavelength dependency. The ladder polymers do not show the smooth curve that PF2/6 follows. Instead, they present an anisotropy curve that follows the vibronics of MeLPPP.

Fluorescence anisotropy (and associated angles) of MeLPPP

Temperature	Peak (λ_{ex} = 425 nm)	Low Energy Plateau (λ_{ex} = 435-445 nm)	High Energy Plateau (λ_{ex} = 455 nm)	Angular Difference
290 K	0.21 (34 °)	0.18 (36 °)	0.25 (30 °)	6 °

Fluorescence anisotropy (and associated angles) of 2,6-NLP

Temperature	Peak (λ_{ex} = 420 nm)	Low Energy Plateau (λ_{ex} = 425-435 nm)	High Energy Plateau (λ_{ex} = 460 nm)	Angular Difference
290 K	0.17 (38 °)	0.14 (41 °)	0.26 (29 °)	12 °
165 K	0.20 (35 °)	0.17 (38 °)	0.29 (25 °)	13 °

Table 5.1: Steady-state fluorescence anisotropy values for MeLPPP and 2,6-NLP in dilute solutions of MCH. The angle between absorption and emission transition dipole moments, calculated via equation 2.36, is given in brackets. The angular difference corresponds to the difference between the high and low energy plateaux. The error on the anisotropy is ± 0.01. These show that as the temperature decreases the angle between absorption and emission similarly decreases.

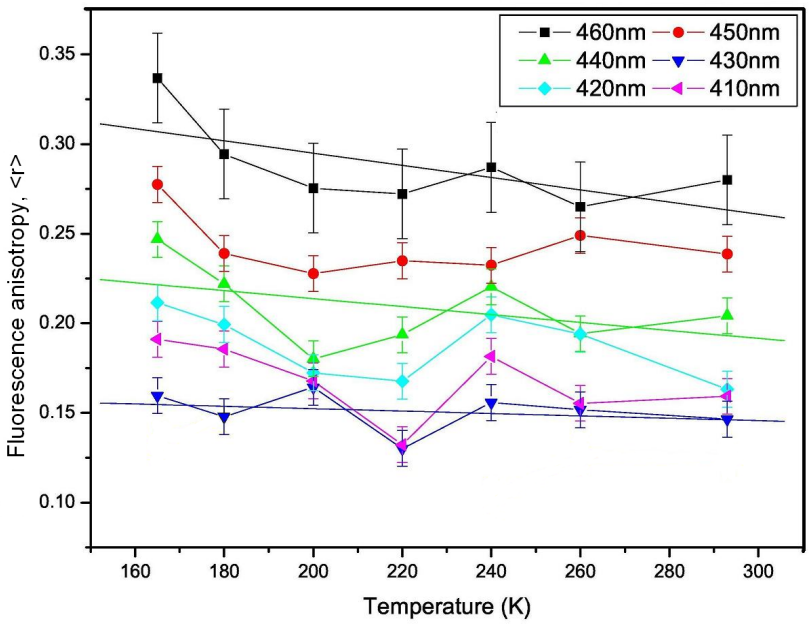

Figure 5.6: Anisotropy temperature profiles of 2,6-NLP in MCH for different excitation wavelengths ranging between 410 nm to the red-edge at 460 nm. Linear trendlines and representative error bars are shown on the graph.

There is a very slight increase in fluorescence anisotropy as the temperature is reduced in 2,6-NLP (shown in Figure 5.6). This temperature dependence is seen for all excitation wavelengths, but it more pronounced at the low energy excitation wavelengths. Excitation at low energy creates a red-edge effect similar to that seen in Chapter 4, Figure 4.4. It means that a single site is probed and therefore fluorescence anisotropy values will tend to the natural anisotropy of the polymer. The natural anisotropy for 2,6-NLP at $\lambda_{ex} = 460$ nm has been estimated as 0.36 ± 0.05 corresponding to an angle of $15° \pm 15°$ (via equation 2.36) between the absorption and emission transition dipole moments. The large error in the angle arises from the extrapolation of the experimental data. Conversely, fluorescence anisotropy in polyfluorenes only shows temperature independence for the peak emission wavelength and a temperature dependence at the red-edge of the absorption spectrum (Figures 4.4, 4.6 and 4.8 in Chapter 4).

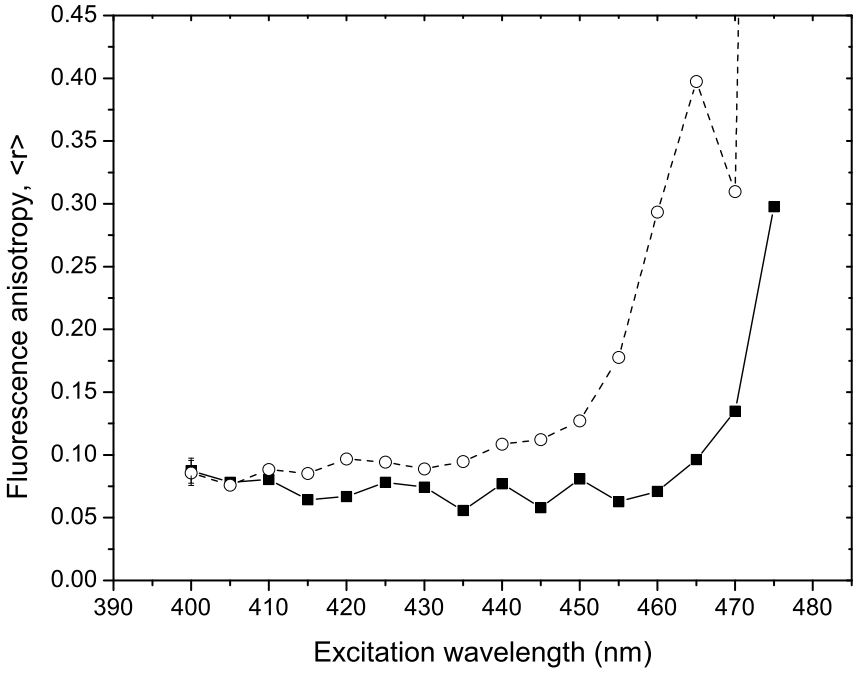

Figure 5.7: Excitation anisotropy spectra of MeLPPP (squares) and 2,6-NLP (circles) as spun cast films. The graph shows that the fluorescence anisotropy is very low until the on-set of the red-edge. These low fluorescence anisotropy values at the lower excitation wavelengths arise from the molecules lying in the plane of the film.[73] It also shows that the data from spun films do not have the same structure as that from dilute solutions shown in Figure 5.4 and 5.5. The emission wavelength is 485 nm for both films. Representative error bars are shown on the graph.

In spun cast films of both polymers, all the emission wavelength dependent anisotropy is lost resulting in flat excitation anisotropy spectra up to the onset of the red-edge effect, as shown in Figure 5.7. The low anisotropy value, approximately 0.1, is independent of excitation wavelength in contrast to the results from the polymers in solution. If an orientation of the polymer chains is imposed, the polymer's anisotropic nature can be investigated further through polarised spectroscopy. This is presented in the following chapter where the polymers are incorporated into polyethylene films and then mechanically stretched.

5.6 Discussion

Fluorescence anisotropy measures the average angle between the absorption and emission transition dipole within a polymer system giving vital information about the excitation migration from the initially excited absorption site to the lower energy emission site. Without excitation migration, or other processes (molecular rotation or conformational change), then a constant anisotropy value across the excitation spectrum with a value close to the theoretical maximum (0.40) would be expected. This would indicate the presence of only one type of chromophore with a transition dipole moment orientation very close to that of the absorption.[51,172] If rotation and conformational relaxation (twisting of the backbone) can be eliminated, then any loss of anisotropy can be used to describe the exciton motion.

The narrow and highly structured absorption and emission spectra of MeLPPP and 2,6-NLP shown in Figures 5.4 and 5.5 have already been used to establish that the ladder polymers are rigid. Their structure limits any conformational motion of the backbone and reduces torsional motions and hence the inhomogeneous broadening due to vibrations.

The previous work on short chain polymers in Chapter 4 has been used to show that polymers of greater than 20 monomer units in length do not undergo appreciable rotation during their fluorescence lifetime. It is estimated that the ladder-type polymers may have rotated through approximately 0.1 ° in their fluorescence lifetime.[90] Whilst this loss should only be a small background loss, it will be present in all measurements and could explain some of the deviation from the maximum anisotropy (0.40) even at low temperatures. Some fluorescence anisotropy may also be lost through reabsorption or scattering of the emitted light (see Chapter 2, section 2.5.8). However, the majority of the anisotropy loss, equivalent to $\sim 15\,^{\circ}$, must be due to a process that is electronic in origin especially in 2,6-NLP, which only has an average of twenty-one units. As the conjugation length is approximately twelve units in length it is unlikely that a polymer chain can support more than one chromophore and thus excitation migration will be unlikely to occur.

Another common cause of anisotropy loss is aggregation. MeLPPP and other ladder polymers can form yellow emitting aggregates in the solid state, these are absent in dilute solution[45,105,119,131,134] (see Figure 5.1) and the absorption spectra of the polymers appears similar to those produced by J-aggregates. (J-aggregates are typically identified by a narrow and well structured intense absorption that is red-shifted with respect to the monomer unit.[70]) However, recent work in the OEM Group, Durham University, has shown that the fluorescence spectrum of MeLPPP is comprised entirely of vibronics, even in the solid state. These vibronics were linked to specific bond vibrations for a single chain.[173] Since the fluorescence spectrum mirrors the absorption spectrum (shown in Figures 5.1 and 5.2) it can be assumed that the structure in the absorption spectrum is a result of vibronic modes and not due to J-aggregates.

It has also been found that higher concentration solutions have lower anisotropy (not shown) which is comparable with that of the spun films. This large depolarisation (loss in anisotropy) which can be considered a change in dipole orientation shows the presence of inter-chain interactions at high concentrations but not at the low concentrations used in this work. It can therefore be safely assumed that the polymer does not form large aggregates in the highly dilute solutions.

However, the possibility of dimer (two molecules held together with inter-molecular forces) or small aggregate formation at such low concentrations cannot be ignored. If the emission occurs from isolated single molecules or small tightly-bound aggregates, the temperature independence of the emission spectra suggest that any energy transfer must be an intra-molecular process that is intrinsic to this conjugated polymer. The excitation dependent behaviour of the anisotropy (Figures 5.4 and 5.5) must, therefore, be attributed to either the chain or to the small aggregate.

The shape of the excitation anisotropy spectrum of 2,6-NLP (Figure 5.5) is unchanged by reduced temperatures. It can be deduced that the anisotropy loss is not associated with thermal excitation of the backbone (i.e. conformational relaxation), which is consistent with the ladder polymers being rigid systems, and that fluorescence anisotropy loss is a fundamental electronic process. Electronic processes, such as exciton migration, are not limited by thermal energy.

The excitation anisotropy spectra of MeLPPP and 2,6-NLP, with their two apparent peaks, are most unlike the excitation anisotropy spectrum of the poly (9,9-di-ethylhexyl) fluorene oligomers which show only one broad peak (see Figures 4.6 and 4.8 in Chapter 4). PF2/6$_{N=20}$ presents a steady increase in anisotropy with excitation wavelength until it reaches a plateau (saturation point) which was explained in the previous chapter as a form of site-selectivity. In the ladder polymers investigated here, the site-selective behaviour of the major electronic transition is dissimilar to that found in PF2/6 (shown in Figure 5.4 and 5.5). The expected smooth curve is interrupted by a large loss of anisotropy in the regions between the two absorption peaks at λ_{ex} = 435 - 445 nm in MeLPPP and λ_{ex} = 425 - 435 nm in 2,6-NLP.

A plateau of constant fluorescence anisotropy is most commonly used to identify electronic transitions in small molecules.[167,174–177] In most of those cases it was known that there were two or more transitions and fluorescence anisotropy measurements were used to measure the angle between them. The ladder polymers are comprised of a narrow distribution of conjugation lengths each of which could be considered to be a separate transition. Therefore the ladder polymers can be considered to support a series of electronic transitions. The measurements here (Table 5.1) show that the upper and lower energy limits of the electronic transitions have an angle of approximately 6 ° (for MeLPPP) and 13 ° (for 2,6-NLP) between them.

Figure 5.3 shows that the emission anisotropy of the ladder polymers is constant for a single excitation wavelength. This indicates that there is only one emission site along the polymer chain. A second transition with a different transition dipole moment to the first would appear as a region with a different emission anisotropy value.[51] Therefore in this case, the difference in excitation anisotropy across the absorption spectrum must arise from an angular dependence of the absorption transition dipole moment.

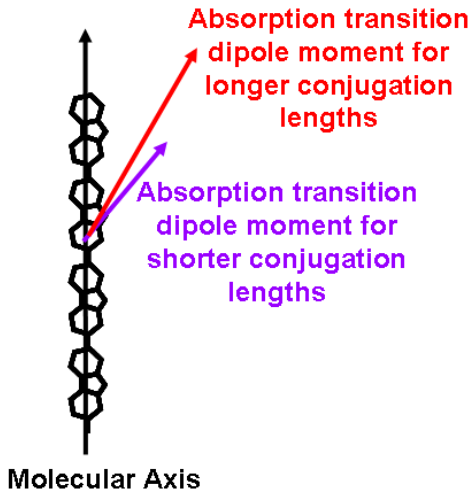

Figure 5.8: Schematic to show the possible orientation directions of the absorbance transition dipole moment for the shortest conjugated lengths and the longest conjugated lengths, i.e. upper and lower units of the conjugated length distribution. The data contained in this chapter, shows that the distribution of conjugated lengths have a localisation angle between 0 and $\sim 10^\circ$ dependent upon the conjugation length. The localisation angle is the angle between the absorbance transition dipole moment and the backbone.

The evidence here gives the limits of the the angular dependence of the absorption transition dipoles for the conjugation length distribution. The upper energy limit (shortest conjugation length) is located approximately 10° from the lower limit (longest conjugation length) as shown in Figure 5.8.

The region of strong absorbance at approximately 420 nm in the absorption spectra of the ladder polymers is due to the first vibronic replica of the electronic transition. Both peaks are broadened by the small distribution of available conjugation lengths. (The conjugation length is small due to the low polydispersity of the polymer.). The replication of the vibronic states is the explanation for the observed extra peak in the excitation anisotropy spectra (Figures 5.4 and 5.5.). Instead of seeing just one red-edge effect (as with PF2/6 in the previous chapter) there is one for every red-edge of each vibronic replica. The presence of multiple vibronic replicas will disguise the red-edge of each adjacent replica, lowering the observed fluorescence anisotropy value. The short conjugation length limit is also masked by the influence of an adjacent replica. However the data does show that there is a range of angles across the conjugation length distribution. The same effect is observed in PF2/6, i.e. is there is a range of absorption angles across the conjugation length distribution. However, inhomogeneous broadening has masked the effect of multiple red-edge effects to produce smooth anisotropy curves.

Both MeLPPP and 2,6-NLP show relatively high values of anisotropy (0.26 ±0.01) at room temperature at their emission maxima (Figures 5.4 and 5.5). This value increases as the temperature decreases and the natural anisotropy of the polymer 2,6-NLP was estimated to be 0.36 ± 0.05. This corresponds to a very small angle between the absorption and emission transition dipole moment orientations, implying that at this low energy edge, the dipole moments are almost parallel. However, as the excitation energy increases the angle between the absorption and emission transition dipoles meaning that they cannot both be parallel to the molecular axis (see Figure 5.8). The reason for this must be electronic in origin because other anisotropy loss processes (twisting, rotating and aggregation) have already been ruled out.

The origin of electronic transitions in conjugated polymers has been debated for many years and photoconductivity investigations have yielded some promising answers. Studies by Köhler *et al.*[178] on the conjugated polymer in poly(2-methoxy-5-(2'-ethylhexyloxy)-*p*-phenylene vinylene) (MEH-PPV) revealed the possibility of localised and delocalised transitions depending upon where the transition originated. Off-axis transition dipole moments are thought to arise from transitions from localised states to delocalised states (or vice-versa) which give rise to substantial photocurrents. Large photocurrents have been observed in MeLPPP[128] so, it can be assumed that transitions from localised to delocalised states can occur in this polymer. If it is assumed that the emission transition dipole moment is oriented along the chain axis[a], the results here suggest that shorter conjugation lengths, which have been found to be approximately 10 ° off-axis, are localised in the ground state. The excited state is therefore more delocalised and oriented with the molecular axis. As discussed above, the absorption transition dipole moment orientation angle decreases with the excitation energy until it is parallel to the emission transition dipole moment which is assumed to be along the axis. This implies that as the excited state increases in length it lies parallel with the molecular axis.

It was hypothesised in the previous chapter that as an electronic state grew in size, it encompassed more of the polymer backbone and changed the orientation of the transition dipole moments associated with it. It is therefore implied that the atomic structure of the backbone will also play a part in the orientation of the transition dipole moments it supports.

Due to its naphthylene ring, the conjugated polymer 2,6-NLP is subject to a small deviation along the monomer unit (shown in Figure 2.26), which in turn results in a small step-like pattern along the backbone. It is likely to be the absorption transition dipole moment of its shorter conjugation lengths is more influenced by this structural motif, whereas, as the conjugation length increases over more carbon-carbon bonds the influence of the step-like pattern is reduced, leading to a dipole oriented more along the chain.

[a]The assumption that the emission transition dipole moment is parallel to the molecular backbone is based on the fact that conjugation is along the molecular axis. However, to confirm the above hypothesis, it was necessary to investigate the relationship between the two transition dipoles and the backbone. This was done in Chapter 6 and it was found that the emission transition dipole is parallel to the molecular axis.

Whilst the monomer unit of MeLPPP is straighter than 2,6-NLP, during its synthesis the polymer chain growth is not consistently linear in direction. Directional change occurs at regular intervals producing kinks in the backbone. The angle between the backbone segments is approximately 60° due to the fused nature of the polymer backbone (as discussed in Chapter 2, section 2.6.2.). Single molecule studies of MeLPPP have proposed that this kink results in neighbouring chromophores with dipole moments that are at large angles[67,130] (shown in Figure 2.12) which would provide considerable depolarisation if viewed on a small scale. Such large angular changes were not observed here because the fluorescence anisotropy is measured for an average of many molecules in a solution. The naphthylene ring in 2,6-NLP causes the dipole to lie further off axis in the monomer unit than the MeLPPP resulting in a larger angle between the long and short conjugation length limits.

Recent work on MEH-PPV has also discovered an ultrafast dipole reorientation that is thought to be caused by a structural relaxation of the chain.[48] It was proposed that dynamic localisation of the exciton arises from the fact that the ground state can undergo torsional motion. MeLPPP and 2,6-NLP are rigid and cannot undergo such structural changes and this suggests that as the wavefunction delocalises along the polymer chain, the transition dipole evolves with it. It is proposed here that the dipole of the monomer unit is oriented off-axis but as the number of monomer units encompassed by a wavefunction increases the influence of individual monomer units becomes diluted and the overall dipole is governed by the alignment of the backbone. This will result in a rapid depolarisation as the excitation moves to a more energetically stable state. This process would be augmented by structural relaxation in flexible polymers and result in a much greater anisotropy loss.

5.7 Conclusion

This chapter has described the first photophysical results of the newly synthesised ladder-type polymer poly(naphthylene-phenylene) (2,6-NLP). The chapter has also investigated the fluorescence anisotropy excitation spectra of dilute solutions of two ladder-type polymers, MeLPPP and the newly synthesised 2,6-NLP. The results are different from the previously observed behaviour of the flexible conjugated polymer, PF2/6, described in Chapter 4. These earlier results indicate that the anisotropy loss was due to a combination of excitation migration and conformational relaxation. By using rigid-rod ladder-type polymers, which cannot undergo conformational relaxation, it has been possible to study the fluorescence anisotropy loss only as a result of pure electronic on-chain processes.

The ladder-type polymers present a wavelength dependent excitation anisotropy spectrum that follows the vibronics of the polymers absorption (excitation) spectrum. This indicates that the angle between the absorption and emission transition dipole moments changes with wavelength. The anisotropy is independent of emission wavelength indicating that the difference arises from an angular dependence of the absorption transition dipole moment across the distribution of possible conjugation lengths.

This is consistent with the absorption transition dipole moment for shorter conjugation lengths being off-axis (i.e. oriented away from the polymer backbone). These off-axis transition dipole moment indicates that the ground state is localised and that the excited state is delocalised.

The shape of the anisotropy was unchanged by temperature and lowering the concentration of the solution increased the anisotropy providing further confirmation that this property is an intra-chain property. It is noted that whilst the experiments were carried out in dilute solutions, it was not entirely possible to eliminate the possibility that the polymer forms dimers or small aggregates. Though the effect of these is thought to be small.

Low temperature anisotropy results have provided a value for the natural anisotropy of 2,6-NLP is 0.36 ± 0.05 which will be used later in this thesis.

If the polymers can be held in an aligned matrix it will be possible to investigate the angle of the absorption transition dipole for the longest and shortest conjugation lengths relative to each other and to the polymer's backbone. It will also be possible to confirm that the angle the emission transition dipole moment is parallel to the backbone. This is fully detailed and discussed in the next chapter.

Chapter 6

Locating the Absorption and Emission Transition Dipole Moments

6.1 Introduction

This chapter contains the details and results of experiments undertaken to determine the orientation of the absorption transition dipole moments in three conjugated polymers. Poly (9,9-di(ethylhexyl)fluorene) (PF2/6) and two ladder-type poly (*para*-phenylene)s (MeLPPP and 2,6-NLP) were incorporated into aligned polyethylene matrices and these films were investigated by a number of techniques including x-ray diffraction. The x-ray diffraction study of the orientation of PF2/6 is part of a collaborative research project that has culminated in the journal paper entitled *A concentration effect on the oriented microstructure in tensile drawn polyfluorene-polyethylene blend* which has been accepted for publication by Macromolecules in 2009. This chapter specifically details the physical analysis undertaken to determine the orientation of the absorption transition dipole moment relative to the polymer backbone, (an angle denoted by α, see Figure 6.1) of the conjugated polymers.

Steady-state fluorescence anisotropy has already been used to determine that there is an angular separation of the absorption and emission transition dipole moments (the natural anisotropy) of these polymers. To understand the fundamental relaxation processes of excitons on these conjugated backbones, it is essential to know the angle of the absorption transition dipole moment relative to the backbone.

The extra information on the angle, α, combined with the natural anisotropy results of Chapter 5 will also locate the orientation of the emission transition dipole moment relative to the backbone. This will help to explain the changes that occur as the ground state develops into the state which emits light. An angular change between these two states will be indicative of a change in localisation of the exciton.

6.1.1 Brief background

In an aligned polymer film there are three angles that need to be determined before a discussion of the change in exciton localisation can be carried out. These are schematically shown in Figure 6.1 and are: the angle between the absorption and emission transition dipole moments (θ); the angle between the absorption transition dipole moment and the polymer backbone (α) and, the angle between the polymer backbone and the alignment direction (ε). This chapter reports on experiments used to find angle ε and hence α. The natural anisotropy, θ, having already been measured in earlier experiments (Chapters 4 and 5).

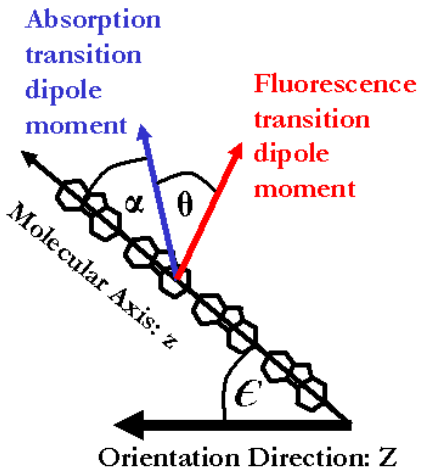

Figure 6.1: Schematic to show the molecular directions and angles between the transition dipole moments. The angle between the macroscopic alignment direction and the polymer backbone is denoted ε and can be determined through x-ray diffraction, Raman spectroscopy and polarised fluorescence. The angle α between the backbone and the absorption transition dipole moment is determined through linear dichroism spectroscopy and the angle θ between the absorption and emission transition dipole moment is found by fluorescence anisotropy. θ for the polymers investigated in this thesis have already been found in Chapters 4 and 5

The angle ϵ between the alignment direction and the polymer backbone has been determined by three different experimental techniques: not all were used for all the polymers. X-ray diffraction was used to study all the films; Raman Spectroscopy was used for a MeLPPP film and polarised fluorescence was used for each polymer. Three different techniques were used because of the suitability for the samples involved. X-ray diffraction allows for the study of long range order in a sample. Polarised Raman spectroscopy studies short range order relating to the position of known bonds in the molecule: when that piece of information is not available, then a fluorescence anisotropy technique can be used to study short range order. Each of these techniques measures the order parameter, Φ, (as defined in Chapter 2, equation 2.19). The techniques are dealt with in separate sections. Each of these sections include a brief explanation of the background and theory, the results and a discussion of them.

The angle α between the polymer backbone and the absorption transition dipole moment has been determined using a polarised absorption technique called linear dichroism. This technique finds the difference in absorption parallel and perpendicular to an alignment direction. An existing experimental set-up was adapted and the control program altered to measure the linear dichroism directly. It was also necessary to verify the results using a commercially available spectrometer. A separate section holds the background, theory, results and discussion of the linear dichroism experiment.

The results from these experiments were combined with the angles between the absorption and emission transition dipole moments determined in Chapters 4 and 5 to describe the electronic process that occurs in a polymer after excitation with light. The results of all the separate sections are brought together in a final discussion section.

6.2 Determination of the order parameter via x-ray diffraction.

Having made stretch aligned films via the technique described in Chapter 3 it was important to quantify the degree of alignment within them. This was done by determining the order parameter of the films. X-ray diffraction is a technique that has been used to study the long range order in many materials including polymer films.[179,180]

6.2.1 Introduction to x-ray diffraction

X-ray scattering can be used to investigate a great number of phenomena including one of the more famous twentieth century scientific discoveries; the structure of DNA; many other applications can be found in standard texts e.g.[181–184] The technique of x-ray diffraction has also been used to investigate the long range order of crystals by observing x-rays scattered from planes of atoms. The improvements of experimental methods and high energy, high flux x-ray sources (synchrotrons) has made it easier to study structures and contribute to various scientific fields.

The basic theory of x-ray diffraction relies on elastic scattering from atoms in a sample that lie in crystal planes. The waves scattered from multiple crystal planes can interfere constructively if the path difference for the light is a multiple of the wavelength used. Bragg's Law[13,185] describes the scattering pattern that arises from the constructive interference:

$$n\lambda = 2d\sin\theta \tag{6.1}$$

where λ is the wavelength of light, d is the separation of the crystal planes and θ is the angle of incidence (to the crystal plane). It is usual, in x-ray diffraction, to work with scattering vectors and reciprocal space. The scattering vector, $\mathbf{q}$, is a unit of reciprocal space and can be related to the separation of the crystal planes in real space by:

$$\mid \mathbf{q} \mid = \frac{2\pi}{d} \tag{6.2}$$

The scattering vector, $\mathbf{q}$, is given by the difference between the incident beam vector ($\mathbf{k}_i$) and the scattered beam vector ($\mathbf{k}_f$) given by equation 6.3:

$$\mathbf{q} = \mathbf{k}_f - \mathbf{k}_i \tag{6.3}$$

The vectors can be resolved into three orthogonal directions: where the xz plane defines the conventional scattering plane as shown in Figure 6.2. In the case of elastic scatter where $\mid \mathbf{k} \mid = 2\pi/\lambda$:[185]

$$\mathbf{q} = \begin{pmatrix} \mathrm{q_x} \\ \mathrm{q_y} \\ \mathrm{q_z} \end{pmatrix} = \frac{2\pi}{\lambda} \begin{pmatrix} \cos\theta_f \cos\varphi - \cos\theta_i \\ \cos\theta_f \sin\varphi \\ \sin\theta_f + \sin\theta_i \end{pmatrix} \tag{6.4}$$

here, θ_i is the angle between the incident beam and the sample; θ_f is the angle between the sample and the beam as it exits; φ is the azimuthal angle, away from the xz plane. Since $\mathbf{q}$ is a unit of reciprocal space, it can be used to directly measure the physical properties of the material under investigation using equation 6.2.[186]

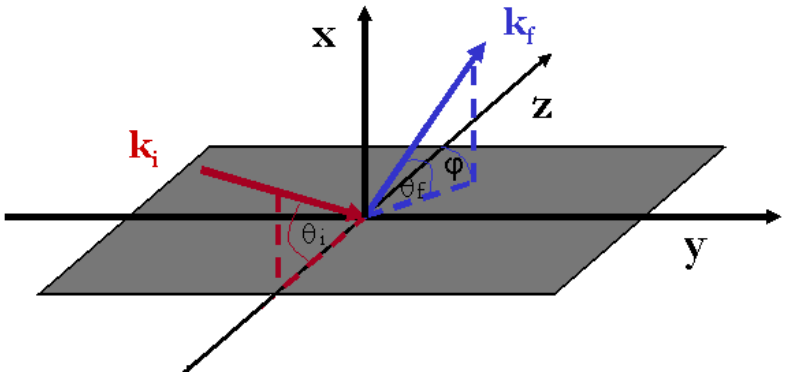

Figure 6.2: Schematic of x-ray scattering and the molecular geometry used in the x-ray work. The incident x-ray beam, $\mathbf{k}_i$, is indicated by the red arrow is in the xy plane and makes an angle θ_i with the sample (which is in the yz plane). The scattered x-ray beam, $\mathbf{k}_f$, indicated by the blue arrow and makes the angle θ_f with the sample and φ with the xz plane.

Each distinct array of atoms, whether from a semiconductor crystal or an amorphous glass, gives a characteristic pattern of scattered intensity. This pattern is the Fourier transform of the scattering objects, which in the case of x-rays is the spatial distribution of the electron density. The scattered intensity can be recorded directly with a CCD camera or by moving a point detector in real space such that it covers the scattered beam in reciprocal space.

When the atoms are held within a fixed repeating lattice (e.g. a crystal or aligned polymer), then the x-rays scattered from individual atoms coherently interfere with each other and a detailed interference pattern following Bragg's Law will be recorded. However, if the material lacks any long range order (i.e. it is amorphous) then the scattering pattern observed is a broad peak centred on the "nearest neighbour distance". These patterns are combined for scattering from an isotropic randomly oriented distribution of equally sized particles (e.g. spun cast polymer film or a powder) and is visually represented as a diffuse "powder" ring at a scattering vector, **q**, defined by the spacings between the planes of atoms.

6.2.2 Previous use of x-ray diffraction for polymers

A particular form of grazing incidence x-ray diffraction (GIXD), is used to study the surface of a sample or very thin films.[116,181,186] GIXD has proved to be a very successful technique for studying thin spun luminescent polymer films. The structure of common polymers such as luminescent polyfluorene derivatives, PFO[187] and PF2/6,[72,91,115,188] poly(3-hexylthiophene)(P3HT),[189,190] as well as the alignment layer used in polarised OLEDs, polyimide[191] and many other polymers,[192–194] have been determined with this method. GIXD, with an angle of incidence of the x-ray of $< 1\,^\circ$, has been used here to determine the alignment of polymer chains and the existence and size of crystallites.

Work has also been conducted on blends of a host polymer and a guest luminescent polymer to investigate the maximum concentration of the guest that can be incorporated in the host before phase segregation occurs. Blending of polymers permits variation in phase from complete miscibility to macrophase separation. This behaviour has significant implications for the control of microstructures within polymer light emitting devices and photovoltaics.[195,196]

Phase segregation is the term given to a blended film where the components separate into domains containing either the guest or the host at a micro or macroscopic level. For a polyethylene (PE) host with a poly(2-butyl,5-(2'-ethylhexyl)-1,4-phenylene vinylene) (BuEH-PPV) guest it was found that at 30% guest the isotropic films were composed of an even distribution of crystallites, but as the film was stretched it became an even distribution of aligned, individual chains.[197]

Part of this work was to investigate whether the behaviour of PF2/6 was similar to BuEH-PPV and three different concentrations of PF2/6 blends were made and studied. GIXD has previously been used to investigate the packing structure of thermotropically aligned PF2/6 films.[72,116,198] In such cases, the polymer was spun on a rubbed polyimide (PI) layer and the grooves created by the rubbing process serve as an alignment layer. Images taken with a two-dimensional MarCCD camera at the XMaS beamline at the European Synchrotron Radiation Facility (ESRF) have already been published by Knaapila *et al.*[72,116,198,199] and used to prove that there are three different stacking patterns within aligned PF2/6 and that annealing the film controls the surface morphology.

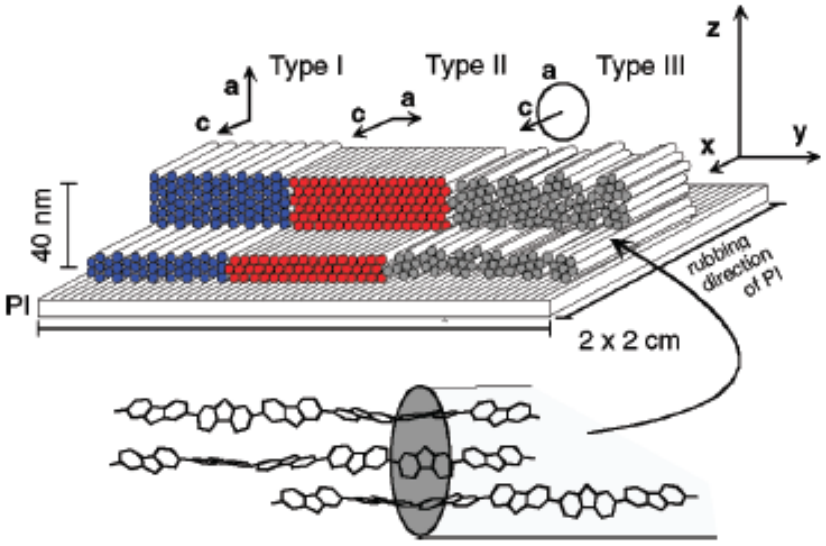

Figure 6.3: Diagram to show the hexagonal packing in PF2/6. The diagram shows the three possible orientations of PF2/6 chains on a rubbed (aligned) polyimide (PI) layer. The individual PF2/6 chains pack together into three different types of crystallites: Type I and type II have a hexagonal unit cell and type III have very little order in the equatorial plane (perpendicular to the film). Type I and II have their secondary axes perpendicular and parallel to the film plane. Axes labeled c and a represent the primary and secondary axes of the hexagonal unit cell. Schematic from *Crystal Growth & Design* and adapted with kind permission of the author.[199]

The three types of packing are shown in Figure 6.3. The helical chains form crystallites that align with the rubbed PI surface. The chains can remain unoriented in the equatorial plane. (The meridional and equatorial refer to the x axis and zy plane respectively.). (Type III) or create a hexagonal unit cell (Type I and II). Type I and II have their secondary axes perpendicular and parallel to the film plane respectively. It is the primary meridional 0021 reflection from the hexagonal unit cell in type I and II that can be seen in GIXD experiments.

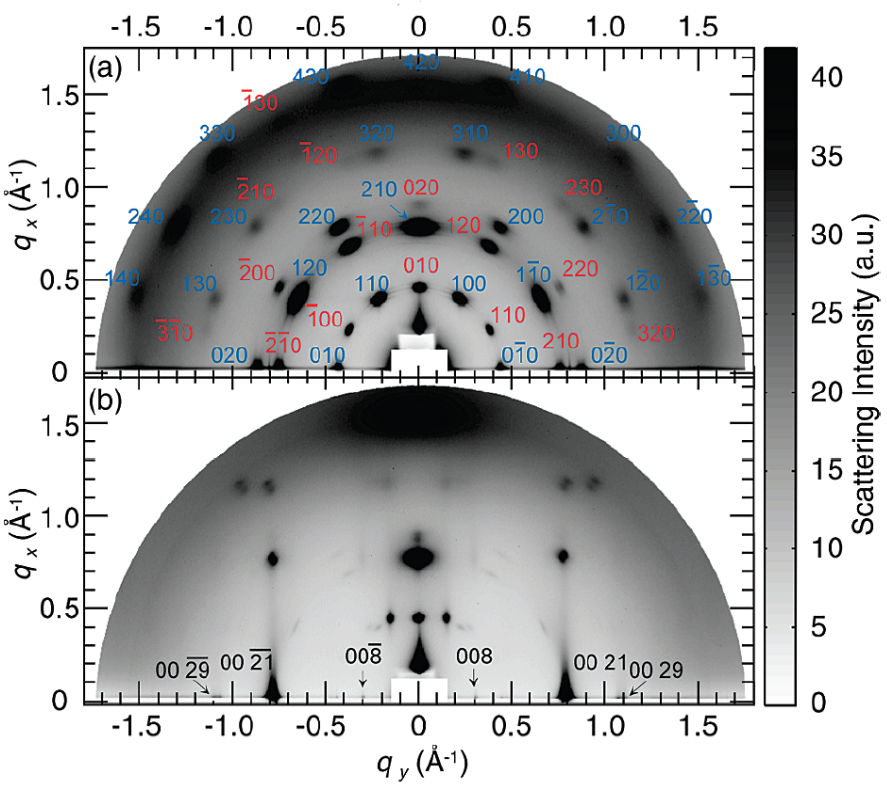

Figure 6.4: GIXD image from the aligned PF2/6 film in Knaapila *et al.*[199] (a) Film alignment defined as the rubbing direction is perpendicular to the beam (b) Film alignment parallel to the beam. The indices marked show the primary reflections of the two types of packing in PF2/6. Reproduced from *Crystal Growth & Design* with kind permission of the author.

Two GIXD images of an aligned PF2/6 on a rubbed PI substrate held perpendicular and parallel to the x-ray beam have been reproduced here (Figure 6.4) to show the positions of the primary meridional 0021 reflections of the hexagonal packing (at $\mathbf{q} \simeq \pm(0.77)$ Å^{-1}) and the primary reflections (Shown as dark points) at $q_y = 1.00$ Å^{-1}.[199]

6.2.3 Experimental: XMaS beamline

To investigate the extent of alignment in the stretched polymer films containing (9,9-di(ethyl hexyl)fluorene) (PF2/6) and ladder-type poly(*para*-phenylene)s MeLPPP and 2,6-NLP, grazing incidence x-ray diffraction (GIXD) measurements were made. The GIXD experiments were carried out at the XMaS beamline[200]at the European Synchrotron Radiation Facility (ESRF) in Grenoble, France, during a visit in 2006. The beam (12 keV) was monochromated using a double Si(111) (silicon) crystal and focused on the sample through 0.2 mm (vertical) × 2 mm (horizontal) slits. To reduce the background, an additional set of anti-scatter slits were placed very close to the sample. The samples (∼ 10 mm × 5 mm) were mounted with cyanoacrylate (superglue) on cleaved silicon wafers. In the geometry used, the z axis is always perpendicular to the film plane (xy0) and the incident beam lies along the x axis in the xz plane, as shown in Figure 6.2. The mounted sample was oriented such that the stretch direction was parallel to the x axis. To prevent radiation damage to the sample and minimise air scatter the samples were placed in a Helium atmosphere at slightly above atmospheric pressure during the measurements. When the film is stretched, the surface becomes slightly buckled. However by using such a small sample, it was possible to use a reflected laser beam

to orient the film in the xy plane. The films rested slightly above their silicon substrate and it was possible to position the sample such that the x-ray beam passed through the film (i.e. θ_i=0). No change in the GIXD patterns was recorded after prolonged exposure to the high flux beam were observed. Data were recorded with a 2D MarCCD detector as a function of the azimuthal angle (φ) around the z axis. $\varphi = 0\,^\circ$ was defined such that the scattering plane was co-incident with the stretching direction. Each measurement on the 2D detector records the scattered intensity as a function of reciprocal space parallel (q_y) and perpendicular (predominantly q_z) to the film's surface. By measuring the intensity of a reflection as a function of φ, it was possible to extract the in-plane mosaic of the film and hence allow the order parameter of the polymer to be determined.

Several samples with differing concentration of PF2/6 were investigated. Films with 15%, 7% and just less than 1% of PF2/6 were created and stretched up to 30 times their original length. Larger isotropic films of MeLPPP and 2,6-NLP spun onto silicon were also used to identify the polymer's powder diffraction rings. The configuration of the system for these measurements was the same, but it was necessary to use a slight angle of incidence for the measurements because these films were much thinner. This angle was 0.15 ° for the MeLPPP film and 0.10 ° for the 2,6-NLP film, close to the critical angle of total external reflection for these materials.

6.2.4 Results and discussion

The results from this work are predominantly qualitative and have been used in conjunction with the published results of Knaapila *et al.*[72] to show that the reflections recorded with the CCD camera are those of aligned PF2/6. Figure 6.5 shows the data from an aligned PE matrix containing 15% PF2/6. Only reflections of pure phases are observed, which indicates that PF2/6 exists as separate crystallites within the crystalline PE matrix and not as separate chains within PE unit cells. The image shows the primary reflection of the PF2/6 is at $q_y = 0.77\text{Å}^{-1}$. This corresponds to the previously published data corresponding to the hexagonal packing[72,116,198,199] and Figure 6.4. There is a low intensity reflection from the other crystal planes. Whilst very faint and difficult to see in these images, the first (equatorial) hexagonal reflection at $q_y = 1.00\text{Å}^{-1}$ is present. It most easily seen in the raw data rather than in Figure 6.5. This indicates the same hexagonal packing that occurs in annealed aligned films is also present in this highly concentrated film, a schematic of which is shown in Figure 6.3.

In lower concentration films, shown in Figures 6.6 and 6.7, the meridional 0021 reflections occur but with reduced intensity. Indeed the 7% film (Figure 6.6) shows very clear peaks at this position indicating that the film remains highly aligned. The reflections from the hexagonal packing vanish in the images from the 1% film. This is due to the low intensity scattering as a direct result of the lack of structural order corresponding to this vector. It is, therefore, hypothesised that the hexagonal packing is absent in such low concentrations. It appears that at this concentration the results are compatible with the polymer being fully dissolved in the PE matrix and the PF2/6 chains are well separated. This is fully supported by later results from photoluminescence studies (in section 6.4) which show that the emission from the low concentration films is comparable to the emission from a dilute solution.

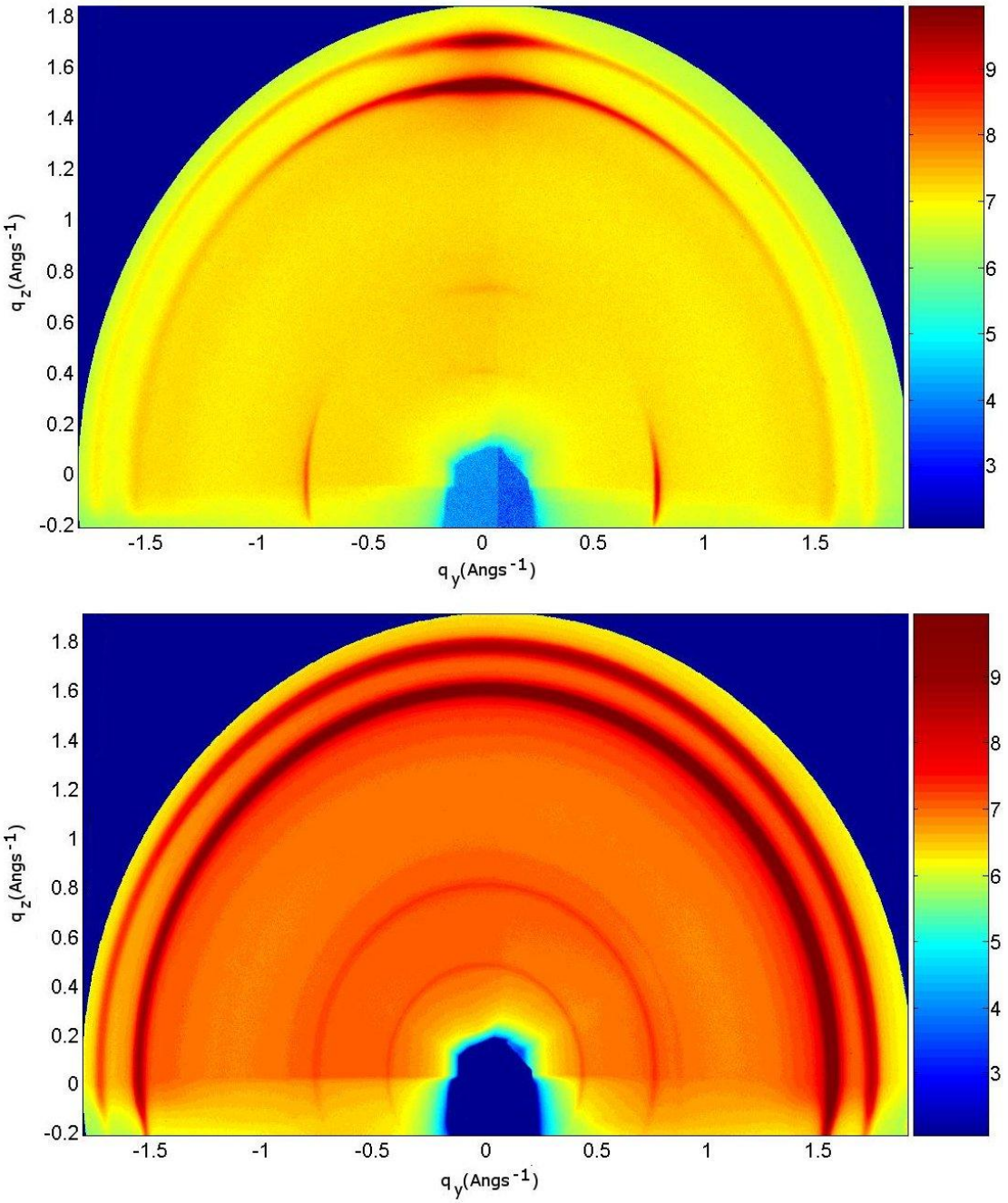

Figure 6.5: GIXD image of a stretch aligned polyethylene host film containing 15% PF2/6 guest. Top: Film alignment is perpendicular to the beam. Bottom: Film alignment is parallel to the beam. The top image shows well defined partial rings at $q_y = 0.77$ Å^{-1} and at $q_y = 0.50$ Å^{-1}. Faint curves are also apparent at $q_y = 1.00$ Å^{-1}. These are most prominent halfway up the image level with the number 6 in the colour key. The pair of rings at $q_y = 1.50$ Å^{-1} and $q_y = 1.75$ Å^{-1} correspond to scattering from the polyethylene host. The colour mapping has been changed between the images to allow the features to be more prominent.

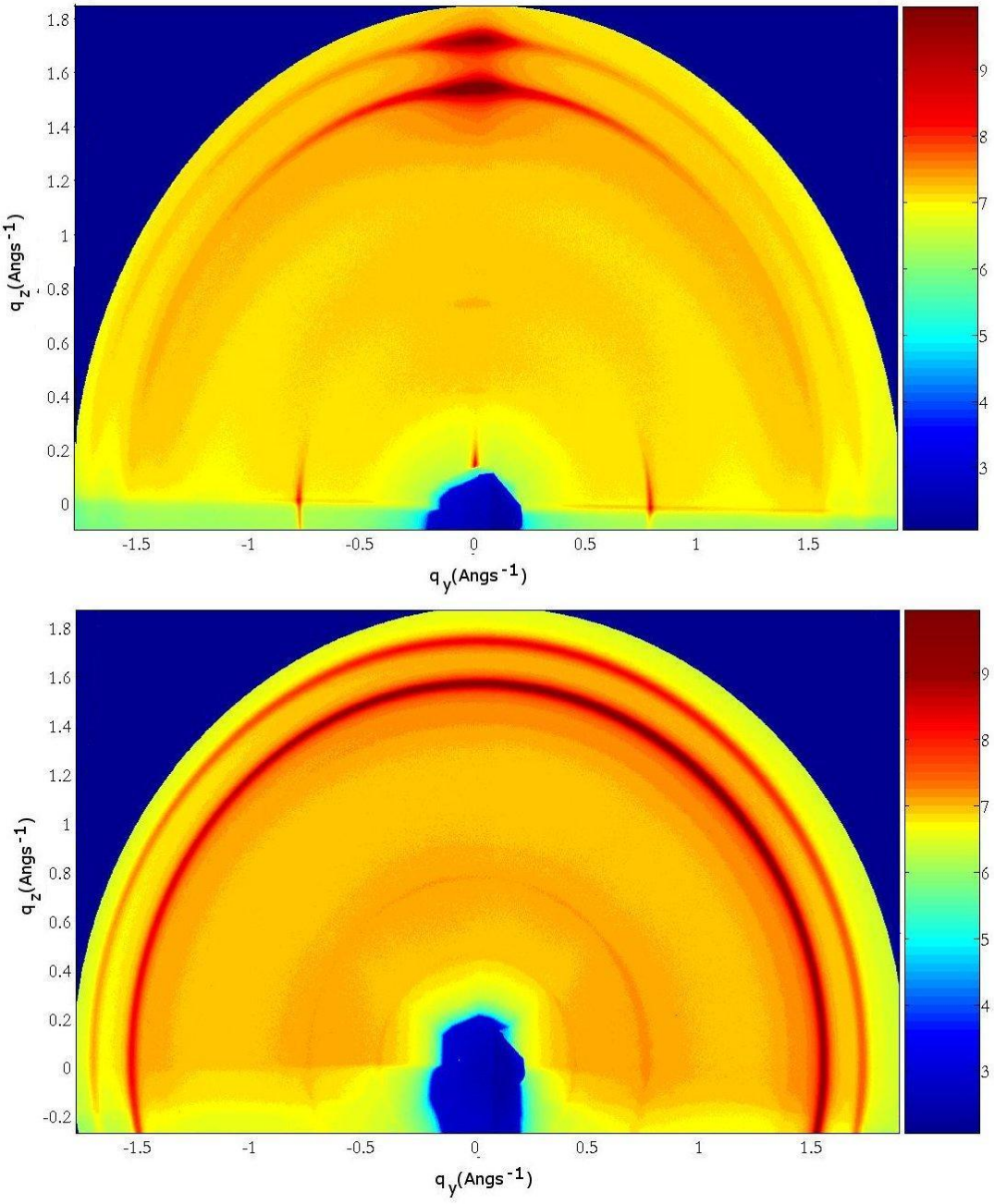

Figure 6.6: GIXD image of a stretch aligned polyethylene host film containing 7% PF2/6 guest. Top: film alignment is perpendicular to the beam. Bottom: film alignment is parallel to the beam. The top image shows well defined points rings at $q_y = 0.77$ Å^{-1}, a faint ring at $q_y = 0.50$ Å^{-1}. Faint curves are also apparent at $q_y = 1.00$ Å^{-1}. These are most prominent halfway up the image level with the number 6 in the colour key. The pair of rings at $q_y = 1.50$ Å^{-1} and $q_y = 1.75$ Å^{-1} correspond to scattering from the polyethylene host. The colour mapping has been changed between the images to allow the features to be more prominent.

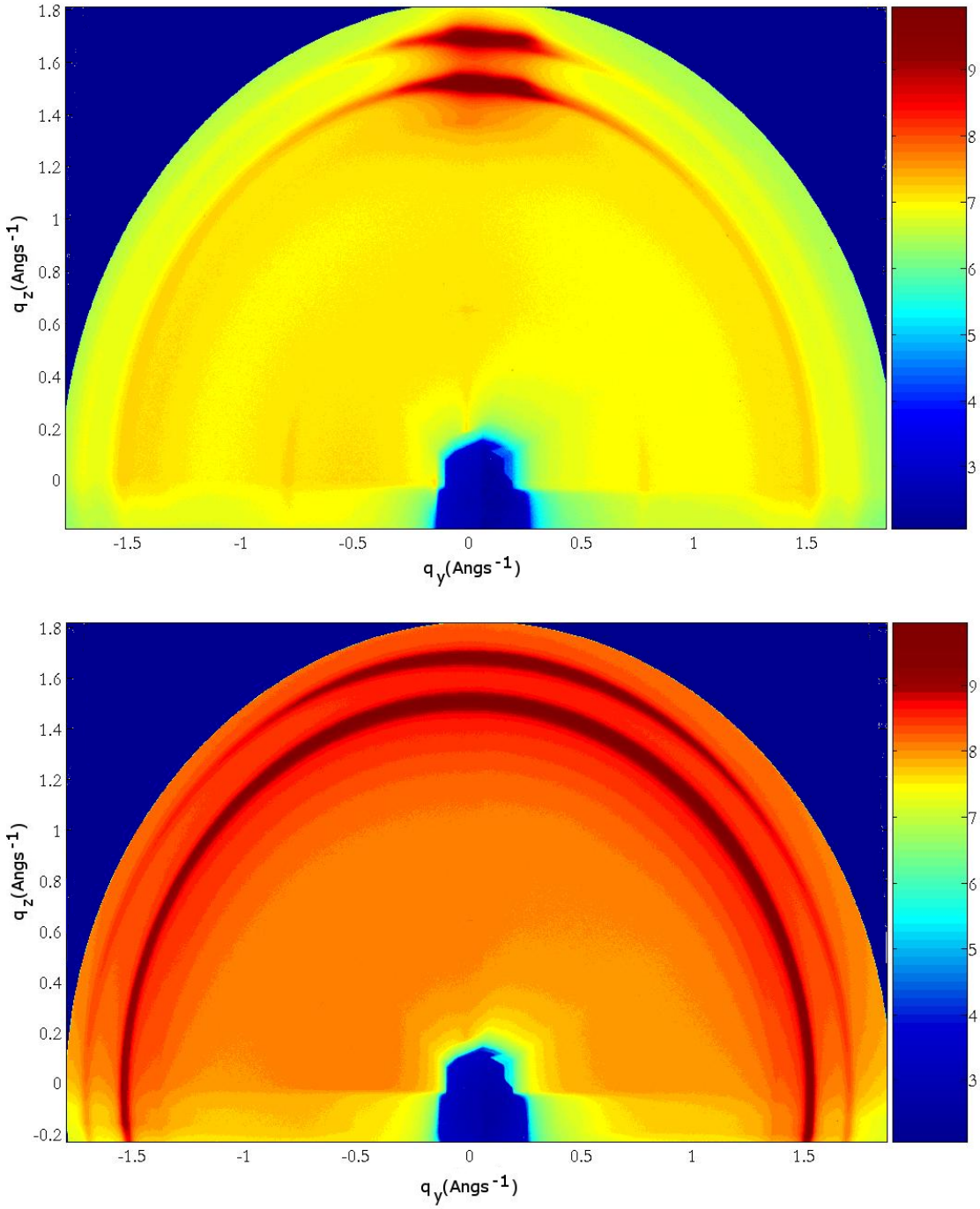

Figure 6.7: GIXD image of a stretch aligned polyethylene host film containing <1% PF2/6 guest. Top: film alignment is perpendicular to the beam. Bottom: film alignment is parallel to the beam. The top image shows a faint ring at $q_y = 0.77$ Å^{-1}. The pair of rings at $q_y = 1.50$ Å^{-1} and $q_y = 1.75$ Å^{-1} correspond to scattering from the polyethylene host. The colour mapping has been changed between the images to allow the features to be more prominent.

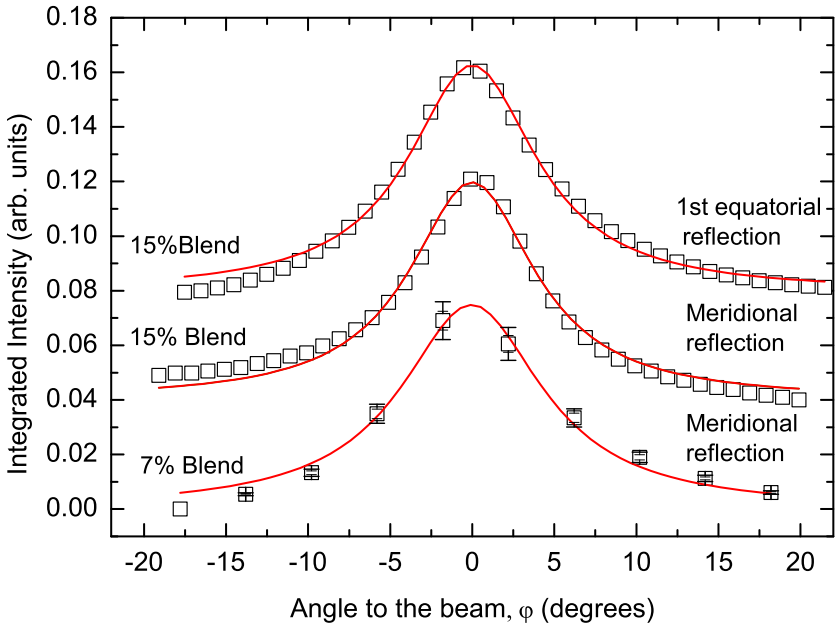

Figure 6.8: Integrated intensities of the first (equatorial) hexagonal reflections and meridional 0021 reflections of stretched PF2/6 - PE matrices. Percentages refer to the PF2/6 fraction. Lorentzian fits, from which the width of the orientation was evaluated are shown by the solid red lines. Figure made with the assistance of Dr M. Knaapila.

The intensity of the first order reflections was measured from the results of the azimuthal scans. An intensity was derived for each angle about the azimuth (or z-axis) φ. This data was plotted as a function of φ and fitted with a Lorentzian curve in the analysis package Microcal Origin 7.0, by Dr M. Knaapila. The Lorentzian fits (shown in Figure 6.8) were then used to determine the full width half maximum (FWHM) for each distribution of intensity. This value gives the average angle that the crystallites, and the polymer chains in them, makes with the stretch direction (ε). These angles were found to be 10.7 $\pm$ 0.2 $^\circ$ for the first hexagonal reflection in the 15% film; 8.9 $\pm$ 0.2° for the meridional reflection of the same film and 10.5 $\pm$ 0.3° for the lower concentration 7% film.

The lowest concentration film ($>$ 1%) did not show as clear hexagonal reflections and as such when the procedure was repeated for these data sets, it was not possible to get a good Lorentzian fit. This is due to the fact that the crystallites are reduced in size or do not exist.

Using equation 2.19 as an approximation which is assumed to be valid for thin films, the order parameter, Φ is between 0.93 - 0.95. This is very close to the order parameter published for polyethylene sheets[201,202] confirming that the stretching technique works very well for this polymer. The order parameter confirms that all the PF2/6 is highly aligned within a very small spread of angles about an average angle of 12° (from equation 2.19)

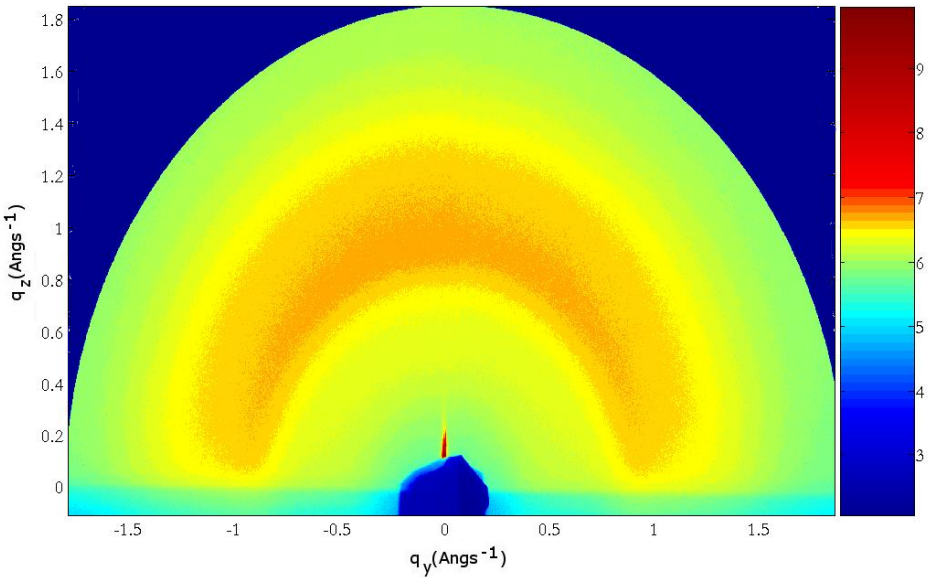

Figure 6.9: GIXD image from the isotropic cyanoacrylate sample. The image shows a broad ring at $\mathbf{q_y} = 1.00$ Å^{-1}, which indicates the powder ring for the superglue.

The two rings that appear in all the images come from the PE matrix images. PE is a randomly oriented crystalline solid and early x-ray diffraction studies have found two powder rings[202–204] corresponding to the two main reflections at 110 and 200 at $q_y \simeq 1.5$ Å^{-1} and 1.7 Å^{-1}.[190,205] Other studies have been carried out on stretched PE films and, as the films are extended to over 50 times, their original length the powder rings condense to single points confirming that the entire film becomes more textured. But even in films stretched to 30 times, the rings are still observed[197,203,206] with the orientation remaining complex because not all the original crystallites are aligned.[207]

The conclusion of this work is, that whilst PE powder rings are observed here, the polymer contained within the matrix is aligned with a high degree of long range order. The powder ring at approximately $q_y = 1$ is from the cyanoacrylate (as shown in Figure 6.9). Every attempt was made to limit the amount of the adhesive that was in the path of the x-ray beam and in most cases, it only appears as a slight halo around the PF2/6 reflection points and can only be observed in the raw data.

Figures 6.10 and 6.11 show the powder diffraction rings for MeLPPP and 2,6-NLP respectively. Given that the structure of the polymers is very similar the fact the scattering vector is $\mathbf{q} \approx 1.5$ Å^{-1} for both polymers is not surprising. The value also corresponds to the reflection of the PE host which is why it is impossible to separate the PE and these conjugated polymers rings in the stretched films (Figures 6.12 and 6.13). The high intensity scattering distribution at $q_z = 1.50$ Å^{-1}, $q_y = 0.00$ Å^{-1} of the images indicates that these polymers are not totally aligned. This broad peak is also evident in the data from the PF2/6 blends but without another reflection to monitor, another physical method must be used to find the order parameter in these films.

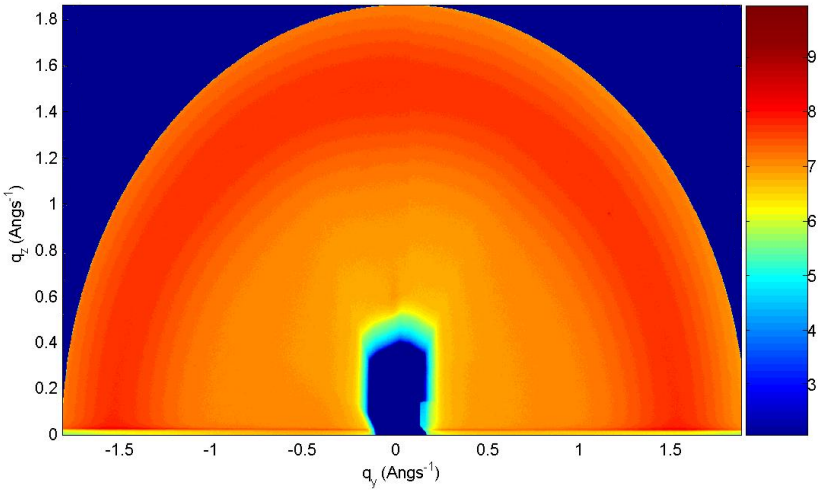

Figure 6.10: GIXD image of an isotropic spun MeLPPP film. Image taken with a scattering angle, θ = 0.15. The image shows a wide ring centered at approximately $q_y = 1.50$ Å^{-1}. This scattering vector corresponds to powder rings from the MeLPPP indicating there is no alignment in the film.

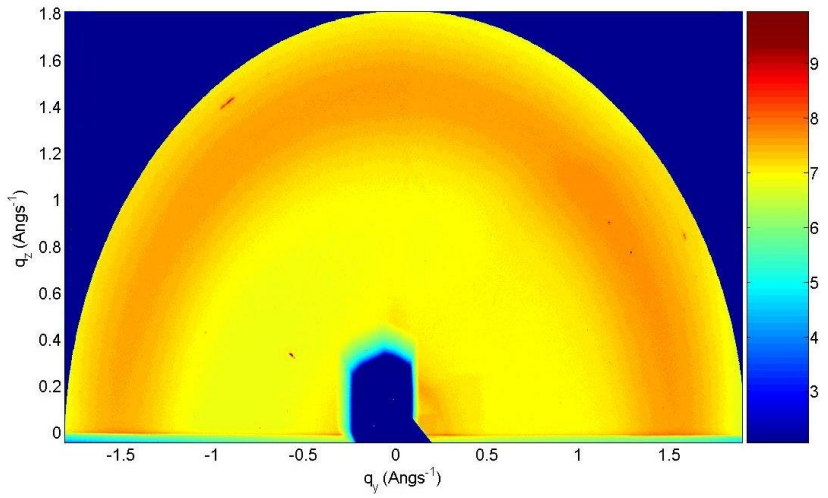

Figure 6.11: GIXD image from the spun isotropic 2,6-NLP film. Image shows a wide ring centered at approximately $q_y = 1.50$ Å^{-1}. This scattering vector corresponds to the power rings from 2,6-NLP, indicating there is no alignment in the film.

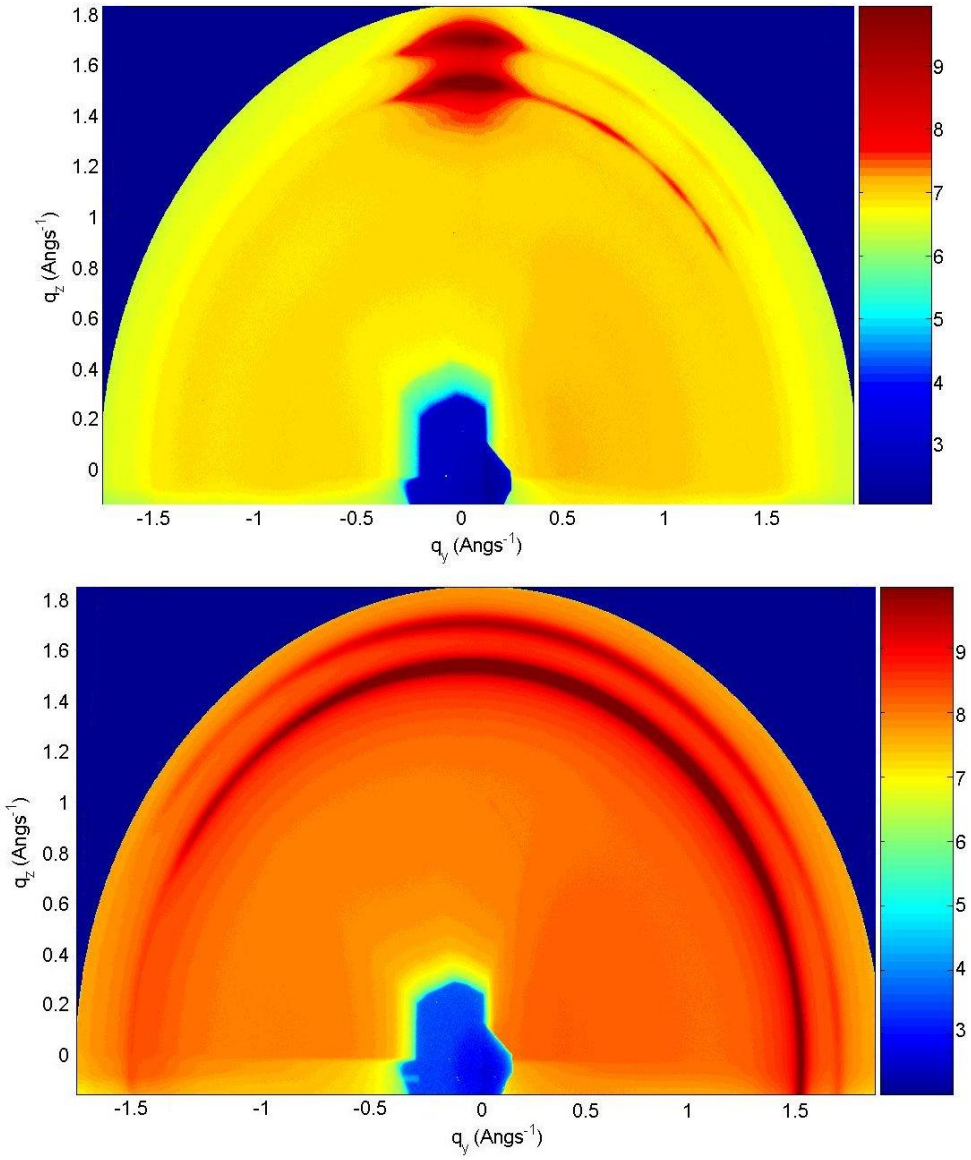

Figure 6.12: GIXD image of a stretch aligned polyethylene host film containing $< 1\%$ MeLPPP guest. Top: film alignment is perpendicular to the beam. Bottom: film alignment is parallel to the beam. The top image shows a high intensity scattering distribution, shown red on the diagram, at $\mathbf{q_z} = 1.50$ Å^{-1}, $\mathbf{q_y} = 0.00$ Å^{-1}. The pair of rings at $\mathbf{q_y} = 1.50$ Å^{-1} and $\mathbf{q_y} = 1.75$ Å^{-1} correspond to scattering from the polyethylene host. The colour mapping has been changed between the images to allow the features to be more prominent.

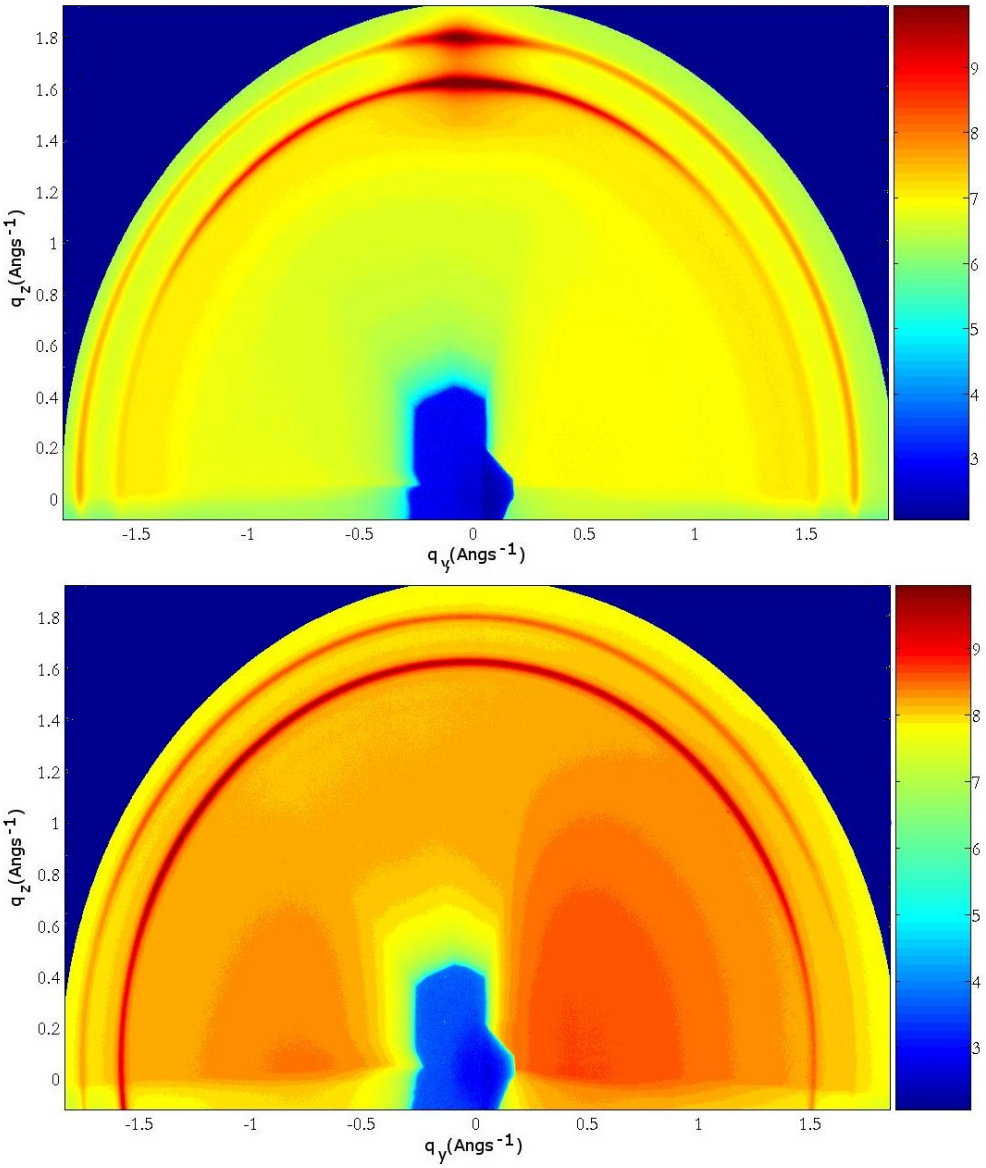

Figure 6.13: GIXD image of a stretch aligned polyethylene host containing $< 2\%$ 2,6-NLP guest. Top: film alignment is perpendicular to the beam. Bottom: film alignment is parallel to the beam. The top image shows a high intensity scattering distribution, shown red on the diagram, at $\mathbf{q_z} = 1.50$ Å^{-1}, $\mathbf{q_y} = 0.00$ Å^{-1}. The pair of rings at $\mathbf{q_y} = 1.50$ Å^{-1} and $\mathbf{q_y} = 1.75$ Å^{-1} correspond to scattering from the polyethylene host. The colour mapping has been changed between the images to allow the features to be more prominent.

6.2.5 Discussion of the microphase segregation in PF2/6

Earlier blend work by Heeger *et* al. showed that, at high concentration of BuEH-PPV guest in a PE host, before stretching the guest polymer formed crystallites and stretching separated the chains. This finding can be compared with the data from stretched PF2/6 15% blend presented in Figure 6.5. The meridional reflections present arise from the hexagonal unit cell indicative of Type I or II structures that PF2/6 is known to form (as shown in Figure 6.3). This means that hexagonal crystallites still exist in stretched films of high concentration PF2/6 blends.

It is known that BuEH-PPV can form entanglements, i.e. bridges, that "tie" crystallites together.[197] As the blend is drawn, the tensile forces stretch the bridges and force the crystallites to break. As the stretching continues, the crystallites are destroyed.

PF2/6 has a lower alkyl chain density compared with BuEH-PPV has with PE. This reduces the compatibility between guest and host and the forces between guest and host in PF2/6 blends are lower than in BuEH-PPV i.e. less entanglements can form between PF2/6 crystallites. Therefore, as the films are drawn, the crystallites are not totally destroyed.

This explanation does not explain the lack of hexagonal crystallites in the blends of low concentration PF2/6 as it would require the number of entanglements to increase as the concentration decreased which is unlikely. Here, it is thought that the low concentration results in a a better miscibility of the guest polymer leading to smaller crystallites and a higher proportion of isolated chains.

6.2.6 Conclusions

The x-ray diffraction experiments have been successfully used to investigate the order parameter in stretched polyethylene films hosting one of the conjugated polymers. The study has shown that PF2/6 films have long range order. The order parameter was estimated to be between 0.93 - 0.95 for this blend. This corresponds to a small distribution of angles about the average angle 12 °. The study has also shown that hexagonal packing in PF2/6 is present in higher concentration blends ($\sim$ 15%) and that it is not present in low concentrations ($\sim$ 1% PF2/6). The latter is explained by a more thorough isotropic distribution of molecules in the blend. It is hypothesised that the former is a result of clumps of PF2/6 forming a phase segregated aggregate that are not broken up as the film is stretched.

X-ray diffraction experiments on 'pure' films of MeLPPP and 2,6-NLP have indicated that the powder reflections coincided with the polyethylene host and the cyanoacrylate glue. There were no other reflections that were dependent on the angle the sample made with the beam. It has already been shown that it is difficult to observe reflections in low concentration blends. Therefore, it is most likely that there is no long range order in these films . The short range order of these films were, therefore, investigated and the results for PF2/6 were used to confirm the validity of the results of the fluorescence anisotropy technique. The order parameters were also used in the later calculations to determine the angles of the transition dipole moments.

6.3 Determination of the order parameter via Raman Spectroscopy

6.3.1 Introduction to Raman spectroscopy

Raman spectroscopy is a technique used to provide information on the bonds and their orientation within a molecule. The Raman process involves inelastic scattering of light and allows the vibrational and rotational energy to be measured. Thus the motions available to electronic (covalent) bonds can be determined.

In elastic (or Rayleigh) scattering, a photon is scattered by a molecule and its energy is unchanged. However, inelastic scattering can occur if the molecule undergoes a change in vibrational or rotational energy (ΔE) then the final energy (E_γ) of the scattered photon is equal to its original energy plus (or minus) the energy loss (or gained) by the molecule. It is defined thus:[208]

- $E_\gamma = E_0 + \Delta E$: Stokes's scattering
- $E_\gamma = E_0 - \Delta E$: Anti-Stokes's scattering

where E_γ is the energy of the scattered photon, E_0 is the initial energy of the photon and ΔE is the change in energy of the molecule. In most cases, the photon is scattered directly from the molecule without any loss or gain of energy, indeed Stokes's or anti-Stokes's scattering occurs less than once per ten million incident photons. For this reason highly sensitive Raman microscopes are used to record these infrequent events. The equipment used in this work is fully described in the next section.

The principles of Raman spectroscopy rely on the formation of an induced electric dipole moment between atoms in a molecule. The induced dipole moment is a response to the electric field of the incident photon with the molecule becoming polarised. It is most often the case that the dipole moment is created along the bond, as this is the easiest way to vibrate the bonding electrons.

The different bonds, between different types of atoms and their modes of vibration (bending, twisting, stretching etc[208]) have different polarisabilities, that is how readily a covalent bond can be polarised. Different bonds will, therefore, show a different energetic position and scattering intensity in the Raman spectra. Also, the intensity is dependent upon the angle of the electric field of the incoming light, i.e. the linear polarisation of the light. By utilising linear polarised light, it is possible to detect the direction of the bond within the molecule; in an anisotropically oriented sample like a liquid crystal or a stretched film, the direction of the bond relative to the orientation direction can be found. For stretched polyethylene sheets, the polyethylene molecules align with the stretch direction. When a guest conjugated polymer is incorporated into the polyethylene (host), the conjugated polymers are similarly oriented when the film is stretched.[21,23]

When Raman Spectroscopy is carried out using a linearly polarised light source, it is possible to determine the relative alignment of guest and host. For example, assuming that the order parameter of the polyethylene tends to a maximum, it is possible to determine the order parameter of the guest in the film.[209,210]

6.3.2 Experimental: Raman Spectrometer

The alignment of the chemical bonds in the stretched polyethylene films containing a conjugated polymer was studied with a Horiba Jobin-Yvon LabRamHR Raman microscope equipped with a 536 nm laser. The laser beam was focused with a microscope objective (50×) onto a small area of the sample, which was held on a rotatable mount. Since the laser beam was predominantly polarised, partially polarised Raman spectra were taken as the sample was rotated. Great care was taken to ensure that the same area of film was in focus as the film was moved.

6.3.3 Results and discussion

Raman spectra of isotropic films spun cast from low concentration solutions of the two polymers are shown in Figure 6.14 (a and b). The conjugated polymers contain carbon and hydrogen, which will give rise to a range of vibronic modes corresponding to carbon-carbon (C-C) bonds and carbon-hydrogen (CH) bonds. Their structures are shown in Figure 2.26 and it can be seen that there are intra-ring C-C bonds in the aromatic groups, but also inter-ring bonds along the backbone, which join the aromatic groups.

The Raman bands of MeLPPP (Figure 6.14 (b)) have been previously recorded and the results are in agreement. The bands at 1560 cm^{-1} and 1600 cm^{-1} have been attributed to aromatic intra-ring C-C stretching modes. The mode at 1322 cm^{-1} is considered to be the inter-ring C-C stretch mode and can be considered to be along the polymer's backbone.[132,211–213]

The Raman spectrum of 2,6-NLP (a) has not been reported previously and by comparison with other polymers it is believed that the modes around 1600 cm^{-1} correspond to the aromatic C-C stretch. 2,6-NLP is a polymer based on a naphthalene backbone and the Raman spectrum of the polymer was qualitatively compared with those from naphthalene and naphthalene based molecules. Naphthalene and its derivatives all have a mode between 1400 cm^{-1} and 1450 cm^{-1}, the intensity and structure of which varies depending on the substituent group attached to the rings in the base molecule.[214] For example, 1,5-dimethylnaphthalene, which has methyl groups at the same position that 2,6-NLP has side groups, shows a more structured Raman spectrum. The structure of this peak is also enhanced in other dimethylnaphthalenes with peaks distributed between 1400 cm^{-1} and 1425 cm^{-1} depending on the location of the methyl groups.

The length of the side chain broadens this peak, obscuring the structure. 1-Naphthaleneneactic acid methyl ester, which is a naphthalene molecule with a long side chain in the same position that 2,6-NLP has a side chain, presents a broad Raman peak at 1425 cm^{-1}. It is therefore hypothesised that the mode at 1405 cm^{-1} arises from the vibrational modes of the long chains attached to the naphthalene unit and the bonds between adjacent rings. Further

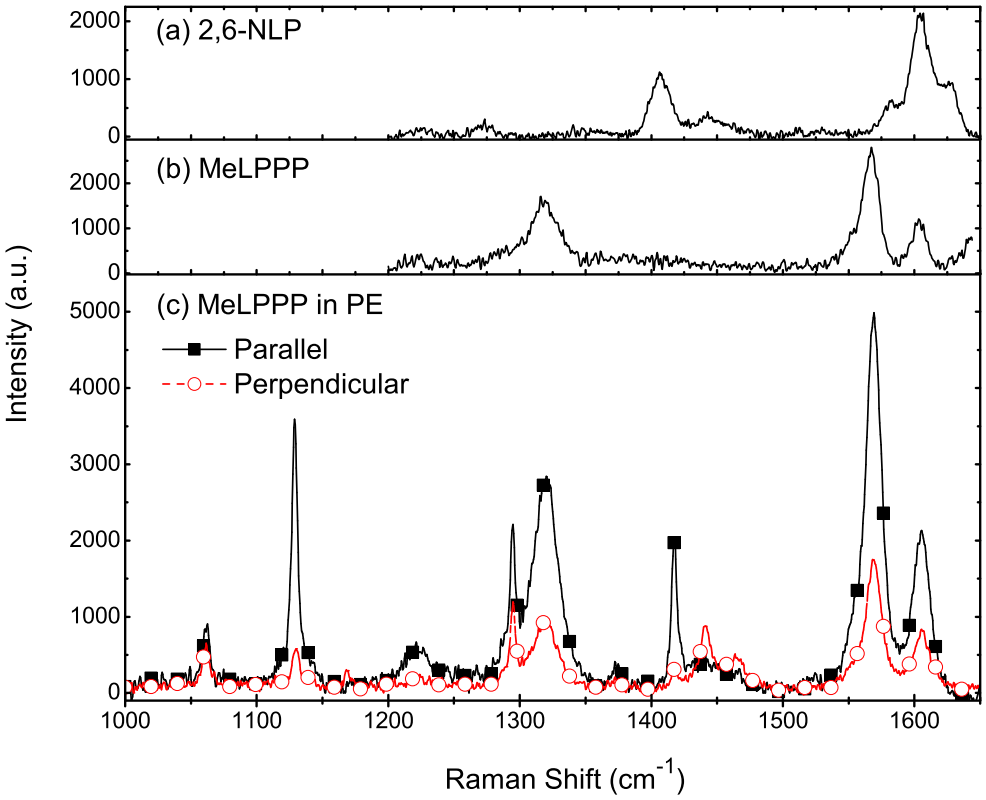

Figure 6.14: Raman spectra of (a) 2,6-NLP (spun cast film) (b) MeLPPP (spun cast film) and (c) stretch oriented PE film doped with MeLPPP parallel (black squares) and perpendicular (red circles) to a fixed arbitrary direction. This PE film doped with MeLPPP was stretched to 8 times its original length. The spectrum of 2,6-NLP in (a), shows a Raman band at approximately 1405 cm^{-1} and a broad structured band between 1575 cm^{-1} and 1650 cm^{-1}. It is hypothesised in the text that the first band corresponds to vibrational modes of the side groups and the broad band correspond to C-C vibrational modes. The spectrum of MeLPPP in (b) shows bands at 1560cm^{-1} and 1600 cm^{-1} which are intra-ring carbon-carbon (C-C) stretching modes. A third band at 1322 cm^{-1} corresponds to the inter-ring C-C stretch mode along the polymer's backbone.[132,211–213] The spectra in (c) show the Raman shift of both the MeLPPP and the PE. By comparing (b) and (c) the Raman bands of PE are clearly evident at 1060 cm-1, 1130 cm-1 (both C-C stretching modes) and 1440 cm-1 (methylene vibrational mode). The spectra in (c) also show how the intensities of the bands change as the film is rotated by 90°. Note that the MeLPPP C-C band at 1322 cm^{-1} and the PE C-C band at 1130 cm^{-1} behave similarly (they decrease with the rotation) but the PE band at 1442 cm^{-1} behaves oppositely and increases with the rotation.

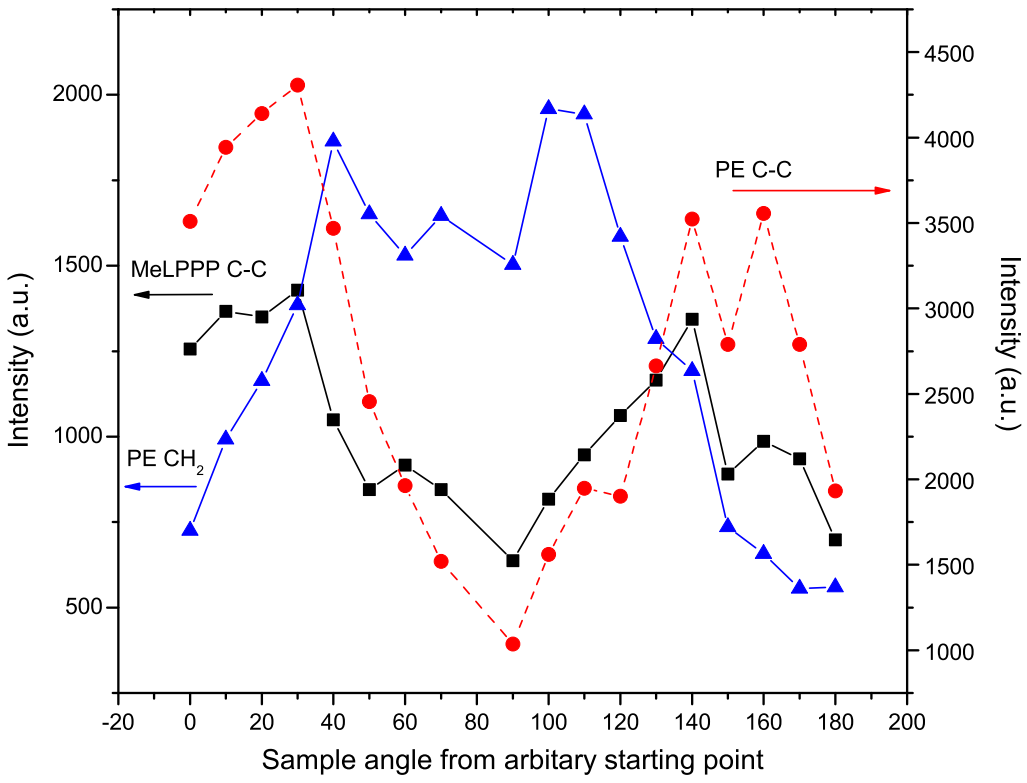

Figure 6.15: Intensity of Raman shift of different vibrational modes of a MeLPPP doped PE stretched film that is rotated around the beam axis. The figure shows the MeLPPP inter-ring mode at 1322 cm^{-1} (squares) and the PE C-C stretching mode at 1130 cm^{-1} (circles). These modes correspond to the backbones of the polymers and vary with angle in the same way. Therefore, they can be considered to be aligned with each other. Data from the PE CH_2 bending mode at 1442 cm^{-1} (triangles) is also shown. This confirms that the two PE modes are at 90°.This also indicates that the PE is better oriented than the MeLPPP within it. Note that the PE C-C mode and the MeLPPP C-C mode are on different scales.

investigations to resolve the spectrum in more detail are needed before a thorough assessment can be made. Neither of the modes described have a known orientation in relation to the backbone of 2,6-NLP, indeed the backbone is solely comprised of aromatic groups. Therefore, films with this polymer could not be used for the polarised work. The order parameter for these films was determined via a different method.

The Raman spectrum of a mechanically stretched PE film doped with MeLPPP in two orthogonal orientations is shown in Figure 6.14 (c). In addition to the MeLPPP bands at 1560 cm^{-1}, 1600 cm^{-1} and 1322 cm^{-1}, which have been previously described, it is dominated by the PE bonds. Peaks at 1060 cm^{-1} and 1130 cm^{-1} are the C-C asymmetric and symmetric stretching modes,[215] and around 1440 cm^{-1} there are many modes from the vibrational motion of the methylene groups.[216,217] Stretching undoped PE leads to the backbone becoming aligned with the stretching direction and the order parameter is generally high.[209,210] It is clear from

Figure 6.14 that it is possible to take partially polarised spectra by rotating the anisotropic film in an ordinary Raman microscope equipped with a strongly polarised laser and whilst it is not equipped with an analyzer, it was possible to use the PE bands as an internal standard to qualitatively determine how oriented the dopant polymer is.

The results of rotating the film and monitoring the intensity of the C-C modes in both the MeLPPP and the PE can be seen in Figure 6.15 (in particular the black squares and red circles). Both of these modes correspond to a polymer backbone. The data is very noisy, but it can be seen that it follows the expected pattern of decreasing and increasing in Raman shift intensity as the film is rotated. Since it can be seen that the two backbone modes change at the same angle it is assumed that the MeLPPP backbone is aligned with the PE backbone to some extent. The intensity of the C-C stretching mode in PE varies significantly more than that in the MeLPPP leading to the assumption that the order parameter of the MeLPPP is less than that of the PE.

The data shown in Figure 6.15 was used to quantitatively estimate the order parameter of the MeLPPP. The ratio of peak to trough for the PE 1130 cm^{-1} band is 4.15. The ratio of the the peak to trough for the MeLPPP 1322 cm^{-1} band is 2.24. The ratio indicates that the order parameter of the MeLPPP is approximately half (0.54) of the PE order parameter. Studies into the alignment of PE have shown that it is possible to achieve an order parameter of 1.[201,202] On this assumption the order parameter for the incorporated MeLPPP is approximately 0.54.

One of the PE methylene bending modes has been shown on the Figure 6.15 to highlight that it is polarised perpendicular to the backbone as expected from its chemical structure in Figure 2.26.

6.3.4 Conclusions

Rotating a stretch aligned polyethylene blend containing the conjugated polymer MeLPPP, while recording the intensity of the Raman bands of the polyethylene backbone and the conjugated polymer backbone, has been used to estimate the short range order of an MeLPPP film stretched eight times. The order parameter of this film was determined to be $\sim$0.54.

The Raman bands of 2,6-NLP could not be assigned to a unique band direction on the backbone and, therefore, this technique could not be used for this particular conjugated polymer blend.

6.4 Determination of the order parameter via fluorescence anisotropy

6.4.1 Introduction to fluorescence anisotropy of aligned films

As the x-ray and Raman methods for order parameter determination could not be successfully applied to 2,6-NLP, due to the lack of long range order and the lack of a known Raman band relative to the polymer backbone, it was necessary to find a technique that would work. Published texts have referred to methods determining the polymer's alignment in a film via polarised fluorescence.[23,73] The technique relies on knowing the angle the polymer emits at relative to the angle that it absorbs at (i.e. the natural anisotropy, r_0) and recording the intensity of emission parallel and perpendicular to the exciting light. From the ratio of these it is possible to determine an angle for the polymer's backbone relative to the stretch direction, ε (which is related to the order parameter via equation 2.19). In essence, it is a more advanced version of the linear dichroism technique which can determine the order parameter from polarised absorption measurements if the angle between the backbone and the absorption transition dipole moment is known.

This method can be carried out in a commercial L-format spectrofluorimeter (a fluorimeter with a 90 ° angle between the excitation and emission ports) provided that the instrument's polarisation response function can be taken into account. Damerau and Hennecke derived the mathematics for this method in their 1995 paper[218] and it has been used with some success to determine the order parameter of various films and fibres.[100,219–224]

Fluorescence from a molecule is often described as a tensor of rank four because it is the product of the absorption and emission tensors (both rank two).[23,73] The total fluorescence tensor ($\mathbf{F}$) is comprised of nine individual terms:

$$\mathbf{F} = \begin{pmatrix} F_{XX} & F_{XY} & F_{XZ} \\ F_{YX} & F_{YY} & F_{XY} \\ F_{ZX} & F_{ZY} & F_{ZZ} \end{pmatrix}$$

where X Y & Z refer to the experimental geometry as shown in Figure 6.16 and is related to the molecular geometry of the polymer by the orientation distribution function. If the orientation distribution function is uniaxial (which the stretched films are assumed to be) then the order parameter Φ can be determined from equation 2.19:

$$\Phi = \frac{1}{2}(3\langle\cos^2\varepsilon\rangle - 1) \tag{6.5}$$

Equation 2.19 is used to calculate the order parameter from an angle in the molecular geometry of an aligned film. Using the fluorescence anisotropy method for determining the order parameter relies on knowing the natural anisotropy value (r_0) of the molecule to find the value of ε (the angle between the stretch direction and the molecular backbone.

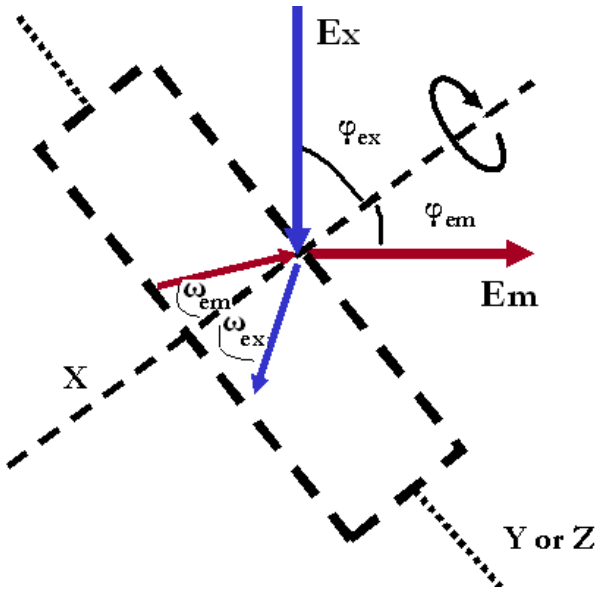

Figure 6.16: Schematic of the geometry used in fluorescence anisotropy measurements of stretched films in an L-format spectrofluorimeter. The excitation beam (large blue arrow, "Ex") and the emission beam (large red arrow, "Em") are at 90 ° to each other. The angle of incidence (φ_{ex}) was 30 ° and $\varphi_{em} = 60\,°$. The angles ω_{em} and ω_{ex} are within the film and depend on the birefringence of the material. The film was positioned in the YZ plane and rotated about the X axis. The stretch direction was parallel to Z axis. For vertical measurements the Z axis is perpendicular to the page and for horizontal measurements, the Z axis is within the page. Figure and text adapted from Figure 2 of T. Damerau and M. Hennecke(1995)[218]

The average cosine of the angle, $\langle \cos^2 \varepsilon \rangle$, can be determined from only three of the tensor components (F_{ZZ}, F_{ZY} & F_{YY}) and the total fluorescence tensor, using the following equations:

$$\begin{aligned} \mathbf{F} &= F_{ZZ} + 4F_{ZY} + 2F_{YY} + 2F_{YX} \\ &= \frac{[(3-2p)F_{ZZ} + 8F_{YY} + 4(3-p)F_{ZY}]}{(3-2p+p^2)} \end{aligned} \tag{6.6}$$

$$\langle \cos^2 \varepsilon \rangle = \frac{1}{2} + \frac{1}{2}\langle \cos^4 \theta \rangle - \frac{16(1-p)\frac{F_{YY}}{F} + 4p\frac{F_{ZZ}}{F} + 4p(1-p)}{(2-3p)^2(3-p)} \tag{6.7}$$

$$\langle \cos^4 \varepsilon \rangle = \frac{16p\frac{F_{YY}}{F} + (12-10p)\frac{F_{ZZ}}{F} + p(6-7p+3p^2)}{(2-3p)^2(3-p)} \tag{6.8}$$

and

$$p = (2 - \sqrt{10r_0})/3 \tag{6.9}$$

The above equations are fully derived in T. Damerau and M. Hennecke(1995).[218]

The three fluorescence tensor components can be evaluated from five of the eight possible polarised spectra that can be taken with the film either horizontal or vertical and the excitation and emission polarisers similarly oriented. The spectra are: I_{Vvv}, I_{Vvh}, I_{Hvv}, I_{Hvh} and I_{Hhv} where $I_{FILM,ex,em}$ represents the intensity of light with film orientation (either horizontal (H)

or vertical (V)) and orientation of the excitation and emission polarisers in the light path: either horizontal (h) or vertical (v)[a]. Also required are the instrumental response functions, G_1 and G_2, which correspond to the effectiveness of the emission and excitation polarisers. Full details of all of these terms and functions can be found in T. Damerau and M. Hennecke *Determination of orientational order parameters of uniaxial films with a commercial 90 degree-angle fluorescence spectrometer* (1995).

The refractive index of the PE films is required. This was assumed to be the refractive index of PE, $n_{PE} = 1.52$ and constant across the spectrum. It is acknowledged that the incorporation of the conjugated molecules may change the refractive index. However, a brief study into changing the refractive index by 0.5 showed that the order parameter changed by only 0.001. Here, the estimated value of the refractive index used was appropriate.

6.4.2 Experimental: Spectrometer

Polarised fluorescence anisotropy from stretch aligned PE films was taken in a Jobin Yvon Fluorolog-3 spectrofluorimeter with a 90 ° geometry as described in section 3.4. A specially designed film holder was used and this allowed rotation of the sample in the plane of the excitation beam which allowed the angles between the excitation φ_{ex} and emission φ_{em} ports to be controlled. In this experiment they were fixed at $\varphi_{ex} = 30\,^\circ$ and $\varphi_{em} = 60\,^\circ$. The sample holder, shown in Figure 3.6, also rotated in the plane normal to the excitation beam such that the orientation of the film could be changed without remounting the film. In all cases the alignment of the film was done by eye. The film stretch direction was oriented within 2 ° of the actual vertical or horizontal. This error was measured with a protractor and was considerably less than is usually estimated in texts (5 °-10 °).[23]

6.4.3 Instrumental response functions (G-factors)

Polarised emission from an isotropic sample is corrected for the anisotropic nature of the emission polariser and the detector using $G_1 = I_{hv}/I_{hh}$. This is the same G-factor used in equation 3.1 in Chapter 3. This can be easily determined by recording the polarised emission from a totally isotropic solution whose emission spectrum coincides with the spectrum of the luminescent molecules (e.g. Fluorescein or Coumarin 6 in methanol). For polarised measurements taken of aligned films, it is imperative to take the effectiveness of the excitation polariser into account and a second instrumentation correction factor, $G_2 = I_{vh}/I_{hh}$, can be determined by recording polarised excitation spectra of an isotropic solution whose absorption spectrum corresponds with the luminescent molecule's spectrum. Here, the G_2 factor was determined with two dyes (Coumarin 120 and Coumarin 500) which together, cover an excitation wavelength range from 275 nm to 475 nm.

[a]For example: I_{Hvh} corresponds to the intensity from a film held with its alignment horizontal, the excitation polariser vertical and the emission polariser horizontal

6.4.4 Experimental: samples

Polyethylene films containing one of the three polymers were investigated with this technique. They were made using the method described in Chapter 3. To ensure the fluorescence anisotropy method could be relied upon, the PF2/6 film was made from the same sample that had been tested with x-ray diffraction. The PF2/6 film tested here was cut from the same stretched strip of polyethylene directly adjacent to the film used in the x-ray study. The comparison of the results was used to estimate the uncertainty in the measurement.

6.4.5 Results and discussion

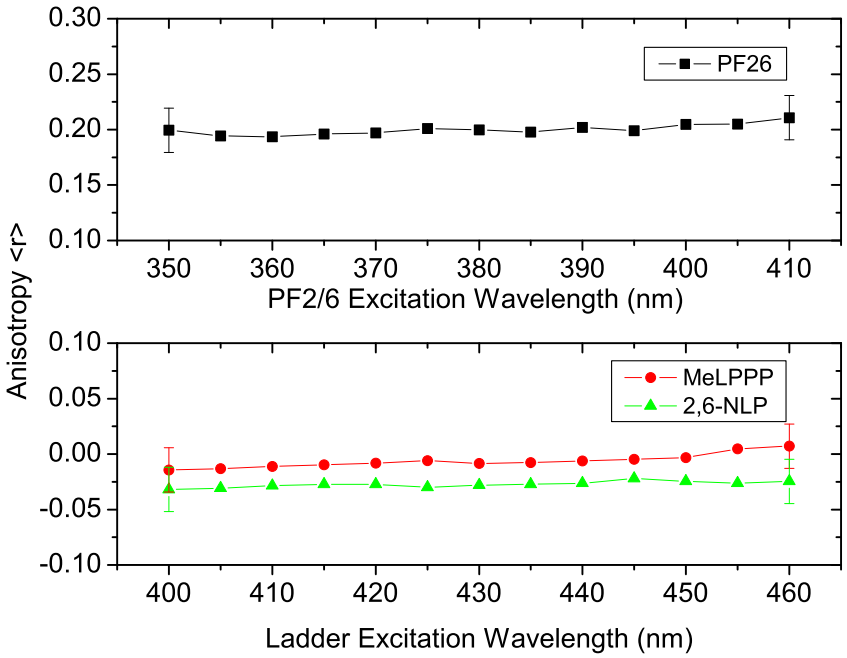

Figure 6.17: Excitation anisotropy spectra of isotropic PF2/6- (squares), MeLPPP- (circles) and 2,6-NLP- (triangles) polyethylene with representative error bars.

The natural anisotropy of the molecules is not always easily determined especially when the molecules are incorporated into a host. It is often necessary to measure the anisotropy in an isotropic film to estimate the effect the host has upon it. Figure 6.17 shows the excitation anisotropy spectra for the three polymers in an isotropic PE matrix. These are the precursor films to the stretch aligned films (as shown at the top and middle of Figure 3.1). PF2/6 shows the highest anisotropy in the PE matrix, a value of 0.20 ± 0.02, which is higher than the 0.10 value which is typically found for isotropic films[23, 225] (for example, the spun cast ladder films in Figure 5.7).

The higher value of anisotropy in the isotropic PF2/6 film arises from the liquid crystalline behaviour of the polymer. A value of 0.1 would have implied that the polymer and associated transition dipole moments are aligned parallel to the Petri dish. This increased the value to 0.2, means that there is a further alignment of the molecules during the casting procedure.

PF2/6 is a liquid crystalline polymer[115,226] and is has been hypothesised in this chapter to form microcrystallites in PE at high concentrations. It follows that fluorescence anisotropy value measured here is a result of probing these aligned crystallites, which in the isotropic film have no preferential direction. Instead of yielding a value close to the natural anisotropy, 0.32 ± 0.04, there is some excitation energy transfer between differently oriented crystallites lowering the anisotropy value to 0.2.

The ladder polymers in an isotropic blend, by contrast, present an anisotropy of value of zero (MeLPPP) or just below zero (2,6-NLP) implying either that all the the uniaxial rods are aligned at the magic angle, 54.7° to the vertical, or that the films are amorphous. Alternatively they may form a mosaic of crystallites that are all oriented differently. The isotropic 2,6-NLP blend presents a slightly negative anisotropy (an average of -0.03 ± 0.02) which, corresponds to an average angle of greater than 54.7° for a photoselected distribution. However, it is much more probable that both of these polymers do not lie in the plane of the film, which would give a value of ~ 0.1. Spun films, however, present a value of 0.1 (see Figure 5.7) due to their anisotropic shape (thickness of a few nanometers).

It has been previously thought that MeLPPP is a liquid crystalline polymer, similar to PF2/6, in that the polymer chains orient themselves uniaxially. The results of the blend films indicates that the chains do not align preferentially in isotropic PE. However, when the film is stretched, the excitation anisotropy spectrum follows the absorption spectrum in the same way as the solutions, as shown in Figure 6.18. It is clear that stretching ladder polymer blends forces a uniaxial orientation and destroys the amorphous-like isotropic state. Heeger *et al.* studied BuEH-PPV in PE blends and found that the crystallites could be destroyed through stretching.[197] Photoluminescence studies on the aligned films have shown that the emission is the same as from dilute solutions are considered to be made of isolated molecules. Therefore, as in BuEH-PPV, stretching the ladder type blends isolates the molecules and they can be considered as such for the next part of this work.

As discussed in the x-ray section above (6.2.5), entanglement of adjacent crystallites in a PE blend is the reason for their destruction upon stretching the film. Whilst this seems a good explanation for MeLPPP and 2,6-NLP, further experiments, involving identifying the packing regime of ladder polymers and varying the concentration of the PE blend, would be needed to confirm this hypothesis.

The data from the x-ray work have that the conjugated polymer PF2/6 forms crystalline microphases in the aligned PE. This also showed that as the concentration decreased so did the size of the crystallites until at low 1 % concentrations, the crystallites were effectively single molecules. The total dissolution (miscibility) of the molecules is comparable to the molecules in a dilute frozen solution because in the PE and the host, the conjugated polymer is unable to rotate or twist. For these reasons, PE matrices cause the polymers to behave as they would at a very low temperature. The natural anisotropy of the molecules used in this part of the study were estimated to be the same as those predicted by the low temperature

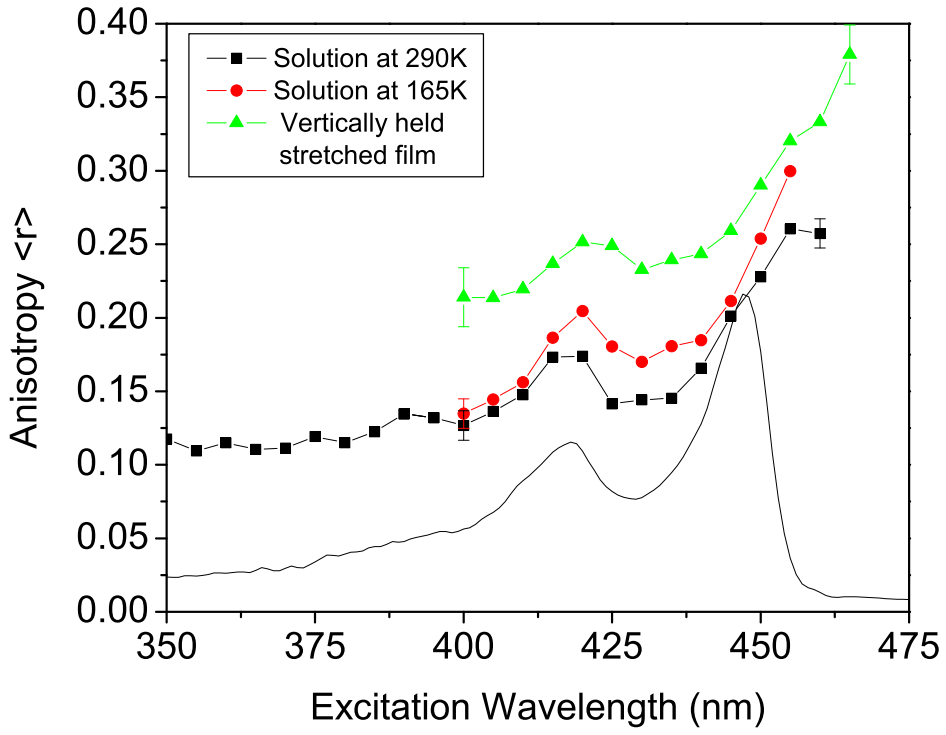

Figure 6.18: Excitation anisotropy spectra of 2,6-NLP in dilute solution at room temperature (squares), 165 K (circles) and in anisotropic PE film stretched 11 times its original length. Also shown is the absorption spectrum of the polymer in dilute toluene solution. Representative error bars are shown on the graph and the film is held vertically.

anisotropy measurements: for PF2/6, $r_0 = 0.32$ (see Chapter 4); 2,6-NLP, $r_0 = 0.36$; and MeLPPP, $r_0 = 0.36$ (see Chapter 5).

To investigate the reproducibility of the films and the measurements, the polarised emission and order parameters were calculated for different PE films. The data from films containing PF2/6 are shown in Figure 6.19 and the angle the polymer chain makes with the perfect orientation direction is approximately 20° (a full list of results is in Table 6.3 below). The order parameter is not explicitly linked to the film's extension and it is clear that each film is unique but measurements taken on films with the same extension made from the same isotropic film do have very similar order parameters as expected. The error on these measurements (taken through repeat readings of the same film) is ± 0.04 which corresponds to an error on the angle of ± 2°.

Two order parameters were returned for similar films, 0.82 ± 0.04 from fluorescence anisotropy measurements and a slightly higher 0.93 ± 0.02 from the GIXD. The order parameter from the x-ray measurements is determined from the orientation of the crystallites, whereas the fluorescence anisotropy measurement comes from individual chains of PF2/6. The analysis for the order parameter value determined by GIXD was carried out for two differently concentrated PE blends. It was shown in section 6.2.4 that at these concentrations, PF2/6

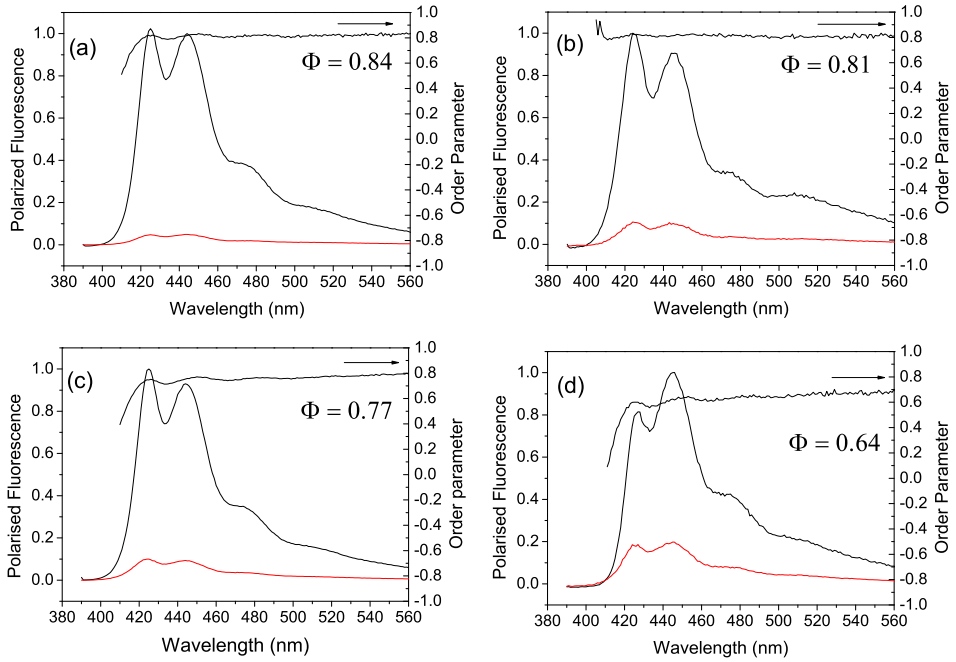

Figure 6.19: Polarised fluorescence and order parameters of stretch aligned $< 1\%$ PF2/6 films. Films stretched 30 times their original length. Films (a) and (b) are taken from the same stretched film. Films (c) and (d) are from the same isotropic batch. The error on the order parameter was $\pm$ 0.04.

formed hexagonal crystallites, in which the chains are aligned with the stretching direction. As the concentration was reduced to $< 1\%$, the size of the crystallites decreased to that of a single molecule. It is assumed that the ordering of the single chains is similar to that of the crystallites. Hence, the order parameter is used to describe such films.

The anisotropy based value comes from two experimentally derived values. In addition to the fluorescence anisotropy experiment, it is dependent upon the successful determination of the natural anisotropy and if this has significant errors then so to does the resulting order parameter. The fluorescence anisotropy value also relies on the alignment of two Glan-Thompson polarisers to produce the polarised light that is used. The synchrotron created x-ray beam, due to its formation, is significantly more polarised and the x-ray results will be more reliable. As such the 0.93 ± 0.02 estimate is the more reliable of the two values and this means that there is an error in Φ of $\pm$ 0.1 meaning an error in ε of $\pm 5^\circ$ for all the fluorescence anisotropy measurements of the order parameter. Order parameters were estimated over the area of strong fluorescence.

The polarised emission and order parameters calculated for different PE films containing ladder polymers are shown in Figure 6.20. It clearly shows that as the extension increases (e.g. the films in Figure 6.20 (b) and (d) are stretched about twice those of (a) and (c)) the order parameter increases. It can also be seen how important it is to calculate the order

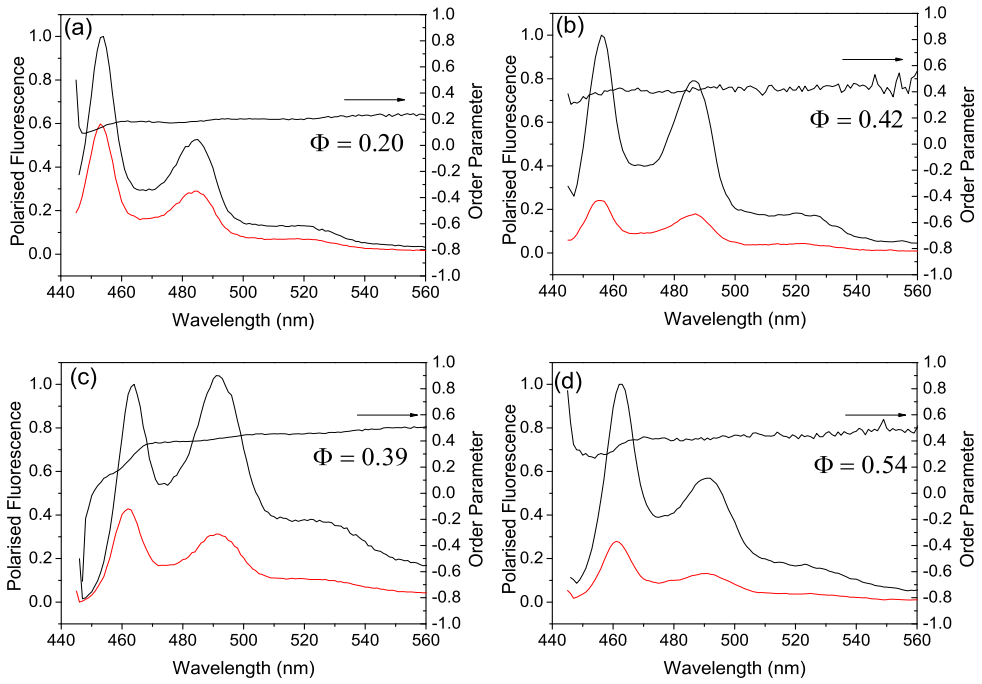

Figure 6.20: Polarised fluorescence and order parameters of stretch aligned 2,6-NLP ((a) and (b) from the same isotropic batch) and MeLPPP ((c) and (d)). The films have been stretched (a) 11, (b) 28, (c) 12 & (d) 20 times. The errors on the order parameter were $\pm$ 0.02**.**

parameter for each individual film made with either of the ladder type polymers. The angle the polymer backbones make with the perfect alignment direction is about $\sim 38^\circ$ for both polymers in highly stretched films and the angles are shown in Table 6.3 below. The order parameter of MeLPPP (Figure 6.20 (c) and (d)) and resulting angles ($35 - 40^\circ$) correspond well to the angle estimated using partially polarised Raman spectroscopy (35°).

The ladder polymers clearly do not orientate as easily as PF2/6 does, neither in the isotropic matrix nor in the stretched films. The data from films of different stretches and the two different polymers confirm that the ladder-type polymers do not align as well as PF2/6. However, there is suggestive evidence in Figure 6.20, that as the film is further extended, more alignment is achieved. This cannot be rigorously proven as each film came from a different strip of the same isotropic matrix. The degree of flexibility in PF2/6 clearly assists the alignment procedure. The crystallites in PF2/6 are formed in the PE and this orientation is carried through as the film is stretched leading to the high order parameters observed. The ladder polymers, thought to also be liquid crystalline, are much more inflexible and yet this liquid crystalline phase is not observed in isotropic blends. The zero fluorescence anisotropy in the isotropic ladder blends suggest an aggregation with no orientation which is broken up as the film is drawn out (as in BuEH-PPV[197]). The polarised emission and absorption (in the next section) indicate that there is a uniaxial distribution. The low value of the order

parameter fits with a similarly low value calculated from Raman spectroscopy. It comes from a wider distribution of the angle ε. The angle calculated for these polymers must be used carefully. However, the results should not be ignored, because PF2/6 can be aligned well and a comparison between the three polymers can be used to explain results in later parts of this thesis.

The lack of aligned crystallites explains why the x-ray diffraction results indicate that the film is amorphous even when stretched to 30 times its original length and there is evidently short range order. The low concentration of the aligned phase is not prominent compared with that of the isotropic phase.

The method of fluorescence anisotropy to determine the order parameter in an aligned film can only give a value of average angle for a homogeneous uniaxial model. For example, microcrystalline domains each with a different domain orientation can give an "average angle" of 10 ° from stretch direction. However, this angle represents the domains rather than the single polymer backbone unless the crystallites are uniaxial.

PF2/6 creates crystallites (as shown in Figure 6.3) that are uniaxial which is confirmed by the x-ray images in section 6.2.4. Therefore, it is safe to assume that the order parameters derived in this section do give the average angle of ε and the values determined can be used in the following sections.

6.4.6 Conclusions

Using the natural anisotropy values found in Chapters 4 and 5, the order parameters of stretched aligned polymer blends were found via a polarised fluorescence technique. The order parameter was unique for each individual film. It was shown that the PF2/6 had a higher order parameter than both MeLPPP and 2,6-NLP. It was shown that PF2/6 films, from the same stretched sample, had the same order parameters within experimental error. It was also shown that films made from the same batch, stretched the same amount, had similar values of the order parameters proving PF2/6 can be aligned well by this method.

The data for MeLPPP and 2,6-NLP suggest that the alignment of these polymers is not as good as they have a lower order parameter. The data also suggest that increasing the amount of stretch increases the order parameter, indicating that the method does indeed align the polymer.

6.5 Conclusions about the order parameter

Three different methods have been used to determine the order parameter of stretched polyethylene films were used. The polyethylene films contained one of three conjugated polymers, poly (9,9-di(ethylhexyl)fluorene) (PF2/6) and one of two ladder-type poly (*para*-phenylene) polymers (MeLPPP and 2,6-NLP).

It was found through x-ray diffraction (GIXD) that PF2/6 aligns well and has a concentration dependent phase segregation effect. When the concentration of PF2/6 in polyethylene is more than 7%, the PF2/6 molecules cluster together and align to form crystallites. For films containing less than 1% PF2/6, it was found that the crystallites were significantly smaller (a single molecule) but assumed to have the same degree of ordering. It has been assumed that as the concentration is reduced the size of the aggregates are significantly reduced but that the order parameter created through stretching remains at a similarly high value for all concentrations. The order parameter was estimated using x-ray diffraction to be 0.93 ± 0.02.

The GIXD method was not suitable for the ladder type films because this polymer does not form aligned crystallites. Instead a polarised fluorescence technique was used to determine the order parameter. Using this method, the estimated order parameter of the PF2/6 was high (> 0.80) confirming that this molecule aligns well by the stretching method. The difference between this value of order parameter derived from the fluorescence anisotropy method and the GIXD experiments is $\Phi \pm 0.1$ which corresponds to an uncertainty in the angle ε of $\pm 10\,^\circ$ for the fluorescence anisotropy method.

Raman spectroscopy was used to investigate a single MeLPPP film stretched eight times. The order parameter was measured relative to the order parameter of polyethylene (assumed to be one). The polarised fluorescence method was used for MeLPPP and 2,6-NLP and it was found that the order parameter for the films was ~ 0.40. The results of the studies on MeLPPP and 2,6-NLP films indicate that these polymers do not align as well as PF2/6. This was explained to be as a result of the rigid backbone of these polymers, whereas it is believed that the PF2/6, because it is more flexible, can be more easily stretched.

The values for the ladder type films should be used cautiously as they come with a large error but the photophysics for these films can be compared with isolated molecules in a frozen solution. This knowledge will assist the explanations in Chapter 7.

6.6 Determination of the angle of the absorption transition dipole moment via linear dichroism

6.6.1 Overview

Using the values of the angle between the polymer backbone and the stretch direction, ε, found in the previous section, the angle the absorption transition dipole makes with the backbone can now be investigated via linear dichroism. This requires the earlier measurements of the order parameter. The low concentration films used to determine the order parameter were studied with polarised absorption spectroscopy. The theory of which can be found in Chapter 2 section 2.5.5.

6.6.2 Experimental

Polarised absorption spectra were taken on equipment constructed in the laboratory and a commercial 2-channel spectrophotometer as described in Chapter 3, section 3.4. Using equation 6.10, it is possible to determine the angle between the polymer's backbone and the absorption transition dipole moment, α.

$$\frac{LD}{3A_{ISO}} = \frac{1}{2}(3\langle\cos^2\alpha\rangle - 1)\Phi \tag{6.10}$$

using the notation in Chapter 2 section 2.5.5.

6.6.3 Results

Figure 6.21 shows the polarised absorbance spectra of a 1% PF2/6 polyethylene blended film stretched 30 times its original length. The figure shows that there is significant absorbance parallel to the film orientation direction and only a smaller amount perpendicular to the film direction. The absorbance perpendicular to the stretch direction is not negligible, giving a dichroic ratio ($A_{\parallel}/A_{\perp}$) of 10. This indicates that the absorption transition dipole is not completely parallel to the stretch direction, but only makes a small angle with it. If the stretch direction and the absorption transition dipole moments are parallel then the dichroic ratio would be very high because the absorption perpendicular would be almost negligible.

The figure also shows the angle between the absorbance transition dipole moment and the backbone, α, shown by red circles. The angles were determined from the linear dichroism data and the order parameter determined by x-ray diffraction, ($\Phi = 0.93$) via equation 6.10.

The angle calculated varies with absorption wavelength. This is unusual for a single chromophore which would normally give a single value. However, conjugated polymers, like PF2/6, support a range of conjugation lengths (as first mentioned in Chapter 2 section 2.3.7.) The data suggests that each conjugation length has a corresponding absorption transition dipole moment confirming the postulate in Chapter 4

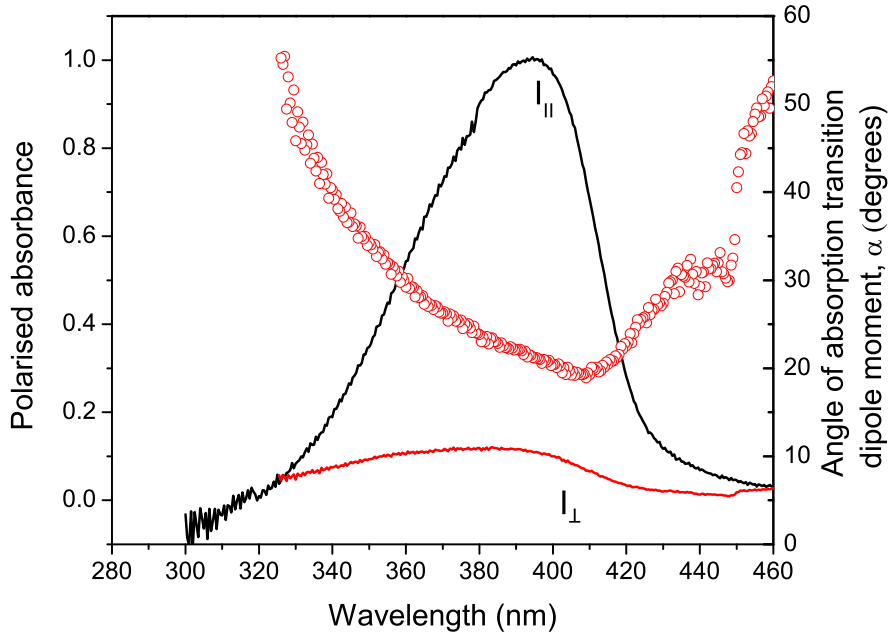

Figure 6.21: An example of a polarised absorbance spectra of aligned $< 1\%$ PF2/6 films stretched 30 times. The graph shows the absorbance parallel (black) and perpendicular (red) to the films alignment direction. These spectra were used to calculate the linear dichroism and using the order parameter determined by GIXD the angle between the backbone and the absorption transition dipole moment were calculated. These angles are shown on the graph by red circles. Angles at the maximum absorption wavelength are tabulated in Table 6.1.)

It was also hypothesised in Chapter 4 that as the conjugated length extends, the transition dipole becomes more aligned with the backbone. The data here shows that at short wavelengths (corresponding to short conjugation lengths) the angle α is large and tends to be a minimum of approximately $20\,^\circ$ at the peak absorbance (corresponding to longer conjugation lengths). Again, the earlier hypothesis for PF2/6 is supported. The angle, α, used later in this work, was determined to be the value of maximum absorbance because this corresponds to the strongest transition.[b]

The data presented in Table 6.1 are taken from experiments on films that had been stretched 30 times their original length. The table includes data from two films taken from the same stretched piece and two from the same isotropic batch that have been stretched independently. It can be seen from the table that the films from the same stretched piece have similar short range order parameters and similar LD values. Those from the same isotropic batch, but a differently stretched piece, have different order parameters. However, they do show that α is between $15\,^\circ$ and $20\,^\circ$.

[b]The data for the film used in Figure 6.21 and that from PF2/6 films that had been stretched 30 times is listed in Table 6.3.

Polymer	Stretch	Order Parameter ±0.02	ϵ ±2°	LD^r	α ±5°
PF2/6*	30	0.93†	12°	0.75	21°
		0.84	20°		15°
PF2/6*	30	0.93†	12°	0.73	22°
		0.81	20°		15°
PF2/6**	30	0.77	23°	0.62	21°
PF2/6**	30	0.64	29°	0.60	12°

Table 6.1: Table of absorption transition dipole angles determined for PF2/6. (ϵ: backbone to film alignment; α: backbone to absorption transition dipole moment; * & ** films were made from the same initial film. Order parameter determined by fluorescence anisotropy measurements and † x-ray diffraction.

For comparison the angles predicted using the order parameter determined by GIXD (0.93) and fluorescence anisotropy (dependent on the film) are shown in the table. It is noted that the 5° difference that occurs in the angle ε is propagated to the angle α, and this changes the absorption transition dipole moment angle by 5°.

Whichever order parameter is used, the absorption transition dipole is shown to be off-chain for the region of highest absorption. The absorption transition dipole corresponding to the blue edges of the conjugation length distribution are even further off-chain (Figure 6.21).

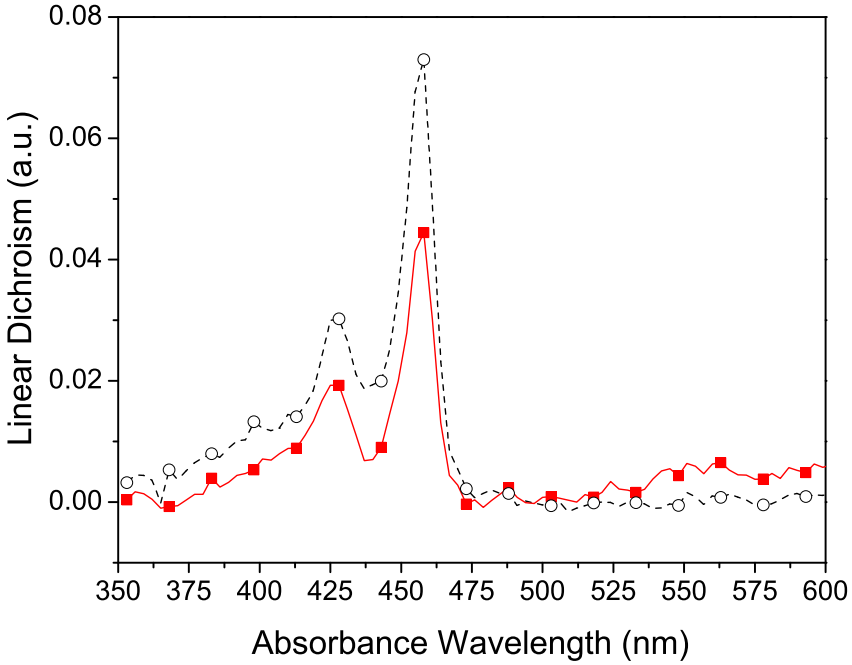

Figure 6.22: Linear dichroism spectra of mechanically stretched polyethylene films doped with MeLPPP stretched 8 (squares) and 12 times (circle). The graphs show that the LD increases as the as the stretching increases. The energetic position of the main absorbance transitions are unaffected by the mechanical process.

The experiments were repeated for films containing the ladder-type polymers showing a similar trend in off-chain absorption transition dipole moment. First, the effect of different stretch ratios is investigated and then the angles of absorption transition dipole moment for the two edges of the conjugation length distribution are listed.

The linear dichroism (LD) results of two mechanically stretched MeLPPP in polyethylene films are shown in Figure 6.22. The films came from the same unoriented sample and were stretched 8 times and 12 times their original length respectively. The figure shows a structure that follows the polymer's absorption spectrum and, as the film is stretched, the LD of the two peaks increases and the LD trough between them decreases. The LD at the two absorption peaks is 0.03 and 0.07 at λ_{abs} = 425 nm and λ_{abs}= 460 nm respectively. The wavelengths between the peaks has an LD of 0.02 at λ_{abs} = 440 nm. Using the order parameter determined by Raman spectroscopy ($\Phi = 0.54$), the angle between the absorption transition dipole and the polymer backbone for the red-edge (455 nm), α_{Red} can be calculated using equation 2.25 to be 18°. The angle between the absorption transition dipole and the backbone varies with excitation wavelength as at the blue-edge of the spectrum (440 nm) $\alpha_{Blue} = 42°$, making an angular difference of 24° across the absorption spectrum for this film.

Whilst the LD increased for the film stretched 12 times its original length, no measurement was taken of its order parameter, so it is not possible to estimate angles from this film. If the order parameter were the same (as assumed above, 0.54) then the average angle α is reduced slightly and the angular distance between the two edges is similarly reduced.

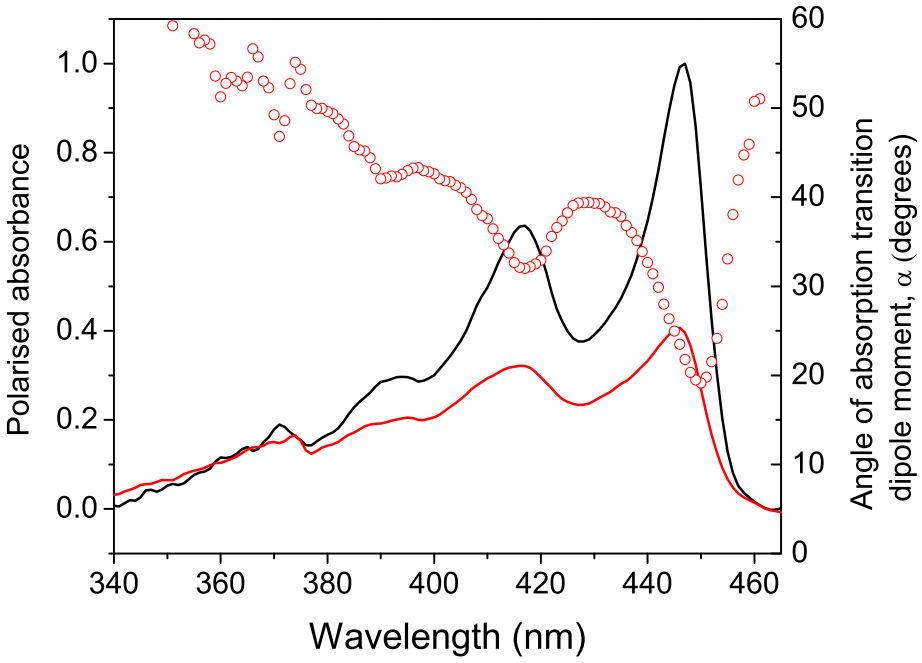

Figure 6.23: An example polarised absorbance spectra of aligned $< 1\%$ 2,6-NLP films stretched 28 times. The graph shows the absorbance parallel (black) and perpendicular (red) to the films alignment direction. These spectra were used to calculate the linear dichroism and using the order parameter determined by fluorescence anisotropy the angle between the backbone and the absorption transition dipole moment were calculated. These angles are shown on the graph by red circles. Angles at the maximum absorption wavelength are tabulated in Table 6.1.

Other films containing the ladder-type polymer were also investigated and were analysed using an order parameter determined by fluorescence anisotropy. Figure 6.23 shows the absorbance parallel and perpendicular to the films stretch direction. The figure shows that there is a dichroic ratio of 2, again indicating that the absorbance transition dipole moment is not aligned parallel or perpendicular to the stretch direction. The figure also shows the angle, α, calculated from equation 6.2, and the order parameter estimated by fluorescence anisotropy.

As with PF2/6, and predicted in Chapter 5, the angle α is dependent upon the absorption wavelength. This is attributed to the change in conjugated length. The angle is smallest at the red-edge of each of the absorption vibronics. This fits with the idea that the longer conjugation lengths are more aligned with the backbone (despite still being at 20° from the backbone). The other point to note is that the angle α varies in the same way (follows the absorption spectrum) as the fluorescence anisotropy follows the excitation wavelength. This supports the idea that it is the absorbance transition dipole moment that varies with wavelength not the emission transition dipole moment. It also confirms that there is a single emission transition dipole. If there was more than one emission transition dipole moment, the fluorescence anisotropy would not be an exact replica of the LD spectrum.

The data from a collection of films containing one of the two ladder polymers are shown in Table 6.2 and contain the angles derived from the results. As with the MeLPPP film above, the data in the table suggest that increasing the extension reduces the angle that the absorption transition dipole moment makes with the backbone. This is not physically possible as the angle is intrinsic to a molecule. Therefore, the data should be interpreted as showing that with increased extension more of the polymers become aligned and the width of the distribution of the angles measured is reduced.

The width of the angular distribution in MeLPPP is broad and is believed to arise from the fact that the backbone is branched (shown in Figure 2.12) and the two units contribute to both polarisations. As the contributions are not necessarily equal they will have the effect of increasing the experimental error.

Polymer	Stretch	Order Parameter	α_{Red}	α_{Blue}	Difference
2,6-NLP*	11	0.20	25°	33°	8°
2,6-NLP*	28	0.42	22°	38°	16°
MeLPPP	8§	0.54	18°	42°	24°
MeLPPP	12	0.39	28°	35°	7°
MeLPPP	20	0.54	5°	22°	13°

Table 6.2: Table of absorption transition dipole angles determined for the ladder-type polymers. (ϵ: backbone to perfect alignment; α: backbone to absorption transition dipole moment; α_{Red} and α_{Blue} refer to the edges of the conjugation length distribution.

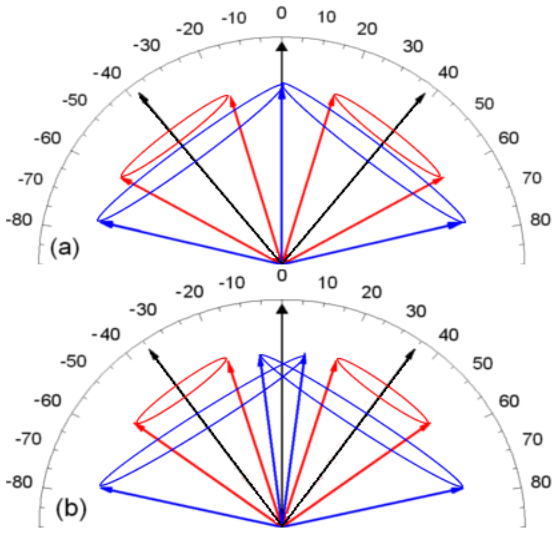

Figure 6.24: Diagram of the location of the the red and blue absorption transition dipole moments lie in (a) 2,6-NLP stretched 28 times its original length and the order parameter determined by fluorescence anisotropy and (b) MeLPPP stretched 8 times its original length and the order parameter determined by partially polarised Raman Spectroscopy.

Table 6.2 and Figure 6.24 show the location of the absorption transition dipoles for the blue peak and red-edge of the polymer's absorption spectrum. They clearly show that the red-edge is localised 20 ° off the chain axis and the blue-edge is up to a further 20 ° from that. The cylindrical rotational symmetry of the transition dipoles around the polymer's backbone has also been indicated in the diagrams.

The results of the linear dichroism (LD) measurements (Figure 6.22) also confirm that there are a range of absorption sites which are at different angles as hypothesised in Chapter 5. The apparent change in alignment of both chromophores with respect to the stretching direction as the mechanical stretching is increased indicates that the polymer is being straightened. Because neither PF2/6 nor MeLPPP show a constant linear dichroism (which would be seen as a constant α) it can be confirmed that earlier assumptions about the polymer conjugation length distribution are valid. Had there been only one absorption dipole orientation, and hence a single chromophore, the linear dichroism across the whole spectrum would have tended to a constant value. Using the order parameter approximated via the Raman spectroscopy, the angle between the absorption transition dipole moment and the backbone for the red-edge, α_{Red}, is ~ 24 ° off that axis (for MeLPPP); whilst not directly confirming the fluorescence anisotropy result, this new result strongly supports the theory outlined earlier. The angle found using the films studied with fluorescence anisotropy shows a much smaller angle (between 7 ° and 13 °) which support the fluorescence anisotropy results.

6.7 Location of the transition dipole moments relative to the polymer's backbone.

6.7.1 Overview

The results of the x-ray diffraction and fluorescence anisotropy have shown that the luminescent polymer, PF2/6, can be aligned in a stretched polyethylene matrix. Similar experiments have shown that MeLPPP and 2/6-NLP can also be aligned to some extent by the stretching method.

The more flexible polymer, PF2/6, has shown the highest dichroic ratio and the highest order parameter of the three polymers studied. It is significantly more aligned than the ladder polymers and forms an angle of $\sim 12^\circ$ with the stretch direction of the PE host and possesses some long range order. In contrast the order parameters of the ladder polymer blends indicate that this angle is $\sim 35^\circ$ for the rigid-rod polymers and that it has very little long range order.

The x-ray diffraction results have also confirmed previous work on stretched PE films that have shown that there is still a large amount of alignment even if the PE does not show the sharp diffraction peaks associated with long range alignment.[202,207] Whilst x-ray diffraction was not successful in determining the order parameter of the ladder type polymer blends, the techniques that study a smaller area (fluorescence anisotropy and Raman spectroscopy) of the sample were successful. It is worth noting that the different techniques give consistent results within $\pm 10^\circ$ error.

Using linear dichroism on the stretch aligned films has allowed the absorption transition dipole moment to be located for each of the polymers. It was found to be up to 21° off-axis. Previous studies of other conjugated polymers have also found that the absorption transition dipole moment is similarly off-axis, in the linear polyenes it was located 15° away from the chain[166] and this value has been confirmed for the conjugated polymer MeH-PPV.[227] This information, coupled with the results from low temperature fluorescence anisotropy measurements in the earlier chapters will allow progress in explaining the behaviour of the excitation. This is dealt with in the following section.

6.7.2 Collation of results

The data collected in Chapter 6 is collated in Table 6.3. Even in tabular form, it can be seen that for all three polymers the angle between the absorption transition dipole moment is very similar to that of the angle between the absorption transition dipole moment and the emission transition dipole moment. The predictions for these angles are related to one another and they are shown in Figures 6.25 and 6.26.

Polymer	Stretch	Order Parameter ±0.02	ϵ ±2°	LD^r	α ±5°	θ ±6°
PF2/6⋆	30	0.93†	12°	0.75	21°	21°
		0.84	20°		15°	
PF2/6⋆	30	0.93†	12°	0.73	22°	21°
		0.81	20°		15°	
PF2/6⋆⋆	30	0.77	23°	0.62	21°	21°
PF2/6⋆⋆	30	0.64	29°	0.60	12°	21°
2,6-NLP⋆	11	0.20	47°	0.14	25°	15°♭
2,6-NLP⋆	28	0.42	38°	0.33	22°	15°
MeLPPP	8	0.54§	35°	0.46	18°	15°
MeLPPP	12	0.39	40°	0.22	28°	15°
MeLPPP	20	0.54	35°	0.54	5°	15°
MeLPPP	25	0.44	38°	0.55	-	15°

Table 6.3: Various polymer angles as determined in this study. (ϵ: backbone to perfect alignment; α: backbone to absorption transition dipole moment; θ: absorption transition dipole moment to emission transition dipole moment. ⋆ and ⋆⋆ films were made from the same initial film. ♭: error for the LPPPs is ±15°.) Order parameter determined by fluorescence anisotropy measurement except †: x-ray Diffraction and §: partially polarised Raman spectroscopy. θ determined from low temperature fluorescence anisotropy and ‡ from Figure 6.18.

These figures show the location of the polymer backbone from the stretch direction at the "average" angle determined via x-ray diffraction. Assuming a uniaxial distribution they also show the average angles the absorption and emission transition dipoles make with the backbone. The diagrams do not show the error on these measurements and are for illustrative purposes only.

The emission transition dipole moment lies in a cone of angle, θ, from the absorption transition dipole moment, but in the figures only the location towards the backbone in the plane of the paper is shown. For completeness, the small angular difference that arises from calculating the positions with the order parameter determined by (a) GIXD and (b) fluorescence anisotropy measurements is shown in Figure 6.25. The diagrams illustrate that the average absorption transition dipole moment location is off axis whereas the emission transition dipole moment is at an angle that is more along the backbone. Both images show that the transition dipole appears to rotate from an off-axis position towards the backbone of the polymer. The cylindrical rotational symmetry of the transition dipoles around the polymer's backbone has also been indicated in the diagrams.

The angle of the transition dipole moments determined for the two ladder polymers are shown in Figure 6.26. But fluorescence anisotropy experiments clearly indicate the rotation of the emission dipole towards the backbone. The schematics in Figure 6.26 ((a) 2,6-NLP and (b) MeLPPP) show that there is a rotation of the transition dipole moments from a state located off-chain to a state more aligned with the chain. In the ladder-type films this rotation is not as complete as PF2/6. This is a result of larger experimental errors (the order parameter measured via fluorescence anisotropy has a large error of ± 10°) and the fact the films have

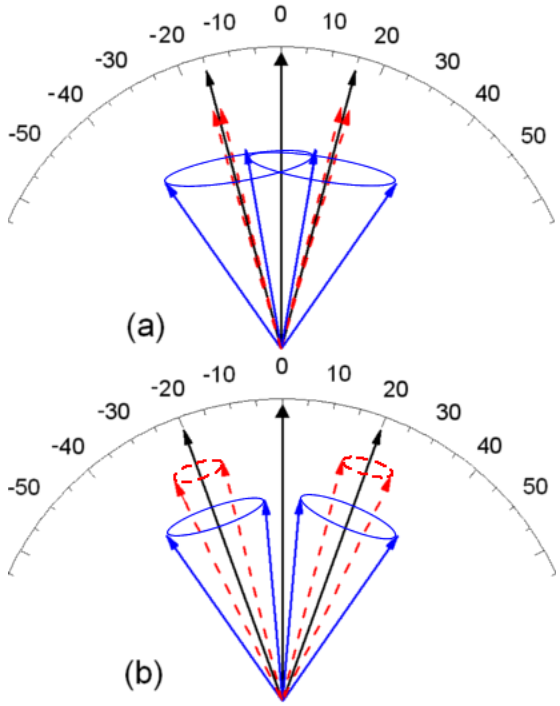

Figure 6.25: Diagram of where the absorption and emission transition dipole moments lie in a PF2/6 film. (a) shows the angles determined with the order parameter determined by GIXD and (b) shows the angles determined with the order parameter determined by fluorescence anisotropy. The short solid arrows indicate the absorption transition dipole moment and the dotted arrows are the emission transition dipole moment.

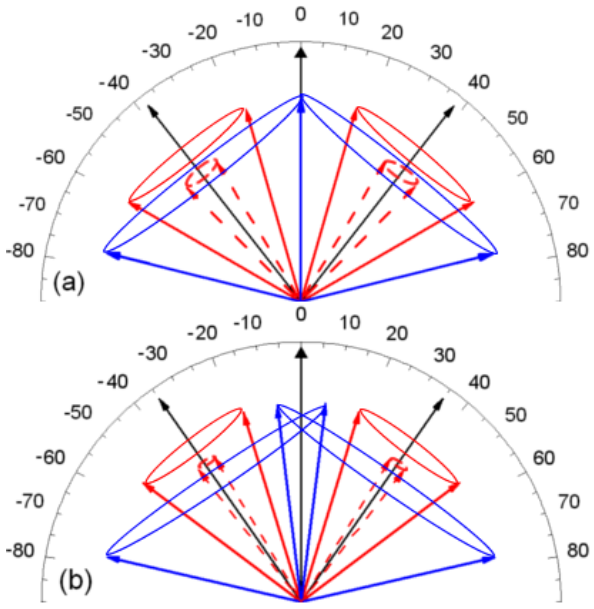

Figure 6.26: Diagram of where the red and blue absorption and its emission transition dipole moments lie in (a) 2,6-NLP stretched 28 times its original length and the order parameter determined by fluorescence anisotropy and (b) MeLPPP stretched 8 times its original length and the order parameter determined by partially polarised Raman Spectroscopy. The short solid arrows indicate the red and blue absorption transition dipole moment and the dotted arrows are the emission transition dipole moment.

a low order parameter. The difference in backbone position that arises due to the two order parameter measurements comes from a combination of two effects. The first, most obvious discrepancy arises from aligning the system by eye which can give an error of up to 3 °. The second discrepancy arises from the fact the two experiments probe different order ranges; x-ray diffraction probes the long order range whilst the fluorescence technique probes the short range. From the results from stretched polymer films it can be seen that the polyethylene is not totally aligned (it would appear as single peaks instead of powder rings if it were) which means there may be areas of the film that have slightly different ordering. This is due to either an imperfect blend or a higher doping concentration. If the PE is not perfectly aligned it would provide a lower estimate of the order parameter on the short scale and there would be a small degree of variation if the two areas probed by the fluorescence anisotropy and the linear dichroism techniques were slightly different. This is entirely feasible since the piece of film studied was 1 cm × 1.5 cm.

Another aspect to take into account is that the equations used in the determination of the order paramter via fluorescence anisotropy contain another experimentally determined value, the natural anisotropy. An estimate for its value was based on a low temperature extrapolation of fluorescence anisotropy results taken in dilute solution, see Chapters 4 and 5. Fluorescence anisotropy of materials in solution does give an excellent estimate of the natural anisotropy[218] but the value can be subject to solvation effects and, as noted previously in this chapter, it is necessary to know the value of the host material's anisotropy. In Figure 6.17, the anisotropy for the isotropic PE blends are presented and the PF2/6 value is about $\langle r \rangle = 0.20 \pm 0.01$. If this value were used, then the order parameter for the films shown in Figure 6.19 (a) and (b) increases to 0.96 (from 0.84) and 0.93 (from 0.81) which is in excellent agreement with the x-ray diffraction results.

This analysis procedure fails when applied to the ladder-type films, where a low natural anisotropy gives rise to an order parameter greater than 1. As suggested previously, this low natural anisotropy is explained by the lack of order in the isotropic phase. It is apparent that when the hot o-xylene solution is poured on to the glass slide it does not affect the ladder-type polymers and force them into order in at least one direction. The random orientation in this plane must not be ignored once the film is stretched and some polymers may not lie in the plane of the film. This has the resultant effect that the transition dipole moments will not lie in that plane either. Since the results presented are for the whole sample, any out of plane polymer will mean the angles determined will be slightly less perfect (as shown in Figure 6.26) and yet still fit with the theory for PF2/6. It can be safely assumed that the PF2/6 molecules do reside in the plane of the film due to the anisotropy value of the isotropic blend.

The schematics, with all their associated errors, do illustrate that the same dipole reorientation process occurs in the flexible PF2/6 and in the more rigid ladder-type polymers. In previous work, this depolarisation has been explained as a result of the polymer's flexibility, where the twisting of the backbone drives the process.[48,81] Here it is shown that this the depolarisation is more fundamental and not necessarily linked to physical conformation change because it lies in a fixed matrix.

In Chapter 4, shortening the polymer chain and removing excitation migration to new sites were observed as an increase in the fluorescence anisotropy. But in no case was the maximum value of fluorescence anisotropy observed. It was explained in Chapter 4 that the conformational relaxation facilitated the fluorescence anisotropy loss in PF2/6. With the polymers immobile in an isotropic host this explanation is not viable, the only explanation left is that the electronic relaxation of the excited state is responsible for the anisotropy loss. This relaxation is equivalent to a conjugation length change of just a few bonds but is enough to cause a significant reorientation of the dipole moments. The interpretation is that as the conjugation length increases the emission transition dipole moment becomes more aligned with the polymer backbone.

This explanation almost fits with Westenhoff *et al.*[81] who have theorised that, as planarisation of the molecule occurs, the excited state extends over a few more adjacent bonds. In this case, it is unlikely that the polymer PF2/6 can undergo total planarisation (or twisting to the same extent as it can in solution) because of the rigid matrix. However, the electronic extension of the excited state is not precluded. A similar process must happen in the ladder polymers independent of phase because it is a rigid-rod that is incapable of planarising.

Ignoring a polymer's flexibility and concentrating solely on the ladder-type polymers, the location of the absorption transition dipole moment relative to the polymer's backbone can be considered. The linear dichroism results suggest that the ground state also behaves in the same way: as the conjugation length increases, the angle between the absorption transition dipole moment and the polymer's backbone reduces. As expected the electronic states are governed by the backbone configuration and as the states delocalise they overcome the crooked nature of the backbone.

Another finding of this work is that PF2/6 undergoes phase segregation in a polyethylene matrix. X-ray diffraction results and fluorescence microscope images have been used to show that microcrystalline regions of PF2/6 guest arise in the PE host. These results do support the concept of phase segregation at higher polymer concentrations and will be the basis for more research into polymer blends. As the concentration is reduced to below 1%, the micocrystallites reduce in size, possibly down to single molecule size. Thus, at low concentrations it can be assumed that these PE films take on the characteristics of dilute solutions suggesting that the molecules are indeed isolated.

This assumption is confirmed by the measurements on the ladder polymers as the fluorescence anisotropy for a stretched film and that of a solution (found in the previous Chapter 5) appear very similar. But given that aggregates can still form, it is not possible to determine whether it is a small aligned aggregate that explains the photophysics. Interestingly, before stretching, the films tend to have an amorphous nature and as they are stretched, they take on the properties of a dilute solution.

6.8 Conclusions

The order parameter of stretched polymer blends (conjugated polymer in polyethylene) was determined through x-ray diffraction, polarised Raman spectroscopy and a fluorescence anisotropy technique. The angle of the backbone to the stretch direction was found to be $\sim 12^\circ$ for PF2/6, $\sim 40^\circ$ for both 2,6-NLP and MeLPPP. The results from different techniques were compared and found to vary with an error of 10°. This is thought to have arisen from the errors associated with fluorescence anisotropy approach as this relies heavily on another experimentally derived value.

Linear dichroism experiments were carried out successfully on the films for which the order parameter had been determined. This data was used with the order parameter measurements to calculate the angle between absorption transition dipole moments and the polymer backbone. The results strongly suggest that the absorption transition dipole moments lie up to 20° off-axis.

The information about the order parameter and the linear dichroism results was then combined with the natural anisotropy values from Chapter 4 (for PF2/6) and Chapter 5 (for 2,6-NLP and MeLPPP). This information gives the angle between absorption transition dipole moment and emission transition dipole moment and was used to determine the relationship between the emission transition dipole moment and the polymer backbone. It was illustrated that one conclusion is that the emission transition dipole moment is along the backbone. This was shown diagrammatically for PF2/6. The results in Chapter 5 showed that the anisotropy varied across the absorption spectrum and this was used in conjunction with linear dichroism to calculate the absorbance angles for the ladder-type polymers. For 2,6-NLP it was found to be dependent upon the order within the film: but the higher energy edge is over 16° from the red-edge, slightly more than predicted by the fluorescence anisotropy results of the previous Chapter 5.

For MeLPPP, it was found to be similarly dependent on order, but is still thought to be $\sim 15^\circ$ further from the red-edge and, therefore, comparable with the anisotropy results. It is conjectured that the longer lengths are delocalised along the polymer's backbone and as the conjugation length shortens, it becomes more localised away from the polymer's backbone.

The reason for the varying absorption transition dipole moment angle with wavelength is due to the distribution of conjugated length supported by a polymer. Each conjugation length has a different absorbance transition dipole moment, dependent upon its length (the angle reduces as the conjugation length increases). It follows that the extension of the conjugation length over more bonds affects the angle. It has been hypothesised that the kinks in the polymer backbone (from flexibility in PF2/6 branched formation in MeLPPP and non-linear backbone in 2,6-NLP) cause this difference.

As a consequence of these findings if these aligned molecules were used in conjunction with a semiconductor LED to create a polarised backlight, the molecules would need to be oriented at 15° to the LED polarisation direction for maximum absorbance. They would also need to be parallel to the transmission axis of the polariser for the maximum transmission efficiency.

These experiments have successfully produced results that show how depolarisation changes. However, they have not proved why it occurs. To understand the process at an electronic level, time resolved studies need to be carried out. Preliminary investigations into polarised single photon counting experiments are reported in the next chapter.

Chapter 7

Time-Resolved Fluorescence Anisotropy Study

7.1 Introduction

This chapter contains the first time-resolved spectroscopy on the newly synthesised polymer, poly(naphthylene-phenylene) (2,6-NLP) and reports its fluorescence lifetime. The chapter also reports on time-resolved fluorescence anisotropy measurements carried out on polymers in solution, spun cast films and in an inert aligned PE matrices. In particular, this chapter contains further experimental work on the polymers poly[9,9-di(ethylhexyl)fluorene] (PF2/6), methyl-substituted ladder-type poly(*para*-phenylene) (MeLPPP) and 2,6-NLP. These experiments investigate the fluorescence anisotropy decay time which reveals more information about the processes behind the fluorescence anisotropy loss in these polymers.

Time-resolved fluorescence anisotropy measurements (TRAM) are used to study the fluorescence anisotropy changes over very short timescales. The anisotropy loss is the orientation change between the absorption and emission transition dipole moments and is sometimes referred to as fluorescence depolarisation. This term is used because the initial polarisation represents the orientation of the absorption transition dipole moment and the final polarisation represents the orientation of the emission transition dipole moment. The change between them constitutes a depolarisation.

In Chapters 4 and 5 the steady state fluorescence anisotropy of the polymers PF2/6, MeLPPP and 2,6-NLP was investigated. In all cases, the fluorescence anisotropy was observed to be less than the theoretical maximum, even at low temperatures. In Chapter 4 the anisotropy loss in the flexible PF2/6 was explained as a consequence of excitation energy transfer to different sites along the chain. A smaller anisotropy loss was still observed in short oligomers that are unable to support excitation energy transfer. This was explained to be a result of the the planarisation of the polymer's backbone. The results in Chapter 5 were used to suggest that the anisotropy loss in the inflexible MeLPPP was due to exciton migration, perhaps between adjacent orthogonal chromophores. Depolarisation in 2,6-NLP, another rigid polymer, could only be due to an electronic process on chain. Using TRAM and measuring the anisotropy decay times, it is hoped, that the mechanisms proposed in these earlier chapters can be confirmed.

TRAM allows fluorescence anisotropy decays to be observed from the maximum anisotropy to the steady-state value. The maximum can only occur if the absorption and emission transition dipole moments are parallel. If the decay starts at an anisotropy less than the theoretical maximum (0.40), it confirms the presence of another anisotropy loss process which is intrinsic to the molecule. TRAM is then used to monitor the fluorescence anisotropy loss from the

early-time anisotropy to the steady state value.

TRAM also estimates the anisotropy decay time (sometimes called the depolarisation time) which can be used to determine the mechanisms responsible for the anisotropy loss. A slow anisotropy decay time implies that the mechanism is likely to be due to a physical change in the molecule. An electronic process will occur much faster than a physical process and fluorescence depolarisation due to this will occur in less than one picosecond.[48,228]

In Chapters 4 and 5 the natural anisotropy of the three polymers was evaluated. Each of the polymers presented a high natural anisotropy (0.32 for PF2/6 and 0.36 for ladder) but none of them presented a natural anisotropy of the theoretical maximum 0.40. This suggests that there is a process responsible for a fundamental anisotropy loss.

In an attempt to uncover the fundamental anisotropy loss process, all three polymers were investigated using TRAM. To be able to solely investigate the intrinsic anisotropy loss process, the short, rigid-rod polymer 2,6-NLP was studied in preference to the other two polymers. Its length and structure both stop the common anisotropy loss processes that the other two suffer from. The short length of the polymer reduces, if not eliminates the possibility for exciton migration. This is because polymers of such a short length cannot support more than one chromophore. The rigidity of the polymer removes conformational motion.

By studying 2,6-NLP in different media (highly dilute solution, spun films and aligned PE matrices,) it was confirmed that this polymer does not rotate in solution (another anisotropy loss mechanism). Comparison of the results from different media has highlighted an anisotropy loss process that is independent from the polymer's surroundings. This comparison has also showed that the intrinsic anisotropy loss that happens on the molecular level.

The TRAM results of the other polymers were also compared with this short, rigid-rod molecule to compare the anisotropy loss processes within them. It was ascertained that the intrinsic anisotropy loss is the same as in other conjugated polymers.

None of the experiments revealed an early-time anisotropy of greater than the natural anisotropy of the molecule. This indicates an anisotropy loss process that occurs faster than the resolution of the experimental equipment.

7.2 Previous Research

Time-resolved anisotropy measurements (TRAM) have been used successfully in several scientific fields including chemistry[229–231] , physics[232–234] and most importantly biology.[235–238] This interdisciplinary technique studies the fluorescence anisotropy as a function of time and is most frequently used to study structures, conformational changes and rotation in biological molecules[77,154,155,239–241] and conjugated polymers.[242–245] Very recently it has also been used to observe fluorescence depolarisation in an attempt to understand the physical processes of conjugated polymers after excitation.[246–248]

TRAM are usually made by recording polarised emission as a function of time and the only limit for the experiment is the temporal resolution of the equipment used. For example, single photon counting methods (as described in Chapter 3) with a time resolution of tens of picoseconds are used to measure rotation times of long proteins. The advent of increasingly faster laser response systems has meant that it is possible to probe earlier into the electronic time frame of a molecule's excited life. Using three-pulse photon-echo experiments it has been possible to investigate processes that occur on the 100 fs timescale and hypothesise as to what happens prior to this.[44,228,249]

Other ultrafast (faster than 1 ps) techniques have been employed by some groups to investigate what is rapidly becoming a very important topic.[47,48,52,250] The anisotropy loss is linked to electronic relaxation within the polymer and this is either energy transfer or excitation migration to defects. Both of these processes can hinder the efficiency of devices made of conjugated polymers. Once the processes have been identified and understood, the information can be used to limit these detrimental migration processes.

Dykstra *et al.* have recently listed the anisotropy loss processes and their time frames in the flexible polymer MEH-PPV.[228] Their work has linked the movement of excitons through the polymer chain to different time frames. The researchers have hypothesised that intra- and inter-chain migration of the excitons occurs between 1 ps and hundreds of picoseconds after excitation and confirm that this would have a significant effect upon the fluorescence anisotropy. Their work has also hypothesised that fluorescence anisotropy can be lost in less than 100 fs because the exciton is trapped on a specific site as a result of planarization of the backbone. They propose a "dynamic localisation" to explain the fastest anisotropy loss process ($\sim$ 50 fs). This is a process which changes the energy and shape of the excited state but the excitation is essentially localized on a polymer segment.[48]

The work of Dykstra *et al.* and many other experimentalists has been carried out on flexible polymers, that is polymers that can undergo torsional motion about their backbones (the same as is hypothesised to occur in PF2/6). This key fact about the structure has played an important role in the explanation of their data. The TRAM experiments carried out here, to understand the intrinsic anisotropy loss (from 0.40 to the natural anisotropy), were carried out on rigid polymers. It is hoped that the measurements will further extend the knowledge of the polymers already investigated in this thesis and confirm the processes hypothesised to exist within them. An important additional finding will be the comparison of depolarisation results from a wholly rigid polymer to those already published.

7.3 Time-resolved Fluorescence Anisotropy Measurements - Theory

Measuring the evolution of fluorescence anisotropy decay can be done with several methods including photon echo, polarised pump-probe and time correlated photon counting (TCSPC). TRAM using a TCSPC technique has been very successfully used in the biological sciences.[158,251,252] Here, an existing TCSPC experiment, with a resolution of 7 ps was adapted to measure polarised decays. The TCSPC system, described in Chapter 3 section 3.4.8 and shown in Figure 3.8, had additional polarisers placed before and after the sample.

As explained in Chapter 2, the fluorescence anisotropy is a measure of the average angular difference between the absorption and emission transition dipole moments. This difference can only be observed during the fluorescence lifetime of the polymer and equation 2.26 can be made into a function of time to give.[51]

$$\langle r(t)\rangle \;=\; \frac{I_{\parallel}(t) - I_{\perp}(t)}{I_{\parallel}(t) + 2I_{\perp}(t)} \tag{7.1}$$

where $I_{alignment}$ is the intensity of the emission, and $\parallel$ and $\perp$ are the relative alignment of the excitation and emission polarisers. In an experimental situation equation 7.1 becomes:

$$\langle r(t)\rangle \;=\; \frac{I_{vv}(t) - GI_{vh}(t)}{I_{vv}(t) + 2GI_{vh}(t)} \tag{7.2}$$

where $I_{ex,em}$ represents the intensity of light with orientation of the polariser in the light path: either horizontal (h) or vertical (v). The fluorescence anisotropy can also be described as a function of time, in particular by a series of exponentials of the rotational correlation times (or anisotropy decay times), Θ_i:

$$\langle r(t)\rangle \;=\; \sum_{i=1}^{m} B_i \exp(-t/\Theta_i) \tag{7.3}$$

where B_i is the pre-exponential factor.

This equation assumes that the molecule is a spherical rotator and that it has only one rotational correlation time. It has already been shown in Chapter 4 that the rotation of the polymers investigated is extremely limited, therefore the rotational correlation time refers solely to the electronic on-chain depolarisation processes in this case. The emission comes from sites that are only reached due to depolarisation processes. This means that all the emission components contribute to the overall depolarisation (anisotropy loss). This assumption means that the polarised emission decays can be written as a series of terms involving the fluorescence lifetimes, τ_{fi}, and the rotational correlation times Θ_i by Lakowicz[51] and Hauer *et al.*[153]

$$I_{Magic}(t) = \sum_{i=1}^{n} A_i \exp(-t/\tau_{fi}) \quad (7.4)$$

$$I_{\parallel}(t) = I_{vv}(t)$$

$$= \frac{1}{3} I(t)[1 + 2r(t)] = \sum_{i=1}^{n} A_i \exp(-t/\tau_{fi})[1 + 2\sum_{j=1}^{m} B_j \exp(-t/\Theta_j)] \quad (7.5)$$

$$I_{\perp}(t) = GI_{vh}(t)$$

$$= \frac{1}{3} I(t)[1 - r(t)] = \sum_{i=1}^{n} A_i \exp(-t/\tau_{fi})[1 - \sum_{j=1}^{m} B_j \exp(-t/\Theta_j)] \quad (7.6)$$

To analyse the experimental data the following procedure was used: experimental polarised fluorescence data was first globally analysed with the above equations to retrieve $I_{\parallel}(t)$ and $I_{\perp}(t)$. The fits were then used to create an anisotropy decay via equation 7.2 which was then fitted with equation 7.3 in Microcal Origin Pro 7 to find the rotational correlation times.

7.4 Experimental

The time-resolved fluorescence decays and anisotropy measurements were made with the time-correlated single photon counting equipment described in section 3.4.8 in Chapter 3. This was achieved by the addition of a polariser in the emission collection optics. In particular, the emission polariser was aligned at the magic angle for isotropic (Magic angle: $I_{Magic}(t)$) decays and parallel or perpendicular relative to the vertically polarised excitation in order to collect the polarised decays $I_{\parallel}(t)$ and $I_{\perp}(t)$ respectively. The same integration times were used for both polarised decays and were kept as short as possible to give at least 6,000 counts at the peak(no more than 600s). The laser was deemed to be stable for these durations.

The analysis procedure (described in section 3.4.11) involved deconvoluting the magic angle decays first to determine the fluorescence lifetime. This value was then included in the analysis employed to fit each polarised decay. The polarised decays were fitted as a series of exponentials as per the expansion of the equations 7.5 and 7.5. The fitted polarised decays were then used to model the anisotropy decay using equation 7.2 which was fitted to a sum of two rotational correlation terms as in equation 7.3.

However the more typical method, of fitting for the rotational correlation coefficients directly, was also employed and it was found to deliver the same Θ_1 value. The data presented is from the indirect method to show that time-resolved fluorescence anisotropy can be analysed very simply and with less sophisticated fitting software. The only limit with this method is the number of terms required in the fitting procedure: for two fluorescence lifetimes and two rotational correlation coefficients then six terms are required. All the information pertaining to the rotational correlation coefficients is contained within the series exponential fit, but it is accessed when the anisotropy decay is analysed.

The process was repeated for several emission wavelengths corresponding to the emission spectrum of the polymers. These values are clearly indicated in the text.

The time-resolved fluorescence anisotropy technique was carried out on the short rigid-rod polymer 2,6-NLP. Three different hosts for the polymer were investigated: highly dilute solution (isotropic), thin spun cast film (isotropic) and within a polyethylene blend (anisotropic). Solutions of the conjugated polymer in either toluene or methylcyclohexane (MCH) were made with a concentration of 3 mg/mL. This resulted in absorbance of 0.1 O.D. at the maximum absorbance wavelength and removed reabsorption effects. The isotropic spun cast film was made from a 10 mg/mL toluene solution. The anisotropic polyethylene blend was stretched 30 times its original length and had an order parameter of 0.42 (as determined by a fluorescence anisotropy technique in Chapter 6section 6.4. Full details of sample preparation can be found in Chapter 3 section 3.3. These experiments were used as a basis for comparison with the results from a rigid, but branched polymer MeLPPP, studied in dilute solution only and with a flexible polymer, PF2/6, which was studied in solution, spun isotropic film and PE matrix.

7.5 Isotropic time-resolved emission of 2,6-NLP results and discussion

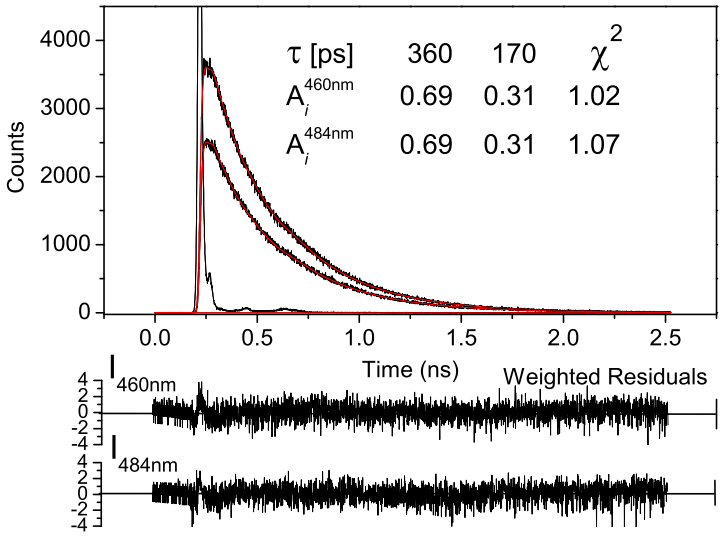

Figure 7.1: Raw data (black) and model from global analysis (red) for fluorescence decays of 2,6-NLP in MCH. The excitation wavelength was 454 nm and emission was collected at 460 nm and 484 nm. Beneath the figure the weighted residuals of the analytical fit are shown. The fluorescence lifetimes and pre-exponential factors found by global analysis are also stated. The small residuals and the low χ^2 factor indicate that the parameters are a good fit for the raw data. The results corresponding to the other decays are collated in Table 7.1

This section contains the first report of the fluorescence lifetimes of naphthylene-substituted ladder-type poly (*para*-phenylene) (2,6-NLP). The lifetimes found in this part of the work will be used in the time-resolved anisotropy measurements that follow this section 2,6-NLP is a newly synthesised ladder-type polymer. Ladder-type materials are known for their blue-green emission and rigid backbone conformation. The absorption and emission of the polymer are

shown in Figure 5.1. It can be seen that the spectra contain very narrow peaks meaning that there is only a small change between the ground and excited states orbital configurations. The fluorescence lifetimes have been found through time correlated single photon counting (TCSPC described in Chapter 3) in toluene and MCH. The results will be compared with those from the existing ladder polymer methyl- substituted ladder-type poly (*para*-phenylene) (MeLPPP) which is also measured here.

Fluorescence lifetimes have been found for two excitation wavelengths; one at the peak absorption (448 nm) and the other at the red edge of the absorption spectrum (454 nm), and two emission wavelengths (peak and red edge of the emission). The two excitation wavelengths were chosen to enable an investigation into two parts of the conjugation length distribution. Exciting at the wavelength of maximum absorption means that there are a number of lower energy electronic sites for an excitation to move to before recombination and emission which leads to a longer lifetime. The number of sites with lower energy is reduced by exciting at the low energy edge of the conjugation length distribution. This should be revealed as a shorter lifetime because the excitation does not move to a new site. Decays were also recorded for two different emission wavelengths which allows a global fitting procedure to be carried out. Global analysis is a procedure that allows the data for different emission wavelengths to be fitted simultaneously and assumes that the lifetimes are identical. By increasing the amount of data, the global analysis and deconvolution process can be assumed to be more accurate than for a single data set. Overall four decays were recorded for each polymer in each solvent.

The data was globally fitted for pairs of emission wavelengths: an example of this analysis is shown in Figure 7.1. The figure shows the raw data, the analysis from the fitting procedure and the weighted residuals. It can be seen that the analysis is a very close fit to the raw data. This is explicitly indicated by the small weighted residuals which indicate the difference between the raw data and the model created from global analysis. The χ^2 factor evaluates this difference for the whole data set and a value close to 1, as here (1.02 and 1.07), shows that the model fits for the whole data set.

The experimental data was analysed with a single exponential resulting in large residuals and a poor χ^2 factor, thus the best fit was achieved for two exponential terms. There is a small spike in the residuals which coincides in time with the instrument response function (IRF). This is most likely to have arisen from a slight scattering of light in the finite width of the IRF. Global fitting with a third exponential term did not locate a short lifetime responsible for the spike. Since the spike is very small and present in all the experiments it is considered to be a systematic experimental artefact. It is discussed in the results of the time-resolved anisotropy measurements in the following section.

The small residuals and χ^2 factor close to unity indicates that the fluorescence lifetimes and pre-exponential are appropriate for the raw data. The lifetimes found (360 ps and 170 ps) are both well above the resolution limit of the equipment (7 ps) and they are separated by at least twice the lowest lifetime. Therefore, they can be considered to be two separate lifetimes that have been successfully resolved.

Solvent	λ_{ex}[nm]	λ_{em} [nm]	τ_1 [ps]:(A_1)	τ_2 [ps]:(A_2)	Fit quality χ^2
MCH	448	454	**367** (0.71)	**229** (0.29)	1.06
		483	**367** (0.59)	**229** (0.41)	1.05
	454	460	**360** (0.69)	**169** (0.31)	1.02
		485	**360** (0.69)	**169** (0.31)	1.07
Toluene	448	454	**338** (0.75)	**219** (0.25)	1.08
		483	**367** (0.71)	**202** (0.29)	1.04
Global	*448*	*454*	*350* (*0.68*)	*212* (*0.32*)	*1.15*
analysis		*483*	*350* (*0.82*)	*212* (*0.18*)	*1.14*
	454	460	**335** (0.73)	**173** (0.27)	1.04
		485	**335** (0.74)	**173** (0.26)	1.05

Table 7.1: Analysis parameters of the fluorescence decays of 2,6-NLP in MCH and toluene. All but the data from excitation at 448 nm have been globally analysed. The global analysis of this set increased the χ^2 factor but has been included in the table in italics to show this.

The data acquisition and analysis was repeated for toluene solution and the lifetimes and pre-exponentials and χ^2 factors are also listed in Table 7.1. The data was mostly analysed globally because this improves the reliability of the analysis procedure to find the real lifetimes. In the case of excitation at 448 nm globally fitting the data increased the χ^2 factor and the weighted residuals as shown in the table. Lower residuals were achieved by fitting the data individually. The table shows for the excitation wavelength 448 nm that the lifetimes and pre-exponential factors found are very close to each other and within 10 ps for the shorter lifetime and 20 ps for the longer lifetime and this corresponds well with the global analysis.

In all cases, the fluorescence decays from 2,6-NLP were analysed better (low residuals and χ^2 close to unity) with two clearly separated lifetimes. For solutions in MCH and excitation at the peak absorption wavelength (448 nm) the lifetimes are 370 ± 20 ps and 21 ± 10 ps, with the longer lifetime making up approximately 70 % of the decay. For excitation wavelengths at the edge of the polymer's absorption spectrum (454 nm) the two lifetimes remain. The longer lifetime is unchanged within the error (∼ 360 ps) but the shorter lifetime is reduced to 170 ps. The contributions of the two lifetimes stay the same with ∼ 70% for the longer lifetime and ∼30% for the shorter.

The effect of solvent is small. In toluene, which is less viscous than MCH, the longer lifetime is shortened to 350 ± 20 ps. This shorter lifetime is still within the error of the MCH data and cannot be positively identified as a definite shortening. The shorter lifetime remains unchanged as a function of solvent. The data clearly show that 2,6-NLP supports two separate lifetimes. They are not affected significantly by solvent viscosity which rules out physical motion as an explanation of either of the lifetimes.

The lifetimes are, however, affected by excitation wavelength. The longer lifetime is independent of excitation wavelength which suggests an electronic process that is independent from the conjugation length distribution. The shorter lifetime is dependent up on the excitation wavelength. Exciting at the maximum absorption wavelength corresponds to the mean conjugation length and this gives a longer time than exciting at the edge of the distribution (which has longer conjugation lengths). The increase in conjugation length will be accompanied by in increase in vibronic couplings between the excited state and vibronic levels. In turn the non-radiative decay routes will increase in significance and this contribution will cause an decrease in the lifetime of the state.[a]

Solvent	λ_{ex}[nm]	λ_{em} [nm]	τ_1 [ps]:(A_1)	τ_2 [ps]:(A_2)	Fit quality χ^2
MCH	448	458	**316** (1)		1.06
		490	**316** (1)		1.05
	454	460	**316** (0.91)	**167** (0.09)	1.02
		492	**316** (0.92)	**167** (0.08)	1.07
Toluene	448	458	**322** (1)		1.08
		490	**322** (1)		1.04
	454	460	**319** (0.91)	**163** (0.09)	1.04
		492	**319** (0.94)	**163** (0.06)	1.05

Table 7.2: Analysis parameters of the fluorescence decays of MeLPPP solutions. All of the decays were globally analysed in pairs.

The same data acquisition and analysis procedure were repeated for MeLPPP. Good fits were found via global analysis and the lifetimes and pre-exponential factors are listed in Table 7.2. The polymer was excited at the peak and the edge of the absorption spectrum (conjugation length distribution) and decays were recorded for emission at the peak and the red edge of the emission spectrum. The results show that MeLPPP has a single exponential (∼320ps) when exciting on the blue edge of the absorption peak confirming the fluorescence lifetime reported by different groups.[54,122,253] Dias *et al.* also noted that for emission in the red, it was necessary to include a small proportion of a second lifetime to fit the data well.[54] In these experiments, when exciting on the red edge, the main fluorescence lifetime does not change significantly but it was necessary to include a small percentage (<9%) of a second shorter lifetime (∼165ps) to obtain a good fit. This second lifetime is very similar to the shorter lifetime in 2,6-NLP. Again the effect of solvent is very small.

It is observed that MeLPPP has only one fluorescence lifetime when excited at the peak of the conjugation length distribution and two at the edge. It is noted that the lifetime dominates (> 90%) in the decay from excitation at the edge of the conjugation length distribution. This long lifetime (320 ps) is on the same timescale as that in 2,6-NLP (350 ps) but it is the second, shorter lifetime that highlights the similarities of the two polymers.

[a] Section 2.5.10 has the relevant equations.

It has already been seen, through a spectroscopic comparison in Chapter 5, that these two polymers can be considered to be very similar electronically. They are also both rigid and, in solution, do not rotate significantly within their fluorescence lifetimes. The evidence that the lifetimes are also very similar serves to support the suggestion above that the electronic states are also very similar, if not identical.

The data in Tables 7.1 and 7.2 show that the lifetimes of 2,6-NLP and MeLPPP are very similar and have similar photophysics. The tables also confirm good fits have been made through the analysis procedure. Finding the fluorescence lifetimes is a vital first step for the analysis of time-resolved anisotropy measurements. It is very important to note that any rotational lifetimes found in the next section, that are longer than the fluorescence lifetimes found here, cannot be relied upon because it is only possible to observe the polymer within the fluorescence lifetime.

7.6 Time-resolved fluorescence anisotropy measurements - Results

The results of the time-resolved anisotropy measurements (TRAM) and analysis for the polymers are presented in this section. This section contains the anisotropy decay times and the early-time anisotropy values for each polymer in solution when excited at the peak and the red-edge of their absorption spectra. In addition, 2,6-NLP and PF2/6 were investigated in aligned film form and these results are presented.

Raw data was acquired as two polarised decays, I_{vv} and I_{vh} for each of two excitation wavelengths and two emission wavelengths. The samples were excited at the peak and the edge of the conjugation length distribution to investigate the effect of limiting the number of sites to which an excitation can migrate. It is thought that, if the excitation is unable to move to different sites, the dipoles should remain almost parallel and the anisotropy should be high. Similarly, if an excitation is free to move away from the initial site then the anisotropy should be reduced.

These measurements allow an investigation into the initial anisotropy and the anisotropy decay times. The anisotropy will be the maximum anisotropy of 0.40 unless there is an anisotropy decay time much faster than the resolution of the system. In this case it is only possible to record the earliest anisotropy and a comparison with the maximum and the previous natural anisotropy results (Chapters 4 and 5) can be made.

Polarized decays at a specific excitation and emission wavelength were globally analysed in pairs with the equations 7.5 and 7.6 using lifetimes found through isotropic decays (e.g. in the previous section). The pairs were fitted simultaneously and it was assumed that the anisotropy lifetimes are identical for I_{vv} and I_{vh}. This assumption is valid for the polarised decays because the same processes will affect both polarisation configuration.[51]

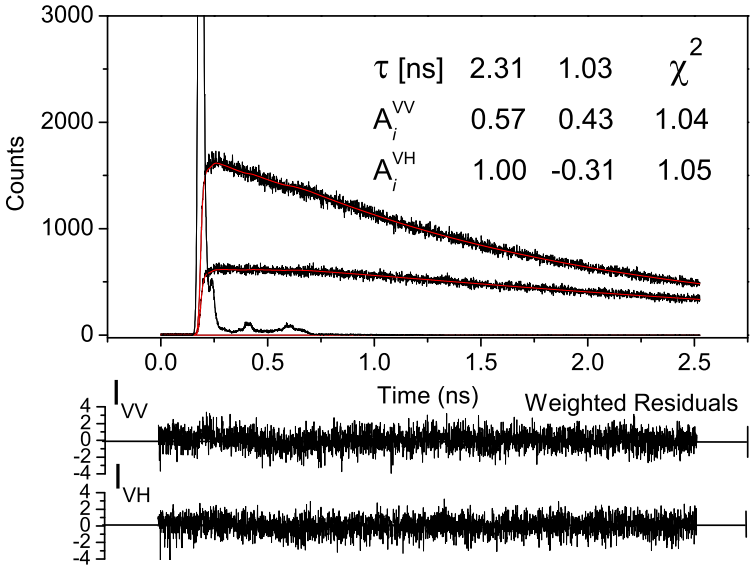

Figure 7.2: Global analysis and residuals for polarised fluorescence decays of Coumarin 6 in Ethylene Glycol with excitation wavelength = 448 nm and emission wavelength at 510 nm. The fluorescence lifetimes and pre-exponential factors found are also given. These value correspond with those found by Kapusta *et al.* in[160]

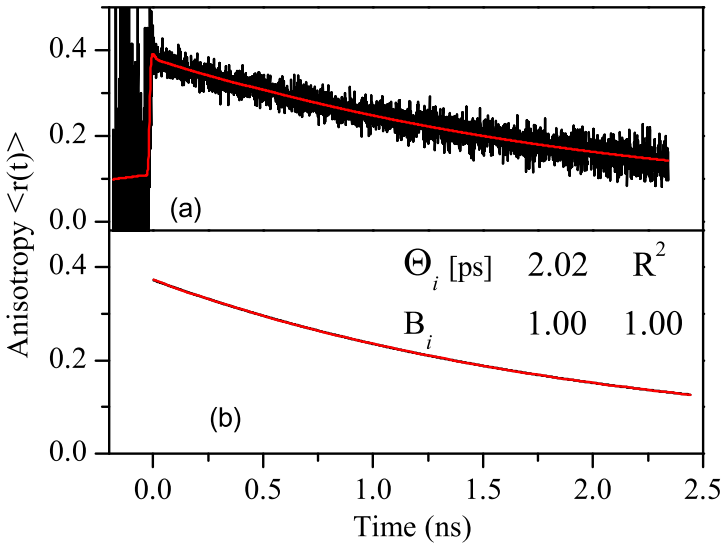

Figure 7.3: Raw data (a) and model (b) anisotropy decay of Coumarin 6 in dilute Ethylene Glycol solution excited at 454 nm and emission recorded at 485 nm. (Time axis has been zeroed to the midpoint of the pulse for clarity). The fluorescence lifetimes and pre-exponential factors found are also given. These value correspond with those found by Kapusta *et al.* in[160]

An example of the global analysis is shown in Figure 7.3. The figure shows the raw polarized decays of Coumarin 6 in ethylene glycol excited at 448 nm and emission collected at 510 nm (the peak of the molecule's emission spectrum). The figure also shows the residuals from the global analysis and the χ^2 fit parameter that gauges the suitability of the fit. The residuals are small and uniform about zero and The χ^2 parameter is close to unity , all of which mean that the model is a good fit to the data. Two exponentials (2.31 ns and 1.03 ns) were required to achieve fit the data and create the model. These two values correspond with those found by Kapusta et al. (2.31 ns and (average) 1.02 $\pm$ 0.04 ns).

The models for the polarized decays were then used in further analysis of the fluorescence anisotropy decay. This involved creating a model of the fluorescence anisotropy decay which was fitted with a first order exponential decay in Microcal Origin and this provided a value for the rotation lifetime of Coumarin 6 in ethylene glycol. The raw decay and model anisotropy decay are shown in Figure 7.3 and the anisotropy decay time was found to be 2.03 ns. The figure clearly shows that there is a single decay time and there is no additional decay on the timescale of the resolution of the system (5 ps). Kapusta *et al.* measured the decay of the anisotropy to be 2.08 $\pm$ 0.03. The value measured here is within two standard errors of this value.[160]

A further set of examples of polarized decay, global analysis results and the fluorescence anisotropy decay models for 2,6-NLP in a dilute MCH solution excited at 454 nm and with emission measured at 483 nm are now considered. Figure 7.4 shows the raw data, the model created by global analysis and the residuals from the fit. The small weighted residuals and χ^2 parameter close to unity indicate that the model used to analyse the data is a good fit. Three exponentials were required to achieve this fit and two correspond closely to the two fluorescence lifetimes of 2,6-NLP. The final lifetime is very fast. Figure 7.5 (a) shows the raw, anisotropy created from the polarised decays before deconvolution of 2,6-NLP in MCH excited at 454 nm. It can be seen that the early time anisotropy is almost at the natural anisotropy predicted in an earlier chapter ($r_0 \sim 0.36$ found in Chapter 5) but is masked by the noise and that it decays quickly to the steady-state value. Figure 7.5(b) shows the anisotropy decay curve created from the functions determined by the individual decays and has not been reconvoluted. This shows an almost immediate loss of anisotropy before a much slower decay to the steady-state value measured for this sample. The R^2 value gives an indication of the suitability of fit and in this case, it is close to one (close to ideal). Two anisotropy decay lifetimes were required to fit the fluorescence anisotropy decay: 7 ps and 542 ps.

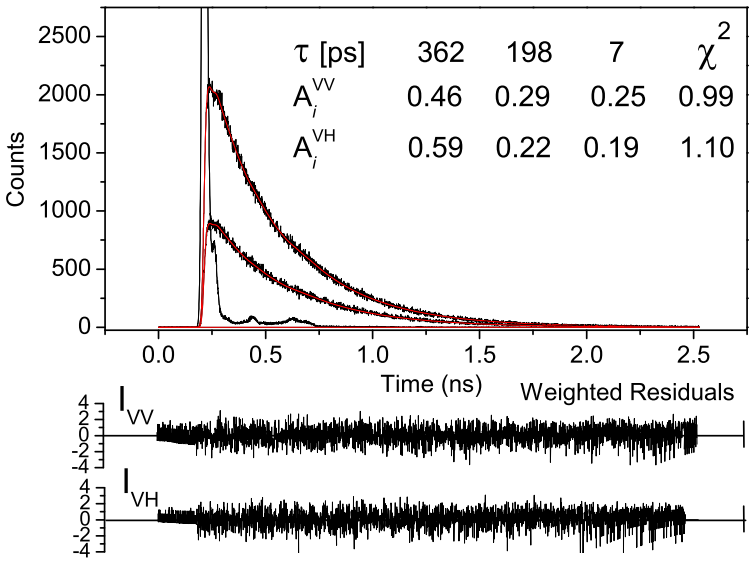

Figure 7.4: Global analysis and residuals for polarised fluorescence decays of 2,6-NLP in MCH with excitation wavelength at 454 nm and emission wavelength at 484 nm. The fluorescence lifetimes and pre-exponential factors found are also given. Data corresponding to the other polarised experiments is collated in Table 7.3

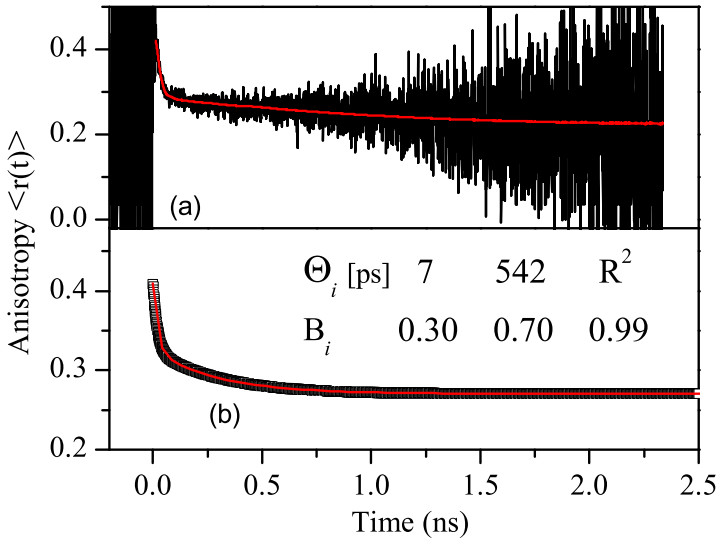

Figure 7.5: Raw data (a) and model (b) anisotropy decay of 2,6-NLP in dilute MCH solution excited at 454 nm and emission recorded at 484 nm. (Time axis has been zeroed to the midpoint of the pulse for clarity). The fluorescence lifetimes and pre-exponential factors found are also given. Data corresponding to the other polarised experiments is collated in Table 7.3.

Solvent	λ_{ex}[nm]	λ_{em} [nm]	Θ_1 [ps]:(B_1)	Θ_2 [ps]:(B_2)	R^2	$r_0^\dagger$	$r_\tau^\star$
Toluene	448	454	**13** (0.53)	**587** (0.47)	0.99927	0.28	0.23
		484	**11** (0.63)	**952** (0.37)	0.99987	0.25	0.23
	454	460	**10** (0.49)	**500** (0.51)	0.99971	0.28	0.25
		484	**12** (0.57)	**780** (0.43)	0.99927	0.29	0.25
MCH	448	454	**11** (0.68)	**549** (0.32)	0.99985	0.28	0.17
		483	**14** (0.41)	**963** (0.59)	1	0.26	0.17
	454	460	**12** (0.47)	**666** (0.53)	0.99920	0.37	0.22
		484	**7** (0.30)	**542** (0.70)	0.99985	0.37	0.22

Table 7.3: Analysis parameters of the 2,6-NLP anisotropy decay models created from individual polarised decays. Table contains data for the 2,6-NLP which has a natural anisotropy of 0.36 (as estimated in Chapter 5). † Early-time anisotropy created from fit parameters of the individual polarised fluorescence decays. ⋆ Steady-state fluorescence anisotropy taken with 2 second integrations. Values ± 0.01.

The fluorescence anisotropy decay times found for 2,6-NLP in different solvents are listed in Table 7.3. The table clearly shows that 2,6-NLP decays are well fitted (low χ^2) with two decay lifetimes. The pairs of lifetimes comprise a very short decay time ($\sim 10ps$) and a longer decay, which ranges from 540 ps to 960 ps. The longer decay is always much longer than the fluorescence lifetime of 2,6-NLP found above (350 ps) and as such cannot be accurately determined. Only its existence can be confirmed and that it is a factor of ten longer than the short lifetime. As a result only the shorter lifetime will be fully investigated here. The shorter lifetime lies within a range of ±6 ps for all the data collected. This spread may be due to the polymer's behaviour or due to the fact that each anisotropy decay was analysed separately for each pair of emission wavelengths. There is no apparent dependence on the anisotropy decay lifetime with either excitation or emission lifetime. But because the values are close, global analysis would confirm the independence of the lifetimes from emission wavelength and possibly reveal further information on dependence upon excitation wavelength. This type of analysis was not possible. It is assumed that the short lifetime is, therefore, (10 ± 6) ps and inherent to the polymer.

Table 7.3 also gives the early-time anisotropy (denoted r_e) and the steady-state anisotropy (r_τ) for 2,6-NLP in solution. As can be seen the early-time anisotropy values are higher than the steady state values confirming a loss of anisotropy within the polymer's fluorescence lifetime. The r_e values are not at the theoretical maximum of 0.40 nor the natural anisotropy estimated from the results in Chapter 5. This deviation from the maximum means that there is a loss that has occurred within the instrument response time of 5 ps. This means that there are at least two anisotropy loss processes occurring: one that lowers the early time anisotropy and occurs in less than 5 ps and at least one longer process that is responsible for the steady-state value.

The early-time anisotropy value and the steady-state value are dependent upon excitation wavelength. Excitation at 448 nm (peak absorption wavelength) leads to the biggest deviation from the maximum value, whereas excitation at 454 nm (red-edge of the absorption spectrum) produces very high anisotropy values. There is one case where the early-time anisotropy is approximately the same as the estimated natural anisotropy measure in Chapter 5. Exciting 2,6-NLP in MCH solution at 454 nm, the edge of the absorption spectrum, reveals an early-time anisotropy of 0.38 indicating that it is a special case which is discussed below.

Solvent	λ_{ex}[nm]	λ_{em} [nm]	Θ_1 [ps]:(B_1)	Θ_2 [ps]:(B_2)	R^2	$r_e^{\dagger}$	$r_\tau^{\star}$
Toluene	448	458	**45** (0.53)	**359** (0.47)	1	0.28	0.07
		490	**5** (0.79)	**195** (0.21)	0.99999	0.19	0.07
	454	460	**13** (0.60)	**260** (0.40)	0.99996	0.28	0.11
		492	**10** (0.63)	**204** (0.37)	0.99996	0.22	0.11
MCH	448	458	**33** (0.57)	**324** (0.43)	1	0.21	0.09
		490	**3** (0.24)	**15** (0.76)	0.99155	0.27	0.09
	454	460	**19** (0.50)	**256** (0.50)	0.99999	0.33	0.12
		492	**19** (0.60)	**295** (0.40)	0.99998	0.26	0.12

Table 7.4: Analysis parameters of the MeLPPP anisotropy decay models created from individual polarised decays. Table contains data for the ladder-type polymers only. † Early-time anisotropy created from fit parameters of the individual polarised fluorescence decays. ⋆ Steady-state fluorescence anisotropy taken with 2 second integrations. Values ± 0.01.

The experiments and analysis were repeated for the ladder polymer, MeLPPP, and the results are listed in Table 7.4. As with the 2,6-NLP results, the data were best fitted with two anisotropy decay lifetimes comprising a very short time ($\sim$ 20 ps) and a longer lifetime ($\sim$ 260 ps). In most cases, the longer lifetime is very close to the fluorescence lifetime of the polymer, 320 ps[54, 122, 253] and, therefore, cannot be considered a highly accurate value. However, the findings do confirm the existence of a long time anisotropy loss process. The shorter lifetime is, as in 2,6-NLP, a factor of ten smaller than the longer time. It is also dependent upon the excitation wavelength. Exciting at 448 nm produces longer times than exciting at 454 nm. The short lifetime value for MeLPPP at 454 nm in toluene is the same as the short lifetime intrinsic to 2,6-NLP in both solvents.

Table 7.4 also shows the early-time anisotropy and steady-state anisotropy for MeLPPP in solutions. The early-time anisotropy is not at the maximum 0.40 nor at the natural anisotropy estimated for MeLPPP in Chapter 5. However, the values recorded are in line with those for 2,6-NLP. The values do not reflect the dependence of the anisotropy on the excitation wavelength that the steady-state values show. The early-time anisotropy is also dependent on the observation (chosen emission) wavelength and the value decreases as the emission moves into the red whereas steady-state anisotropy has once again been found to be independent of observation wavelength. In general, 2,6-NLP has a much higher anisotropy than the MeLPPP for both early-times and steady-state.

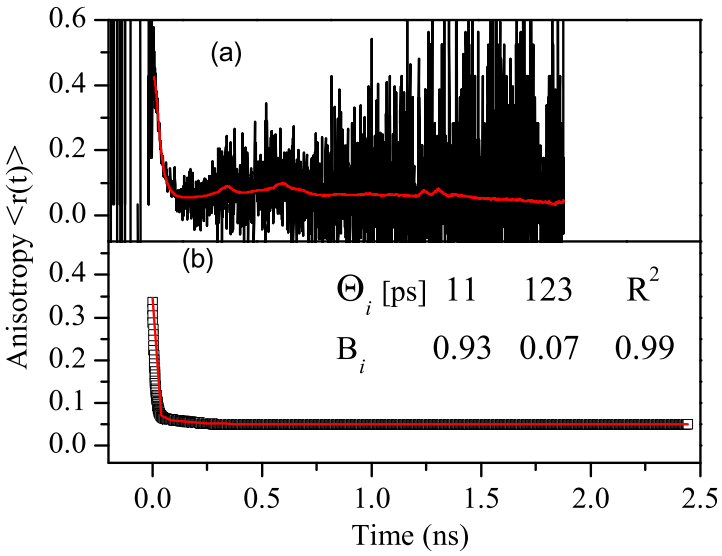

Figure 7.6: Anisotropy decay from isotropic spun thin film of 2,6-NLP, held parallel with respect to excitation beam. Raw data (a) and model (b). Excited at 454 nm, emission recorded at 485 nm. (Time axis has been zeroed to the midpoint of the pulse for clarity). The fluorescence lifetimes and pre-exponential factors found are also given.

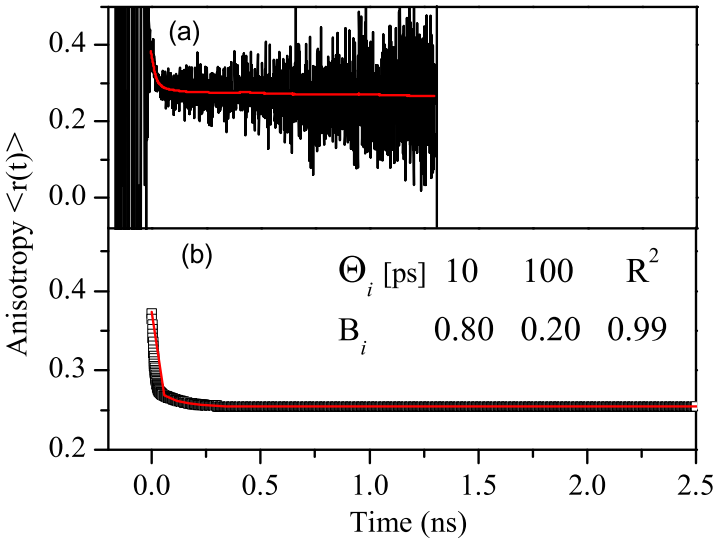

Figure 7.7: Anisotropy decay from stretched thin film of 2,6-NLP in PE, held parallel with respect to excitation beam. Raw data (a) and model (b). Excited at 454 nm, emission recorded at 485 nm. (Time axis has been zeroed to the midpoint of the pulse for clarity). The fluorescence lifetimes and pre-exponential factors found are also given.

In order to rule out rotation as a major source of anisotropy decay 2,6-NLP was investigated in film form. The polymer was spun cast into a thin isotropic film. It was also incorporated in a PE film which was then stretched to give the system small scale order. The same procedure as used for solution data analysis was followed for the film and PE data.

Figure 7.6 shows the raw anisotropy decay data, deconvoluted model and the model anisotropy decay for 2,6-NLP in isotropic film. It is clear that the almost immediate anisotropy loss observed in solution decays (Figure 7.5) is also present in isotropic film. However, the early-time anisotropy, and the value it tends to, are very different from the solution work. The values of early-time anisotropy are listed in Table 7.5 and are lower than the natural anisotropy (0.36) and the equivalent solution data (also shown in the table).

Figure 7.7 shows the raw anisotropy decay data, deconvoluted model and the model anisotropy decay for 2,6-NLP in an anisotropic stretched PE film. The film was stretched 30 times its original length. Here, the early anisotropy value is the same as measured in the solution decays and the data are listed in Table 7.5.

Polymer	Form	λ_{ex} [nm]	λ_{em} [nm]	Θ_1:(B_1) [ps]	Θ_2:(B_2) [ps]	Θ_3:(B_3) [ps]	$r_0^\star$	$r_e^\dagger$
2,6-NLP	MCH Solution	454	485	**7** (0.30)	**542** (0.70)	-	0.36	0.37
	Spun film	454	485	**11** (0.93)	**123** (0.07)	-	0.36	0.34
	stretched film	454	485	**10** (0.80)	**100** (0.20)	-	0.36	0.38
PF2/6	MCH solution	385	410	**11** (0.30)	**116** (0.45)	**823** (0.25)	0.34	0.23
	stretched film	385	410	**11** (1)	-	-	0.36	0.93

Table 7.5: Anisotropy decay times and early-time anisotropy values for 2/6-NLP and PF2/6 in different states this table is to do with the comparison between sf and pf data $\star$ means found in Chapter 5 and † means early time anisotropy found with decays.

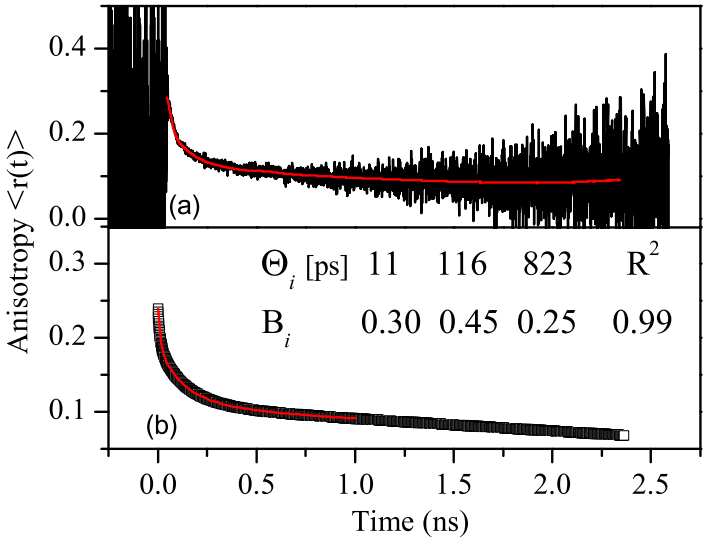

Figure 7.8: Anisotropy decay from PF2/6 in dilute MCH solution. Raw data (a) and model (b). Excited at 385 nm, emission recorded at 410 nm. (Time axis has been zeroed to the midpoint of the pulse for clarity). The fluorescence lifetimes and pre-exponential factors found are also given.

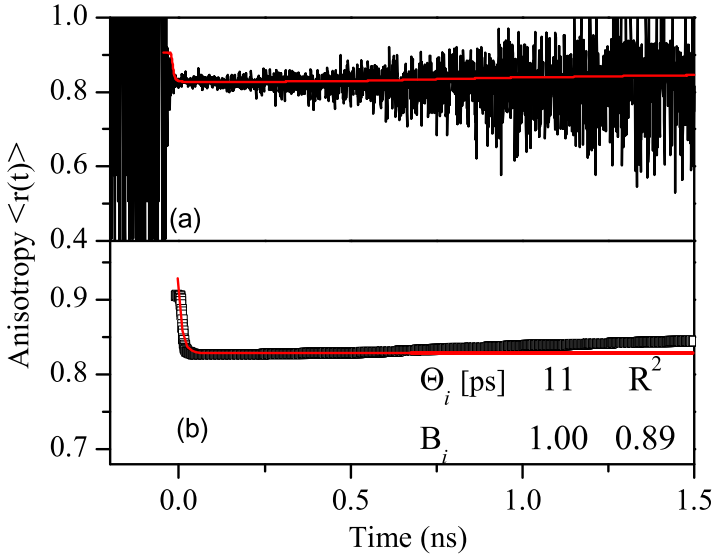

Figure 7.9: Anisotropy decay from stretched thin film of PF2/6 in PE, held parallel with respect to excitation beam. Raw data (a) and model (b). Excited at 385 nm, emission recorded at 410 nm. (Time axis has been zeroed to the midpoint of the pulse for clarity). The fluorescence lifetimes and pre-exponential factors found are also given.

Similar experiments were also carried out for PF2/6 in MCH solution and stretch PE film. Figures 7.8 and 7.9 show the raw data, models and fits of these experiments. The fluorescence lifetime was measured prior to the investigations and found to be the reported by Dias *et al.*.[54] The anisotropy decays and pre-exponential factors are tabulated in Table 7.5. The results for the solution required three lifetimes to fit the data well (low R^2), one of which is greater than the fluorescence lifetime of the polymer and is, therefore, unreliable. The second longest is $\sim$ 110 ps and the shortest is 11 ps. In stretched film form, only one anisotropy lifetime is required to describe the data. This short time is 11 ps and is the same as in solution. As can be seen, PF2/6 in two different media present almost the same short lifetime as 2,6-NLP in its three different media.

The early-time anisotropies for PF2/6 in solution and PE film are also given in Table 7.5. For experiments in solution this is lower than the natural anisotropy found in Chapter 5. There is still some angular loss in the anisotropic film which suggests that the transition dipole moment moves through a small angle, θ. This sample has long range order (shown by x-ray diffraction experiments in Chapter 6) and equation 7.7 fully defined in Chapter 2 can be used to estimate this angle.

$$\langle r \rangle = \frac{(3\langle \cos^2 \theta \rangle - 1)}{2} \tag{7.7}$$

An early-time anisotropy value of 0.9 is recorded from the raw anisotropy and the model and gives an angular loss of $\sim 15^\circ$. This angle fits with our estimate from the regression from the temperature dependent fluorescence anisotropy data found in Chapter 4. This equation cannot be applied to the data from the 2,6-NLP film because this matrix only has short range order, similar to that found in a solution.

7.7 Discussion

Time-resolved anisotropy measurements (TRAM) allow the evolution of the transition dipole moment orientation from absorption transition dipole moment to emission transition dipole moment to be observed. This method has allowed the observation of the change from the maximum recorded anisotropy to the steady state value. The work so far in this thesis has hypothesised that the orientational change of the dipoles is from off the chain axis to along the chain. The results presented above have shown that ladder-type poly(naphthylene-phenylene) (2,6-NLP) has a fluorescence anisotropy decay time that is independent of the molecular environment. The data also show that this anisotropy decay time is the same as for another conjugated polymer, PF2/6, in solution and anisotropic film and MeLPPP in solution. They strongly suggest that the anisotropy decay process is intrinsic to all these conjugated polymers and is one that occurs in different types of polymers and in their different media. These new results are used to build on the concepts presented in Chapter 5 and 6 and to confirm that the anisotropy loss process from theoretical maximum to natural anisotropy is electronic in origin is an elongation of the electronic state through the conjugation length distribution and that the loss from the natural anisotropy to steady-state value is also an electronic process but due to exciton migration.

Elimination of fluorescence anisotropy loss processes

Fluorescence anisotropy loss in molecules can be caused by many processes as discussed in section 2.5.8 in Chapter 2 . The main loss processes are: (1) rotation of the entire molecule; (2) planarisation and associated elongation of the electronic state; (3) migration to an adjacent chromophore that is at an angle to the first; (4) inter-chain excitation migration possibly within an aggregate; intra-chain migration via hopping to lower energy states and (5) an elongation of the electronic state through the conjugation length distribution. Scattering and re-absorption are also causes of small anisotropy loss on the timescale of the fluorescence lifetime but will not cause a significant loss in highly dilute solutions. Systematic investigations in previous chapters has ruled out many of the fluorescence anisotropy loss processes in 2,6-NLP.

In Chapter 4 , PF2/6$_{N=20}$ was shown not to rotate significantly in its fluorescence lifetime. 2,6-NLP is the same length as PF2/6$_{N=20}$ and, therefore, would not be expected to rotate significantly despite having a longer fluorescence lifetime. The rotation of an entire molecule is hypothesised to be comparatively slow ($\sim \times 10^{-4\,\circ}$ ps^{-1} which corresponds to a rotation of $\sim 0.1^{\circ}$ in its fluorescence lifetime and a change in anisotropy of much less than 0.01 (which is the error in the measurements). As such rotation cannot be responsible for the significant anisotropy loss observed. The mathematical model used to analyse the data is specific for a spherical rotator and is most often used by researchers to calculate the molecule's rotation time.[51,80] In previous chapters the rigid-rod nature of the 2,6-NLP molecules has been relied upon. Therefore, a spherical rotator model is not the most appropriate to determine the rotation time of these polymers. It is a good approximation for the rotation of a small molecule such as Coumarin 6. The spherical rotator is still applicable for the polymer because, as mentioned above, the rate of rotation is particularly low for the polymers and the model is being used specifically to measure the rotation of the transition dipole moments. These are point dipoles so a spherical rotation model is a suitable approximation.

In Chapter 4, two anisotropy loss processes were observed in PF2/6 one of which was a conformational motion that planarised the molecule and elongated the electronic state. In Chapter 5 it was confirmed that 2,6-NLP is a rigid-rod polymer that is already planarised. This rules out planarization as a cause of anisotropy loss in 2,6-NLP. Also in Chapter 5 it was observed that rigid-rod polymers undergo fluorescence anisotropy loss. In MeLPPP, this was partially explained as a result of the branched backbone (see Figure 2.12) which has the potential to create a large angle between adjacent chain segments. 2,6-NLP does not have the same branching defects in its structure and is much more linear. Transfer between adjacent chromophores could not induce such large anisotropy changes in 2,6-NLP and anisotropy values are expected to remain high. Chapter 5 showed that large aggregates did not form in low concentration solutions of 2,6-NLP. Inter-chain energy transfer within an aggregate can cause a substantial anisotropy loss (as mentioned in Chapter 2 section 2.5.8). The side groups on 2,6-NLP are sufficient to separate the backbones such that the aggregates cannot form. However, the possibility of small aggregates or dimers could not be ruled out and could

be a cause of the fluorescence anisotropy loss. The concentrations of the solutions used here were deliberately kept low to avoid aggregates and to separate the molecules. Calculations, based on the concentration of the solutions have been used to estimate the average separation between molecules. As discussed in Chapter 2 section 2.4.4, transfer can only happen when the molecules are in close proximity ($\sim$ 6 nm). The length estimated for the solutions is nearer $\sim$ 300 nm, making inter-chain energy transfer interactions very highly unlikely.[139]

Aggregates are most likely to form in isotopic spun films, yet there is no difference in anisotropy decay lifetime between 2,6-NLP in solution or in film. It was expected that the aggregate behaviour would be more prominent and give a faster decay lifetime in film. In a film, inter-chain transfer can occur more easily due to the close proximity of the molecules. The similar lifetime in solution and in film suggests that the same process occurs in both media. Whilst this could be aggregation it is more likely that it is intrinsic on-chain exciton dynamics because of the low probability of aggregates in solution (discussed above).

Small aggregates would explain the rapid anisotropy loss in 2,6-NLP but this mechanism would also occur for the other polymers. If this were the case, the dipole alignment within the aggregate would have to retain some polarization because the fluorescence is not completely depolarized. This suggests that the aggregates would have to be comprised of a small number of ordered molecules e.g. dimers. The same argument would then need to be used for both MeLPPP and PF2/6 because the data collected here suggest that all the systems are alike. In general the MeLPPP and PF2/6 are considered to be isolated because of their similar behaviour to many other individual polymer chains e.g. MEH-PPV and polyfluorenes.[106] The implications of the aggregate argument would be that conjugated polymers are never truly isolated. The steric chemistry of different chains has been used to confirm that other molecules are separated,[106] therefore, it is assumed that in dilute solution the electronic processes in 2,6-NLP occur on an individual chain and intra-chain process do not occur.

In films, however, the aggregate argument is more difficult to dismiss because of the significant loss in anisotropy which is enhanced by the close proximity of molecules. Co-facial aggregates are known to cause significant depolarisation[47] and this is a valid explanation of anisotropy loss in isotropic films. However, aggregates are not observed in isotropic films of MeLPPP and 2,6-NLP. MeLPPP is reported to form yellow emitting aggregates[135,136] and these are not present in the fluorescence spectra in Figure 5.2). Because of the similarities in 2,6-NLP and MeLPPP, this leads to the conclusion that molecules do not form aggregates or, if it does, they do not affect the fluorescence spectra in the way that has been reported previously.

In Chapter 4 the length of the oligomers was found to limit the intra-chain excitation migration. It was found that oligomers of less than ten units could not support many sites to which an excitation could migrate. 2,6-NLP is approximately 21 monomer units long and, in theory though unlikely, may support more than one chromophore: intra-chain hopping between states would cause some fluorescence anisotropy loss.

In Chapters 5 and 6 it was hypothesized that the elongation of the excited state through the conjugation length distribution could cause fluorescence anisotropy loss from the maximum value 0.40. 2,6-NLP is capable of supporting a distribution of conjugation lengths and the distribution is narrow. (The narrowness gives rise to the well-defined vibronic replicas of the transition, evident in both the absorption and emission spectra of each polymer (see Figure 7.5)). It is expected that the absorption and emission transition dipole moments of these states are parallel as the two states did not change between transitions. However, as shown in Chapter 5 there is still significant depolarisation even at when the very red-edge of the density of states is excited (i.e. with low energy excitation wavelengths in 2,6-NLP, as shown in Table 7.3) . Since fluorescence anisotropy in solution depends on photo selection, (only molecules with dipoles oriented parallel to the electric field of the illuminating photons are excited), it has been possible to record the orientational evolution of the dipole moment as the excited state relaxes.

The experimental technique and the subsequent analysis were successfully tested for Coumarin 6 in ethylene glycol (see Figures 7.2 and 7.3). Coumarin 6 is a small highly luminescent molecule. It is just larger than a monomer unit of 2,6-NLP and is a known, almost spherical, rotator. The global analysis of polarised decays produced model decays that correspond (within error) to those found by previous authors.[160] The fluorescence anisotropy decay model and subsequent analysis of the decay gave a rotational time of 2.03 ns which is two standard errors from that previously published. (Propagation of the error in lifetime into this complex function estimates the error at 0.2 ns. This is a specific case for Coumarin 6 and the error is smaller for the other measurements.) This evidence gives good reliability of the experimental method used and high confidence in the results it yields.

The results for Coumarin 6 do not show an anisotropy decay on the 10 ps time scale which is measured for all of the polymers. There was no change in the experimental set-up between taking the measurements, proving that the short decay observed is intrinsic to the conjugated polymers and not an experimental artefact. Therefore, this decay is real for the polymers and not a systematic experimental error.

Having ruled out many of the common anisotropy loss processes the suitability of the spherical rotator model global analysis is confirmed. The mathematical model used to analyse the polarised decays (see equations 7.5 and 7.6) relies on the assumption that all fluorescence components contribute to the anisotropy decay.[80] This was a particular concern when analyzing 2,6-NLP because, unlike MeLPPP and PF2/6, it has two fluorescence lifetimes. This makes the mathematical model (see equations 7.5 and 7.6) more complicated and more subject to errors. If one of theses lifetimes did not contribute to the fluorescence anisotropy, the model would not be appropriate. However, since only electronic (fluorescence) contributions remain the applicability of the analysis method used in this experiment is confirmed.

7.7.1 Discussion of remaining processes in 2,6-NLP

All but three major anisotropy loss processes have been ruled out by studying 2,6-NLP in dilute solution. The remaining processes are inter-chain migration (in small aggregates), intra-chain migration via hopping to lower energy states and an elongation of the electronic state through the conjugation length. The discussions above have highlighted how limited inter- and intra-chain migration are in 2,6-NLP, but they are still worth considering.

The data from 2,6-NLP in solution indicates that there are three different anisotropy processes. Table 7.3 lists three pieces of information about 2,6-NLP in solution: that it has two lifetimes; the lifetimes are independent of solvent; and that the early-time anisotropy is not 0.40. The processes are identified as: a very long lifetime due to a slight rotation; a dominant picosecond scale process, which is electronic; and an ultrafast (< 5 ps) process, responsible for the early-time anisotropy less than 0.40, which is also electronic in origin. Each of these processes is discussed separately below.

Several hundreds of picoseconds fluorescence anisotropy loss.

The longer of the two lifetimes cannot be clearly resolved in this experiment because it is considerably longer than the polymer's fluorescence lifetime. It does however exist and it is significantly (about three times) the fluorescence lifetime. It is thought to arise from the slight rotation undergone by the molecule ($\sim 0.1\,^{\circ}$) because it is not the most dominant process involved in anisotropy loss.

Ten picosecond fluorescence anisotropy loss.

The shorter anisotropy lifetime is dominant. It is due to an electronic process that is responsible for up to half the total anisotropy loss. The timescale is approximately (12 ± 5) ps for all excitation wavelengths. The lifetime is independent of excitation and emission wavelength and solvent, and is, therefore, intrinsic to the polymer. Dykstra *et al.* have hypothesized that anisotropy loss on this timescale is electronic in origin either intra- or inter-chain energy transfer.[228] . This lifetime appears in all of the anisotropy decays for three different polymers and in different media. The origin of this lifetime is discussed below.

Ultra-fast fluorescence anisotropy loss.

The maximum fluorescence anisotropy was not observed for 2,6-NLP and an electronic process is deduced to be responsible for it. It has already been discussed in Chapters 4 and 5 that the natural anisotropy is not 0.40 and that the molecule has an intrinsic angle between absorption and emission transition dipole moments. The evolution of this process (from absorption to emission transition dipole moment) is not observed in the time resolution of this experiment. The anisotropy loss from 0.40 to the natural anisotropy must occur in under 5 ps (the experimental resolution. From the description of anisotropy loss processes by Dykstra *et al.*, a process occurring in under 5 ps must be electronic in origin.[228] thus confirming the ideas outlined in earlier chapters in this thesis.

7.7.2 Discussion of remaining processes in MeLPPP

The data in Table 7.4 can be interpreted to show that the three processes identified in 2,6-NLP also occur in MeLPPP. However, in this polymer, the longer lifetime is on the scale of the fluorescence lifetime indicating that the process causing it, which is not dominant, is scattering or reabsorption. Both these processes can occur on this timescale. The MeLPPP solutions were slightly higher concentration than 2,6-NLP and, therefore, scattering is the most convincing reason. The short lifetime in MeLPPP is approximately 15 ps and within the error of that of 2,6-NLP. It is responsible for the majority of the anisotropy loss. This means that intra-chain migration between branched segments is possible in this polymer. Once again the maximum value of anisotropy is not reached proving that there is an ultrafast anisotropy process. Like 2,6-NLP, MeLPPP is rigid and, therefore, any anisotropy loss cannot be ascribed to conformational motion.

As predicted above, the early-time and steady-state anisotropy values are lower in MeLPPP than in 2,6-NLP, due to the shape and chain length of MeLPPP. MeLPPP is a longer chain than 2,6-NLP and can support more than one energetic site. The findings fit with the earlier hypothesis that the lightning shaped backbone of MeLPPP enhances the anisotropy loss process compared with 2,6-NLP. For 2,6-NLP and MeLPPP the results for excitation at the peak absorption wavelength produce lower anisotropy values suggesting an enhancement of the anisotropy because of excess excitation energy. The excess energy applied to MeLPPP initiates hopping to other states which produces a small effect in 2,6-NLP because this latter polymer is much shorter.

7.7.3 Discussion of remaining processes in PF2/6

These results and findings are not solely linked in rigid-rod ladder-type polymers, the short anisotropy lifetime in PF2/6 corresponds directly with the 2,6-NLP lifetime. Figures 7.8 and 7.9 show that the PF2/6 can be studied in the same way as 2,6-NLP. The results listed in Table 7.5 show that PF2/6 has three anisotropy decay lifetimes. The two lifetimes present in 2,6-NLP, a short time of $\sim$ 12 ps and a lifetime much longer than the fluorescence lifetime are also present in PF2/6. (In PF2/6 the lifetime, 11 ps, is within the error for 2,6-NLP). The existence of the two lifetimes in PF2/6 is explained in the same way as for 2,6-NLP i.e. the much longer one is due to a slight rotation of the molecule and the short lifetime is an electronic process. The similarity in lifetime between PF2/6 and 2,6-NLP suggests that the same process occurs in both polymers.

PF2/6: Several tens picoseconds fluorescence anisotropy loss

The results for PF2/6 in solution present a third anisotropy lifetime of 100 ps which is ascribed to conformational twisting of the polymer backbone. Three lifetimes are only observed in PF2/6 in solution: only the 100 ps lifetime is not present in the data from 2,6-NLP in the same solvent. The main difference between the two polymers is the flexible backbone in PF2/6. It therefore follows that this lifetime arises as a result of the polymer's flexibility. As discussed here in Chapter 4, conformational twisting (resulting in planarization) alone is not sufficient

to change the anisotropy unless it is coupled with an elongation of the electronic state. It is therefore concluded here, that the 100 ps lifetime is created by the process of planarisation and elongation. The anisotropy decay result confirms that the fluorescence lifetime observed by Dias *et al.* between 30 ps and 100 ps is indeed due to conformational twisting.

Confirmation of chain isolation in PE films

The high early-time anisotropy value of PF2/6 in anisotropic film suggests that the molecules are well separated and that the system acts like a frozen solution. The x-ray work in chapter 6 has suggested that the domain size in PF2/6 blends is small or molecular chain sized. The early-time anisotropy results correspond to the natural anisotropy of the "average" molecule i.e. an isolated molecule or dimer. The results of PF2/6 in anisotropic films are identical to that of an isolated small planar molecule (2,6-NLP). This suggests that the molecules do not form large aggregates in the matrix and, as discussed above, they are immobile, much like a molecule in a frozen solution. Given the dilute solution is not thought to form large aggregates, it can be assumed that the small domains measured in chapter 6 are indeed single molecules. This set of results also confirms the postulation in Chapter 6 that the guest conjugated molecules in a stretched polyethylene host are completely dissolved.

7.7.4 Interpretation of the two fast anisotropy loss processes.

The data have shown that there are three fluorescence anisotropy decay times for polymers studied in solution. At least two of these are fast processes that can only be electronic in origin. These are the ultra-fast process that occurs in less than the experimental time resolution and the $\sim$ 11 ps decay. The processes are now discussed separately.

Ultra-fast fluorescence anisotropy loss process in all polymers studied

The three polymers did not show the maximum anisotropy, 0.40, in solution or in an anisotropic stretched film proving that there is another anisotropy loss process that occurs in less than 5 ps. Figure 7.9 gives an early-time anisotropy corresponding to the natural anisotropy found in Chapter 4 and not the maximum anisotropy. This loss of anisotropy must take place on a time scale less than the resolution of the equipment. This is the same phenomenon observed in 2,6-NLP where the maximum anisotropy measured was the natural anisotropy.

The fluorescence anisotropy is incontrovertibly linked to a reorientation of the transition dipole moments and it is shown here to occur in under 5 ps. Indeed Lanzani[254] reports such an anisotropy loss that occurs faster than 5 fs as judged from his ultra-fast measurements. The change from maximum to natural anisotropy occurs as the emission transition dipole moment rotates from being parallel to the absorption dipole to its final state. This is a finite process and will not cause total depolarisation of the polymer. Chapters 4, 5 and 6 have showed that the ground states of the polymers are localised up to 20° off the chain long axis, (with higher energy states in 2,6-NLP even further axis.) indicative of localised initial excitons. It has also been shown that the emission transition dipole moment is oriented parallel to the

backbone. This is the first time that an ultrafast electronic change to the excited state have been linked to the microscopic alignment of the polymer backbone. More importantly the time-resolved anisotropy measurements have revealed that this process occurs in under 5 ps. Processes under this time must be electronic.

The origin of this ultrafast anisotropy loss is linked to the electronic behaviour of the polymers and is ascribed to the elongation of an excited state over longer conjugation lengths. Earlier chapters discussed the concept that the ground state was localised on a segment and that the excited state was more delocalised along the polymer chain. The interpretation of the change in dipole orientation from maximum to natural anisotropy is that the exciton wavefunction spreads out after it is created becoming more delocalised along the chain axis. It is still localized (located) on a chain segment (which can be the entire chain in small fully conjugated polymers) but it is elongated over a longer conjugation length, compared with the ground state.

Experiments published by other researchers on experimental systems with a shorter resolution time have also recorded very fast depolarization (anisotropy loss) times. (For example, ultrafast transient absorption anisotropy on fully conjugated MEH-PPV present a depolarisation lifetime of < 1 ps,[255] ultrafast time-resolved fluorescence of P3HT show sub-100 fs lifetimes.[256] Work on discotic molecules has also shown the depolarization to be sub 1 ps.[63,257–259]). In many cases these very short lifetimes were explained as "dynamic localization", a process which changes the energy and shape of the excited state but the excitation is localized on a polymer segment.[48] [b]

In some of the experiments mentioned above, the polymers were flexible and part of the delocalisation was explained as a result of a physical motion. By working with a short rigid polymer we have confirmed that the elongation process that is known as dynamic localization is simply a result of an electronic relaxation process. It is perhaps better referred to as "dynamic delocalisation". It is therefore proposed that since this process is the same in flexible and rigid molecules that the true process is entirely electronic and that it is an electronic extension of the exciton wavefunction over adjacent bonds after initial excitation i.e. the conjugation length dynamically increases to accommodate the exciton. Most importantly the work here suggests that it is inherent to all conjugated polymers.

Ten picosecond fluorescence anisotropy loss in all polymers studied

All three polymers presented a fluorescence anisotropy loss of approximately 11 ps. In all cases this was the dominant fluorescence decay lifetime and it accounted for up to half the anisotropy loss between the natural anisotropy and the steady-state value. Where 2,6-NLP was excited at the red-edge of the conjugation length distribution, this short lifetime was responsible for all of the anisotropy loss. Anisotropy loss on this timescale can be caused by inter- or intra-chain migration or a further electronic process.

[b] The polymer segments were created by conjugation breaks caused by a flexible backbone.

This lifetime is independent of structure in three of the polymers studied here and it is assumed that it will also be inherent to other conjugated polymers. This lifetime could be explained a number of different ways, depending on the experimental data interpreted. For example, in solid-state, the lifetime could correspond to inter-chain migration which is expected to dominate. Yet, it has been proven here that these molecules are isolated (in solution) and the same lifetime is recorded, ruling out inter-chain contributions. Also, should two or more processes occur, the experiment would not be able to resolve them, making the interpretation of the data even more difficult. Here, the experimental considerations eliminated many fluorescence anisotropy processes in an attempt to explain the fundamental fluorescence loss in a conjugated polymer.

PF2/6 held in an anisotropy matrix further confirms that the short lifetime is electronic in origin. When PF2/6 is held in a rigid matrix of polyethylene (PE) only one anisotropy decay is recorded: this is the 11 ps lifetime. The other two lifetimes that were present in solution are absent in the film data. These were ascribed to either inter- or intra- molecular motion. Their absence in solid state confirms their origin and the fact that molecules are held rigid and immobile in a PE matrix. The 11 ps decay is therefore not a physical process but at such a rate it can only be electronic.

Exciting at the red-edge of the absorption spectrum of 2,6-NLP produces higher early and steady-state anisotropy values because the number of anisotropy loss processes are limited. 2,6-NLP is a rigid-rod polymer capable of supporting a distribution of conjugation lengths: as the conjugation increases over more bonds, the corresponding energy of the chromophore decreases. The change in fluorescence anisotropy is also connected to this change in conjugation length. By exciting just the edge of the conjugation length distribution it is possible to select a low energy site. The low energy of the site limits the number of processes that can occur, the main one, as found for PF2/6$_{N=20}$ in Chapter 4 , is the cessation of excitation hopping to lower energy sites. Therefore, for excitation wavelengths at 454 nm in (the short polymer) 2,6-NLP in MCH, there is little doubt that there are no other states for an excitation to travel to. Therefore, exciton hopping is not responsible for anisotropy loss in 2,6-NLP when excited at the red-edge.

The origin of the electronic anisotropy loss with a lifetime of 11 ps could be a function of the chain length. PF2/6 is not believed to form aggregates in dilute solution and therefore rules out this intra-chain migration as a major cause of anisotropy loss. Side-chains in the PF2/6 should prevent the molecules forming aggregates. However, this cannot be totally ruled out and is a possibility for anisotropy loss as it is in 2,6-NLP. The polymer PF2/6 used here has $\sim$ 60 monomer units meaning that it is very likely to support inter-chain excitation migration as shown in Chapter 4. Inter-chain migration is a known cause of fluorescence anisotropy loss (see Chapter 2 and section 2.5.8) especially in coiled polymers like PF2/6. This process occurs on the 10 ps time scale.[228] Exciton hopping between segments has been previously reported by other groups for different polymers such as PDOPT,[81] MEH-PPV[260]and partially conjugated MEH-PPV.[48] These reports all report a lifetime of $\sim$ 10 ps.

The electronic anisotropy loss process in PF2/6 is not aggregation but could be inter-chain hopping down through energetically lower states of the coiled chain.

However, the lifetimes in 2,6-NLP and PF2/6 are the same which means that the same process or processes occur in both polymers. The extent of anisotropy loss in the polymers depends upon excess excitation energy as does the early-time anisotropy. This may be because other anisotropy loss processes take place on the same timescale. The data in Table 7.5 indicates that PF2/6 and 2,6-NLP have the same short lifetime in solution and in stretched film. The origin of the 11 ps lifetime has been discussed in 2,6-NLP to be due to exciton hopping when there is enough excess excitation energy. And, in the case of PF2/6, there is a large number of sites for an excitation to hop down indicating that the 11 ps lifetime is at least partially explained by exciton hopping. However, there is still no clear explanation of the anisotropy loss process when exciton hopping is eliminated.

Whilst an explanation for the anisotropy loss process is, at present, unclear, the findings do work towards further understanding of the electronic processes within polymers. The work has shown that there is a fundamental anisotropy loss on he picosecond timescale (as well as on the ultra-fast time-scale). Therefore in future work of this kind, it is no longer appropriate to ascribe anisotropy loss solely to a property of the polymer under test. The interpretation of the decays on this lifetime plays an important role in the understanding of electronic properties in polymers and the efficiency of devices. It is strongly suggested that further work should be undertaken to resolve the different processes that occur on this time scale. For example, what role is played by solvent rearrangement in solution and what are the effects do adjacent chains have on the orientation of the emission transition dipole moments? These questions are of particular importance for research into solid-state polymer devices which rely on the close packing of chains.

Comments on planarisation assisted fluorescence anisotropy loss

The value of both the early-time and steady-state fluorescence anisotropy in PF2/6 is lower in solution than in film which indicates that the conformational twisting and the associated planarisation assist the electronic process. As stated above holding the polymer in a rigid matrix removes the physical motion of the molecule. As a result the number of anisotropy loss processes is reduced to one and the early time anisotropy is equivalent to the natural anisotropy of the polymer. The steady state anisotropy is also very high, indicating that there has been little contribution of the electronic anisotropy process. Indeed close observation of Figure 7.9 shows that the fast decay is very short lived. It is theorised that the anisotropy loss process is hindered by the molecule's surroundings i.e. that it is held rigidly. As mentioned above the effect of the rotation is very small, meaning that the conformational motion helps the electronic process responsible for anisotropy loss.

It was suggested that the electronic process was either hopping down the chains or an elongation of the excited state through the conjugation length distribution. Exciton hopping would be able to overcome the twisted backbone to reach lower energy sites that were not collinear

with the original site. But it is the planarisation that is key to assisting this process which is why the anisotropy loss rate is seen for a short period of time. The planar polymer 2,6-NLP shows only a small anisotropy loss at red-edge excitation. However, when it has enough excess energy, the anisotropy loss is greater. This gives further credence to the idea that the planarisation assists the anisotropy loss. The findings here support the theory of Westenhoff *et al.* who first suggested that conformational twisting was linked with planarisation.[81] The data here has been used to postulate that the 11 ps decay, that is independent of phase and polymer is electronic and most likely to be inter-chain excitation migration.

7.8 Conclusions

Time-resolved fluorescence anisotropy measurements (TRAM) have been successfully carried out on a time correlated single photon counting system in Durham University. TRAM were used to monitor the evolution of the fluorescence anisotropy decay in polymers that show unexpected fluorescence anisotropy. Ladder type polymers are linear and planar and not expected to have a difference in dipole between absorption and emission.

By using a short, rigid polymer naphthylene poly(*para*-phenylene) (2,6-NLP) 2,6-NLP many of the common fluorescence anisotropy processes (significant rotation, planarisation, intra-chain migration) were automatically ruled out leaving just purely electronic processes. These can only be excitation migration and an elongation of the excited state to encompass longer conjugation lengths.

The data have shown that the major decay route has an anisotropy decay of 10 ps. The results of the polymer held in different media (solution, thin spun film and anisotropic polyethylene matrix) show the anisotropy decay rate as being independent of the polymer's surroundings. This is likely to be inter-chain migration.

At no point was the maximum anisotropy, 0.40, observed; instead only the natural anisotropy was recorded. Therefore the loss from the maximum had to occur in under 5 ps, the resolution limit of the experimental equipment. Again this process must be electronic process that rotates the emission transition dipole moment from parallel to the absorption transition dipole moment to its final orientation. Work in previous chapters hypothesised that this was due to increased delocalisation of the excited state. Here a further step is hypothesised that this is a "dynamic delocalisation" caused by the elongation of the excited state across adjacent molecular bonds.

We have shown that a popular concept of "dynamic localisation" is applicable to our work with the understanding that the final excited state is located on a polymer segment, but it is further delocalised over a longer conjugation length.

The fast fluorescence anisotropy decay that is observed in the rigid-rod polymer, is also present in the more flexible polyfluorene poly[9,9-di(ethylhexyl)fluorene](PF2/6). This proves that conformational changes are not wholly responsible for fluorescence depolarisation. However results have shown that the flexibility of the polymer enhances the anisotropy loss processes.

Finally, the data presented here confirms the assumptions made in earlier chapters. Specifically that long chain polymers (over 20 monomer units in length) do not rotate significantly in solution. That 2,6-NLP, MeLPPP and PF2/6 do not form large aggregates in solution or in stretched polyethylene matrices. That the individual molecules are well separated in dilute solution and in PE matrices and that excitations remain on a single chain when excited on the red edge.

Chapter 8

Conclusions

The work contained in this thesis has increased the understanding of the interaction between conjugated polymers and linearly polarised light. The work has concentrated on blue emitters because these are particularly important due to their rarity. The x-ray data collected for this thesis has been used in an international collaboration to investigate phase morphology of blended films. This thesis also includes the first photophysical report on a newly synthesised conjugated polymer.

Four different blue emitting conjugated polymers from two different classes of polymer were studied. The results from the flexible polyfluorene derivatives were compared with those from the inflexible ladder-type poly(*para*-phenylene) (LPPP). This comparison was made to further understand the photophysical processes that occur on polymers and to investigate the difference between polymers whose excited state can undergo conformational relaxation (flexible) with those that cannot (inflexible).

The study has also provided further understanding of the angle between of the absorption and emission transition dipole moments (anisotropy). These dipole moments govern the polarisation of the emission and absorption transitions. Appreciating the orientation of these relative to the backbone of the polymer will reveal a fundamental understanding of luminescent polymers.

This work continues the work of Dias et al, whose results from time resolved single photon counting measurements, led them to postulate that there were two distinct physical processes in the polyfluorene derivative poly[9,9-di(ethylhexyl)fluorene] (PF2/6). A conformational motion, which is a rotational twist about the chain axis, and excitation migration of excitons from one state to an energetically lower state.

Initially, PF2/6 was investigated through polarised spectroscopy and the work performed showed that its anisotropy increased with the excitation wavelength, rising smoothly to a steady-state value at the red edge of the polymers absorption spectrum. The natural (inherent) anisotropy was estimated from low temperature anisotropy measurements taken with excitation wavelength at the red edge of the spectrum. This value showed that there is an angular separation between the absorption and emission transition dipole moments for this polymer. Three short chain oligomers, which limited the exciton hopping but not the conformational twisting, were studied in addition to PF2/6. Overall, the results of these low temperature experiments confirmed the existence of the two processes in polymer as postulated by Dias *et al.*

To verify that one of the two processes responsible for the excitation wavelength anisotropy change was due to conformation relaxation it was necessary to study the two processes separately. By choosing a ladder-type polymer which, due to its structure, eliminated conformational motion, it was possible to study excitation migration This class of ladder-type polymer was represented by two materials: Methyl-substituted-LPPP (MeLPPP) and napthylene-LPPP (2,6-NLP). They were investigated by the same methods and it was identified that these polymers did not behave in exactly the same way as the polyfluorene derivatives. It was found that their anisotropy is also dependent upon the excitation wavelength, but instead of reaching a steady state value at the red-edge of the spectrum, the LPPPs has a peak before reaching this plateau. The peak in anisotropy is at the same wavelength as the vibronic peak in the absorption spectrum. It was found that the orientation of the absorption transition dipole moment is dependent upon the absorption wavelength.

The results of low temperature work showed that as with the PF2/6, the natural anisotropy of the LPPPs indicated that there is an angular separation between the absorption and emission transition dipole moments. This new result did not fit with the accepted theory that all the transitions were parallel because they were thought to be aligned along the polymeric chain.

Further experiments were then undertaken to locate the angle between the absorption and the polymer chain. From this knowledge and the natural anisotropy results found previously, it was possible to locate the relative positions of the emission and the backbone.

To do this the experiments required the known orientation of the polymer backbone and this was achieved by mechanically aligning the polymer and measuring the orientation distribution of the chains. A method of fabrication used by other workers was developed and adapted to make suitable aligned films. Polyethylene films, containing approximately 1% of the polymer under investigation, were stretched to approximately 30 times their original length. To find the orientation distribution of the polymer (or how well aligned the polymer was in the film) the films were investigated with a number of techniques, including X-ray diffraction, polarised Raman spectroscopy and fluorescence anisotropy.

The results, using these films, showed that the PF2/6 had a high degree of long range order and that the average angle the polymer backbone made with the stretching direction was small. Whereas the MeLPPP and 2,6-NLP results indicated a short range order and a wider distribution of orientation angles. The average angle the backbone made was quite large.

Having rebuilt the existing apparatus and enhanced the control program, polarised absorption spectra (linear dichroism) were obtained. The results of this experiment provided strong evidence that the absorption transition dipole moment was not aligned with the backbone in any of the polymers used. These conclusions are in agreement with those found experimentally for other similar conjugated polymers by Shang et al.[166]

Using the natural anisotropy results found previously, it was postulated that the emission transition dipole moment of PF2/6 was oriented parallel and along the polymer backbone. Although the results for the LPPP films are not as conclusive, they still present evidence

that is not inconsistent with the same behaviour. The structural similarity of the polymer backbones leads to the conclusion that the emission transition dipole moments lie along the backbone.

Having already found that all the polymers exhibit a significant anisotropy loss across the absorption spectrum, investigations were carried out to measure the rate of this loss. An existing picosecond time resolved single photon counting system was adapted allowing individually polarised decays were measured. Using the standard equation for anisotropy, these decays were combined to create an anisotropy decay.

PF2/6 and the two ladder-type polymers were investigated in this way. The polymers were studied in dilute solution to compare with the steady state results and in thin isotropic and aligned films.

It was discovered that there was one main decay mechanism responsible for the immediate anisotropy loss. This mechanism was independent of the form the polymer was in and, to the limit of the experiment: independent of polymer. The majority of the anisotropy was lost in under 5 ps, the limit of the equipment.

It is expected that a decay route due to physical deformation would be on the order of several picoseconds and an electronic process would be much faster. Whilst the equipment here could not resolve the decay times, the measurements do confirm that the anisotropy loss process is electronic in origin.

Comparing the rates for the flexible PF2/6 and the ladder-type polymers has shown that the major anisotropy loss is the same for both polymers. The fact that the decay time is similar for the polymer in solution and in films, indicates that this is a process that is intrinsic to both polymers. This theory with previous reports of ultrafast depolarisation has been explained as “dynamic localisation” of the exciton.

For the first time it has been possible to link the microscopic chain order with basic electronic processes yielding new and important information on exciton relaxation and dynamic conjugation length changes during the initial period after photoexcitation.

Throughout this thesis the origin of the fluorescence anisotropy loss (Fluorescence depolarisation) in conjugated polymers has been investigated and theorised about. Investigations herein have systematically removed excitation migration, rotation and conformational motion yet, fluorescence depolarisation still occurs. When combined with the time resolved results it was proposed that this fast electronic process is an inherent property of all conjugated polymers. From observations of the dipole orientation change from off-axis to on-axis with increasing conjugation length, it is believed that the exciton delocalises to create a longer conjugation segment. This elongation of the excited state is responsible for the fluorescence depolarisation from the theoretical maximum to the natural anisotropy. Because the process is electronic, it occurs in a timescale to fast for the experiments herein, but other sources have recorded unknown depolarisation processes to occur in under 100 fs.

This thesis has also increased the knowledge of the behaviour of conjugated polymers in blends. Through x-ray diffraction experiments it was discovered that high concentrations of conjugated polymers in polyethylene form phase segregate aggregates which can be ordered, but not separated, through stretching. The work also showed that low concentration blends simulated the solution phase of the conjugated polymer, thought to be due to a thorough dissolution of the polymer in the host. These findings are particularly useful for controlling the internal microstructures of light emitting and voltaic devices.

References

[1] C. K. Chiang, C. R. Fincher Jr, Y. W. Park, A. J. Heeger, H. Shirakawa, E. J. Louis, S. C. Gau, and A. G. MacDiarmid. Electrical conductibility in doped polyacetylene. *Phys. Rev. Lett.*, 39(17):1098 – 1101, (1977).

[2] J. H. Burroughes, D. D. C. Bradley, A. R. Brown, R. N. Marks, K. MacKay, R. H. Friend, P. L. Burns, and A. B. Holmes. Light-emitting diodes based on conjugated polymers. *Nature*, 347:539–541, (1990).

[3] A.R. Blythe and D. Bloor. *Electrical properties of polymers*. Cambridge University Press, Cambridge, UK, second edition, (2008).

[4] R. H. Friend, R. W. Gymer, A. B. Holmes, J. H. Burroughes, R. N. Marks, C. Taliani, D. D. C. Bradley, D. A. Dos Santos, J. L. Brédas, M. Logdlund, and W. R. Salaneck. Electroluminescence in conjugated polymers. *Nature*, 397(6715):121–128, (1999).

[5] C. D. Müller, A. Falcou, N. Reckefuss, M. Rojahn, V. Wiederhirn, P. Rudati, H. Frohne, O. Nuyken, H. Becker, and K. Meerholz. Multi-colour organic light-emitting displays by solution processing. *Nature*, 421:829–833, February (2003).

[6] C.R. Towns, I. Grizzi, M. Roberts, and A. Wehrum. Conjugated polymer-based light emitting diodes. *J. Luminesc*, 122-123:976–979, (2007).

[7] S. R. Forrest. The path to ubiquitous and low-cost organic electronic appliances on plastic. *Nature*, 428(6986):911–918, (2004).

[8] A. Sugimoto, H. Ochi, S. Fujimura, A. Yoshida, T. Miydera, and M. Tsuchida. Flexible OLED displays using plastic substrates. *IEEE J Sel Top Quant Electron*, 10(1), (2004).

[9] R. H. Friend. Materials science: Polymers show their metal. *Nature*, 441(7089):37, (2006).

[10] SAMSUNG. http://www.samsungmobile.co.uk/products/jet/showroom/index.html. Website: Downloaded 20/08/09 13.22, (2009).

[11] NOKIA. http://europe.nokia.com/find-products/devices/nokia-n85/tech-specs. Website: Downloaded 20/08/09 13.22, (2009).

[12] SONY. http://www.sony.co.uk/product/nws-x-series/nwz-x1050. Website: Downloaded 20/08/09 13.25, (2009).

[13] E. Hecht. *Light*. Addison-Welsey, Harlow, England, third edition, (1998).

[14] M. Chapple. *The complete A-Z Physics handbook*. Hodder & Stoughton, London, UK, (2001).

[15] B. H. Bransden and C. J. Joachain. *Physics of atoms and molecules*. Longman Scientific and Technical, Essex, England, first edition, (1983).

[16] R. P. Feynman, R. B Leighton, and M. Sands. *The Feynman Lectures on Physics*, volume 1. Addison-Welsey Publishing Company, Inc., London, 1st edition edition, (1965).

[17] P. A. Tipler. *Physics for scientists and engineers*. W. H. Freeman and Company, New York, fourth edition, (1999).

[18] D. S. Kliger, J.W. Lewis, and C.E. Randall. *Polarized light in optics and spectroscopy*. Academic Press, San Diego, (1990).

[19] F Mandl. *Quantum Mechanics*. John Wiley & Sons, Chichester, UK, (1992).

[20] A. Gilbert and J. Baggot. *Essentials of Molecular Photochemistry*. Blackwell Scientific Publications, Oxford, 1st edition edition, (1991).

[21] A. Rodger and B. Norden. *Circular Dichroism and Linear Dichroism*. Oxford Chemistry Masters. Oxford University Press, Oxford, 1 edition, (1997).

[22] N. J. Turro. *Modern Molecular Photochemistry*. University Science Books, (1991).

[23] E. W. Thulstrup and J. Michl. *Elementary Polarization Spectroscopy*. VCH Publishers (UK) Ltd., Cambridge, (1989).

[24] J. C. Kotz and P. Treichel Jr. *Chemistry and Chemical Reactivity*. Saunders College Publishing, London, UK, third edition, (1998).

[25] A. L. Companion. *Chemical Bonding*. McGraw-Hill Book Company, London, (1979).

[26] F. A. Cotton, G. Wilson, and P. L. Gaus. *Basic Inorganic Chemistry*. John Wiley & Sons, Inc, New York, third edition, (1995).

[27] H Zollinger. *Color chemistry: Syntheses, properties and applications of organic dyes and pigments*. VCH Publishers, Inc, New York, 2nd edition, (1991).

[28] M. Pope and C. E. Swenberg. *Electronic Processes in Organic Crystals and Polymers*, volume 1. Oxford University Press, 2nd edition, (1999).

[29] H. L. Vaughan and S. M. King. Private discussions on the topic of branching in melppp, (2007).

[30] S. M. King. *Ultrafast processes and excited state dynamics in conjugated polymers*. Phd, Physics Department, Durham University, (2008).

[31] U Scherf and H. L. Vaughan. Personal communications on the topic of polydispersities of materials provided and the possible branching in melppp, (2004).

[32] P.W. Atkins. *Concepts in Physical Chemistry*. Oxford University Press, Oxford, UK, first edition, (1995).

[33] C. Kittel. *Introduction to Solid State Physics*. John Wiley & Sons, Inc, 7th edition, (1996).

[34] A. J. Heeger. Semiconducting and metallic polymers: The fourth generation of polymeric materials (nobel lecture)13. *Angewandte Chemie International Edition*, 40(14):2591–2611, (2001).

[35] W. P. Su, J. R. Schrieffer, and A. J. Heeger. Solitons in polyacetylene. *Physical Review Letters*, 42(25):1698 LP – 1701, (1979).

[36] W. P. Su, J. R. Schrieffer, and A. J. Heeger. Soliton excitations in polyacetylene. *Physical Review B*, 22(4):2099 – 2111, (1980).

[37] S. F. Alvarado, P. F. Seidler, D. G. Lidzey, and D. D. C. Bradley. Direct determination of the exciton binding energy of conjugated polymers using a scanning tunneling microscope. *Phys. Rev. Lett.*, 81(5):1082 – 1085, (1998).

[38] J.-L. Brédas, J. Cornil, and A. J. Heeger. The exciton binding energy in luminescent conjugated polymers. *Advanced Materials*, 8(5):447–452, (1996).

[39] D. Moses, J. Wang, A. J. Heeger, N. Kirova, and S. Brazovskii. Singlet exciton binding energy in poly(phenylene vinylene). *Proc. Nat. Acad. Sci. U.S.A.*, 98(24):13496, (2001).

[40] I. G. Scheblykin, A. Yartsev, T. Pullerits, V. Gulbinas, and V. Sundström. Excited state and charge photogeneration dynamics in conjugated polymers. *J. Phys. Chem. B.*, 111(23):6303–6321, (2007).

[41] I. Avgin and D. L. Huber. Excitons in disordered polymers. *J. Luminesc*, 122-123:389–392, (2007).

[42] G. D. Scholes and G. Rumbles. Excitons in nanoscale systems. *Nature Materials*, 5(9):683–696, (2006).

[43] W. J. D. Beenken and T. Pullerits. Spectroscopic units in conjugated polymers: A quantum chemically founded concept? *Journal of Physical Chemistry B*, 108(20):6164–6169, (2004).

[44] T. E. Dykstra, V. Kovalevskij, X. Yang, and G. D. Scholes. Excited state dynamics of a conformationally disordered conjugated polymer: A comparison of solutions and film. *Chem. Phys.*, 318(1-2):21–32, (2005).

[45] A. Köhler, J. Grüner, R. H. Friend, K. Müllen, and U. Scherf. Photocurrent measurements on aggregates in ladder-type poly(p-phenylene). *Chem. Phys. Lett.*, 234:456–461, (1995).

[46] J. G. Muller, E. Atas, C. Tan, K. S. Schanze, and V. D. Kleiman. The role of exciton hopping and direct energy transfer in the efficient quenching of conjugated polyelectrolytes. *Journal of the American Chemical Society*, 128(12):4007–4016, (2006).

[47] M. H. Chang, M. J. Frampton, H. L. Anderson, and L. M. Herz. Intermolecular interaction effects on the ultrafast depolarization of the optical emission from conjugated polymers. *Phys. Rev. Lett.*, 98(2):027402, (2007).

[48] A. Ruseckas, P. Wood, I. D. W. Samuel, G. R. Webster, W. J. Mitchell, P. L. Burn, and V. Sundström. Ultrafast depolarization of the fluorescence in a conjugated polymer. *Phys. Rev. B*, 72(11):115214, (2005).

[49] Y. Ding, X. S. Wang, and F. C. Ma. Mechanism of forster-type hopping of charge transfer and excitation energy transfer along blocked oligothiophenes by si-atoms. *Chemical Physics*, 348(1-3):31–38, (2008).

[50] G. Ramakrishna, A. Bhaskar, P. Bauerle, and T. Goodson. Oligothiophene dendrimers as new building blocks for optical applications. *Journal of Physical Chemistry A*, 112(10):2018–2026, (2008).

[51] J. R. Lakowicz. *Principles of Fluorescence Spectroscopy*. Plenum Publishers, New York, 2nd edition, (1999).

[52] E. Collini and G. D. Scholes. Coherent intrachain energy migration in a conjugated polymer at room temperature. *Science*, 323(5912):369–373, (2009).

[53] T. G. Bjorklund, S-H. Lim, and C. J. Bardeen. Use of picosecond fluorescence dynamics as an indicator of exciton motion in conjugated polymers: Dependence on chemical structure and temperature. *J. Phys. Chem. B*, 105(48):11970–11977, (2001).

[54] F. B. Dias, A. L. Macanita, J. Sexias de Melo, H. D. Burrows, R. Guentner, U. Scherf, and A. P. Monkman. Picosecond conformational relaxation of singlet excited polyfluorene in solution. *J. Chem. Phys*, 118(15):7119–7126, (2003).

[55] T. W. Hagler, K. Pakbaz, K. F. Vossm, and A. J. Heeger. Enhanced order and electronic delocalization on conjugated polymers orientated by gel processing in polyethylene. *Phys. Rev. B*, 44(16):8652–8666, (1991).

[56] R. Kersting, B. Mollay, M. Rusch, J. Wenisch, G. Leising, and H. F. Kauffmann. Femtosecond site-selective probing of energy relaxing excitons in poly(phenylenevinylene): Luminescence dynamic and lifetime spectra. *J. Chem. Phys*, 106(7):2850–2864, (1997).

[57] E. J. W. List, J. Partee, J. Shinar, U. Scherf, K. Müllen, E. Zojer, W. Graupner, and G. Leising. Solid state effects in the electronic structure of ladder-type poly(p-phenylene)s and oligo(p-phenylene)s. *Synth. Met.*, 111-112:509–513, (2000).

[58] S. Tretiak, A. Saxena, and R. L. Martin. Conformational dynamics of photoexcited conjugated molecules. *Phys. Rev. Lett.*, 89(9):097402, (2002).

[59] B. J. Schwartz, T-Q. Nguyen, J. Wu, and S. H. Tolbert. Interchain and intrachain exciton transport in conjugated polymers: ultrafast studies of energy migration in aligned MEH-PPV/mesoporous silica composites. *Synth. Met.*, 116(1-3):35–40, (2001).

[60] H. Bässler and B. Schweitzer. Site-selective fluorescence spectroscopy of conjugated polymers and oligomers. *Acc. Chem. Res.*, 32(2):173–182, (1999).

[61] S. A. Bagnich, H. Bässler, and D. Neher. Exciton dynamics in ladder-type methyl-poly(para-phenylene) doped with phosphorescent dyes. *J. Luminesc*, 112((1 - 4)):377–380, (2005).

[62] P. Bojarski, A. Synak, L. Kulak, and A. Kubicki. Electronic excitation energy migration in partly ordered polymeric films. *J. Fluoresc.*, 16(3):309–316, (2006).

[63] H. S. Cho, H. Rhee, J.K. Song, C.-K. Min, M. Takase, N. Aratani, S. Cho, A. Osuka, T. Joo, and D. Kim. Excitation energy transport processes of porphyrin monomer, dimer, cyclic trimer, and hexamer probed by ultrafast fluorescence anisotropy decay. *J. Am. Chem. Soc.*, 125(19):5849–5860, (2003).

[64] E. J. W. List, C. Creely, G. Leising, N. Schulte, A. D. Schlüter, U. Scherf, K. Müllen, and W. Graupner. Excitation energy migration in pi-conjugated polymers. *Synth. Met.*, 1(119):659–660, (2001).

[65] E. J. W. List and G. Leising. Excitation energy migration assisted processes in conjugated polymers. *Synth. Met.*, 141(1-2):211–218, (2004).

[66] A. Ruseckas, M. Theander, L. Valkunas, M. R. Andersson, O. Inganäs, and V. Sundström. Energy transfer in a conjugated polymer with reduced inter-chain coupling. *J. Luminesc*, 76 & 77:474–477, (1998).

[67] J. G. Müller, J. M. Lupton, J. Feldmann, U. Lemmer, and U. Scherf. Ultrafast intramolecular energy transfer in single conjugated polymer chains probed by polarized single chromophore spectroscopy. *Appl. Phys. Lett.*, 84(7):1183–1187, (2004).

[68] K. Becker and J. M. Lupton. Efficient light harvesting in dye-endcapped conjugated polymers probed by single molecule spectroscopy. *Journal of the American Chemical Society*, 128(19):6468–6479, (2006).

[69] S. C. J. Meskers, R. A. J. Janssen, J. E. M. Haverkort, and J. H. Wolter. Relaxation of photo-excitations in films of oligo- and poly-(para-phenylene) derivatives. *Chem. Phys.*, 260:415–439, (2000).

[70] A. Eisfeld and J. S. Briggs. The J-band of organic dyes: lineshape and coherence length. *Chem. Phys.*, 281(1):61–70, (2002).

[71] N. C. Maiti, S. Mazumdar, and N. Periasamy. J- and H-aggregates of porphyrin-surfactant complexes: Time resolved fluorescence and other spectroscopic studies. *J. Phys. Chem. B*, 102:1528 – 1538, (1998).

[72] M. Knaapila, B. P. Lyons, K. Kisko, J. P. Foreman, U. Vainio, M. Mihaylova, O. H. Seeck, L-O. Palsson, R. Serimaa, M. Torkkeli, and A. P. Monkman. X-ray diffraction studies of multiple orientation in poly(9,9-bis(2-ethylhexyl)fluorene-2,7-diyl) thin films. *J. Phys. Chem. B.*, 107(45):12425–12430, (2003).

[73] J. Michl and E. W. Thulstrup. *Spectroscopy with Polarized Light: Solute Alignment by photoselection, in Liquid Crystals, Polymer and Membranes*. VCH Publishers, Inc, 2nd edition, (1995).

[74] P. G. de Gennes and J. Prost. *The Physics of Liquid Crystals*. Clarendon, Oxford, (1993).

[75] L-O. På lsson, H. L. Vaughan, and A. P. Monkman. Polarised optical spectroscopy applied to investigate two poly(phenylene vinylene) (PPV) polymers with different side structures. *J. Chem Phys*, 125(16):Art. No. 164701, (2006).

[76] R. V. Bensasson, E. J. Land, and T. G. Truscott. *Excited States and Free Radicals in Biology and Medicine: Contributions from Flash Photolysis and Pulse Radiolysis*. Oxford University Press, (1993).

[77] B. Valeur. *Molecular Fluorescence: Principles and Applications*. Wiley-VCH, Weinheim, (2002).

[78] M. Hennecke. On the transfer of excitation energy in poly(p-phenylenevinylene) as studied by fluorescence depolarization. *Synth. Met.*, 41:1281–1284, (1991).

[79] P. Bojarski, A. Kaminska, L. Kulak, and M. Sadownik. Excitation energy migration in uniaxially oriented polymer films. *Chem. Phys. Lett*, 375(5-6):547–552, (2003).

[80] D. V. O'Connor and D. Phillips. *Time Correlated Single Photon Counting*, volume 1. Academic Press (London) Ltd, London, (1984).

[81] S. Westenhoff, W. J. D. Beenken, R. H. Friend, N. C. Greenham, A. Yartsev, and V. Sundström. Anomalous energy transfer dynamics due to torsional relaxation in a conjugated polymer. *Phys. Rev. Lett.*, 97(16), (2006).

[82] S. Westenhoff, W. J. D. Beenken, A. Yartsev, and N. C. Greenham. Conformational disorder of conjugated polymers. *J. Chem. Phys.*, 125(15), (2006).

[83] M. Leclerc. Polyfluorenes: Twenty years of progress. *J. Polym. Sci., Part A Polym. Chem.*, 39:2867, (2001).

[84] W. Wu, M. Inbasekaran, M. Hudack, D. Welsh, W. Yu, Y. Cheng, C. Wang, S. Kram, M. Tacey, and M. Bernius. Recent development of polyfluorene-based rgb materials for light emitting diodes. *Microelectronics Journal*, 35(4):343–348, (2004).

[85] U. Scherf and E. J. W. List. Semiconducting polyfluorenes - towards reliable structure-property relationships. *Adv. Mater.*, 14(7):477, (2002).

[86] M. Fukuda, K. Sawada, and K. Yoshino. Synthesis of fusible and soluble conducting polyfluorene derivatives and their characteristics. *J. Polym. Sci., Part A Polym. Chem.*, 31(10):2465–2471, (1993).

[87] N. Miyaura and A. Suzuki. Palladium-catalyzed cross-coupling reactions of organoboron compounds. *Chem. Rev.*, 95(7):2457, (1995).

[88] T. Yamamoto. π-conjugated polymers with electronic and optical functionalities: Preparation by organometallic polycondensation, properties, and applications. *Macromol. Rapid Comm.*, 23(10-11):583, (2002).

[89] A. C. Grimsdale and K. Müllen. Emissive materials, nanomaterials: Polyphenylene-type emissive materials: Poly(para-phenylene)s, polyfluorenes and ladder polymers. *Adv. Polym. Sci*, 199:1–82, (2006).

[90] G. Fytas, H-G. Nothofer, D. Vlassopoulos, and G. Meier. Structure and dynamics of nondilute polyfluorene solutions. *Macromolecules*, 35(2):481–488, (2002).

[91] M. Knaapila, M. Torkkeli, and A. P. Monkman. Evidence for 21-helicity of poly 9,9-bis(2-ethylhexyl)fluorene-2,7-diyl. *Macromolecules*, 40(10):3610–3614, (2007).

[92] M. Arif, C. Volz, and S.M. Guha. Chain morphologies in semicrystalline polyfluorene: Evidence from Raman scattering. *Phys. Rev. Lett.*, 96:025503, (2006).

[93] A. L. T. Khan, P. Sreearunothai, L. M. Herz, M. Banach, and A. Köhler. Morphology-dependent energy transfer within polyfluorene thin films. *Phys. Rev. B*, 69(8):art. no. 085201, (2004).

[94] F. B. Dias, J. Morgado, A. L. Macanita, F. P. da Costa, H. D. Burrows, and A. P. Monkman. Kinetics and thermodynamics of poly(9,9-dioctylfluorene) beta-phase formation in dilute solution. *Macromolecules*, 39(17):5854–5864, (2006).

[95] C. C. Kitts and D. A. Vanden Bout. The effect of solvent quality on the chain morphology in solutions of poly(9,9'-dioctylfluorene). *Polymer*, 48(8):2322 – 2330, (2007).

[96] M. Knaapila, V. M. Garamus, F. B. Dias, L. Almasy, F. Galbrecht, A. Charas, J. Morgado, H. D. Burrows, U. Scherf, and A. P. Monkman. Influence of solvent quality on the self-organization of archetypical hairy rods - branched and linear side chain polyfluorenes: Rodlike chains versus "beta-sheet" in solution. *Macromolecules*, 39(19):6505–6512, (2006).

[97] A. Cadby, P. A. Lane, H. Mellor, S. J. Martin, M. Grell, C. Giebeler, D. D. C. Bradley, M. Wohlgenannt, C. An, and Z. V. Vardeny. Film morphology and photophysics of polyfluorene. *Phys. Rev. B*, 62(23):15604–15609, (2000).

[98] M. Grell, W. Knoll, D. Lupo, A. Meisel, T. Miteva, D. Neher, H.-G. Nothofer, U. Scherf, and A. Yasuda. Blue polarized electroluminescence from a liquid crystalline polyfluorene. *Adv. Mater.*, 11(8):671–675, (1999).

[99] W. Z. Liang, Y. Zhao, J. Sun, J. Song, S. L. Hu, and J. L. Yang. Electronic excitation of polyfluorenes: A theoretical study. *J. Phys. Chem. B.*, 110(20):9908–9915, (2006).

[100] B. Schartel, V. Wachtendorf, M. Grell, D. D. C. Bradley, and M. Hennecke. Polarized fluorescence and orientational order parameters of a liquid-crystalline conjugated polymer. *Phys. Rev. B*, 60(1):277–283, (1999).

[101] H. D. Burrows, J. Seixas de Melo, C. Serpa, L. G. Arnaut, A. P. Monkman, I. Hamblett, and S. Navaratnam. S1→t1 intersystem crossing in -conjugated organic polymers. *J. Chem Phys*, 115(20):9601–9606, (2001).

[102] A. Kobayashi, M. Todorokihara, K. Fujihara, and H. Naito. Polarized fluorescence of poly(9,9-dioctylfluorene) thin films on polyimide alignment layers. *Synth. Met.*, 135-136:295–296, (2003).

[103] E. J. W. List, M. Gaal, R. Guentner, P. Sandiucci de Freitas, and U. Scherf. The role of keto defect sites for the emission properties of polyfluorene-type materials. *Synth. Met.*, 139:759763, (2003).

[104] G. Mauthner, M. Collon, E. J. W. List, F. P. Wenzl, M. Bouguettaya, and J. R. Reynolds. Elimination of defect-induced color stabilities in polymer light-emitting devices. *J. Appl. Phys.*, 97:063508, (2005).

[105] M. Gaal, E. J. W. List, and U. Scherf. Excimers or emissive on-chain defects. *Macromolecules*, 36:4236–4237, (2003).

[106] S. I. Hintschich, C. Rothe, S. Sinha, A. P. Monkman, P. Scandiucci de Freitas, and U. Scherf. Population and decay of keto states in conjugated polymers. *J. Chem. Phys*, 119(22):12017–12022, (2003).

[107] X. H. Yang, D. Neher, C. Spitz, E. Zojer, J. L. Brédas, R. Guntner, and U. Scherf. On the polarization of the green emission of polyfluorenes. *J. Chem. Phys.*, 119(13):6832–6839, (2003).

[108] C. Rothe, S.I. Hintschich, L-O. På lsson, A. P. Monkman, Guentner R., and U. Scherf. Pressure dependent radiative quantum yields of the prompt and delayed luminescence of polyfluorene films. *Chem. Phys. Lett*, 360(1-2):111–116, (2002).

[109] D. Neher. Polyfluorene homopolymers: Conjugated liquid-crystalline polymers for bright blue emission and polarized electroluminescence. *Macromol. Rapid Commun.*, 22(17):1366–1385, (2001).

[110] C. Bauer, G. Urbasch, H. Giessen, A. Meisel, H-G. Nothofer, D. Neher, U. Scherf, and R. F. Mahrt. Polarized photoluminescence and spectral narrowing in an orientated polyfluorene thin film. *ChemPhysChem*, 3:142–146, (2000).

[111] M. Grell and D. D. C. Bradley. Polarized luminescence from oriented molecular materials. *Adv. Mater.*, 11(11):895–905, (1999).

[112] M. Grell, D. D. C. Bradley, M. Inbasekaran, and E.P. Woo. A glass-forming conjugated main chain liquid crystal polymer for polarized electroluminescence applications. *Adv. Mater.*, 9(10):798–802, (1997).

[113] T. Miteva, A. Meisel, M. Grell, H. G. Nothofer, D. Lupo, A. Yasuda, W. Knoll, L. Kloppenburg, U. H. F. Bunz, U. Scherf, and D. Neher. Polarized electroluminescence from highly aligned liquid crystalline polymers. *Synth. Met.*, 111-112:173–176, (2000).

[114] M. Tammer, R. W. T. Higgins, and A. P. Monkman. High optical anisotropy in thin films of polyfluorene and its affect on the outcoupling of light in typical polymer light emitting diode structures. *J. Appl. Phys.*, 91(7):4010–4013, (2002).

[115] M. Knaapila, R. Stepanyan, B. P. Lyons, M. Torkkeli, T. P. A. Hase, R. Serimaa, R. Guntner, O. H. Seeck, U. Scherf, and A. P. Monkman. The influence of the molecular weight on the thermotropic alignment and self-organized structure formation of branched side chain hairy-rod polyfluorene in thin films. *Macromolecules*, 38(7):2744–2753, (2005).

[116] M. Knaapila, R. Stepanyan, B. P. Lyons, M. Torkkeli, and A. Monkman. Towards general guidelines for aligned, nanoscale assemblies of hairy-rod polyfluorene. *Adv. Funct. Mater.*, 16(5):599 – 609, (2006).

[117] B. He, J. Li, Z. Bo, and Y. J. Huang. Highly polarized blue luminescence from the oriented poly(9,9-dioctylfluorene)/polyethylene blending films. *Macromolecules*, 38(16):6762 – 6766, (2005).

[118] D. Hertel, U. Scherf, and H. Bässler. Charge carrier mobility in a ladder-type conjugated polymer. *Adv. Mater.*, 10(14):1119–1122, (1998).

[119] U. Lemmer, S. Heun, R. F. Mahrt, U. Scherf, M. Hopmeier, U. Siegner, E. O. Göbel, K. Müllen, and H. Bässler. Aggregate fluorescence in conjugated polymers. *Chem. Phys. Lett.*, 240:373 – 378, (1995).

[120] J. G. Müller, U. Scherf, and U. Lemmer. Two step charge carrier generation in a ladder-type conjugated polymer. *Synth. Met.*, 119(1-3):395–396, (2001).

[121] U. Scherf and K. Müllen. A soluble ladder polymer via bridging of functionalized poly(p-phenylene)-precursors. *Makromol. Chem., Rapid commun*, 12:489–497, (1991).

[122] F. Laquai, A. K. Mishra, M. R. Ribas, A. Petrozza, J. Jacob, L. Akcelrud, K. Müllen, R. H. Friend, and G. Wegner. Photophysical properties of a series of poly (ladder-type phenylene)s. *Adv. Funct. Mater.*, 17(16):3231–3240, (2007).

[123] R. Hildner, U. Lemmer, U. Scherf, M. van Heel, and J. Köhler. Revealing the electron-phonon coupling in a conjugated polymer by single-molecule spectroscopy. *Adv. Mater.*, 19(15):(1978), (2007).

[124] H. D. Burrows, J. Seixas de Melo, C. Serpa, L. G. Arnaut, M. da G. Miguel, A. P. Monkman, I. Hamblett, and S. Navaratnam. Triplet state dynamics on isolated conjugated polymer chains. *Chem. Phys.*, 285(1):3–11, (2002).

[125] J. Stampfl, W. Graupner, G. Leising, and U. Scherf. Photoluminescence and uv-vis absorption study of poly (para-phenylene)-type ladder-polymers. *J. Lumin.*, 63:117–123, (1995).

[126] U. Scherf, A. Bohnen, and K. Müllen. The oxidized states of a (1,4-phenylene) ladder polymer. *Makromol. Chem*, 193:1127–1133, (1992).

[127] B. S. Nehls, S. Füldner, E. Preis, A. Farrell, and U. Scherf. Microwave-assisted synthesis of 1,5-and 2,6-linked naphthylene-based ladder polymers. *Macromolecules*, 38:687–694, (2005).

[128] S. Barth, H. Bässler, U. Scherf, and K. Müllen. Photoconduction in thin films of a ladder-type poly-para-phenylene. *Chem. Phys. Lett.*, 288:147 – 154, (1998).

[129] B. Schweitzer, G. Wegmann, D. Hertel, R. F. Mahrt, H. Bässler, F. Uckert, U. Scherf, and K. Müllen. Spontaneous and stimulated emission from a ladder-type conjugated polymer. *Phys. Rev. B*, 59(6):4112 – 4118, (1999).

[130] F. Schindler, J. Jacob, A. C. Grimsdale, U. Scherf, K. Müllen, J. M. Lupton, and J. Feldmann. Counting chromophores in conjugated polymers. *Angewandte Chemie-International Edition*, 44(10):1520–1525, (2005).

[131] U. Scherf. Ladder-type materials. *J. Mater. Chem*, 9:1853–1864, (1999).

[132] D. Somitsch, F. P. Wenzl, G. Leising, P. Wilhelm, U. Scherf, K. O. Annan, and P. Knoll. Temperature dependent structural stability of ladder type poly(p-phenylenes). *Synth. Met.*, 119:349–350, (2001).

[133] J. W. Blatchford, T. L. Gustafson, A. J. Epstein, D. A. Vanden Bout, J. Kerimo, D. A. Higgins, P. F. Barbara, D-K. Fu, T. M. Swager, and A. G. MacDiarmid. Spatially and temporally resolved emission from aggregates in conjugated polymers. *Phys. Rev. B*, 54(6):3683 – 3686, (1996).

[134] A. Haugeneder, U. Lemmer, and U. Scherf. Exciton dissociation dynamics in a conjugated polymer containing aggregate states. *Chem. Phys. Lett.*, 351(5-6):354–358, (2002).

[135] D. Hertel, H. Bässler, U. Scherf, and H. H. Hörhold. Charge carrier transport in conjugated polymers. *J. Chem Phys*, 110(18):9214–9222, (1999).

[136] R. F. Mahrt, T. Pauck, U. Lemmer, U. Siegner, M. Hopmeier, R. Hennig, H. Bässler, E. O. Göbel, P. Haring Bolivar, G. Wegmann, H. Kurz, U. Scherf, and K. Müllen. Dynamics of optical excitations in a ladder-type pi-conjugated polymer containing aggregate states. *Phys. Rev. B*, 54(3):1759 – 1765, (1996).

[137] J. M. Lupton. On-chain defect emission in conjugated polymers - Comment on Exciton dissociation dynamics in a conjugated polymer containing aggregate states [A. Haugeneder, U. Lemmer, U. Scherf, Chem. Phys. Lett. 351 (2002) 354]. *Chem. Phys. Lett.*, 365(3-4):366–369, (2002).

[138] F. B. Dias, M. Knaapila, A. P. Monkman, and H. D. Burrows. Fast and slow time regimes of fluorescence quenching in conjugated polyfluorene-fluorenone random copolymers: The role of exciton hopping and dexter transfer along the polymer backbone. *Macromolecules*, 39(4):1598–1606, (2006).

[139] S. M. King, C. Rothe, and A. P. Monkman. Triplet build in and decay of isolated polyspirobifluorene chains in dilute solution. *J. Chem Phys*, 121(21):10803–10808, (2004).

[140] E. J. W. List, C. Creely, G. Leising, N. Schulte, A. D. Schluter, U. Scherf, K. Müllen, and W. Graupner. Excitation energy migration in highly emissive semiconducting polymers. *Chem. Phys. Lett*, 325(1-3):132–138, (2000).

[141] B. P. Lyons, K. S. Wong, and A. P. Monkman. Study of the energy transfer processes in polyfluorene doped with tetraphenyl porphyrin. *J. Chem Phys*, 118(10):4707–4711, (2003).

[142] C. Bauer, H. Giessen, B. Schnabel, E. B. Kley, C. Schmitt, U. Scherf, and R. F. Mahrt. A surface-emitting circular grating polymer laser. *Adv. Mater.*, 13(15):1161, (2001).

[143] R. Harbers, P. Strasser, D. Caimi, R. F. Mahrt, N. Moll, D. Erni, W. Bächtold, B. J. Offrein, and U. Scherf. Enhanced feedback and experimental band mapping of organic photonic-crystal lasers. *J. Opt A: Pure Appl. Opt*, 8:S273–S277, (2006).

[144] J. G. Müller, J. M. Lupton, J. Feldmann, U. Lemmer, M. C. Scharber, N. S. Sariciftci, C. J. Brabec, and U. Scherf. Ultrafast dynamics of charge carrier photogeneration and geminate recombination in conjugated polymer: fullerene solar cells. *Phys. Rev. B*, 72(19), (2005).

[145] J. G. Müller, M. Scharber, U. Lemmer, J. Feldmann, U. Scherf, and N. S. Sariciftci. Ultrafast spectroscopy of polaron pairs in polymer solar cells. *Synth. Met.*, 137(1-3):1475–1476, (2003).

[146] A. Wohlgenannt and Z. V. Vardeny. Photophysics properties of blue-emitting polymers. *Syth Met*, 125(1):55–63, (2001).

[147] Y. Goto, I. Kakinoki, M. Noto, and M. Era. Efficient polarized blue electroluminescent device using oriented p-sexiphenyl thin film. *Curr. Appl. Phys.*, 5:19–22, (2005).

[148] S. F. Chung, T. C. Wen, W. Y. Chou, and T. F. Guo. High luminescence polarized polymer light-emitting diodes fabricated using aligned polyfluorene. *Jpn. J. Appl. Phys., Part 2*, 45(1-3):L60–L63, (2006).

[149] A. Cirpan, L. Ding, and F. E. Karasz. Optical and electroluminescent properties of polyfluorene copolymers and their blends. *Polymer*, 46(3):811–817, (2005).

[150] Lyons. B. P and H Vaughan. Discussions on the methodology of spun film manufacture and subsequent use of the films in optical experiments, (2003).

[151] B. P. Lyons and A. P. Monkman. A comparison of the optical constants of aligned and unaligned thin polyfluorene films. *J. Appl. Phys.*, 96(9):4735–4741, (2004).

[152] B. P. Lyons and A. P. Monkman. The role of exciton diffusion in energy transfer between polyfluorene and tetraphenyl porphyrin. *Phys. Rev. B*, 71(23):235201, (2005).

[153] J.A. Hauer, S.S. Taylor, and D.A. Johnson. Binding-dependent disorder-order transition in pkiα;: A fluorescence anisotropy study. *Biochemistry*, 38(21):6774–6780, (1999).

[154] E. Deprez, P. Tauc, H. Leh, J.-F. Mouscadet, C. Auclair, and J-C. Brochon. Oligomeric states of the hiv-1 integrase as measured by time-resolved fluorescence anisotropy. *Biochemistry*, 39(31):9275–9284, (2000).

[155] A. Volkmer, V. Subramaniam, D. J. S. Birch, and T. M. Jovin. One- and two-photon excited fluorescence lifetimes and anisotropy decays of green fluorescent proteins. *Biophysical Journal*, 78(3):1589–1598, (2000).

[156] A. V. Digris, V. V. Skakoun, E. G. Novikov, A. van Hoek, A. Claiborne, and A. Visser. Thermal stability of a flavoprotein assessed from associative analysis of polarized time-resolved fluorescence spectroscopy. *European Biophysics Journal with Biophysics Letters*, 28(6):526–531, (1999).

[157] J. C. Brochon, P. Tauc, F. Merola, and B. M. Schoot. Analysis of a recombinant protein preparation on physical homogeneity and state of aggregation. *Anal. Chem.*, 65(8):1028–1034, (1993).

[158] P. Majumder, R. Sarkar, A. K. Shaw, A. Chakraborty, and S. K. Pal. Ultrafast dynamics in a nanocage of enzymes: Solvation and fluorescence resonance energy transfer in reverse micelles. *J. Colloid Interface Sci.*, 290(2):462–474, (2005).

[159] R. Sarkar, A. K. Shaw, M. Ghosh, and S. K. Pal. Ultrafast photoinduced deligation and ligation dynamics: Dcm in micelle and micelle-enzyme complex. *Journal of Photochemistry and Photobiology B: Biology*, 83(3):213–222, (2006).

[160] P. Kapusta, R. Erdmann, U. Ortmann, and M. Wahl. Time-resolved fluorescence anisotropy measurements made simple. *J. Fluoresc*, 13(2):179–183, (2003).

[161] H. L. Vaughan, F. B. Dias, and A. P. Monkman. An investigation into the excitation migration in polyfluorene solutions via temperature dependent fluorescence anisotropy. *J. Chem Phys*, 122(1):014902, (2005).

[162] V.I. Arkhipov, E.V. Emelianova, and H. B¨ assler. Hot exciton dissociation in a conjugated polymer. *Phys. Rev. Lett.*, 82:1321–1324, (1999).

[163] M. D. Lechner and W Martienssen, editors. *Group IV: Physical Chemistry Viscosity of Pure Organic Liquids and Binary Liquid Mixtures*, volume 25 of *Landolt-Brnstein: Numerical Data and Functional Relationships in Science and Technology - New Series*, pages 470–472. Springer, (2009).

[164] B. Brocklehurst and R. N. Young. Rotation of aromatic hydrocarbons in viscous alkanes. 1. methylcyclohexane. *J. Phys. Chem. A*, 103(20):3809–3817, (1999).

[165] M. Hennecke, T. Damerau, and K. Müllen. Fluorescence depolarization in poly(p-phenylphenylenevinylene) and related oligomers. *Macromolecules*, 26:3411, (1993).

[166] Q-Y. Shang, X. Dou, and B. S. Hudson. Off-axis orientation of the electronic transition moment for a linear conjugated polyene. *Nature*, 352(6337):703 – 706, (1991).

[167] H-J. Egelhaaf, L. Lüer, A. Tompert, P. Bäuerle, K. Müllen, and D. Oelkrug. Fluoresecence anisotropy and rotational diffusion of polyene-like molecules in solution. *Synth. Met.*, 115:63–68, (2000).

[168] S. C. J. Meskers, J. Hübner, M. Oestreich, and H. Bässler. Dispersive relaxation dynamics of photoexcitations in a polyfluorene film involving energy transfer: Experiment and monte carlo simulations. *J. Phys. Chem. B*, 105:9139–9149, (2001).

[169] H. L. Vaughan, L-O. På lsson, B. S. Nehls, A. Farrell, U. Scherf, and A. P. Monkman. On the angular dependence of the optical polarization anisotropy in ladder-type polymers. *J. Chem Phys*, 128(4):044709, (2008).

[170] L. Cuff and M. Kertesz. Theoretical prediction of the vibrational spectrum of fluorene and planarized poly(p-phenylene). *J. Phys. Chem.*, 98(47):12223 – 12231, (1994).

[171] D. Hertel, Y. V. Romanovskii, B. Schweitzer, U. Scherf, and H. Bässler. The origin of the delayed emission in films of a ladder-type poly(para-phenylene). *Synth. Met.*, 116:139–143, (2001).

[172] A. Synak, G. Gondek, P. Bojarski, L. Kulak, A. Kubicki, M. Szabelski, and P. Kwiek. Fluorescence depolarization in the presence of exciation energy migration in poartly ordered polymer films. *Chem. Phys. Lett*, 399:114–119, (2004).

[173] E. W. Snedden, R. Thompson, S. I. Hintschich, and A. P. Monkman. Fluorescence vibronic analysis in a ladder-type conjugated polymer. *Chem. Phys. Lett*, 472:80–84, (2009).

[174] K. D. Belfield, M. V. Bondar, O. V. Przhonska, and K. J. Schafer. One- and two-photon photostability of 9,9-didecyl-2,7-bis(n,n-diphenylamino)fluorene. *Photochem. Photobiol. Sci*, 3:138–141, (2003).

[175] K. D. Belfield, M. V. Bondar, O. V. Przhonska, K. J. Schafer, and W. Mourad. Spectral properties of several fluorene derivatives with potential as two-photon fluorescent dyes. *J. Lumin.*, 97(2):141–146, (2002).

[176] S. Kalinin, M. Speckbacher, H. Langhals, and L. B-A. Johansson. A new and versalie fluorescence standard for quantum yield determination. *Phys. Chem. Chem. Phys.*, 3:172 – 174, (2001).

[177] M. P. Lettinga, H. Zuilhof, and M. A. M. J. van Zandvoort. Phosphorscence and fluorscence charaterization of fluorescein deraviatives immobilized in various polymer matrices. *Phys. Chem. Chem. Phys.*, 2:2697 – 3707, (2000).

[178] A. Köhler, D. A. dos Santos, D. Beljonne, Z. Shuai, J. L. Bredas, A. B. Holmes, A. Kraus, K. Müllen, and R. H. Friend. Charge separation in localized and delocalized electronic states in polymeric semiconductors. *Nature*, 392(6679):903–906, (1998).

[179] F. G. Balt´ a Calleja and C. G. Vonk. *X-ray scattering of synthethic polymers*. Elsevier, Amsterdam, (1989).

[180] R. J. Roe. *Methods of X-ray and neutron scattering in polymer science / Ryong-Joon Roe.* Oxford University Press, New York, (2000).

[181] P. H. Fuoss and S. Brennan. Surface sensitive X-Ray scattering. *Annu. Rev. Mater. Sci.*, 20:365 – 390, (1990).

[182] P. Lindner and T. Zemb. *Neutron, X-rays and Light. Scattering Methods Applied to Soft Condensed Matter*. Elsevier Ltd, Oxford, UK, second edition, (2004).

[183] M. Birkholz. *Thin Film Analysis by X-Ray Scattering: Techniques for Structural Characterization*. Wiley-VCH, Weinheim, first edition, (2006).

[184] N. Stribeck. *X-Ray Scattering of Soft Matter*. Springer-Verlag, Berlin, first edition, (2007).

[185] B. K. Tanner. *Introduction to the Physics of Electrons in Solids*. Cambridge University Press, Cambridge, 1st edition, (1995).

[186] J. Als-Nielsen and D. McMorrow. *Elements of Modern X-ray Physics*, volume 1. John Wiley & Sons, New York, (2001).

[187] M. Misaki, S. Nagamatsu, M. Chikamatsu, Y. Yoshida, R. Azumi, N. Tanigaki, Y. Ueda, and K. Yase. Single-crystal-like structure of poly(9,9-dioctylfluorene) thin films evaluated by synchrotron-sourced grazing-incidence X-ray diffraction. *Polymer Journal*, 39(12):1306–1311, (2007).

[188] M. Knaapila, M. Torkkeli, B. P. Lyons, M. R. C. Hunt, T. P. A. Hase, O. H. Seeck, L. Bouchenoire, R. Serimaa, and A. P. Monkman. Influence of star-like iridium complexes in the graphoepitaxy of polyfluorene thin films. *Phys. Rev. B*, 74(21), (2006).

[189] H. C. Yang, T. J. Shin, L. Yang, K. Cho, C. Y. Ryu, and Z. N. Bao. Effect of mesoscale crystalline structure on the field-effect mobility of regioregular poly(3-hexyl thiophene) in thin-film transistors. *Advanced Functional Materials*, 15(4):671–676, (2005).

[190] S. Goffri, C. Muller, N. Stingelin-Stutzmann, D. W. Breiby, C. P. Radano, J. W. Andreasen, R. Thompson, R. A. J. Janssen, M. M. Nielsen, P. Smith, and H. Sirringhaus. Multicomponent semiconducting polymer systems with low crystallization-induced percolation threshold. *Nature Mater.*, 5(12):950–956, (2006).

[191] M. F. Toney, T. P. Russell, J. A. Logan, H. Kikuchi, J. M. Sands, and S. K. Kumar. Near-surface alignment of polymers in rubbed films. *Nature*, 374(6524):709–711, (1995).

[192] N. Reitzel, D. R. Greve, K. Kjaer, P. B. Hows, M. Jayaraman, S. Savoy, R. D. McCullough, J. T. McDevitt, and T. Bjornholm. Self-assembly of conjugated polymers at the air/water interface. structure and properties of Langmuir and Langmuir-Blodgett films of amphiphilic regioregular polythiophenes. *Journal of the American Chemical Society*, 122(24):5788–5800, (2000).

[193] S. Nagamatsu, M. Misaki, M. Chikamatsu, T. Kimura, Y. Yoshida, R. Azumi, N. Tanigaki, and K. Yase. Crystal structure of friction-transferred poly(2,5-dioctyloxy-1,4-phenylenevinylene). *J. Phys. Chem. B*, 111(17):4349–4354, (2007).

[194] Y. Zhang, S. Mukoyama, Y. Hu, C. Yan, Y. Ozaki, and I. Takahashi. Thermal behavior and molecular orientation of poly(ethylene 2,6-naphthalate) in thin films. *Macromolecules*, 40(11):4009–4015, (2007).

[195] E. Moons. Conjugated polymer blends: linking film morphology to performance of light emitting diodes and photodiodes. *J. Phys: Condens Matter*, 14:12235, (2002).

[196] D. Veldman, S. C. J. Meskers, and R. A. J. Janssen. The energy of charge-transfer states in electron donor-acceptor blends: Insight into the energy losses in organic solar cells. *Adv Funct Mater*, 19:1939, (2009).

[197] C. Y. Yang, A. J. Heeger, and Y. Cao. Microstructure of gel-processed blends of conjugated polymer and ultrahigh molecular weight polyethylene. *Polymer*, 41:4113–4118, (2000).

[198] M. Knaapila, B. P. Lyons, T. P. A. Hase, C. Pearson, M. C. Petty, L. Bouchenoire, P. Thompson, R. Serimaa, M. Torkkeli, and A. P. Monkman. Influence of molecular weight on the surface morphology of aligned, branched side-chain polyfluorene. *Adv. Funct. Mater.*, 15(9):1517–1522, (2005).

[199] M. Knaapila, T. P. A. Hase, M. Torkkeli, R. Stepanyan, L. Bouchenoire, H. S. Cheun, M. J. Winokur, and A. P. Monkman. Meridional orientation in biaxially aligned thin films of hairy-rod polyfluorene. *Crystal Growth & Design*, 7(9):1706–1711, (2007).

[200] S. D. Brown, L. Bouchenoire, D. Bowyer, J. Kervin, D. Laundy, M. J. Longfield, D. Mannix, D. F. Paul, A. Stunault, P. Thompson, M. J. Cooper, C. A. Lucas, and W. G. Stirling. The xmas beamline at esrf: instrumental developments and high-resolution diffraction studies. *J. Synchotron Rad.*, 8:1172–1181, (2001).

[201] E. Meirovitch. Esr. observations on stretching-induced molecular mobility and partitioning among sites in polyethylene films. *J. Phys. Chem.*, 88:2629 – 2635, (1984).

[202] R. S. Stein and F. H. Norris. The X-Ray diffraction, birefringence, and infrared dichroism of stretched polyethylene: Part II. *J. Poly. Sci.*, 31(123):327 –, (1956).

[203] A. Brown. X-ray diffraction studies of the stretching and relaxing of polyethylene. *Journal of Applied Physics*, 20(6):552–558, (1949).

[204] R. S. Stein and F. H. Norris. The X-Ray diffraction, birefringence, and infrared dichroism of stretched polyethylene. *J. Poly. Sci.*, 21(99):381–396, (1956).

[205] C. Luo, N. A. Guardala, J. L. Price, I. Chodak, O. Zimerman, and R. G. Weiss. Structural and dynamic investigations of unstretched and stretched ultrahigh molecular weight polyethylene films. 1-pyrenyl attachment by bombardment with 4.5 mev protons and irradiation with ev range photons. *Macromolecules*, 35(12):4690–4701, (2002).

[206] C.P. Lafrance, P. Chabot, M. Pigeon, R. E. Prud'homme, and M. Pezolet. Study of the distribution of the molecular orientation in thick polyethylene samples by X-Ray diffraction, infra-red dichroism, and Raman spectroscopy. *Polymer*, 34(24):5029, (1993).

[207] R. J. Pazur, A. J. J. I. Abdellah, and R. E. Prud'homme. X-ray and birefringence orientation measurements on uniaxially deformed polyethylene film. *Polymer*, 34(19):4004 – 4014, (1993).

[208] C. N. Banwell. Raman spectroscopy. In *Fundamentals of molecular spectroscopy.* McGraw-Hill Book Company (UK) Limited, Maidenhead, (1983).

[209] B. J. Kip, M. vanGurp, S. P. C. van Heel, and R. J. Meier. Orientational order parameter in polyethylene foils - a polarized Raman-spectroscopic study. *J. Raman. Spec.*, 24(8):501 – 510, (1993).

[210] M. S. Lavine, N. Waheed, and G. C. Rutledge. Molecular dynamics simulation of orientation and crystallization of polyethylene during uniaxial extension. *Polymer*, 44(5):1771 – 1779, (2003).

[211] L. Cuff, M. Kertesz, U. Scherf, and K. Müllen. Interpretation of the vibrational spectra of planarized poly-p-phenylene. *Synth. Met.*, 69:683–684, (1995).

[212] S. Guha and M. Chandrasekhar. Photophysics of organic emissive semiconductors under hydrostatic pressure. *Phys. Stat. Sol*, 241(14):3318–3327, (2004).

[213] D. Somitsch, F. P. Wenzl, J. Kreith, M. Pressl, R. Kaindl, U. Scherf, G. Leising, and P. Knoll. The Raman spectra of methyl substituted ladder type poly(p-phenylene). theoretical and experimental investigations. *Synth. Met.*, 138:39–42, (2003).

[214] B Schrader. *Raman/Infrared Atlas of Organic Compounds.* VCH Publishers (UK) Ltd., Cambridge, (1989).

[215] M. C. P. Van Eijk, P. J. R. Leblans, R. J. Meier, and B. J. Kip. Raman-spectroscopic determination of the number of high-stress bearing C-C bonds within high-modulus polyethylene fibers during stress-relaxation. *J. Mater. Sci. Lett.*, 9(11):1263–1265, (1990).

[216] F. J. Boerio and J. L. Koenig. Raman scattering in crystalline polyethylene. *J. Chem Phys*, 52(7):3425 – 3431, (1970).

[217] C. Fagnano, M. Rossi, R. S. Porter, and S. Ottani. A study on solid-state drawn fibers of polyethylene by confocal Raman microspectrometry: evaluation of the orientation profiles of amorphous and crystalline phases across the fiber section. *Polymer*, 42(13):5871 – 5883, (2001).

[218] T. Damerau and M. Hennecke. Determination of orientational order parameters of uniaxial films with a commercial 90 degree-angle fluorescence spectrometer. *J. Chem. Phys.*, 103(14):6232, (1995).

[219] A. Arcioni, C. Bacchiocchi, M. D'Elia, R. Tarroni, and C. Zannoni. Order and mobility of the fluorescent probe 1,6-diphenylhexatriene in a polyester liquid crystal polymer. *Molecular Crystals and Liquid Crystals*, 362:279–288, (2001).

[220] E. M. Aver'yanov. Spectral features of impurity luminescence in uniaxial polymer films and nematic glasses. *Molecular Materials*, 14(3):233–261, (2001).

[221] E. M. Aver'yanov. Spectral features of impurity luminescence in uniaxial polymer films and nematic glasses. *Optics and Spectroscopy*, 91(5):711–723, (2001).

[222] J. Gierschner, M. Ehni, H. J. Egelhaaf, B. M. Medina, D. Beljonne, H. Benmansour, and G. C. Bazan. Solid-state optical properties of linear polyconjugated molecules: pi-stack contra herringbone. *Journal of Chemical Physics*, 123(14), (2005).

[223] C. Luc, S. Clerjon, F. Peyrin, and J. Lepetit. Polarized front-face fluorescence for muscle tissue structure evaluation. *Meas. Sci. Technol.*, 19(5):055705, (2008).

[224] C. Weder, C. Sarwa, C. Bastiaansen, and P. Smith. Highly polarized luminescence from oriented conjugated polymer/polyethylene blend films. *Advanced Materials*, 9(13):1035, (1997).

[225] R. Jimenez, S. N. Dikshit, S. E. Bradforth, and G. R. Fleming. Electronic excitation transfer in the LH2 complex of rhodobacter sphaeroides. *J. Phys. Chem.*, 100(16):6825–6834, (1996).

[226] C. Chi, G. Lieser, V. Enkelmann, and G. Wegner. Packing and uniaxial alignment of liquid crystalline oligofluorenes. *Macrom. Chem. Phys.*, 206:1597–1609, (2005).

[227] T. W. Hagler, K. Pakbaz, and A. J. Heeger. Polarized-electroabsorption spectroscopy of a soluble derivative of poly (p-phenylenevinylene) oriented by gel processing on polyethylene: Polarization anisotopy, the off-axis dipole moment and excited state delocalization. *Phys. Rev. B*, 49(16):10968 –10976, (1994).

[228] T. E. Dykstra, E. Hennebicq, D Beljonne, J Gierschner, G. Claudio, E. R. Bittner, J Knoester, and G. D. Scholes. Conformational disorder and ultrafast exciton relaxation in ppv-family conjugated polymers. *J. Phys. Chem. B*, 113:656667, (2009).

[229] C-K Chee, S Rimmer, R Rutkaite, I Soutar, and L Swanson. Time-resolved fluorescence anisotropy measurements in the study of poly(n-isopropyl acrylamide)-based systems. *J Photoch Photobio A*, 180:1 – 8, (2006).

[230] G. Giraud, H. Schulze, T.T. Bachmann, C.J. Campbell, A.R. Mount, P Ghazal, S.W.J. Khondoker, M.R. Ember, I. Ciani, C. Tlili, A.J. Walton, J.G. Terry, and J Crain. Solution state hybridization detection using time-resolved fluorescence anisotropy of quantum dot-dna bioconjugates. *Chem. Phys. Lett.*, In Press, Corrected Proof, Available online 18 November 2009, (2009).

[231] I Soutar, C Jones, D.M. Lucas, and L Swanson. Applications of time-resolved luminescence anisotropy measurements to the study of polymer dynamics. *J Photoch Photobio A*, 102:87–92, (1996).

[232] D. Tleugabulova, Z. Zhang, Y. Chen, M.A. Brook, and J.D. Brennan. Fluorescence anisotropy in studies of solute interactions with covalently modified colloidal silica nanoparticles. *Langmuir*, 20:848–854, 2004.

[233] A. Bruno, M. Alfé, B. Apicella, C. de Lisio, and P. Minutolo. Characterization of nanometric carbon materials by time-resolved fluorescence polarization anisotropy. *Opt. Laser Eng.*, 44:732 – 746, (2006).

[234] D. Anestopoullos, M. Fakis, L. Polyzos, G. Tsigaridas, P. Persephonis, and V. Giannetas. Study of the isotropic and anisotropic fluorescence of two oligothiophenes by femtosecond time-resolved spectroscopy. *J. Phys. Chem. B*, 109(19):9476–9481, (2005).

[235] A. K. Shaw, R. Sarkar, D. Banerjee, S. I. Hintschich, A. P. Monkman, and S. K. Pal. Direct observation of protein residue solvation dynamics. *Journal of Photochemistry and Photobiology A: Chemistry*, 185(1):76 – 85, (2007).

[236] Y. Pu, W.B. Wang, S. Achilefu, B.B. Das, G.C. Tang, V. Sriramoju, and R.R. Alfano. Time-resolved fluorescence polarization anisotropy and optical imaging of cybesin in cancerous and normal prostate tissues. *Opt. Comm.*, 274:260 – 267, (2007).

[237] T Munaka, H Abe, M Kanai, H Sakamoto, T AMD Nakanishi, T Yamaoka, S Shoji, and A Murakami. Real-time monitoring of antibody secretion from hybridomas on a microchip by time-resolved luminescence anisotropy analysis. *Anal Biochem*, 353:1–6, (2006).

[238] R. Sarkar, A. K. Shaw, S.S. Narayanan, F. Dias, A.P. Monkman, and S. K. Pal. Direct observation of protein folding in nanoenvironments using a molecular ruler. *Bio Phys Chem*, 123:40–48, (2006).

[239] N. Chadborn, J. Bryant, A. J. Bain, and P. O'Shea. Ligand-dependent conformational equilibria of serum albumin revealed by tryptophan fluorescence quenching. *Biophysical Journal*, 76(4):2198–2207, (1999).

[240] O. F. A. Larsen, I. H. M. van Stokkum, A. Pandit, R. van Grondelle, and H. van Amerongen. Ultrafast polarized fluorescence measurements on tryptophan and a tryptophan-containing peptide. *J. Phys. Chem. B.*, 107(13):3080–3085, (2003).

[241] A.P. Dorado and I.F. Piérola. Rotational motions of probes and labels in polyethylacrylate networks studied by time-resolved fluorescence anisotropy. *J Lumin*, 72-74:484–486, (1997).

[242] O. Varnavski, I. D. W. Samuel, L-O. Palsson, R. Beavington, P. L. Burn, and T. Goodson. Investigations of excitation energy transfer and intramolecular interactions in a nitrogen corded distrylbenzene dendrimer system. *J. Chem Phys*, 116(20):8893–8903, (2002).

[243] D. Hu, J. Yu, B. Bagchi, P.J. Rossky, and P. F. Barbara. Collapse of conjugated polymers with chemical defects into ordered, cylindrical conformations. *Nature*, 405(6790):1030–1033, (2000).

[244] J. Schaffer, A. Volkmer, C. Eggeling, V. Subramaniam, G. Striker, and C. A. M. Seidel. Identification of single molecules in aqueous solution by time-resolved fluorescence anisotropy. *J. Phys. Chem. A*, 103(3):331–336, (1999).

[245] P. Toele, H. Zhang, and M. Glasbeek. Femtosecond fluorescence anisotropy studies of excited-state intramolecular double-proton transfer in [2,2'-bipyridyl]-3,3'-diol in solution. *J. Phys. Chem. A.*, 106(15):3651–3658, (2002).

[246] T. Nomoto, H. Hosoi, T. Fujino, T. Tahara, and H. O. Hamaguchi. Excited-state structure and dynamics of 1,3,5-tris(phenylethynyl)benzene as studied by Raman and time-resolved fluorescence spectroscopy. *J. Phys. Chem. A.*, 111(15):2907–2912, (2007).

[247] D. Anestopoulos, M. Fakis, P. Persephonis, V. Giannetas, and J. Mikroyannidis. Excitation energy transfer in a cationic water-soluble conjugated co-polymer studied by time resolved anisotropy and fluorescence dynamics. *Chem. Phys. Lett.*, 421(1-3):205–209, (2006).

[248] S. Westenhoff, C. Daniel, R. H. Friend, C. Silva, V. Sunström, and A. Yartsev. Exciton migration in a polythiophene: Probing the spatial and energy domain by line- dipole förster-type energy transfer. *J. Chem Phys*, 122:094903, (2005).

[249] X. Yang, T. E. Dykstra, and G. D. Scholes. Photon-echo studies of collective absorption and dynamic localization of excitation in conjugated polymers and oligomers. *Phys. Rev. B*, 71:045203, (2005).

[250] E. Collini and G. D. Scholes. Electronic and vibrational coherences in resonance energy transfer along meh-ppv chains at room temperature. *J. Phys. Chem. A*, 113(16):4223–4241, (2009).

[251] E. Deprez, P. Tauc, H. Leh, J. F. Mouscadet, C. Auclair, M. E. Hawkins, and J. C. Brochon. DNA binding induces dissociation of the multimeric form of hiv-1 integrase: A time-resolved fluorescence anisotropy study. *Proc. Nat. Acad. Sci. U.S.A.*, 98(18):10090–10095, (2001).

[252] A. K. Shaw and S. K. Pal. Spectroscopic studies on the effect of temperature on pH-induced folded states of human serum albumin. *Journal of Photochemistry and Photobiology B-Biology*, 90(1):69–77, (2008).

[253] V. Gulbinas, Y. Zaushitsyn, V. Sundström, D. Hertel, H. Bässler, and A. Yartsev. Dynamics of the electric field-assisted charge carrier photogeneration in ladder-type poly(para-phenylene) at a low excitation intensity. *Phys. Rev. Lett.*, 89(10):107401, (2002).

[254] G Lanzani, H. L. Vaughan, and A. P. Monkman. Personal communications at op 2009 in beijing, june 2009 on the topic of ultra-fast depolarization in conjugated polymers., (2009).

[255] M. M-L. Grage, P. W. Wood, A. Ruseckas, T. Pullerits, W. J. Mitchell, P. L. Burn, I. D. W. Samuel, and V. Sundström. Conformational disorder and energy migration in MEH-PPV with partially broken conjugation. *J. Chem Phys*, 118(16):7644–7650, (2003).

[256] N.P. Wells, B. W. Boudouris, M. A. Hillmyer, and D. A. Blank. Intramolecular exciton relaxation and migration dynamics in poly(3-hexylthiophene). *J. Phys. Chem. C*, 111(42):15404–15414, (2007).

[257] P. Martinsson, V. Sundström, and E. Å kesson. An ultrafast time-resolved anisotropy of bacteriochlorophyll a in pyridine. *FEBS Lett.*, 465:107–109, (2000).

[258] O. Varnavski, T. Goodson, L. Sukhomlinova, and R. Twieg. Ultrafast exciton dynamics in a branched molecule investigated by time-resolved fluorescence, transient absorption, and three-pulse photon echo peak shift measurements. *J. Chem Phys B*, 108(29):10484–10492, (2004).

[259] A. T. Yeh, C. V. Shank, and J. K. McCusker. Ultrafast electron localization dynamics following photo-induced charge transfer. *Science*, 289(5481):935–938, (2000).

[260] M. M-L. Grage, T. Pullerits, A. Ruseckas, M. Theander, O. Inganäs, and V. Sundström. Conformational disorder of a substitued polythiophene in solution revealed by excitation transfer. *Chem. Phys. Lett*, 339:96–102, (2001).